AD-A075 163 BELL HELICOPTER TEXTRON FORT WORTH TX F/G 1/3
INVESTIGATION OF THE CRASH-IMPACT CHARACTERISTICS OF ADVANCED A--ETC(U)
SEP 79 J D CRONKHITE, T J HAAS, V L BERRY DAAJ02-77-C-0062
UNCLASSIFIED USARTL-TR-79-11 NL

1 OF 3
AD
A075163

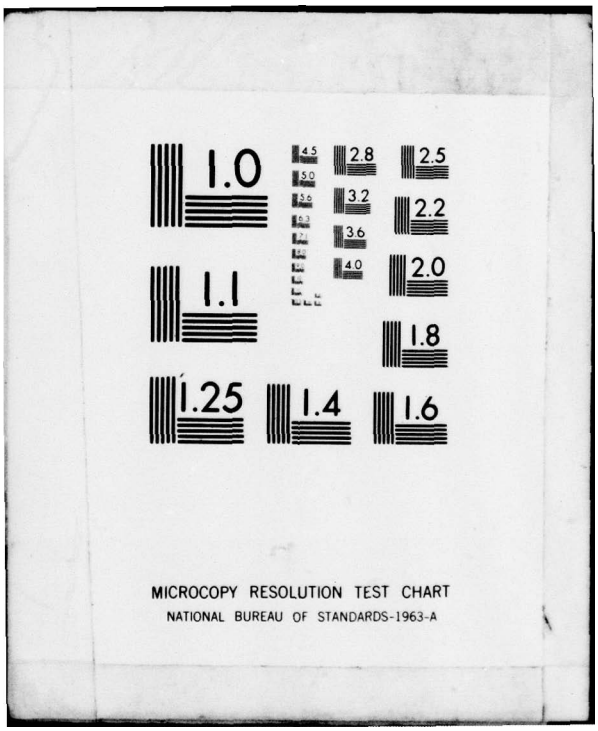
1.0
1.1
1.25
1.4
1.6
1.8
2.0
2.2
2.5
2.8
3.2
3.6
4.0
4.5
5.0
5.6
MICROCOPY RESOLUTION TEST CHART
NATIONAL BUREAU OF STANDARDS-1963-A

USARTL-TR-79-11

INVESTIGATION OF THE CRASH-IMPACT CHARACTERISTICS OF ADVANCED AIRFRAME STRUCTURES

J. D. Cronkhite, T. J. Haas, V. L. Berry, R. Winter
BELL HELICOPTER TEXTRON
P. O. Box 482
Fort Worth, Tex. 76101

September 1979

Final Report

Approved for public release;
distribution unlimited.

Prepared for

APPLIED TECHNOLOGY LABORATORY
U. S. ARMY RESEARCH AND TECHNOLOGY LABORATORIES (AVRADCOM)
Fort Eustis, Va. 23604

APPLIED TECHNOLOGY LABORATORY POSITION STATEMENT

This report was prepared by Bell Helicopter Textron under the terms of Contract DAAJ02-77-C-0062. The objective of this effort was to investigate the crash-impact characteristics of advanced troop transport helicopter airframe structures constructed of composite materials. This was achieved by: (1) surveying literature and organizations on the subject of advanced airframe crashworthiness; (2) developing design concepts; (3) analytically investigating the ability of advanced helicopter structures to comply with MIL-STD-1290; and (4) assessing the state of the art of designing crashworthy advanced helicopter structures.

The technical manager for this program was Mr. George T. Singley, III, Safety and Survivability Technical Area, Aeronautical Systems Division.

James D. /Cronkhite, Thomas J. Haas,
Victor L. /Berry Robert/Winter

UNCLASSIFIED
SECURITY CLASSIFICATION OF THIS PAGE (When Data Entered)

REPORT DOCUMENTATION PAGE	READ INSTRUCTIONS BEFORE COMPLETING FORM
1. REPORT NUMBER: USARTL-TR-79-11	2. GOVT ACCESSION NO. / 3. RECIPIENT'S CATALOG NUMBER
4. TITLE (and Subtitle): INVESTIGATION OF THE CRASH-IMPACT CHARACTERISTICS OF ADVANCED AIRFRAME STRUCTURES	5. TYPE OF REPORT & PERIOD COVERED: Final Report / 6. PERFORMING ORG. REPORT NUMBER
7. AUTHOR(s): BHT: J. D. Cronkhite, T. J. Haas, V. L. Berry; GAC: R. Winter	8. CONTRACT OR GRANT NUMBER(s): DAAJ02-77-C-0062
9. PERFORMING ORGANIZATION NAME AND ADDRESS: Bell Helicopter Textron (BHT), P. O. Box 482, Fort Worth, Texas 76101 (See supplementary notes)	10. PROGRAM ELEMENT, PROJECT, TASK AREA & WORK UNIT NUMBERS: 62209A 1L262209AH76 00 216 EK
11. CONTROLLING OFFICE NAME AND ADDRESS: Applied Technology Laboratory, U.S. Army Research & Technology Laboratories, Fort Eustis, Virginia 23604 (AVRADCOM)	12. REPORT DATE: September 1979 / 13. NUMBER OF PAGES: 221
14. MONITORING AGENCY NAME & ADDRESS (if different from Controlling Office)	15. SECURITY CLASS. (of this report): Unclassified / 15a. DECLASSIFICATION/DOWNGRADING SCHEDULE

16. DISTRIBUTION STATEMENT (of this Report)

Approved for public release; distribution unlimited.

17. DISTRIBUTION STATEMENT (of the abstract entered in Block 20, if different from Report)

18. SUPPLEMENTARY NOTES

Work under this contract was also performed by:
Grumman Aerospace Corporation (GAC)
Bethpage, New York 11714

19. KEY WORDS (Continue on reverse side if necessary and identify by block number)

Helicopter	Composite
Structure	Fiber reinforced plastic
Airframe	Structure crash simulation
Crashworthiness	Mathematical
Crash impact	Computer model

20. ABSTRACT (Continue on reverse side if necessary and identify by block number)

The purpose of this program was to investigate the crash-impact characteristics of advanced troop transport helicopter airframe structures constructed of composite materials. Currently available information was surveyed on the crash-impact behavior of composite materials, analytical tools for design of crashworthy airframe structures, and airframe structure crashworthiness design criteria. Information on the crash-impact behavior of composite materials was found to be limited. Automotive studies showed that by innovative

DD FORM 1 JAN 73 1473 EDITION OF 1 NOV 65 IS OBSOLETE

UNCLASSIFIED
SECURITY CLASSIFICATION OF THIS PAGE (When Data Entered)

20. Continued.

design, composite materials could function efficiently as energy absorbers to reduce crash-impact loads. Other pertinent studies were found that are currently in progress at Bell Helicopter Textron, the NASA Langley Research Center and the U.S. Army's Research and Technology Laboratories and are summarized. Finally, effects of composite materials on the compliance of airframe structures with current Army crashworthiness requirements are discussed.

Two state-of-the-art, nonlinear, large deflection structure crash simulations are evaluated for use as analytical tools for design of crashworthy composite airframe structures: The Lockheed KRASH analysis and the Grumman DYCAST finite-element analysis. Input structure definition for coarse KRASH analysis was found to be difficult. While it is more complete, the DYCAST detailed analysis needs validation for both metal and composite helicopter-type structure. However, the two programs are seen to complement each other: KRASH for analysis of overall airframe response and DYCAST for detailed analysis of sections which can be input to KRASH.

Design concepts using composite materials are shown that incorporate both the general airworthiness and crashworthiness considerations into the same airframe structure. The crashworthy design criteria used for the concepts were found in TR 71-22, "The Crash Survival Design Guide", and MIL-STD-1290(AV), "Light Fixed- and Rotary-Wing Aircraft Crashworthiness."

A comprehensive research program is recommended to study the crash-impact behavior of composites, develop analytical tools, and develop design concepts and data for crashworthy helicopter airframes constructed of composite materials.

PREFACE

This investigation of the crash-impact characteristics of advanced airframe structures was performed under Contract DAAJ02-77-C-0062, with the Applied Technology Laboratory, U.S. Army Research and Technology Laboratories (AVRADCOM), Fort Eustis, Virginia. George Singley, III, of the Applied Technology Laboratory provided technical direction for the program.

The literature survey, conceptual design study, and analysis evaluations were performed jointly by engineers at Bell Helicopter Textron in Fort Worth, Texas, and Grumman Aerospace Corporation in Bethpage, New York. Principal engineers at Bell Helicopter Textron were James Cronkhite, Thomas Haas, and Victor Berry. The contributions of Robert Vogel at Bell during the conceptual design study are also acknowledged. The principal engineer at Grumman Aerospace Corporation was Robert Winter, who was involved in both the literature survey of analytical methods and the evaluation of the DYCAST structure crash simulation. Also, the contributions of Ronald Cairo, Dr. Alan Pifko, and Dr. James Whiteside at Grumman and their expertise in the areas of composite materials and structure crash simulation are appreciated.

TABLE OF CONTENTS

TABLE OF CONTENTS - Continued

TABLE OF CONTENTS - Concluded

LIST OF ILLUSTRATIONS

LIST OF ILLUSTRATION - Continued

LIST OF ILLUSTRATION - Continued

LIST OF ILLUSTRATION - Continued

LIST OF ILLUSTRATIONS - Continued

LIST OF ILLUSTRATIONS - Continued

LIST OF ILLUSTRATIONS - Continued

LIST OF ILLUSTRATIONS - Concluded

LIST OF TABLES

1. INTRODUCTION

Extensive crashworthiness studies for metal aircraft structures have been conducted in the past. For example, early in 1960 the U.S. Army Transportation Command, now The Applied Technology Laboratory, USARTL (AVRADCOM), initiated a long-range program to study aspects of crashworthiness which culminated in the issuance of a crash survival design guide and the associated military standard (References 1 and 2). Research into the crashworthiness and energy absorption aspects of aircraft structures was initiated in the mid-1960's with studies conducted by General Dynamics-Convair and Aviation Safety Engineering and Research (AvSER) making prime contributions to the understanding and analysis of the energy absorption characteristics of airframe structures (References 3, 4 and 5).

In order to place this study in the proper time perspective, it should be noted that the lag between the initiation of research into conventional airframe impact energy absorption and its incorporation into a design, such as the UTTAS, has been on the order of 8-10 years. Therefore, this study represents the initial effort toward designing a crashworthy composite airframe structure in the mid-1980's.

---

[1] J. Turnbow, D. Carroll, J. Halby, W. Reed, and S. Robertson, CRASH SURVIVAL DESIGN GUIDE, Dynamic Science, USAAMRDL Technical Report 71-22, Eustis Directorate, U.S. Army Air Mobility Research and Development Laboratory, Fort Eustis, Virginia, October 1971, AD-733358.

[2] LIGHT FIXED- AND ROTARY-WING AIRCRAFT CRASHWORTHINESS, MIL-STD-1290(AV), Eustis Directorate, U.S. Army Air Mobility Research and Development Laboratory, Fort Eustis, Virginia, January 1974.

[3] D. L. Greer, J. J. Breeden, and T. L. Heid, CRASHWORTHY DESIGN PRINCIPLES, General Dynamics-Convair, FAA Technical Report ADS-24, Department of Transportation, Federal Aviation Administration, Washington, D.C. 20590, September 1964.

[4] W. H. Reed and J. P. Avery, PRINCIPLES FOR IMPROVING STRUCTURAL CRASHWORTHINESS FOR STOL AND CTOL AIRCRAFT, Aviation Safety Engineering and Research, USAAVLABS Technical Report 66-39, Eustis Directorate, U.S. Army Air Mobility Research and Development Laboratory, Fort Eustis, Virginia, June 1966, AD-637 133.

[5] D. L. Greer, T. L. Heid, and J. D. Weber, DESIGN STUDY AND MODEL STRUCTURES TEST PROGRAM TO IMPROVE FUSELAGE CRASHWORTHINESS, General Dynamics-Convair, FAA Technical Report DS-67-20, Department of Transportation, Federal Aviation Administration, Washington, D.C. 20590, October 1967, AD-666 816.

In recent years, composite materials such as graphite, fiberglass, boron and Kevlar have been used more extensively in the design of aircraft components, both structural and nonstructural. It is reasonable to assume that the helicopter industry will have large numbers of production aircraft with major structural components, such as the fuselage, wings, empennage, blades or landing gear, constructed of composite materials in the near future. Entire composite airframes have already been produced for general aviation type aircraft. It will therefore benefit the industry to have an understanding of the behavior of composite materials in a crash environment before large numbers of production aircraft are in the field.

Two fundamental guidelines to consider when designing the airframe structure for crash impact are first, that a protective shell be maintained around the occupied area and second, that the structure be crushable and absorb energy, thus reducing deceleration forces on the occupants and large masses. An important item to consider when applying composite materials to a crashworthy airframe structure is that these materials generally exhibit a low strain-to-failure characteristic behavior compared to metals. Whereas ductile metals such as 2024 aluminum can tolerate rather large strains, deform plastically, and absorb considerable energy without fracture or separation composites, due to their stress-strain behavior, will be unable to sustain large material deformations and must depend on innovative design configurations to achieve energy absorption. These configurations can provide for energy absorption and force attenuation by surroudning the protective structural shell with a crushable material such as a foam, honeycomb or a crushable composite concept.

Bearing these guidelines in mind, the objectives of this study were the following:

- Survey the literature and determine the existing data base on the crash-impact behavior of composite materials, the analytical methods used to design crashworthy airframe structures, and the current crashworthiness design criteria.

- Apply crashworthiness and airworthiness criteria to an airframe structure constructed of composite materials to arrive at design concepts that will better satisfy the criteria.

- Assess the state of the art of the structural crash simulations to determine their suitability for the analysis of composite structure.

2. LITERATURE SURVEY

2.1 SURVEY OBJECTIVES

The survey of information on the subject of the Crash Impact Characteristics of Advanced Airframe Structure had three objectives. The goals were to discover the existing information on:

- The effects on the crash-impact behavior of airframe structure constructed with composite materials.
- The analytical methods used for designing airframe structures to sustain a crash-impact load and to determine the suitability of these techniques for composite materials.
- The crashworthiness design criteria and their application to airframe structures constructed with composite materials.

An evaluation of the characteristics of composite materials indicates that unique design problems exist during a crash impact which must be solved so the structure can provide a survivable environment.

Composite materials exhibit a characteristically low static strain-to-failure relative to typical aircraft metals (see Figure 1). Consequently, in a crash impact when materials are required to undergo large plastic deformations at high strain rates, a composite material can be at a disadvantage unless the structural design accounts for this low strain-to-failure.

During a crash impact, when compression failure modes dominate the structure, sharp edges that may result can be hazardous to the occupants during the secondary collisions. A design must recognize this and provide a protective shell for the occupants during and after the initial impact.

The low strain-to-failure characteristic also affects the ability of the material to dissipate energy and to effectively redistribute loads in a joint. This characteristic could be detrimental if the lower fuselage is not designed properly or if a joint constraining a large mass item does not contain redundant load paths.

In addition to energy absorption and compression failure modes, there are additional parameters, as shown in Figure 2, which could affect the crash-impact performance of the structure. These parameters were considered when surveying existing information on the crash-impact response of composite

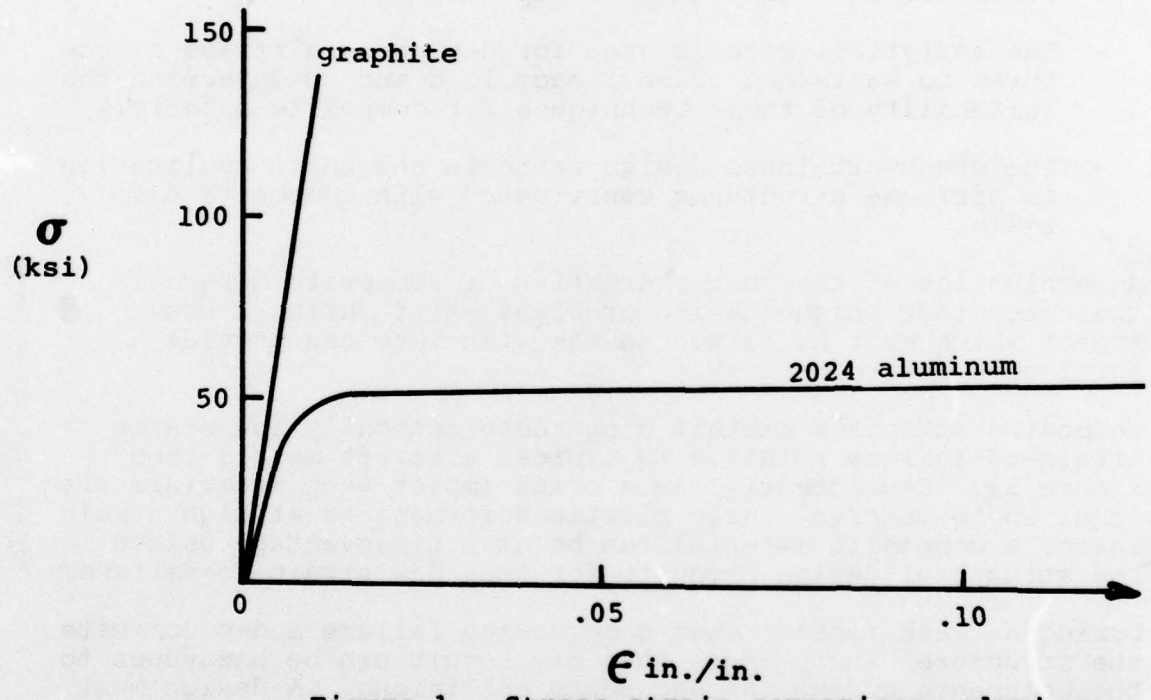

Figure 1. Stress-strain comparison, aluminum vs unidirectional graphite.

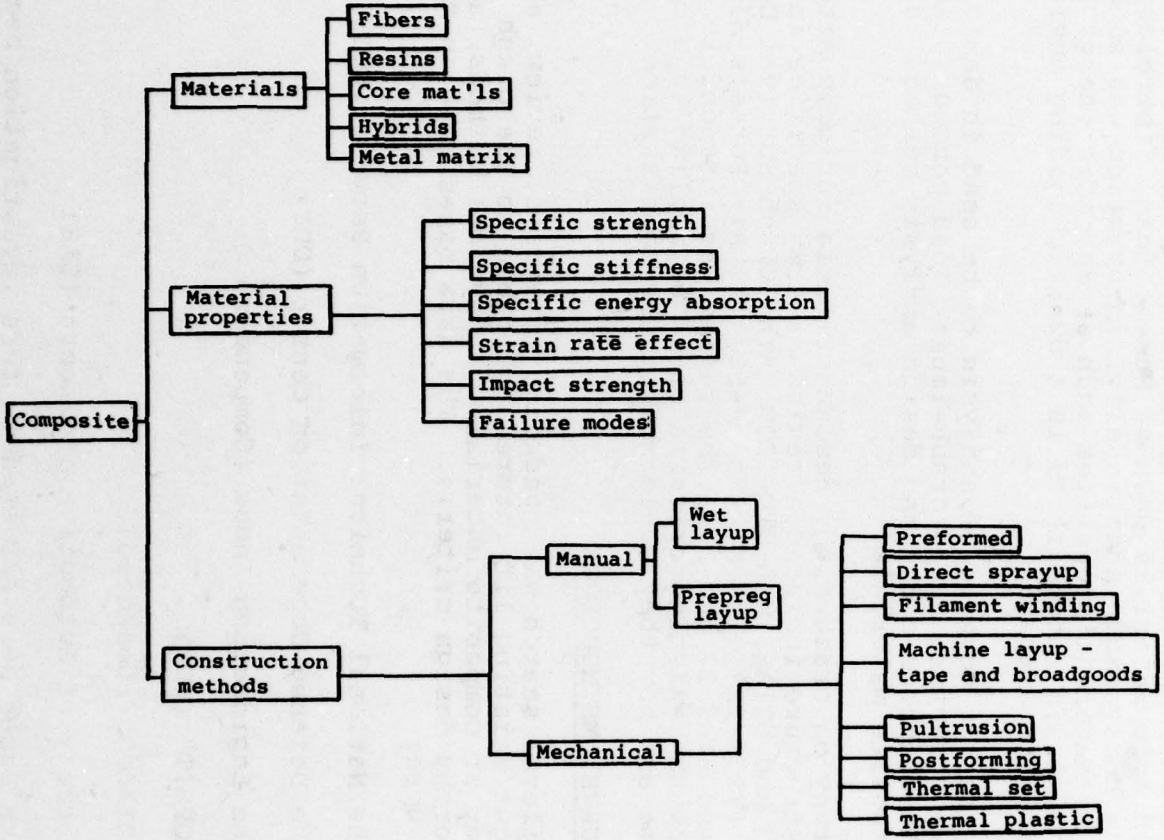

Figure 2. Composite material considerations.

structures. Particular attention was accorded to the constituent materials such as the fibers of Kevlar, graphite, boron, fiberglass and hybrids thereof; the matrices of metal, epoxy, polysulfones, phenolics, polyimides and polyesters; and the sandwich core materials such as Nomex, foam, fiberglass and aluminum honeycomb. Additionally, information was sought about the material properties such as specific energy absorption and strain rate effects in a dynamic-loading environment comparable to a crash.

The search for methods of analysis to be used in designing an airframe structure for a crash-impact load concentrated on suitable computer codes and design analysis methods adapted for composite materials.

The survey on crashworthy design criteria for composite airframe structure included a review of Army specifications for the AAH and UTTAS, MIL-STD-1290, "The Crash Survival Design Guide" (TR71-22), The Navy's AR-56, The Air Force's MIL-A-8865, and FARS 27 and 29. The review was intended to determine how the existing criteria could be applied to a composite airframe and how they would affect the construction.

2.2 SURVEY METHODOLOGY

A multilevel search was conducted to locate, review, and catalogue existing literature applicable to the crash impact behavior of composite materials, analytical methods, and crashworthy design criteria. The data bases used in the survey were:

- The National Technical Information Service (NTIS)
- The Defense Documentation Center (DDC)
- The Engineering Index (Compendex)
- "ORBIT" (SDC)
- "DIALOG" (Lockheed)
- Society of Automotive Engineers (SAE)

Six data bases were surveyed in this investigation because each offered unique advantages which broadened the scope of this study. The information which is cataloged in the National Technical Information Service (NTIS) is derived from publications of the federal, state, and local Government agencies; private industry; and universities. The data which are available through NTIS emphasize the commercial applications.

The information available from the Defense Documentation Center (DDC) is obtained from many of the same sources as NTIS; however, the emphasis is placed on military and defense usage and therefore it provides access to limited distribution and classified documents. The information which can be obtained from NTIS and DDC is usually a report, a standard, or a book. The Engineering Index (COMPENDEX) contains publications of the engineering societies such as the proceedings of conferences, journals, and magazines. The Engineering Index may also include work that is published as a magazine article and is in progress or is anticipated. The SDC "ORBIT" and Lockheed "DIALOG" data bases complement NTIS and DDC and permit a more complete recall of the available information. The Society of Automotive Engineers (SAE) Index represents a good composite of the information which is available in the automotive industry. The automobile industry has preceded the aircraft industry in research into the dynamics of the crash scenario and the protection offered to the occupants by the body shell; therefore, this index provided an excellent background into crashworthiness per se. The information which was retrieved from these data bases was supplemented by material from company files and from unpublished Government and business documents. One of the data bases (DDC) was independently surveyed by both BHT and Grumman while NTIS, COMPENDEX, and SAE were surveyed by BHT only, and "ORBIT" and "DIALOG" were surveyed by Grumman only. The information gathered from these data bases represents a substantial cross section of published reports and articles on crashworthiness, composite materials, energy absorption, failure modes, analytical techniques, and design criteria.

A flow diagram of the literature search methodology used to retrieve information from the data bases and other sources is shown in Figure 3.

To access a data base, NTIS for example, blocks of keywords were formed and input to the system so that all information pertinent to the particular topic could be retrieved. The keyword blocks were then combined to further focus the search on the subject being surveyed until the number of documents was capable of being visually scanned.

2.3 SURVEY RESULTS ON CRASH-IMPACT BEHAVIOR

The logic that was used to make the computerized search of the NTIS and COMPENDEX data bases is shown in Figure 4. The abstracts of the combinations were reviewed for information relative to the use of composite materials in a crash-impact environment or as an energy absorber. The compression failure

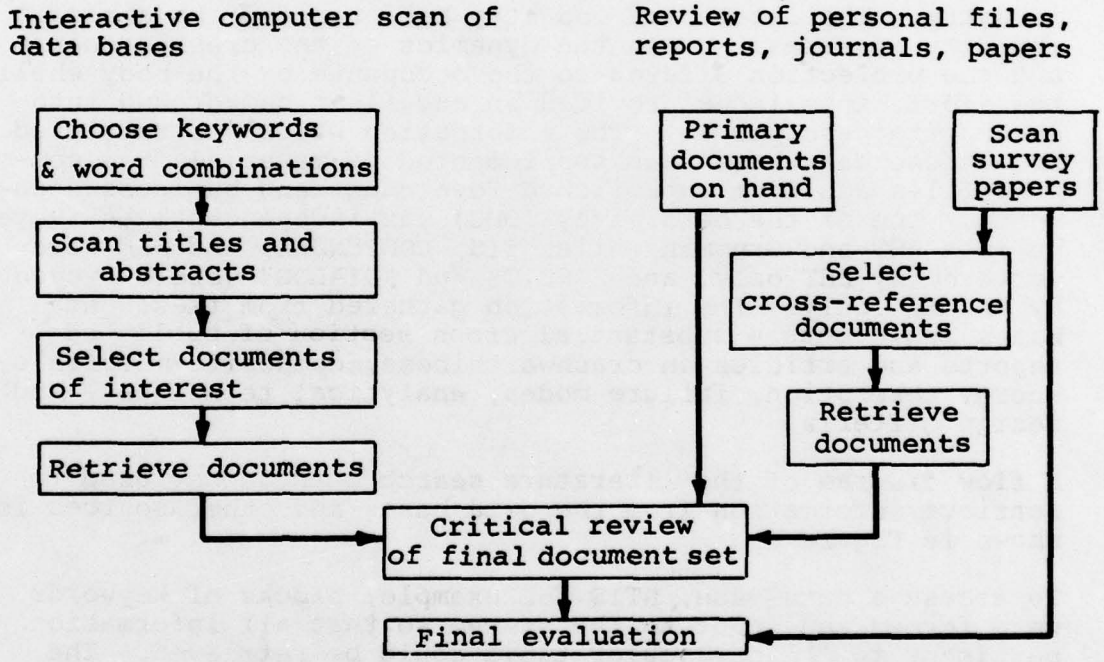

Figure 3. Literature survey methodology.

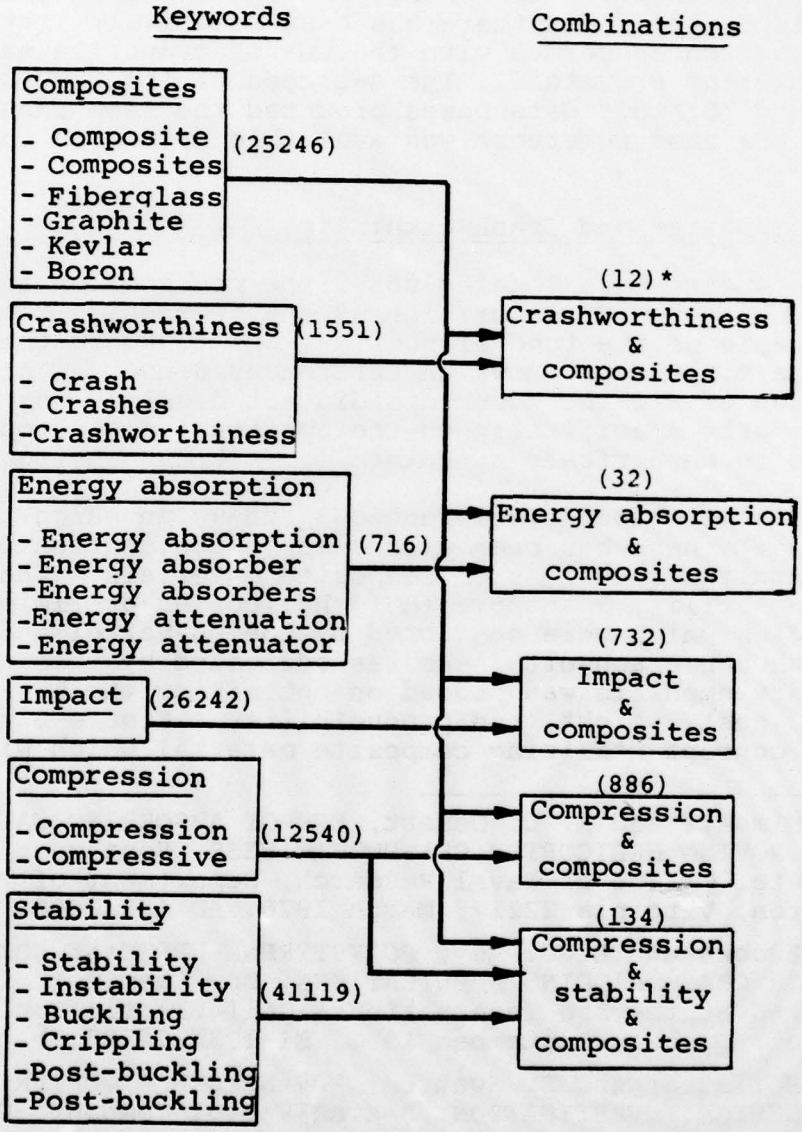

*Numbers in parentheses indicate no. of available references

Figure 4. Search logic - crash-impact behavior of composite materials.

modes were studied to determine their applicability in an impact situation. As is evident from the numbers in the parentheses, there is a great wealth of information about composite materials, crashworthiness energy absorption, and the compression failure modes; but there has been relatively little reported research concerned with the use of composite materials for crashworthy structure. The searches of the SAE, DDC, "ORBIT" and "DIALOG" data bases produced the same result, and at times the same reference was available from more than one source.

2.3.1 Composites and Crashworthiness

Twelve documents were located under the combination of the two keyword subjects, "Crashworthiness" and "Composite Materials." As an example of the type of publications found in the search, two of the titles are shown in References 6 and 7. A visual examination of all the documents did not disclose any published reports specifically on the application of composite materials to an airframe structure for a crash environment.

Two reports were found (References 8 and 9) in which the issue of crashworthiness has been discussed in conjunction with advanced structural designs of composite materials. These were the Medium Utility Transport (MUT) helicopter preliminary design studies which were conducted by Boeing-Vertol and Sikorsky. Although crashworthiness was addressed by these reports, the primary emphasis was placed on optimizing the basic design concepts, cost, weight, and producibility. Figure 5 shows a proposed concept utilizing composite material which will offer

---

[6]C. E. Kimball and R. C. DeHart, ENERGY ABSORBING MATERIALS FOR IMPROVING HELICOPTER CRASHWORTHINESS, Southwest Research Institute, Office of Naval Research, Department of the Navy, Arlington, Virginia 22217, March 1976, AD-A023 006.

[7]J. D. Brooks and L. G. Rey, POLYSTYRENE-URETHANE COMPOSITE FOAM FOR CRASH PADDING APPLICATIONS, Dow Chemical of Canada, Presented at the 3rd International Cell Plastic Conference, Montreal, Quebec, September 1972, EI 1731154583.

[8]D. J. Hoffstedt and S. Swatton, ADVANCED HELICOPTER STRUCTURAL DESIGN INVESTIGATION, Boeing-Vertol Company, USAAMRDL Technical Report 75-56A and B, Eustis Directorate, U.S. Army Air Mobility Research and Development Laboratory, Fort Eustis, Virginia, March 1976, AD A024662, ADA 024478.

[9]M. J. Rich, INVESTIGATION OF ADVANCED HELICOPTER STRUCTURAL DESIGNS, Sikorsky Aircraft Division, USAAMRDL Technical Report 75-59, Eustis Directorate, U.S. Army Air Mobility Research and Development Laboratory, Fort Eustis, Virginia, May 1976, AD-A026 246.

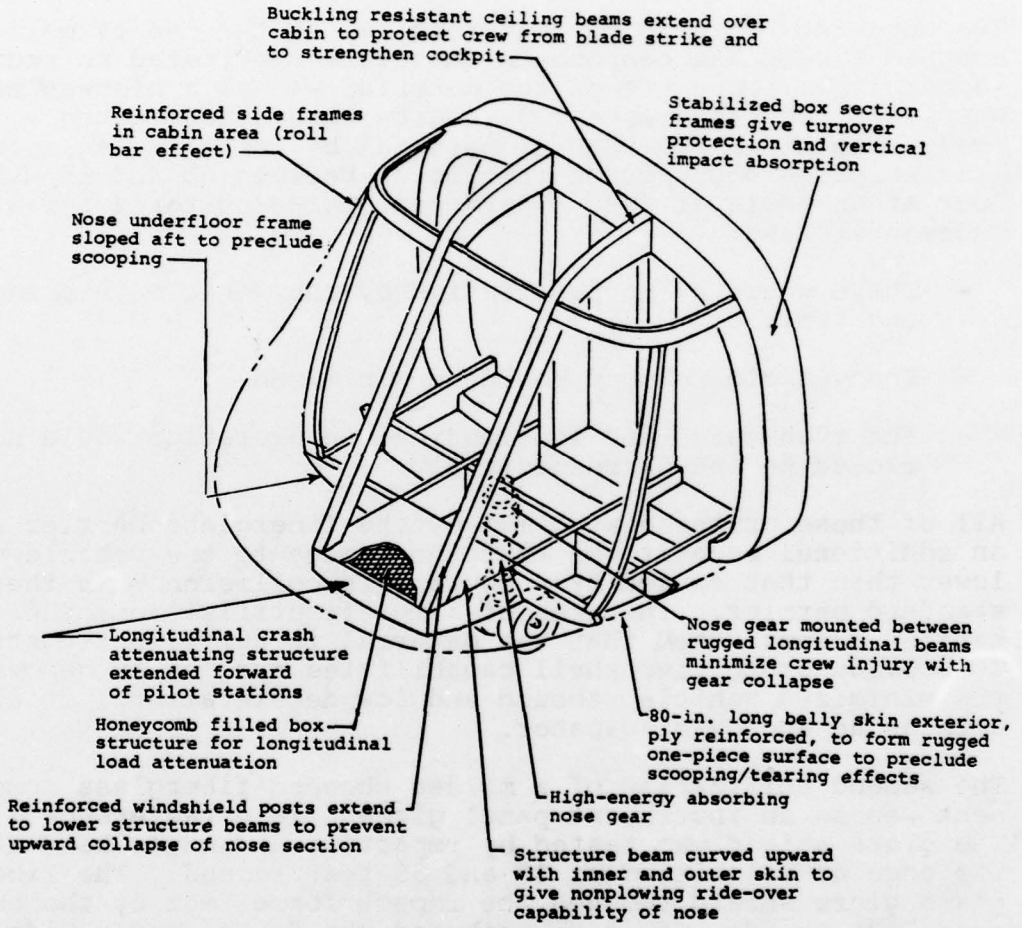

Figure 5. Crashworthy features - forward cabin (Reference 8).

protection for the crew during a longitudinal impact. The main instrument for attenuating the impact force is a box structure filled with aluminum honeycomb. The remainder of the structure is used to provide a protective shell for the occupants with composite materials being used advantageously in the lower skin to form a one-piece antiscooping structure.

Two documents were found that reported on the use of molded chopped fiberglass components that were fabricated to reduce impact loads. One use of the material was as a highway median barrier strip (Reference 10). Tests were conducted on a full-scale segment of the barrier material by impacting an automobile weighing 4500 pounds into it at between 60 and 65 miles/hour at an angle of 25°. There were three criteria for a successful test:

- There would be no penetration by the vehicle into oncoming traffic.
- The vehicle rebound would be minimized.
- The transverse and longitudinal deceleration would not exceed 6g and 8g respectively.

All of these criteria were met by the fiberglass barrier and an additional benefit was that the damage to the vehicle was lower than that caused by a comparable collision with the standard barrier. In terms of aircraft utilization, the barrier demonstrated that the material is sufficiently strong to provide protective shell capabilities and, as evidenced by the minimized vehicle rebound and low decelerations, it also acts as an energy dissipator.

The second utilization of a molded chopped fiberglass component was as an instrument panel glare shield (Reference 11). The glare shield was tested by impacting a dummy's head along its edge at velocities of 30 and 35 feet/second. The fiberglass glare shield reduced the impact force felt by the head from 300g to 60g and it distributed the force over a wide area,

---

[10] Robert M. Riddell, MOLDED FIBERGLASS NARROW MEDIAN BARRIER, Rockwell International, FHWA RD 75 25, Federal Highway Administration, Washington, D.C., December 1974, DB-242555.

[11] E. D. Langston and J. J. Swearingen, EVALUATION OF A FIBERGLASS GLARE SHIELD FOR PROTECTION AGAINST HEAD INJURY, FAA Civil Aeromedical Institute, FAA AM-72-7, Office of Aviation Medicine, Federal Aviation Administration, Washington, D.C., February 1972, AD-740732.

thus lowering the stress level felt by the skull. The glare shield failed, however, leaving a sharp edge sufficient to have produced a fatal head wound. The authors felt that the correction of this fault by a minor design modification could lead to a significant reduction in head injuries.

There were two reports about automobiles that were fabricated in whole or part using fiberglass sandwich construction and tested in a crash environment.

The report by Messerschmitt-Boelkow-Blohm was primarily concerned with the automobile functioning as an electric transport vehicle and only secondarily rates the crashworthy aspects of the construction (Reference 12). The vehicle chassis was constructed of a self-supporting plastic sandwich composed of fiberglass face sheets bonded to a polyurethane foam core. Details of the complete crash test were not available. However, the author stated that the vehicle showed good energy absorption and crushing capability.

The second automotive report was written by the Budd Company, and it was the only document found in the survey on crashworthiness which specifically reported on the use of composite construction for the attenuation of crash-impact forces (Reference 13). The test specimen was a 1974 subcompact, two-door sedan which was modified by replacing the front fenders and the lower longitudinal frames with sandwich panels and tubes constructed of a polyurethane foam core and fiberglass face sheets. Sandwich construction was used, as opposed to monocoque or semimonocoque without a foam assist, on the basis of

---

[12]H. G. Raschbichler, TECHNICAL AND ECONOMIC ASPECTS CONCERNING THE APPLICATION OF THE SELF-SUPPORTING PLASTIC SANDWICH CONSTRUCTION TO ELECTRIC TRANSPORT VEHICLES, Messerschitt-Boelkow-Blohm, Presented at the 3rd International Electric Vehicle Symposium and Exposition, Washington, D. C., February 1974, EI 1750962776.

[13]H. A. Jahnle, FEASIBILITY STUDY OF PLASTIC AUTOMOTIVE STRUCTURE, Budd Company, DOT HS-801-771, U.S. Department of Transportation, National Highway Traffic Safety Administration, Washington, D. C., December 1975, PB 248354.

previous work (References 14, 15, 16) which showed the sandwich construction to be superior in crash energy management.

Prior to constructing the test vehicle, a series of static and dynamic tests was conducted on a variety of specimens to serve as design support. As a result of these tests, a fiberglass cloth reinforced polyester was chosen as the material because of strength, stiffness, cost, and retention of properties at higher temperatures. Additionally, the four basic shapes shown in Figure 6 were tested with and without polyurethane foam filler to develop energy absorption data. Conclusions from these tests were:

- The general mode of failure for the thermoplastic specimens was similar to metals with ductile folding occurring.
- By chamfering the ends of the specimens, an initial peak force (twice as great as the average crushing force) could be eliminated.
- Tapered wall thicknesses reduced the peak loads in curved panels and cylinders during the dynamic tests.
- Cylinders and curved panels develop uniform crush characteristics over long crush distances.
- Square and rectangular elements demonstrated good load absorbing characteristics over short distances up to 3 inches.
- Rigid polyurethane foam increases the crush strength of the fiberglass reinforced polyester cylinders, but the energy absorbed per unit area is not affected by either the foam or the foam density.
- A fiberglass reinforced polyester has a higher specific energy absorption than 2036-T4 aluminum or low carbon steel.

---

[14]R. A. Gallant, X898 - A PASSENGER VEHICLE OF UNITIZED BODY - CHASSIS STRUCTURE OF RP/C, Presented at the 29th Annual Conference of the Reinforced Plastics/Composite Institute, Washington, D. C., February 1974.

[15]H. G. Raschbichler, VEHICLE CHASSIS OF SANDWICH CONSTRUCTION, Modern Plastics, Volume 50, No. 7, July 1973, pp. 76-79, EI 730946605.

[16]S. Shimamura and K. Ishine, A CONTRIBUTION TO THE SAFETY DESIGN OF THE FRP CAR, Presented at the Reinforced Plastics Congress, Brighton, England, November 1974.

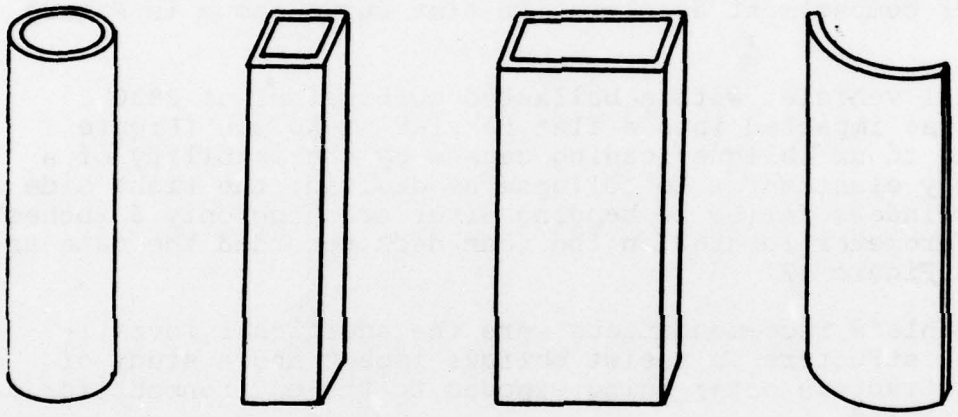

- Glass reinforced polyester (chopped fibers, 0°/90° fabric)
- ABS
- Acrylic
- Polycarbonate

} With and without polyurethane foam filler

Figure 6. Crush specimens (Reference 13).

Based on the dynamic test data, the concept shown in Figure 7 was designed and constructed. When compared to the original automobile, a replacement of 142.8 pounds of steel parts with plastic parts was achieved with a 25 percent weight reduction.

A drop tower test was conducted on one-half of the frontal system at 30 mph. The specimen showed good energy absorption throughout the crush distance of 14 inches. A dynamic analysis using the force-deformation curves of Figure 8 input into the five mass model simulation shown in Figure 9 produced the passenger compartment acceleration-time curve shown in Figure 10.

The actual vehicle, with a ballasted curb weight of 2830 pounds, was impacted into a flat barrier at 50 mph (Figure 11). Due to an oblique loading caused by the inability of a low energy elastomeric to collapse as desired, the right side lower cylinders failed in bending after crushing only 6 inches. An accelerometer located on the rear deck recorded the data as shown in Figure 12.

Among Jahnle's recommendations were the additional investigation of structure to resist oblique impact and a study of plastic structure after being exposed to the environment for a lengthy period.

The conclusions reached, based on the test results, were that a crashworthy reinforced plastic structure can be designed and manufactured; also, that the plastic structure would result in a lower weight vehicle when compared to a steel structure.

In addition to surveying the documented reports on composite construction usage in a crashworthy application, attempts were made to obtain reports on several general aviation type aircraft, among them the Windecker Eagle and the Bellanca Skyrocket, which use a composite sandwich construction. Contacts were made with the companies and the FAA in an effort to discover any reference information on the accident and crash experience of the aircraft, but the attempts were not successful.

2.3.2 Composites and Energy Absorption

The majority of the work in this category has been aimed at improving the energy absorption characteristics of composite materials at the microstructural or local levels, and correlations between this research and its application to the requirements in a crash environment have not been attempted. Typical of this type of information is a paper written by

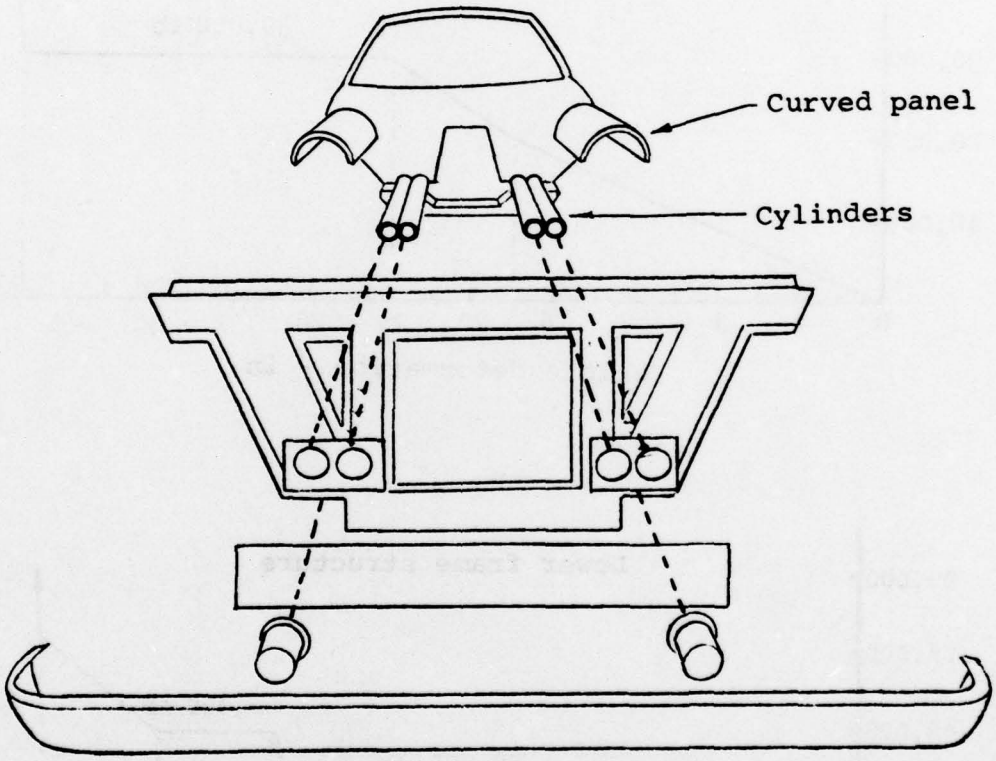

Figure 7. Energy-absorbing frontal structure (Reference 13).

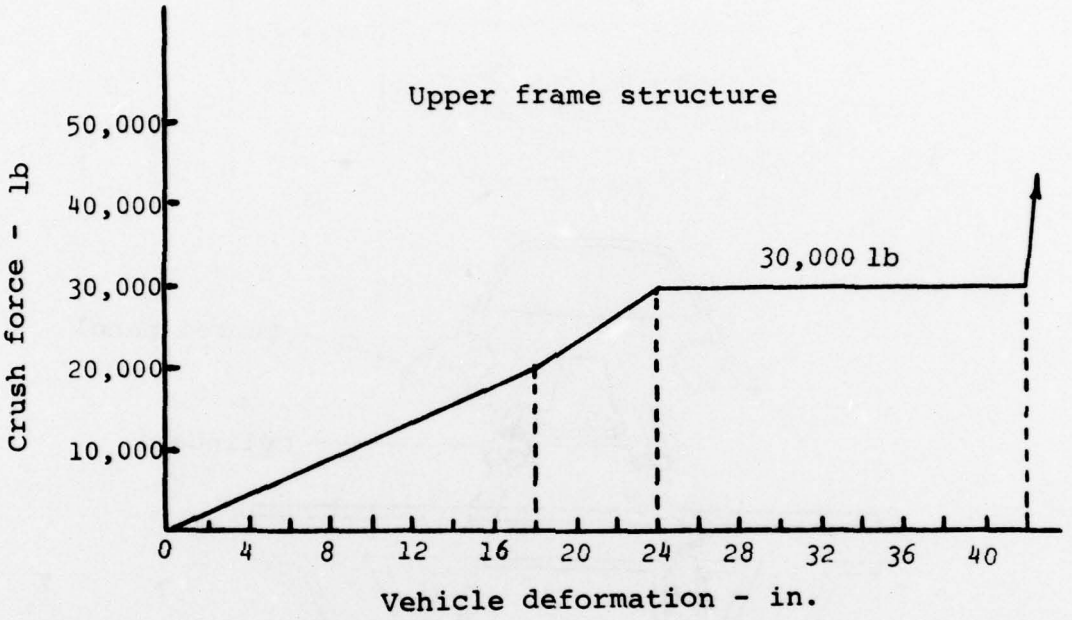

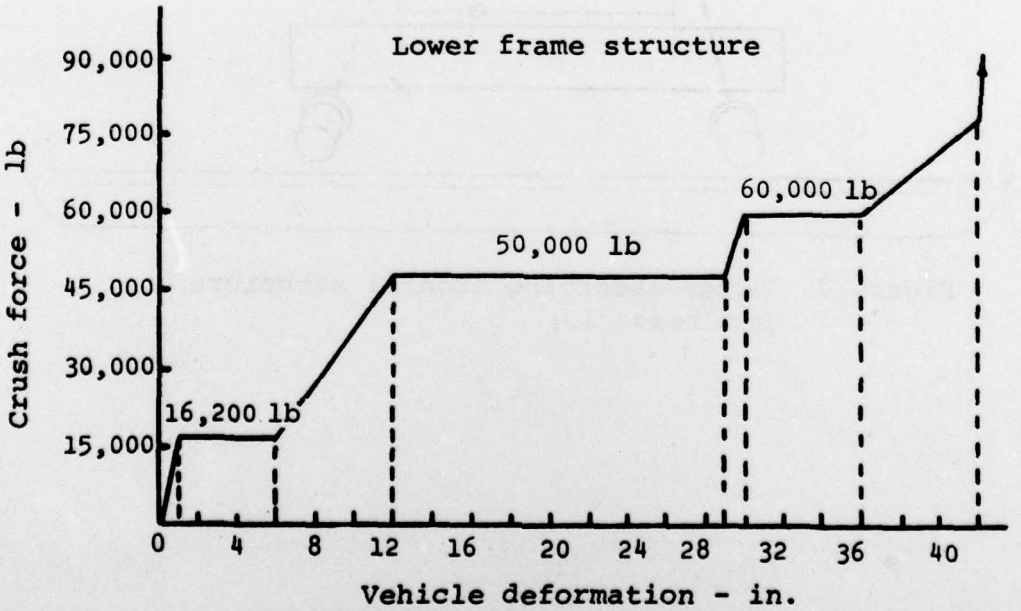

Figure 8. Force-deformation characteristics (Reference 13).

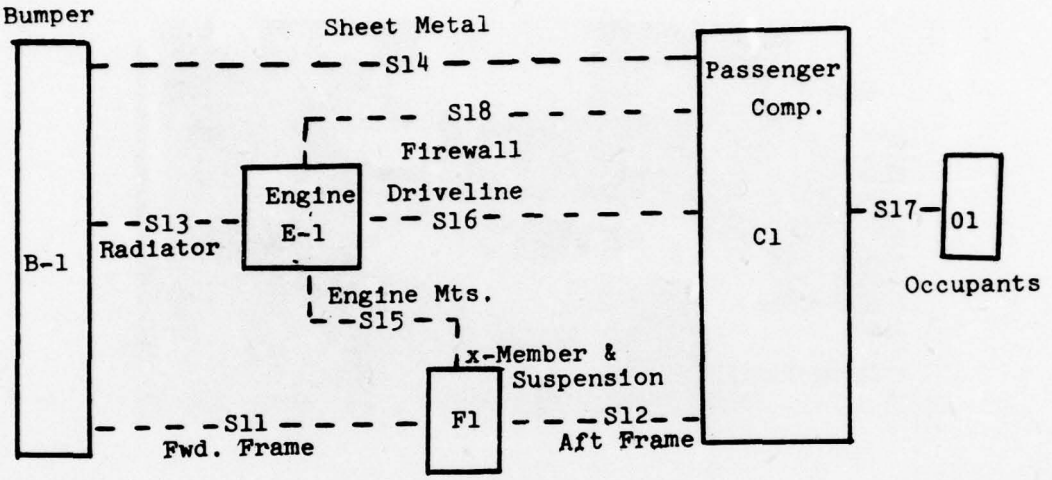

Figure 9. Five mass model crash simulation (Reference 13).

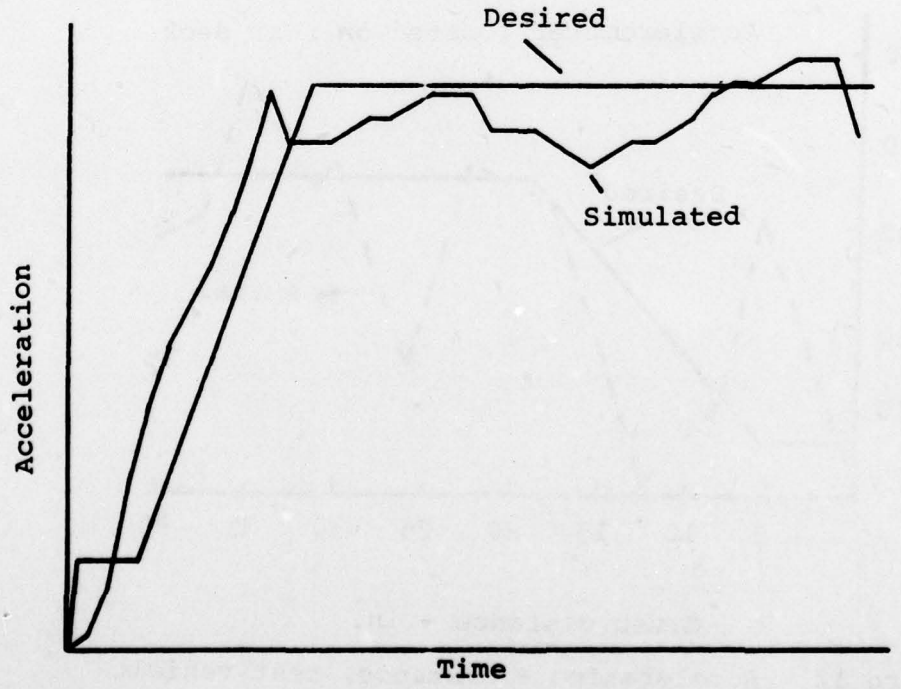

Figure 10. Simulated crush characteristics - 50 mph (Reference 13).

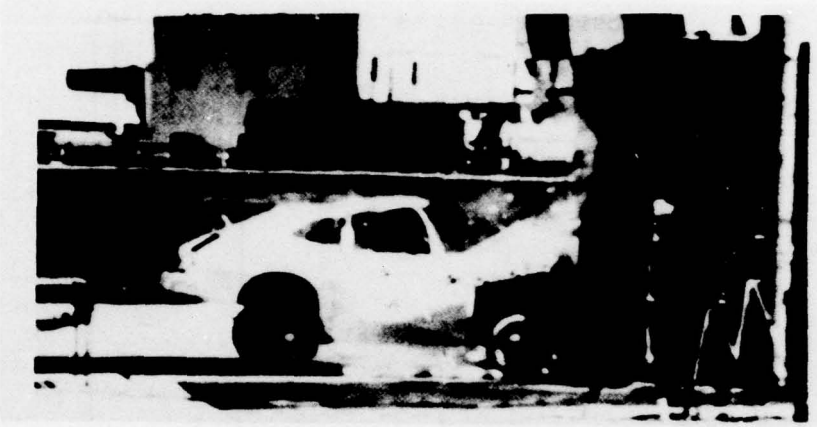

50-mph barrier crash test

Figure 11. Barrier impact test - 50 mph (Reference 13).

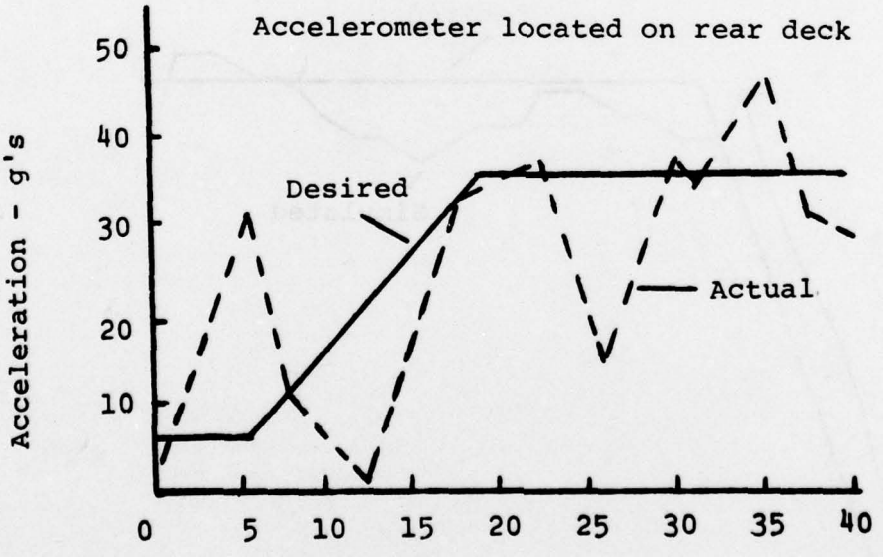

Figure 12. Acceleration - distance, test vehicle (Reference 13).

Millman and Morley of the University of Nottingham in Great Britain (Reference 17). They describe tests of thin sheet specimens containing single layers of unidirectional reinforcement which were impacted in a direction normal to the plane of the sheet by missiles traveling at speeds up to 200 meters/sec. The amount of energy absorbed by the composite specimens is compared to that of austenitic stainless steel specimens under similar test conditions. Their conclusions were that for a weight-to-weight basis the composite materials could theoretically absorb up to 2.5 times as much energy as austenitic stainless steel.

The only articles which addressed the use of composite materials as energy absorbers or attenuators for a crash impact were referring to low velocity applications such as bumpers (References 18, 19, and 20). Typically the bumpers act as springs to absorb, store, and release the energy. A representative paper by Newton of Dunlop Ltd. described a bumper system of laminated rubber and plastic layers wherein a high level of energy is dissipated during deformation, while storing sufficient energy in the rubber layer to return the component to its original configuration.

2.3.3 Composites and Impact

There has been a great deal of research in the area of impact strength of composite materials, but this research has been mainly directed toward local impacts produced by tool drops, foreign objects, projectiles, or particles.

Typical of these articles is a paper written by Lifshitz of the Israel Institute of Technology in Haifa in which he

---

[17] R. S. Millman and J. G. Morley, ENERGY ABSORPTION AT HIGH RATES OF DEFORMATION IN FIBROUS COMPOSITES WITH NON-FRACTURING REINFORCING ELEMENTS, University of Nottingham (GCBA, Britain), Materials Science and Engineering, Volume 23, No. 1, April 1976, pp. 1-10, EI 1761065436.

[18] B. H. Jones, DESIGN AND PRODUCTION OF ECONOMICAL FRP ENERGY ABSORBING SYSTEMS FOR TRANSPORTATION APPLICATIONS, Goldsworthy Engineering Inc., Presented at the SPE National Technical Conference: Plastic in Surface Transportation, Detroit, Michigan, November 1974, EI 1751176050.

[19] R. H. Eshelman, FUTURE BUMPER MATERIALS UP FOR GRABS, Automotive Industry, Volume 147, No. 11, December 1, 1972, pp. 45-47, EI 1730205811.

[20] D. A. Newton, DUNLOP COMPOSITE ENERGY ABSORBING BUMPER SYSTEMS, Dunlop Ltd., Leicester, England, SAE Prepr. No. 750010, 6 pages, EI 1750635832.

describes tests measuring the tensile strength of angle ply balanced laminates of fiberglass/epoxy under dynamic loading conditions (Reference 21).

Another paper written by Eaton describes ballistic damage to graphite/epoxy plates caused by an impactor mass at various velocities (Reference 22). Inspections of local damage were accomplished visually, microscopically, and by x-ray to determine the extent of the damage. The residual strength in tension was measured and was found to be insensitive to damage size effects.

Although the research on local impact damage caused by a projectile does not directly relate to the impacts associated with a crash because different mechanisms for failure are involved, it is important to note that future research in crash impacts will have to account for these local failure mechanisms because they do affect the gross compression failure mode of the structure.

2.3.4 Composites and Compression Failure Mode

During a crash, the compression failure modes of the structure influence the energy absorption and crash-impact behavior of the design. In surveying this category, documents were sought that contained information about the gross compressive behavior, the post-buckling characteristics, and the crushing of the structure. However, the documents found in this search were concerned with predicting the static allowable load of the element. The research into the post-buckling characteristics of compression specimens has centered on predicting the buckling load and in methods to increase it, thereby making the structure more efficient statically.

A typical paper representative of the collection in the survey is that by Spier and Klouman which describes efforts to predict the post-buckling characteristics of flat plates and

---

[21] J. M. Lifshitz, IMPACT STRENGTH OF ANGLE PLY FIBER REINFORCED MATERIALS, Journal of Composite Materials, Volume 10, January 1976, pp. 92-100, EI 760529620.

[22] G. A. Eaton, BALLISTIC DAMAGE OF GRAPHITE/EPOXY PLATES, Naval Post Graduate School, Monterey, California, Master's Thesis, 61 pages, June 1977, AD-A042 29614ST.

channels constructed of graphite/epoxy (Reference 23). The behavior of the plates and channels was observed at and beyond the point of incipient buckling. This load was then compared to the analytical buckling strength calculated by the elastic buckling theory. The authors state that although the behavior of the laminated plates was analogous to that of isotropic metal plate, considerable disparity exists between the incipient buckling load and the calculated value. The load deflection curves for two of the specimens are shown in Figure 13, where P_i^{cr} and P^{cc} represent values obtained by test while P^{cr} is the predicted value.

For comparison, the results of some tests conducted by General Dynamics-Convair to measure the load-deflection characteristics of various plate-stringer panel configurations made of aluminum are shown in Figure 14 (Reference 5). Note that the load-deflection behavior of the integrally stiffened panel is poor in comparison to that of the rolled stringer sections because the failure mode was an explosive fracture; also note that its shape is similar to that of the graphite/epoxy flat plate and channel. Figure 15 shows the data from the rolled zee stringer aluminum panel re-plotted as a load-strain curve and compared with a graphite/epoxy flat plate and a channel specimen taken from the Spier and Klouman paper. These specimens, while having the same approximate static load capability, do not exhibit comparable energy absorption qualities because of their dissimilar failure modes. When the composite specimens fail by delamination and splintering, they are unable to sustain any load resulting in a poor load-stroke performance. The aluminum panel, by contrast, continues to stroke at a reduced load while crippling and folding, thereby providing additional energy absorption.

2.4 CONCLUSIONS ON SURVEY OF PUBLISHED CRASH-IMPACT RESPONSE LITERATURE

The static and fatigue behavior, analytical techniques, environmental effects, manufacturing, processing and nondestructive evaluation techniques relating to composite materials have received attention sufficient to allow their uses as helicopter airframe structure. However, the survey demonstrated that with the exception of some work done in the automotive industry, sufficient attention has not been directed toward those aspects of composite materials which would affect their crashworthiness

---

[23] E. E. Spier, and F. L. Klouman, POST-BUCKLING BEHAVIOR OF GRAPHITE/EPOXY LAMINATED PLATES AND CHANNELS, Presented at Army Symposium on Solid Mechanics, Cape Cod, Mass., September 1976, EI 770534416.

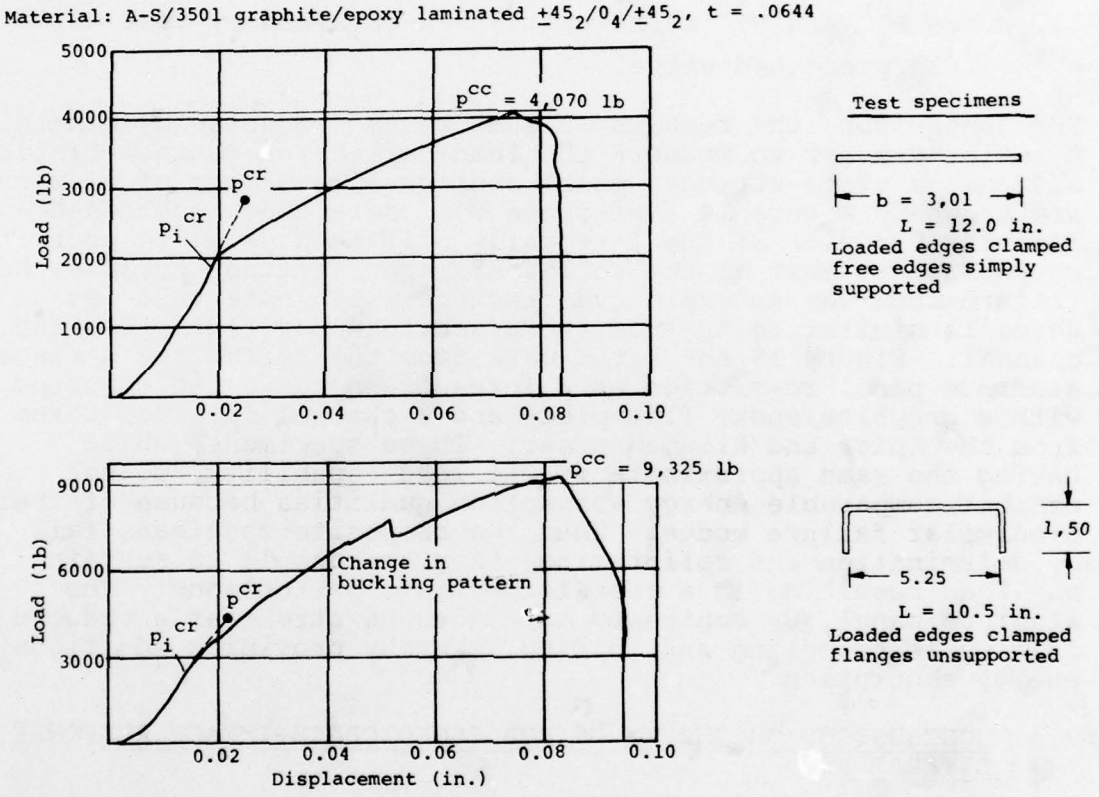

Figure 13. Typical post-buckling behavior of graphite/epoxy laminated structure (Reference 23).

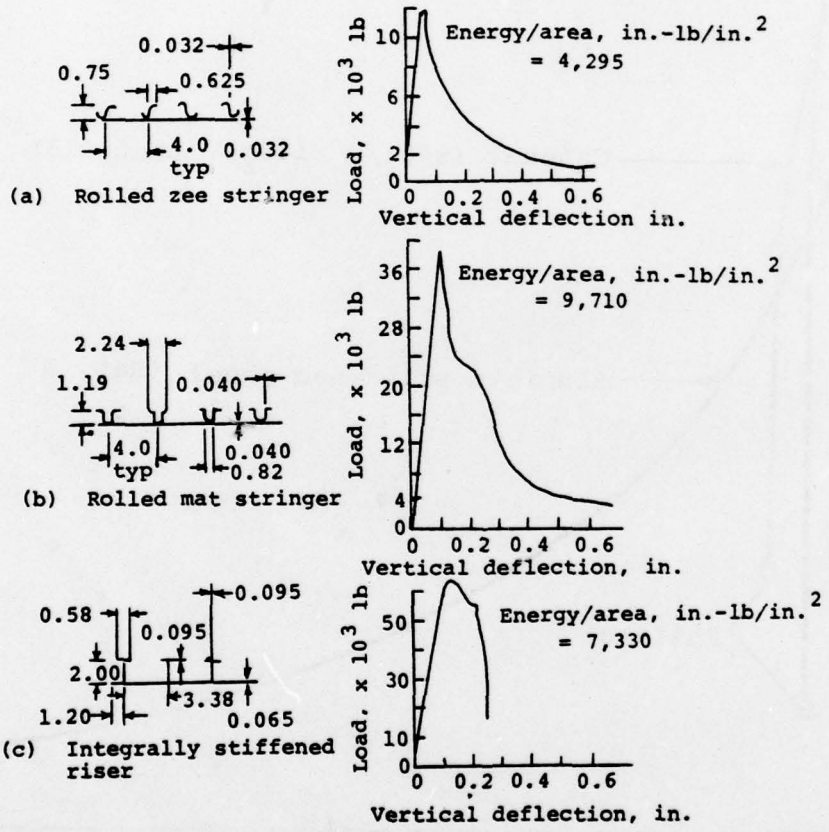

Figure 14. Compressive behavior of aluminum sheet stringer panels (Reference 5).

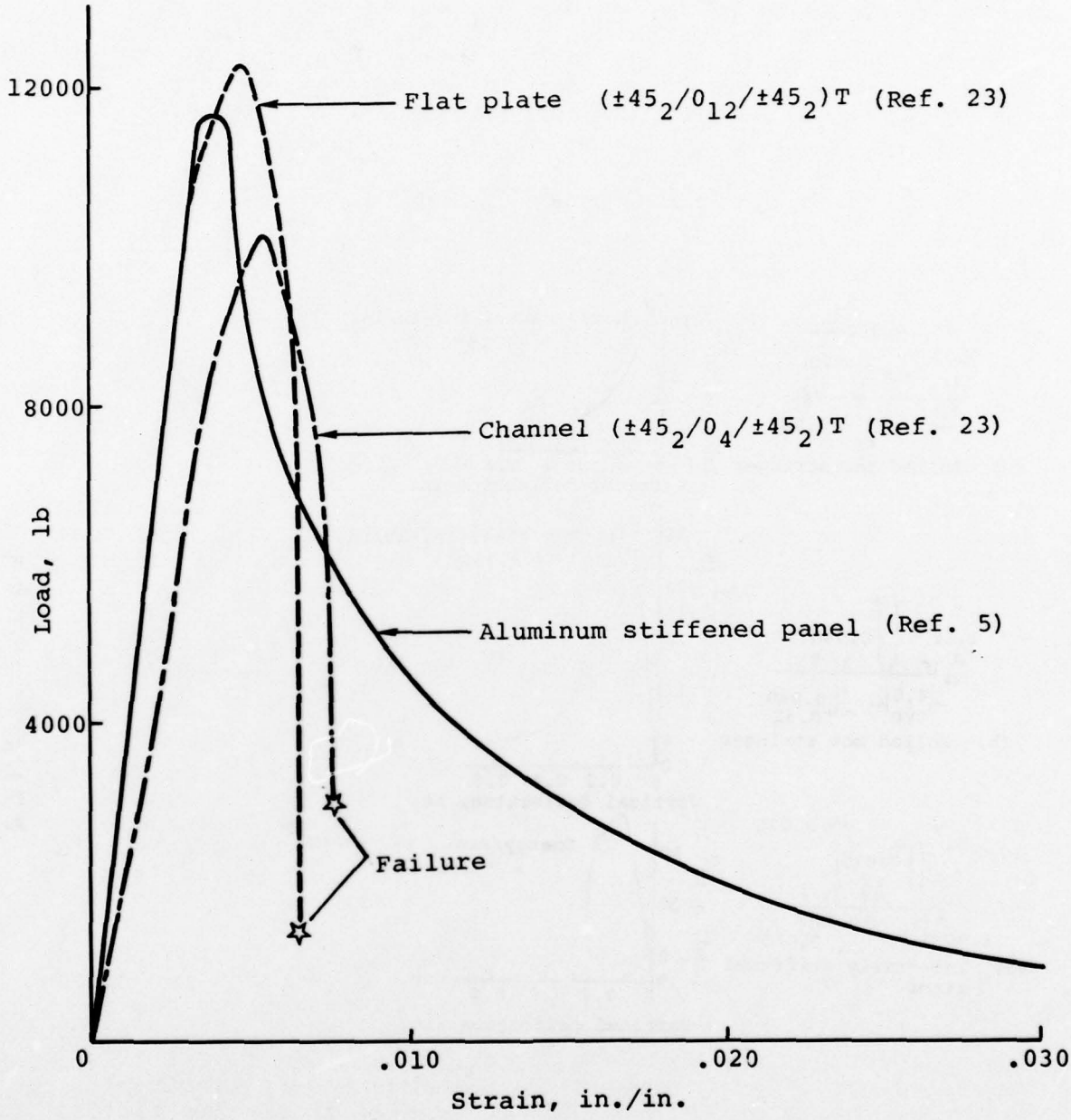

Figure 15. Comparison of post-buckling behavior — aluminum and A-S/3501 graphite/epoxy.

qualities. Consequently, before reliable, lightweight, crashworthy, advanced composite helicopters can be designed, considerably more data is required. These data can be summarized under two major categories: data required to support the analytical crash prediction, and data required to support a vehicle design.

2.4.1 Data Required for Analytical Crash Prediction

The data necessary to support the analytical crash prediction would require research on:

- Evaluation of the crash-impact response of various components of airframe structures
- Characterization of materials
- Failure analysis

As part of the evaluation of the structure, the crash scenario should be better defined in terms of structural attitude, time sequence of events, functions of airframe components, and expected material strain rates. Military Standard MIL-STD-1290 (Reference 2) and USARTL-TR-79-22, the "Crash Survival Design Guide," (Reference 24), should be used as the basis for any future development and should be revised according to the results of such investigations.

Characterization of composite materials at the strain rates expected during a crash impact should concentrate on those parameters which are important in the crash sequence such as energy absorption and compression failure modes plus other factors such as those shown in Figure 2. All of the materials and variables such as matrices, fibers, core materials, and combinations of each will have to be evaluated.

The area of failure analysis needs additional attention because of the complex failure modes of laminated structures for crash-impact loads. Some of the complexities of predicting the response of a metallic structure operating in the inelastic region are apparent. With composite structures, this complexity is magnified not only because of the heterogeneous, anisotropic nature of the material, but also because of those same factors which affect the static performance of the structure such as

---

[24] CRASH SURVIVAL DESIGN GUIDE, USARTL Technical Report 79-22, The Applied Technology Laboratory, U.S. Army Research and Technology Laboratory, (AVRADCOM), Fort Eustis, Virginia (to be published).

manufacturing defects, cure cycle variation, and lamina stacking sequence. Just as is still the case in the static analysis, the fracture and failure prediction techniques need to be checked against observed failure modes so that the analysis can be verified.

2.4.2 Data Required for Vehicle Design Development

To acquire the expertise to design a crashworthy vehicle structure using composite materials, additional data must be obtained about the crash-impact response of structural configurations and materials. Additionally, the records of all advanced composite field components which have been involved in a crash should be reviewed for pertinent data. Finally, a comparison should be made of the crash-impact response of current metallic helicopter structures with advanced composite structures since current requirements are based on experience with metallic structures.

The most direct method of obtaining the crash-impact response of candidate structural components is by structural testing. Analytical techniques used to predict the crash-impact response of components and of the entire structure need to account for component interaction which will require verification by tests before confidence can be established. The emphasis should be placed on the behavior of the structural elements during crash-impact loading, with particular emphasis on the fracture modes peculiar to composites. To obtain data from field components of crashed advance composite structure is difficult since not many such structures currently exist. It is suggested though, that as the numbers of these aircraft increase, a crash investigation team similar to the type already in existence, whose task it is to determine accident causes, be assigned to review the material behavior during the impact.

The metal and advanced composite structures during the crash sequence can only be compared through a controlled laboratory experiment. Analytical comparison will be valid only when the techniques have been verified.

As composite materials increase in usage, the question will arise, as it already has in the basic static design, as to the effect of service life on the crash-impact response. It is reasonable to expect that if things such as low energy impacts (dropped tools, rocks), moisture absorption or desorption, and cycling loads can affect the static compression allowable of a structure, they can also affect the crash-impact response. Therefore, it might be logical to assume that the aircraft design will be such that it would account for this damage and

still produce acceptable occupant protection in the 6000th hour as in the 6th hour of operation.

2.5 RESEARCH-IN-PROGRESS

During the survey of the current data base of information on the crash-impact behavior of composite structures, some pertinent research-in-progress was found that has not been documented or made available to the public. The in-progress programs pertinent to this topic involve:

- The testing of energy-absorbing cylinders by Bell Helicopter Textron.
- Airframe crashworthy design concepts are being studied in a NASA/FAA crashworthiness program.
- The testing of stiffened cylinders and scale models of helicopter fuselage structure under programs sponsored by the U.S. Army Research and Technology Laboratories of *USAAVRADCOM*.

2.5.1 Composite Material Tube Energy Absorbers

Bell Helicopter Textron is conducting a study to investigate the energy absorption characteristics of some composite material deformation concepts. Composite tubes have been filament wound at ±45° angles from three materials: graphite/epoxy, Kevlar/epoxy, and fiberglass/epoxy. The properties of the tubes are given in Table 1.

TABLE 1. BASIC PROPERTIES OF TUBES

Material	Thickness (in.)	Weight/Inch (lb)	Elastic Modulus (psi)
Graphite/epoxy	.033	.01638	2.48×10^6
Kevlar/epoxy	.077	.03212	1.09×10^6
Fiberglass/epoxy	.031	.01890	2.23×10^6

The specimens were statically tested in a Tinius-Olsen testing machine and were compressed on mandrels which had angles of 0°, 15°, 30°, and 45°. Representative failed specimens are shown in Figure 16 for each of the mandrels used. Typical

load-deflection curves for each tube configuration are given in Figure 17. The tubes exhibited progressive failure as illustrated in Figure 18 where a Kevlar/epoxy specimen is shown compressed on a 30° cone. The specific energy absorption attainable is shown to be a function of the angle of cone as well as material. The test results are summarized in Table 2 along with a metal tube of 3003-H14 aluminum alloy for comparison.

TABLE 2. SPECIFIC ENERGY FOR TEST (FT-LB/LB)

Material	Flat	15°	30°	45°
Graphite/epoxy	15200	9200	4100	2300
Kevlar/epoxy	4900	4900	3500	1900
Fiberglass/epoxy	2600	5000	2600	2600
3003-H14 Al	7800	----	----	----

As seen in Table 2, the graphite tested on a flat surface had the highest specific energy capability.

To determine if a static load-deflection test provides usable data for a dynamic application, a drop test was conducted. The test setup for the drop test is shown in Figure 19. A ±45° graphite/epoxy tube 3.5 inches long was impacted with a 122-pound mass dropped from 2 feet. Including the tube deflection, the full drop height was 25.75 inches. The impact velocity of the mass was about 12 feet per second. The specimen attenuated the full 242 foot-pounds of energy without any rebound. Using the energy from the area under the static load-deflection curve, a 1.63-inch stroke was predicted. The dynamic drop measured a 1.75-inch stroke. This is a good indication that static load-deflection information is representative for dynamic loading and shows that composites are potentially good energy absorbers for crash impact.

Further testing has sought to determine the effects of construction methods and angle ply orientation on the specific energy absorption capabilities of the tubes.

Four types of construction methods have been used to manufacture the test specimens. Two specimens have been filament wound at a ±45° angle orientation using the two crossover techniques shown in Figure 20. This figure also shows the method of manufacture used to construct the tubes at ±45° angle orientation when the material is a tape or fabric.

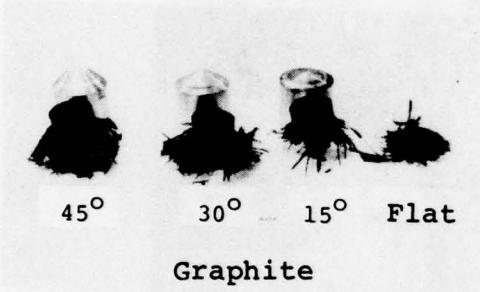

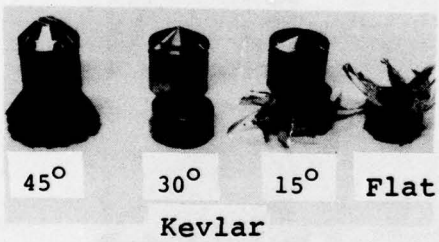

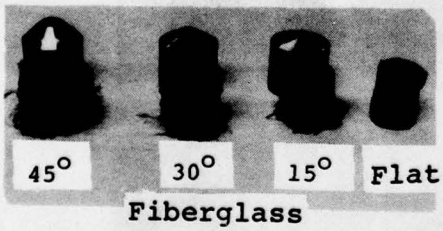

Figure 16. Static crush tests of composite tubes for various anvil angles.

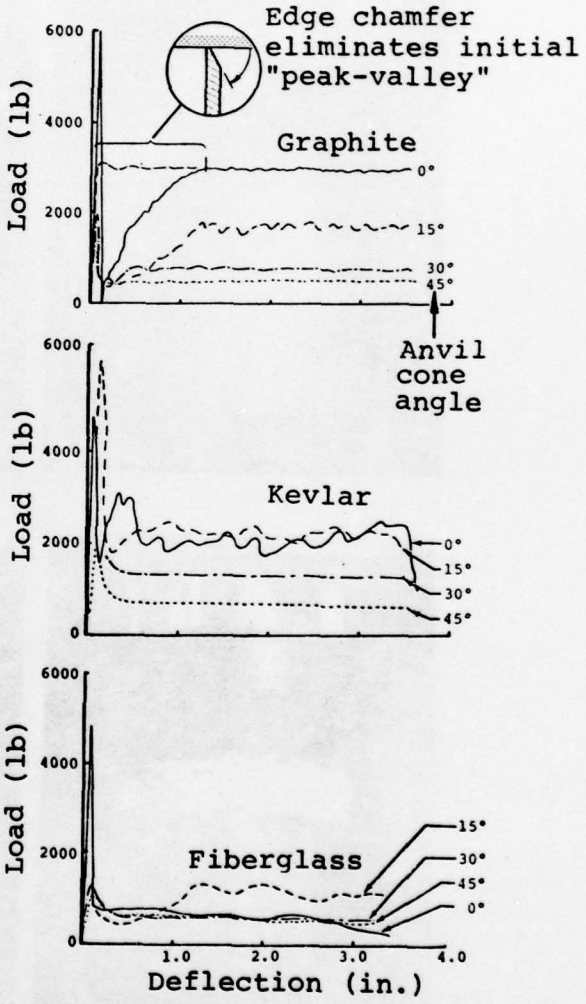

Figure 17. Load-deflection curves for energy-absorbing composite tubes.

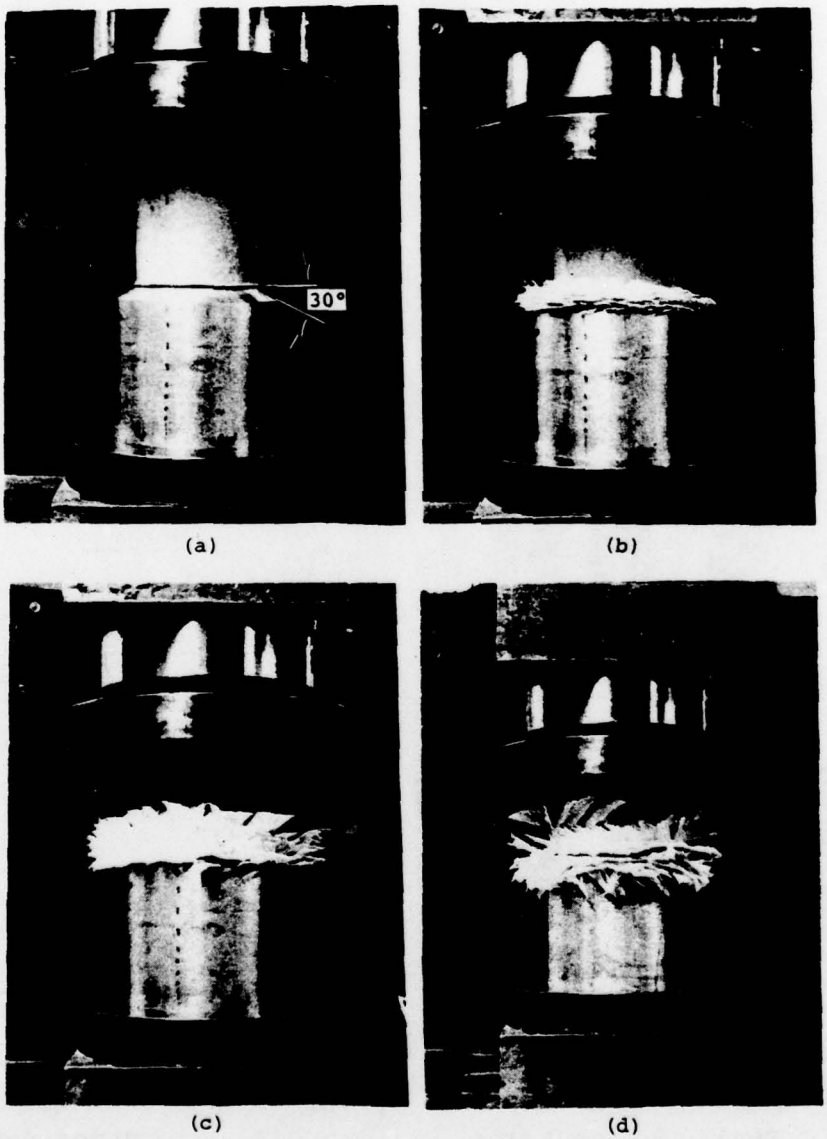

Figure 18. Sequence of static crushing test of Kevlar tube.

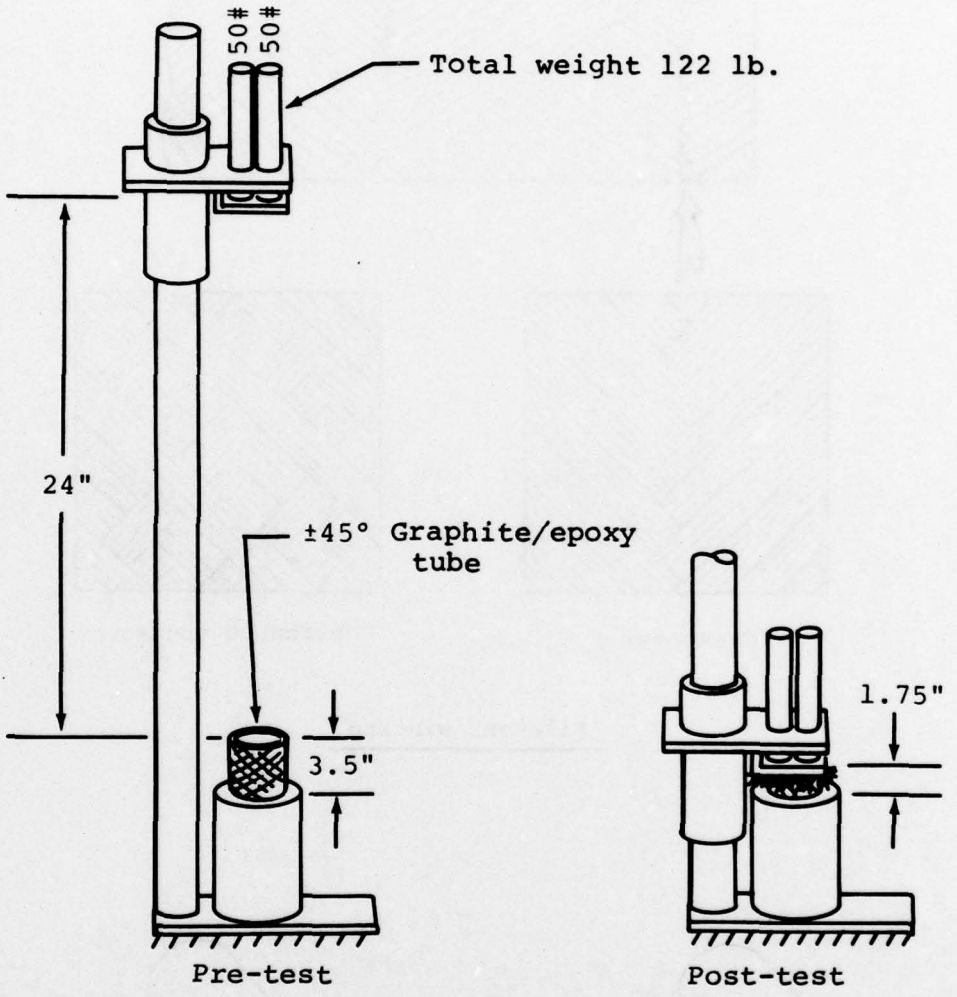

Figure 19. Dynamic drop test of graphite tube.

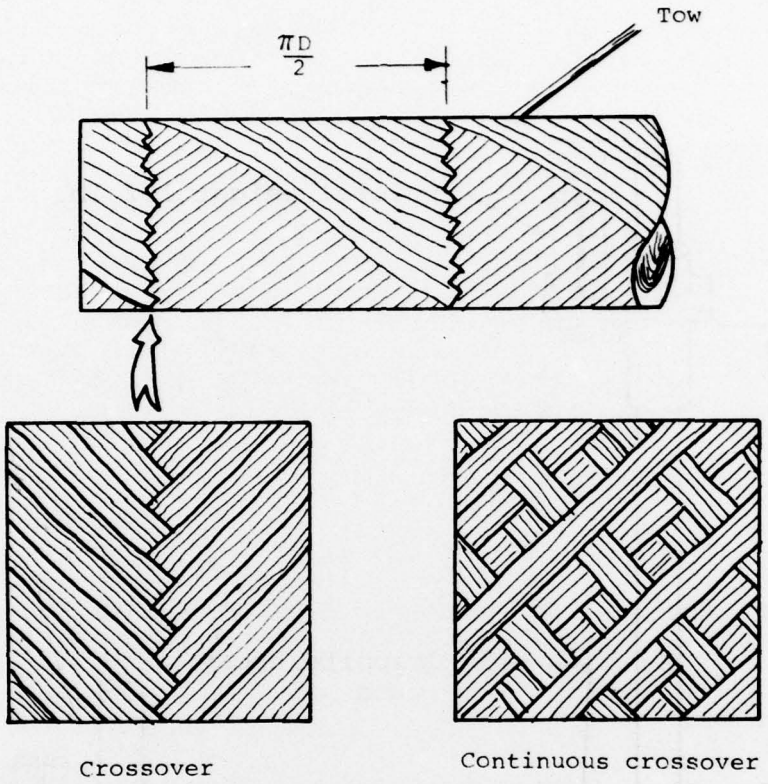

Filament winding

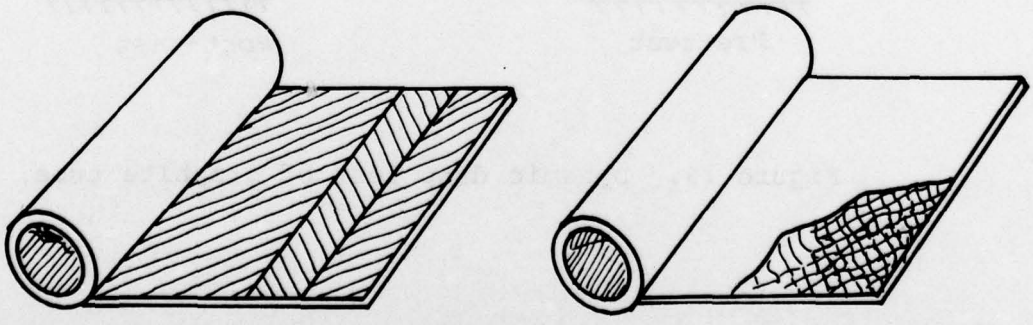

Rolled tape

Rolled fabric

Figure 20. Test specimen construction techniques.

Comparatively speaking, the type of crossover used in the filament-winding process had little effect on the specific energy absorption of the test specimens. Some improvement in the specific energy absorption was noted when the material form was changed to fabric and tape, but since the epoxy was also changed, it is difficult to determine if the increase in this compression mode was due solely to the material form. The greatest increase in specific energy absorption (approximately 66 percent) was obtained when the tape was laid up at 0°, ±35° angle ply orientation (see Figure 21). Further testing will be done to determine an optimum angle ply orientation and material form. It is apparent from Figure 22 References 25 and 26) that composite materials can compete with other materials in an energy-absorbing capacity.

2.5.2 Airframe Crashworthy Design Concepts

A joint FAA and NASA research program is in progress at Langley Research Center to develop valid, practical structural design criteria and improve crashworthiness design technology. The total program is described in Reference 27. NASA, under the direction of R. Thomson, Crash Safety Program Group Leader, is conducting full-scale crash tests of light fixed-wing aircraft, developing analytical techniques and evaluating crashworthy design concepts for seats and airframe structures.

Bell Helicopter is currently under contract with NASA to develop crashworthy design concepts for the fuselage structure of light aircraft. The primary emphasis is on concepts applied to future airframes constructed of metal, but consideration is also being given to concepts applicable to composite structures.

Energy absorbing concepts that can be applied to the lower fuselage structure are currently being designed and will be

---

[25]Smith, H. G., DESIGNING HELICOPTERS FOR IMPROVED CRASH SURVIVABILITY, Presented at the Agard/NATO Aerospace Medical Panel Specialist's Meeting, Oporto, Portugal, June 1977.

[26]Ezra, A. A., and Fay, R. J., AN ASSESSMENT OF ENERGY ABSORBING DEVICES FOR PROSPECTIVE USE IN AIRCRAFT IMPACT SITUATIONS, Dynamic Response of Structures, Pergamon Press, N. Y., 1972, pp. 225-246.

[27]R. G. Thomson and R. C. Goetz, NASA/FAA GENERAL AVIATION CRASH DYNAMICS PROGRAM, A status report, presented at the AIAA/ASME/ASCE/AHS 20th Structures, Structural Dynamics, and Materials Conference, St. Louis, Missouri, April 4-6, 1979.

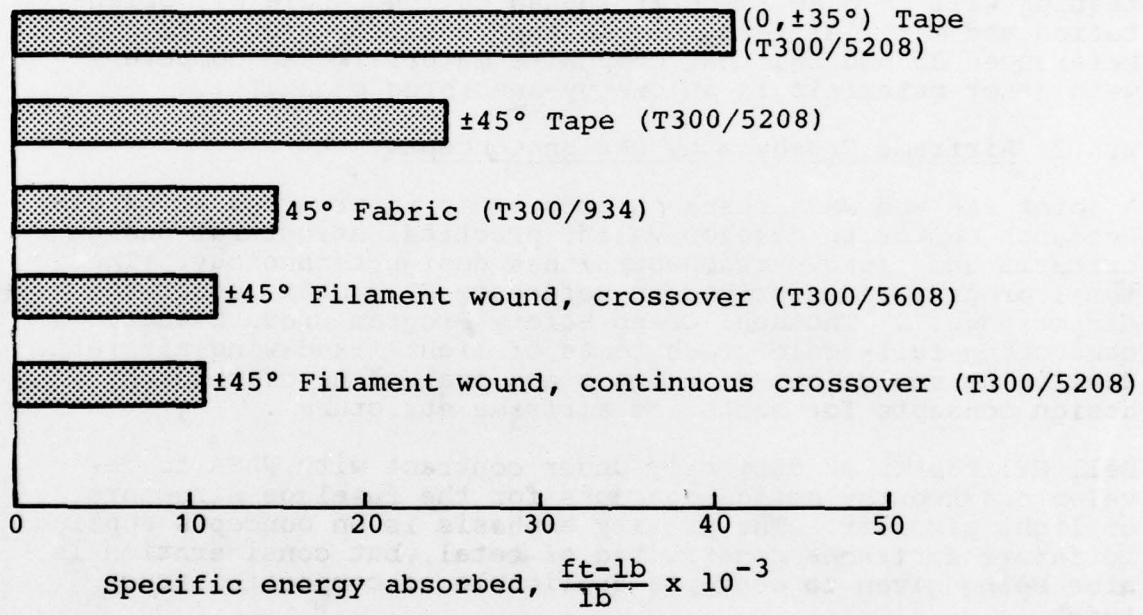

Figure 21. Specific energy absorption of graphite/epoxy tubes.

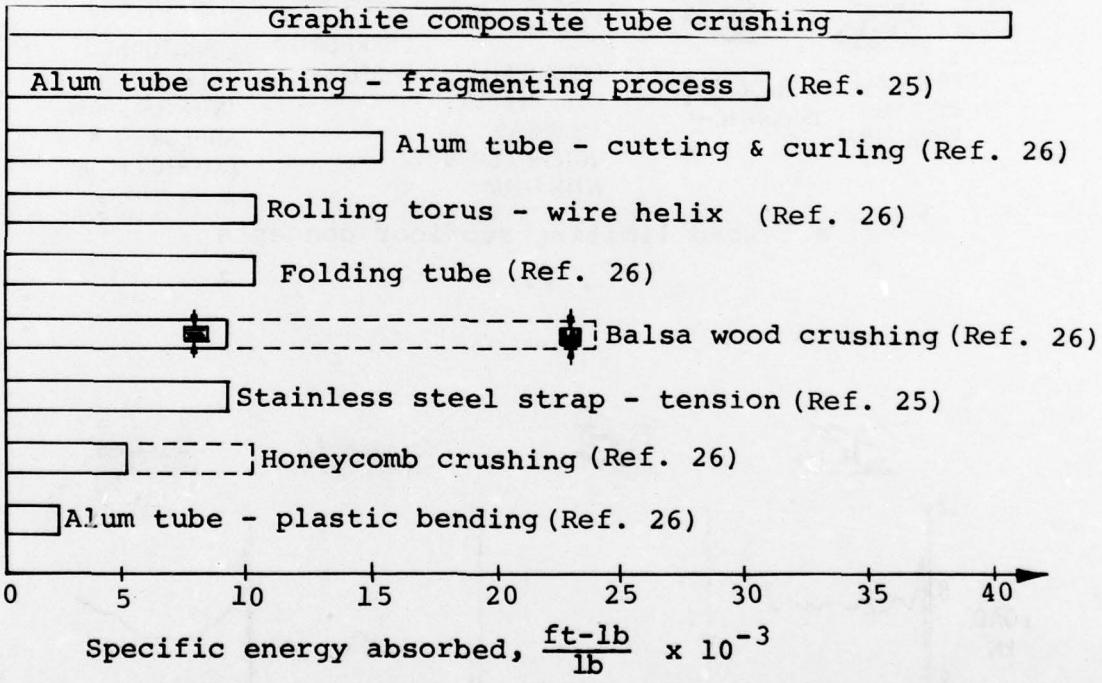

Figure 22. Specific energy absorption comparisons, crushed graphite tube vs other materials.

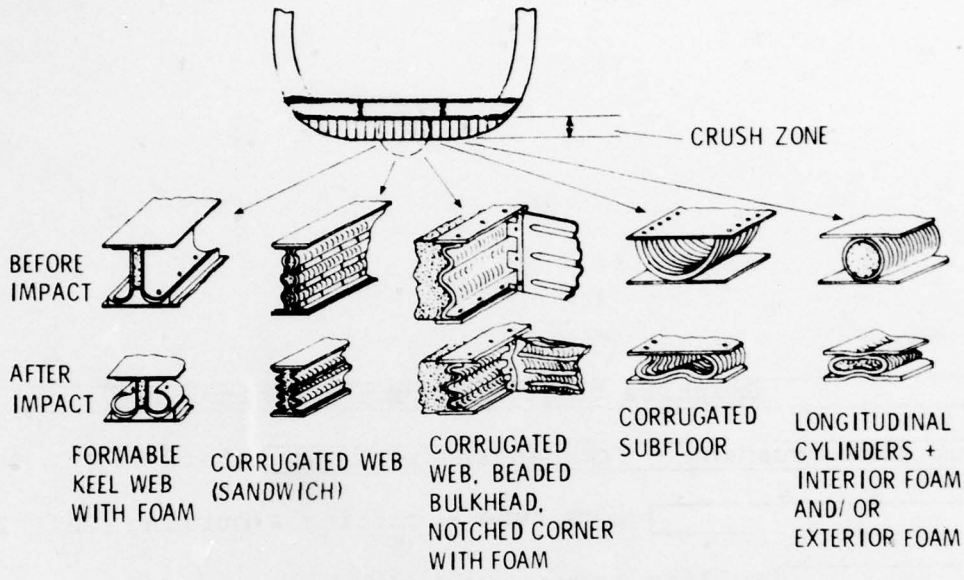

a. Load limiting subfloor concepts

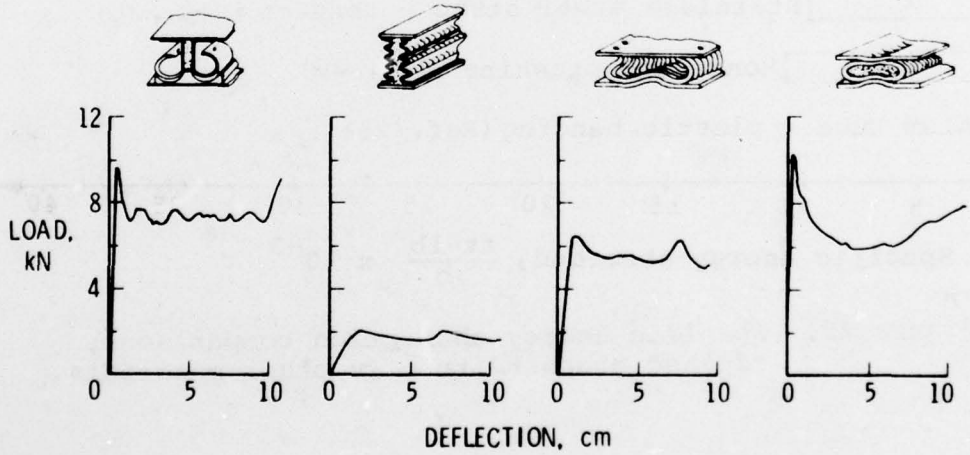

b. Load-deflection curves for load limiting subfloor concepts

Figure 23. NASA airframe crashworthy design concepts (Reference 27).

tested later. Crushable material in the lower fuselage is being designed to attenuate crash forces, absorb energy, and distribute loads to the primary structural shell. Typical examples are shown in Figure 23a. Load-deflection data for some of the concepts is shown in Figure 23b.

2.5.3 Composite Material Stiffened Cylinders

Dr. R. L. Foye of the Research and Technology Laboratories of USAAVRADCOM is attempting to develop an inexpensive test method which will permit the qualitative evaluation of different material/structural concepts with regard to their crushing energy absorption capacity.

The test specimen is a cylindrical shell 9 inches in diameter and 20 inches long with longitudinal stiffeners in the form of hat sections spaced every 90° around the circumference. It was intended that the stringer spacing and cylinder length be representative of the stringer and frame spacing on a utility helicopter fuselage. The cylinders were designed to have the same ultimate axial load allowable and torsional stiffness as a baseline aluminum cylinder.

The materials which have been tested are 7075-T6 aluminum, "E" glass, fiberglass/epoxy cloth, Kevlar 49/epoxy cloth, and graphite/ epoxy. The aluminum cylinder was riveted together with skin overlaps at the stiffener lines while the composite cylinders were co-cured.

The test of the baseline aluminum cylinder displayed failure modes similar to those which occurred during the crushing tests of more complex aluminum monocoque structures. There was local skin buckling, local crippling of the stiffener, plastic bending of the skin and stringer, fastener tearout, and skin tearing. The load-deflection characteristics of this cylinder were also quite similar, qualitatively, to more complex airframe structures.

The composite test specimens, however, displayed a tendency of the stiffeners to split and separate from the skin over their entire length rather than crippling locally. This failure mode produced significantly lower energy absorption when compared to the aluminum baseline (see Figure 24). The results of the tests to date indicate that composites, when configured similar to metal specimens, have a lower energy absorption due mainly to the loss of tension capability across the bond joint.

Future tests are planned using external rather than internal stringers so that the local failure modes may be observed during the loading. Additional parameters to be tested include a comparison of riveted construction and bonded construction, and an evaluation of a sandwich construction relative to a sheet/stringer construction.

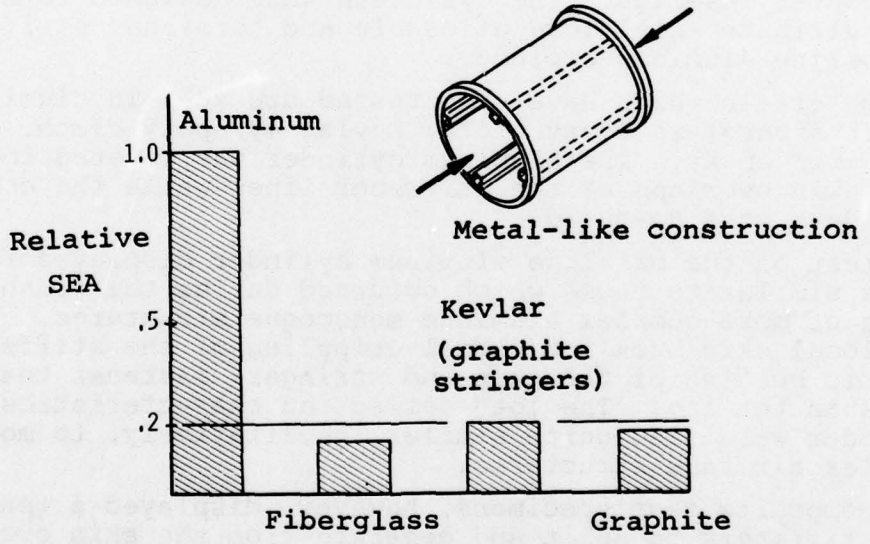

Figure 24. Specific energy absorption (SEA) comparisons of stiffened cylinders.

2.5.4 Scaled Fuselage Section Tests

As a continuation of their test program for determining the energy absorption characteristics of typical helicopter fuselage structure, the Applied Technology Laboratory of the U.S. Army Research and Technology Laboratories, USAAVRADCOM, is conducting a program to investigate the behavior of similar composite structures subjected to the same static and impact conditions. Due to the size limitations of the test equipment at ATL, 1/2-scale specimens were designed by using a dimensional analysis.

An aluminum honeycomb concept which weighed 8.6 percent less than the original structure has been subjected to both a static test and an impact test at 14 fps impact velocity. This concept demonstrated an increase in energy absorption of 82 percent in comparison to the original structure (see Figure 25). Future testing of specimens constructed of graphite and fiberglass is planned.

2.6 SURVEY OF ANALYTICAL METHODS

As the second part of this survey, an investigation was made using the methodology shown in Figure 3 to determine the usefulness of currently available plastic, large deformation structural crash simulations, especially those which can be applied to airframe structures of composite materials. This investigation was aided substantially by previous surveys of the crash simulation literature, particularly those done by Saczalski (Reference 28), McIvor, et al. (Reference 29), and Kamat (Reference 30).

Use can be made of a mathematical crash simulation during the design process, as shown in Figure 26. The key elements in this process are a set of design criteria and a valid crash simulation method. Inputs of structural behavior, which take

---

[28] K. J. Saczalski, MODELLING AND ANALYSIS TECHNIQUES FOR PREDICTION OF STRUCTURAL AND BIODYNAMIC CRASH IMPACT RESPONSE, Finite Element Analysis of Transient Nonlinear Structural Behavior, ASME, New York, Publication AMD Vol. 14, 1975, pp. 99-117.

[29] I. K. McIvor, A. S. Wineman, W. H. Yang, and B. Bowman, MODELLING, SIMULATION, AND VERIFICATION OF IMPACT DYNAMICS, VOL. 2, STATE OF ART, COMPUTER SIMULATIONS OF VEHICLE IMPACT, DOT Report HS-800-997, February 1974.

[30] M. P. Kamat, SURVEY OF COMPUTER PROGRAMS FOR PREDICTION OF CRASH RESPONSE AND ITS EXPERIMENTAL VALIDATION, Measurement and Prediction of Structural and Biodynamic Crash Impact Response, ASME, New York, 1976, pp. 33-48.

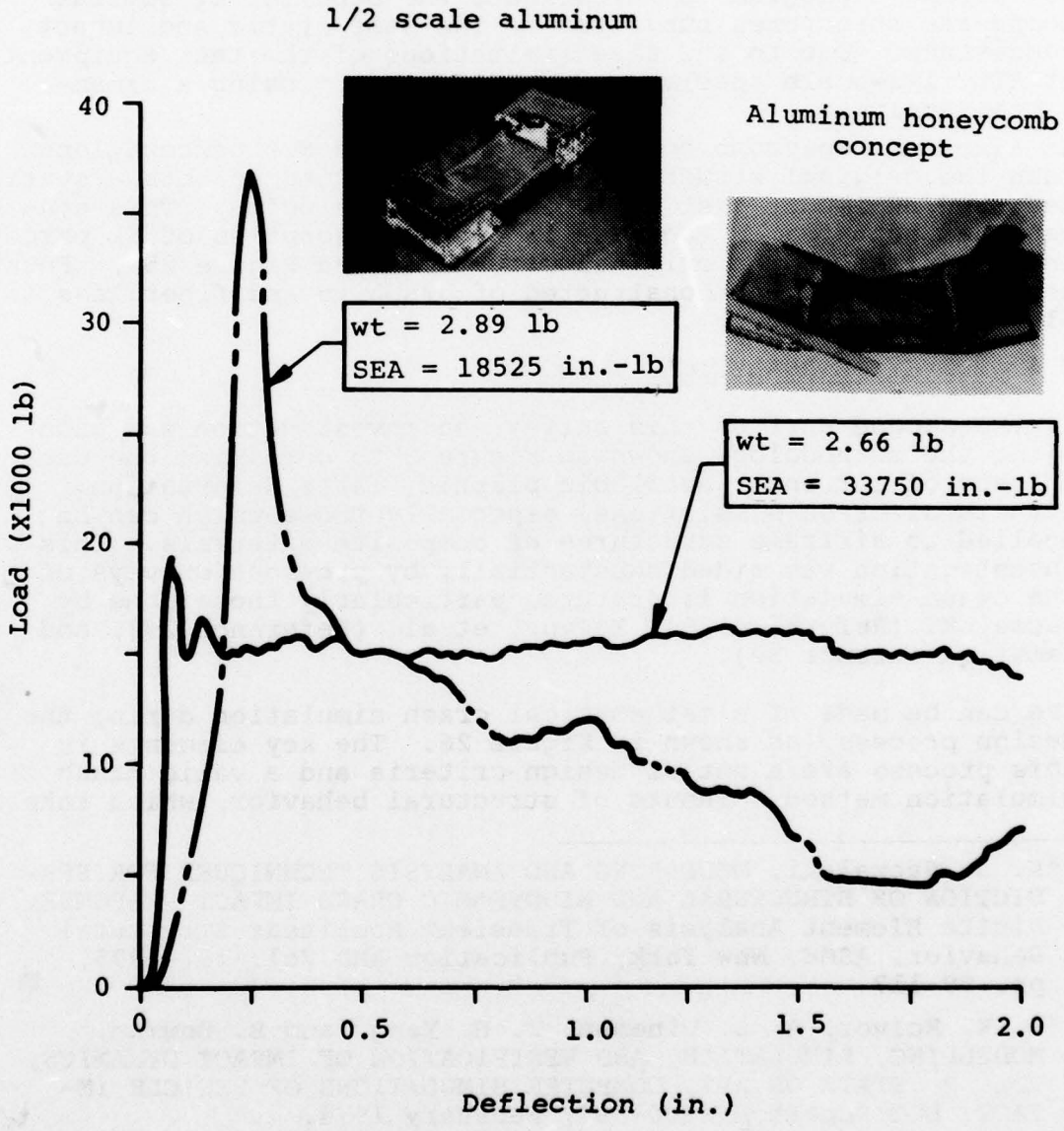

Figure 25. Load-deflection curves for half-scale structure sections.

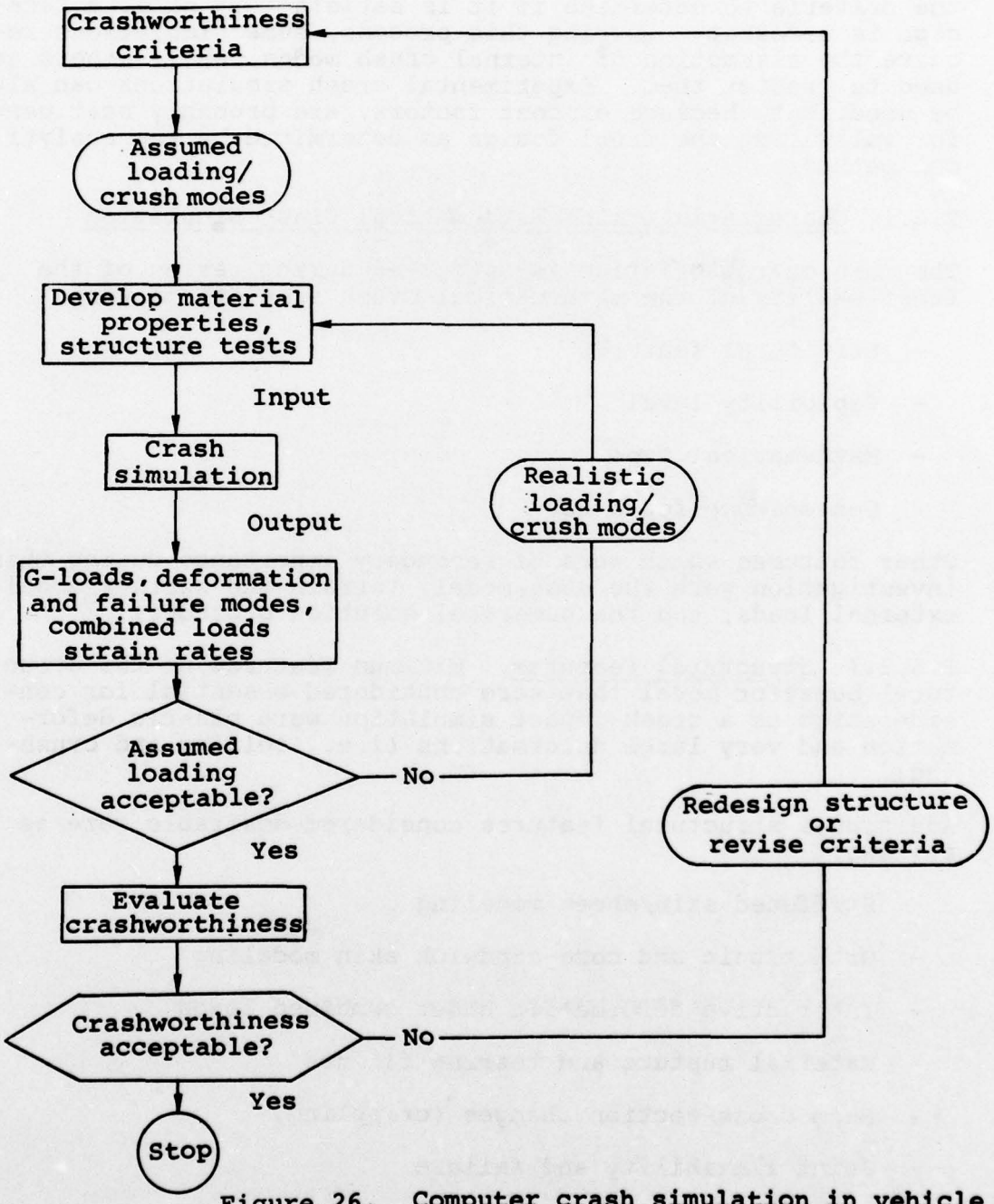

Figure 26. Computer crash simulation in vehicle design process.

the form of stress-strain curves or component crush test data, are used to predict the structure's dynamic response. The crashworthiness of the design can then be evaluated against the criteria to determine if it is satisfactory or if a redesign is necessary. During this process, some simulations require the assumption of internal crush modes, while others are used to predict them. Experimental crash simulations can also be used, but, because of cost factors, are probably best used for validating the final design as determined by the analytical methods.

2.6.1 Characteristics of Mathematical Crash Simulation

The main characteristics investigated during review of the functionality of the mathematical crash simulations were:

- Structural features
- Capability level
- Mathematical type
- Convenience features

Other features which were of secondary importance during this investigation were the mass model, terrain and barrier model, external loads, and the numerical solution procedure.

2.6.1.1 Structural Features. Minimum features of the structural behavior model that were considered essential for consideration as a crash-impact simulation were plastic deformation and very large deformations (i.e., folding and crushing).

Additional structural features considered desirable were as follows:

- Stiffened skin/sheet modeling
- Orthotropic and core-sandwich skin modeling
- Interactive deformation under combined loads
- Material rupture and tearing failure
- Beam cross-section changes (crippling)
- Joint flexibility and failure

For this survey, three broad categories of capability level were established along with their potential uses during design. These levels are as follows:

2.6.1.2 Capability Levels. The single-capability simulations can be used to evaluate gross responses and design trends. They feature:

- Large structural assemblies modeled as single crush elements
- Up to 10 masses, 50 degrees of freedom (unknown in motion equations)
- One- or two-dimensional geometry and motions

The intermediate-capability simulations can be used for studies of structural design parameters and energy dissipation in subassemblies. They feature:

- Structural subassemblies modeled separately, no sheet/skin panel model
- Up to 100 masses, 500 degrees of freedom
- Two- or three-dimensional geometry and motions

The detailed-capability simulations can be used for predicting failure or collapse modes and redesigning individual components. They feature:

- Individual structural components modeled separately, including sheet/skin panels
- More than 100 masses, 500 degrees of freedom
- Three-dimensional geometry and motions

Figure 27 shows specific examples of the capability levels of three mathematical crash simulations as they are applied to automobiles and rotary-wing aircraft.

2.6.1.3 Mathematical Types

2.6.1.3.1 Hybrid type. Requires structural component crush data derived from tests or separate analysis, with:

- Stiffness as input data
- Collapse modes assumed in advance
- Noninteractive collapse and failure under combined loads
- Any testable material or construction
- Simple-to-intermediate capability levels

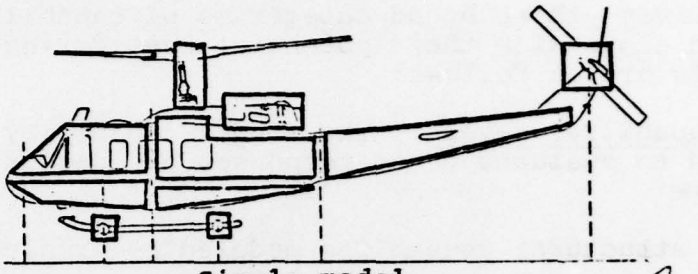

Simple model
"CRASH" - DSI, Gatlin, et al.
(Ref. 36).

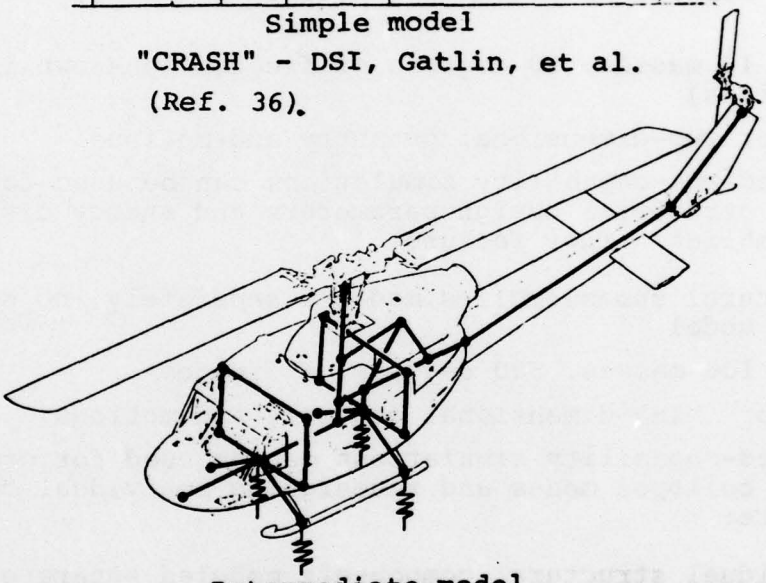

Intermediate model
"KRASH" - Lockheed, Wittlin & Gamon (Ref. 48).

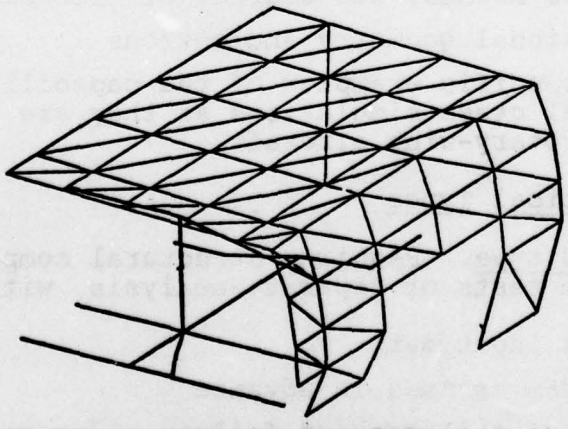

Detailed model
"WRECKER" = Welch & Bruce (Ref. 44).

Figure 27. Examples of mathematical simulation capability levels.

2.6.1.3.2 "Purely" Mathematical (Finite-Element) Type. Requires basic stress-strain data, with:

- Internal stiffness calculations
- Predicted interactive collapse and failure modes (not always)
- Required mathematical stiffness models for advanced materials
- Intermediate to detailed level

The main advantages of the hybrid types are their low computer running cost, their ability to handle any type of construction (if test data are available), and their current availability and user experience. The advantages of the finite-element types are usefulness in analyzing and designing details, theoretical completeness, and very simple material data requirements.

2.6.1.4 Convenience Features. The desired convenience features are input and output graphics to reduce user effort, and a feature that permits the analysis to proceed using sequential time segments with intermediate data examination.

2.6.2 Assessment of Mathematical Crash Simulations

Numerous simple-capability hybrid simulations are available (References 31 through 36, for example). Of these, the two most notable programs are those authored by Herridge and Mitchell of Battelle Columbus Labs and by Gatlin, et al., of Dynamic Science, Inc. The work done by Herridge and Mitchell

---

[31] R. I. Emori, ANALYTICAL APPROACH TO AUTOMOBILE COLLISION, SAE paper 680016, January 1968.

[32] N. Miura and K. Kawamura, ANALYSIS OF DEFORMATION MECHANISMS IN HEAD-ON COLLISIONS, SAE paper 680474, May 1968.

[33] M. Tani and R. I. Emori, A STUDY ON AUTOMOBILE CRASHWORTHINESS, SAE paper 700175, January 1970.

[34] M. M. Kamal, ANALYSIS AND SIMULATION OF VEHICLE-TO-BARRIER IMPACT, SAE paper 700414, May 1970.

[35] J. T. Herridge and J. Mitchell, DEVELOPMENT OF A COMPUTER SIMULATION PROGRAM FOR COLLINEAR CAR/CAR AND CAR/BARRIER COLLISIONS, Battelle Columbus Laboratory for Department of Transportation, Report DOT-HS-800-645, January 1975.

[36] C. I. Gatlin, D. E. Boebel, and S. E. Larsen, ANALYSIS OF HELICOPTER STRUCTURE CRASHWORTHINESS, USAAVLABS Technical Report 70-71A and B, Eustis Directorate U.S. Army Air Mobility Research and Development Laboratory, Ft. Eustis, Virginia, January 1971, AD880680, AD880678.

was directed toward automobile crash impacts, while that done by Gatlin, et al., examined the vertical impact of a helicopter fuselage. This latter program (called "CRASH") simulates the fuselage as rigid masses connected by nonlinear axial and rotary springs in a predetermined arrangement. Both of these simulations are two dimensional.

Of the intermediate-capability programs, the most advanced and perhaps the most widely used hybrid simulation is "KRASH" by Wittlin and Gamon (References 37 and 38). "KRASH" utilizes a three-dimensional arbitrary framework of point masses connected by beams to simulate the fuselage structure. The remaining intermediate-capability programs use finite-element computer codes and include Shieh's work (Reference 39), "CRASH" by Young (References 40 and 41), and "UMVCS" by McIvor, et al. (Reference 42). Shieh idealizes the structure as a two-dimensional array of beams with yielding confined to the plastic hinges at their ends, while "CRASH" and "UMVCS" use three-dimensional models of a framework composed of rods and beams. "UMVCS" could also be considered a hybrid because it requires test data input to define the moment rotation curves for the plastic hinges at the beam ends.

---

[37]M. A. Gamon and G. Wittlin, ANALYTICAL TECHNIQUES FOR PREDICTING VEHICLE CRASH RESPONSE, Lockheed California Company, Aircraft Crashworthiness, University Press of Virginia, Charlottesville, 1975, pp. 605-622.

[38]G. Wittlin and M. A. Gamon, A METHOD OF ANALYSIS FOR GENERAL AVIATION STRUCTURE CRASHWORTHINESS, Measurement and Prediction of Structural and Biodynamic Crash Impact Response, ASME, New York, 1976, pp. 63-81.

[39]R. C. Shieh, BASIC RESEARCH IN CRASHWORTHINESS II - LARGE DEFLECTION DYNAMIC ANALYSIS OF PLANE ELASTO-PLASTIC FRAME STRUCTURES, Calspan Corporation, Report YB-2987-V-7, August 1972.

[40]J. W. Young, CRASH: A COMPUTER SIMULATOR OF NONLINEAR TRANSIENT RESPONSE OF STRUCTURES, Philco-Ford Company, U.S. Department of Transportation, Report Number DOT-HS-091-1-125B, 1972.

[41]R. J. Melosh, CAR-BARRIER IMPACT RESPONSE OF COMPUTER-SIMULATED MUSTANG, Philco-Ford Company, U.S. Department of Transportation, Report Number DOT-HS-091-125A, 1972.

[42]I. K. McIvor, A. S. Wineman, W. J. Anderson, and H. C. Wang, MODELLING, SIMULATION AND VERIFICATION OF IMPACT DYNAMICS - VOL. 4, THREE DIMENSIONAL PLASTIC HINGE FRAME SIMULATION MODULE, University of Michigan, U.S. Department of Transportation, Report Number DOT-HS-800-999, February 1974.

The detailed crash simulations are all three-dimensional finite-element codes with the capability of modeling stringers, beams, and structural surfaces such as skins and bulkhead panels. The four codes currently available are "WHAM" by Belytschko of Northwestern University (Reference 43), "WRECKER" by Welch, et al., of Illinois Institute of Technology (Reference 44), "ACTION" by Melosh, et al., of Virginia Polytechnic Institute of Technology and State University (Reference 45), and "DYCAST" by Pifko, et al., of Grumman Aerospace Corporation (References 46 and 47). "WHAM" currently can be used to idealize a structure which contains only isotropic material. It uses partly interactive yielding; i.e., the effect of shear stresses on plasticity is neglected. "WRECKER" contains the same formulations as "WHAM" but also has the added convenience features of graphics and restart. "ACTION" also has partly interactive yielding, and it can be used only with a structure constructed with isotropic materials. Additionally, "ACTION" also contains an internally varied time step with numerical error controls. "DYCAST" can idealize a structure constructed of orthotropic material. Its features include fully interactive yielding, internally varied time steps with error control, restart, and graphic output.

A summary of the assessment of these specific crash simulations is given in Table 3. Note that the hybrid codes do not account for collapse or failure under combined loads because the crash data inputs are derived from tests with a single load. All of the finite-element codes except Shieh's can account for multiple load components. The crush test can furnish the hybrid computer codes with data to analyze orthotropic laminates and core-sandwich panels, while only "DYCAST" of the finite-element codes can analyze an orthotropic material.

---

[43]T. B. Belytschko, WHAM USER'S MANUAL, University of Illinois, Report 74-B2, 1974.

[44]R. E. Welch, R. W. Bruce, and T. B. Belytschko, DYNAMIC RESPONSE OF AUTOMOTIVE SHEET METAL UNDER CRASH LOADINGS, AIAA Paper 75-793, May 1975.

[45]R. J. Melosh and M. P. Kamat, COMPUTER SIMULATION OF A LIGHT AIRCRAFT CRASH, Journal of Aircraft, Vol. 14, No. 10, October 1977, pp. 1009-1014.

[46]H. Armen, A. Pifko, and H. Levin, NONLINEAR FINITE ELEMENT TECHNIQUES FOR AIRCRAFT CRASH ANALYSIS, Grumman Aerospace Corporation, Aircraft Crashworthiness, University Press of Virginia, Charlottesville, 1975, pp. 517-548.

[47]R. Winter, A. B. Pifko, and H. Armen, CRASH SIMULATION OF SKIN-FRAME STRUCTURE USING A FINITE ELEMENT CODE, Grumman Aerospace Corporation, SAE Paper 770484, April 1977.

TABLE 3. COMPUTER CRASH SIMULATIONS ASSESSMENT

ITEM	HYBRID	FINITE ELEMENT
Plastic collapse & crush with combined loads	All None	All All except Shieh's
Material failure with combined loads	All None	None None
Skin & bulkhead	All (Poorly)	WRECKER, WHAM, ACTION, DYCAST
Anisotropic laminates with cored sandwiches	All All	DYCAST None
Beam cross-section deform. (Crippling)	All	None
Joint deform. & failure	All	None
Strain rate stiffening	KAMAL, HERRIDGE	WRECKER
With local variations	None	WRECKER

None of the evaluated finite-element codes can currently analyze a core sandwich. "WRECKER" is the only one of these codes which will account for strain rate effects in a logical way by determining the local strain rate and adjusting the stiffnesses. All the hybrids can account for joint failure and crippling because these effects are part of the crush test data.

2.6.3 Conclusions and Recommendations on Computer Crash Simulations

The major conclusions of this investigation on computer crash simulations for advanced material applications are:

- There is no satisfactory single existing code
- Hybrid codes are theoretically incomplete
- Finite-element codes currently lack sufficient advanced material capability

The recommendation for current crash simulations on advanced materials is to use "KRASH" with applicable crush test data for the preliminary parametric studies and gross evaluations. For a detail design, "DYCAST" can be used for analyzing orthotropic laminates. However, this code is still under development and has not yet been experimentally verified. It is not currently possible to perform an extensive detailed design evaluation of a structure with sandwich-core construction. This type of construction holds promise for increased energy dissipation with advanced composites.

2.6.4 Application of Crashworthiness Design Criteria to Composite Structures

There are many factors to consider during the design of a crashworthy airframe structure, but for this investigation, only those considerations related to the crash-impact characteristics of composite materials were considered pertinent. If the airframe is to be subjected to a pulse which represents the design impact velocity changes for the 95th percentile potentially survivable accident, then the design considerations shown in Figure 28 must be applied to the airframe to maintain a crashworthy environment for the occupants. Discussions of the crashworthy design considerations can be found in many documents, but the primary reference is the "Crash Survival Design Guide" (Reference 1).

These design considerations have been addressed in civilian and military regulations, standards, and specifications wherein criteria have been formulated. A summary of the available criteria and the crashworthy design considerations addressed by each is presented in Table 4.

By far, the most comprehensive document concerning the requirements for a crashworthy airframe structure is MIL-STD-1290 (Reference 2). MIL-STD-1290, which is based on the design guidelines of the "Crash Survival Design Guide," establishes the minimum crashworthiness design criteria which, when implemented in the initial stages of a systems design, will provide the aircraft with improved crash-safety characteristics. Because these criteria represent a needed capability for crash-impact survivability, modification of this criteria in a manner that would reduce the level of crash protection should not be considered. Although some of the material properties of composites run counter to the material properties preferred for crashworthy structures (e.g., low ductility, fracture and splintering), nothing learned in this investigation indicates that the criteria of MIL-STD-1290 cannot be met by a structure constructed from composite materials.

The Budd Company reports indicate that with a proper design, composite energy absorbers may be used without a weight penalty. Their report, when compared with the work done by Foye, indicates that the sandwich construction will be superior to sheet/stringer construction for absorbing impacts. The median barrier, used to prevent cars from crossing traffic lanes, also indicates that composite materials have the capability of remaining intact under impact forces, which is a requirement for maintaining a protective shell. The test on the glare shield indicates that the failure mode that produced a sharp edge was in itself a hazard. Due to the lack of

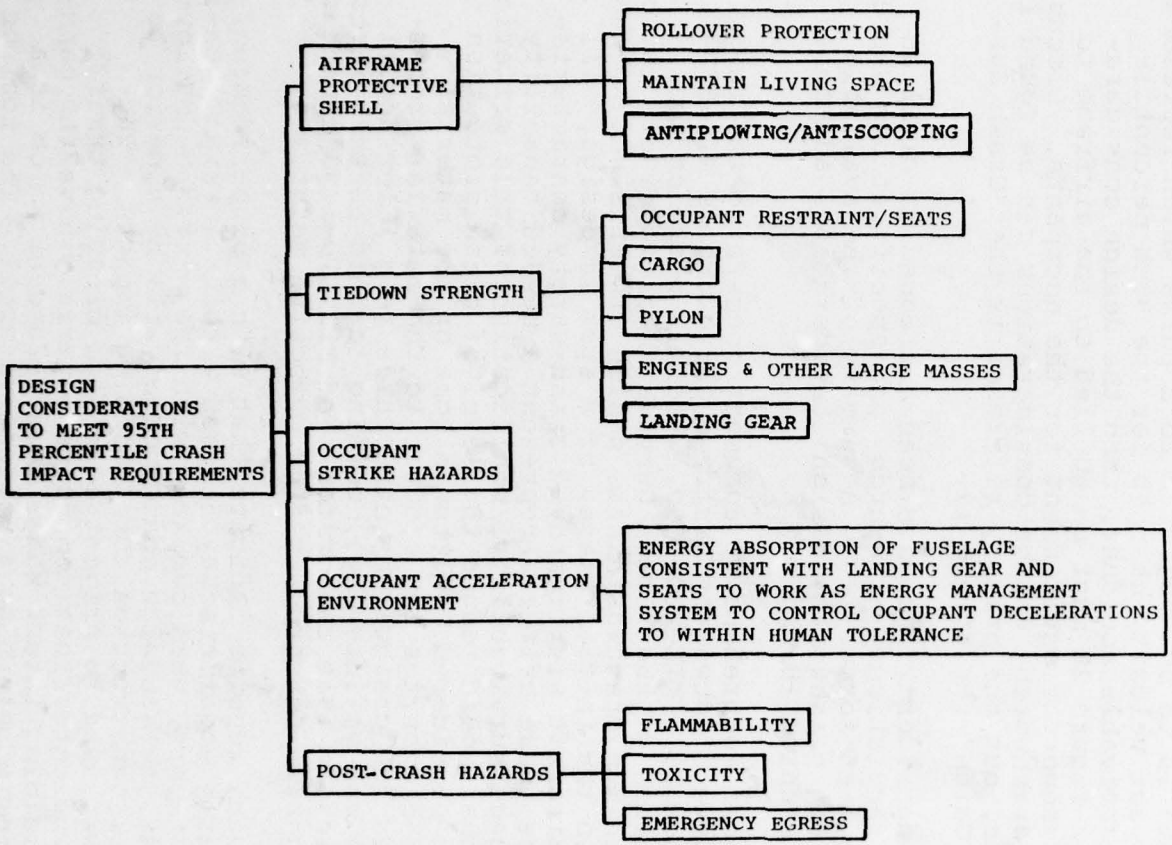

Figure 28. Airframe crashworthiness considerations.

extensive research into the field of crashworthiness of structures constructed from composite materials, it will be difficult to substantiate compliance with the criteria analytically; therefore, numerous section tests and possibly full-scale crash tests will be required.

TABLE 4. AIRFRAME CRASHWORTHINESS CONSIDERATIONS VS CRITERIA

AIRFRAME CRASHWORTHINESS CONSIDERATIONS	ARMY (MIL-STD-1290 & TR 71-22)	NAVY (AR-56)	AIR FORCE (MIL-A-8860 & MIL-A-8865	FAA (FAR 23, 25 27 & 29)
AIRFRAME PROTECTIVE SHELL	•	•		
BREAKAWAY AIRFRAME STRUCTURE	•			
OCCUPANT STRIKE HAZARDS	•			
ENERGY ABSORPTION	•			
POST-CRASH HAZARDS	•			
FAILURE MODES	•			
INERTIA FORCES TIEDOWN STRUCTURE	•	•	•	•

3. DESIGN CONCEPTS

3.1 OVERALL DESIGN CONSIDERATIONS

Overall crashworthiness considerations which are applicable to design of an airframe structure are shown in Figure 29. Composite materials are currently being used to satisfy the basic airframe requirements for normal flight loads, stiffness, and weight; in the future they will also be required to satisfy the crashworthiness criteria.

An example of the dual function that future airframe structures will be asked to fulfill can be illustrated by examining the design requirements for the lower fuselage. To satisfy the crashworthiness design consideration, the lower fuselage should be able to absorb some of the energy due to a crash impact. This would reduce the inertia forces transmitted to the occupants and the large mass items such as the transmission and engine, and it would also help maintain the protective shell by reducing and distributing transmitted loads. In its role as an energy absorber, the fuselage acts in series with other crash force attenuators such as the landing gear and the occupant seats. Additionally, the lower fuselage must be designed to provide the basic strength and stiffness that is required to resist the normal flight loads, while also providing the room to route the controls, wiring, and life-support systems.

3.2 OVERALL FUSELAGE CONCEPTS

Figure 30 presents an illustration of an approach to satisfy the fuselage crashworthy considerations where the primary function is to maintain a protective shell around the occupied area. This can be accomplished by providing rollover strength in the form of elliptical sandwich-stiffened ring frames on the top and sides of the fuselage and a structural floor. Note that in Figure 30 the side fillets are designed to provide better rigidity and corner continuity between the floor and the sidewalls, while they also will act to absorb the energy and to distribute the loads from a side impact. The foam-filled Kevlar tubes will be multifunctional in that they will act as floor beams to satisfy the normal airworthiness criteria of strength and stiffness; they will also function as energy absorbers to react the vertical and lateral crash-impact forces. The heavy sandwich construction with local strap reinforcement on the lower mold-line surface will act as a shear and axial load path to satisfy the normal airframe requirements, while functioning as a skid during a longitudinal impact to prevent plowing and gouging. A common post-crash hazard is entrapment of the occupants due to the collapse

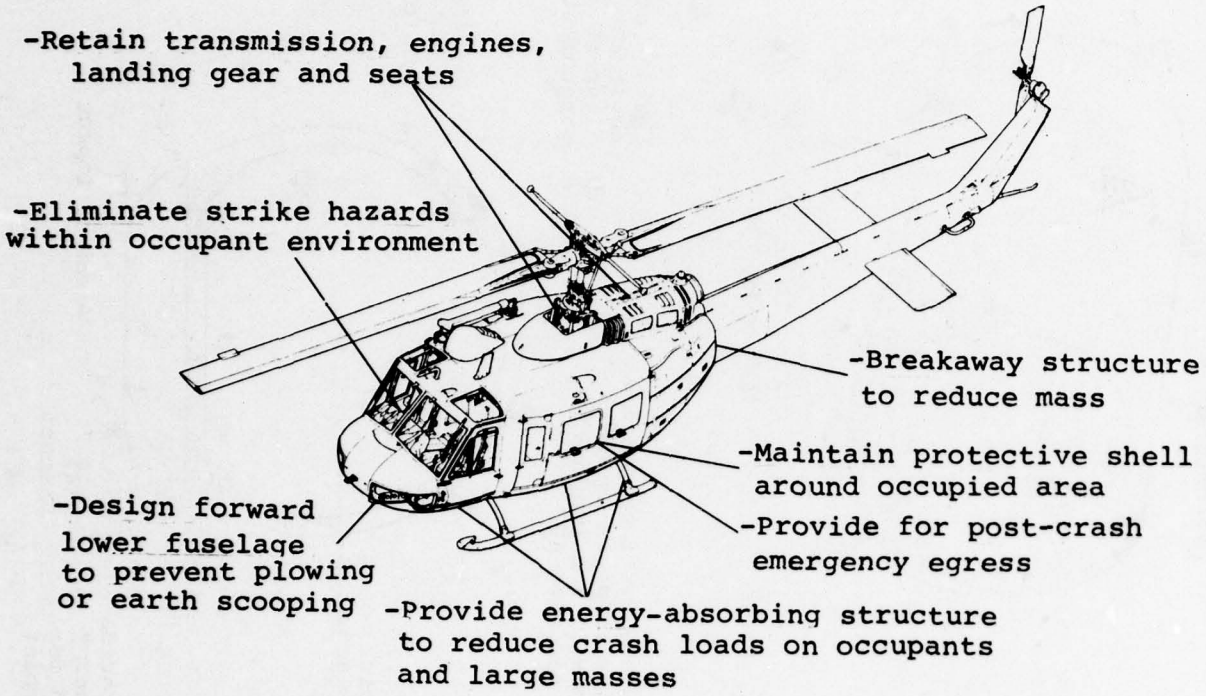

Figure 29. Airframe structure crashworthy design considerations.

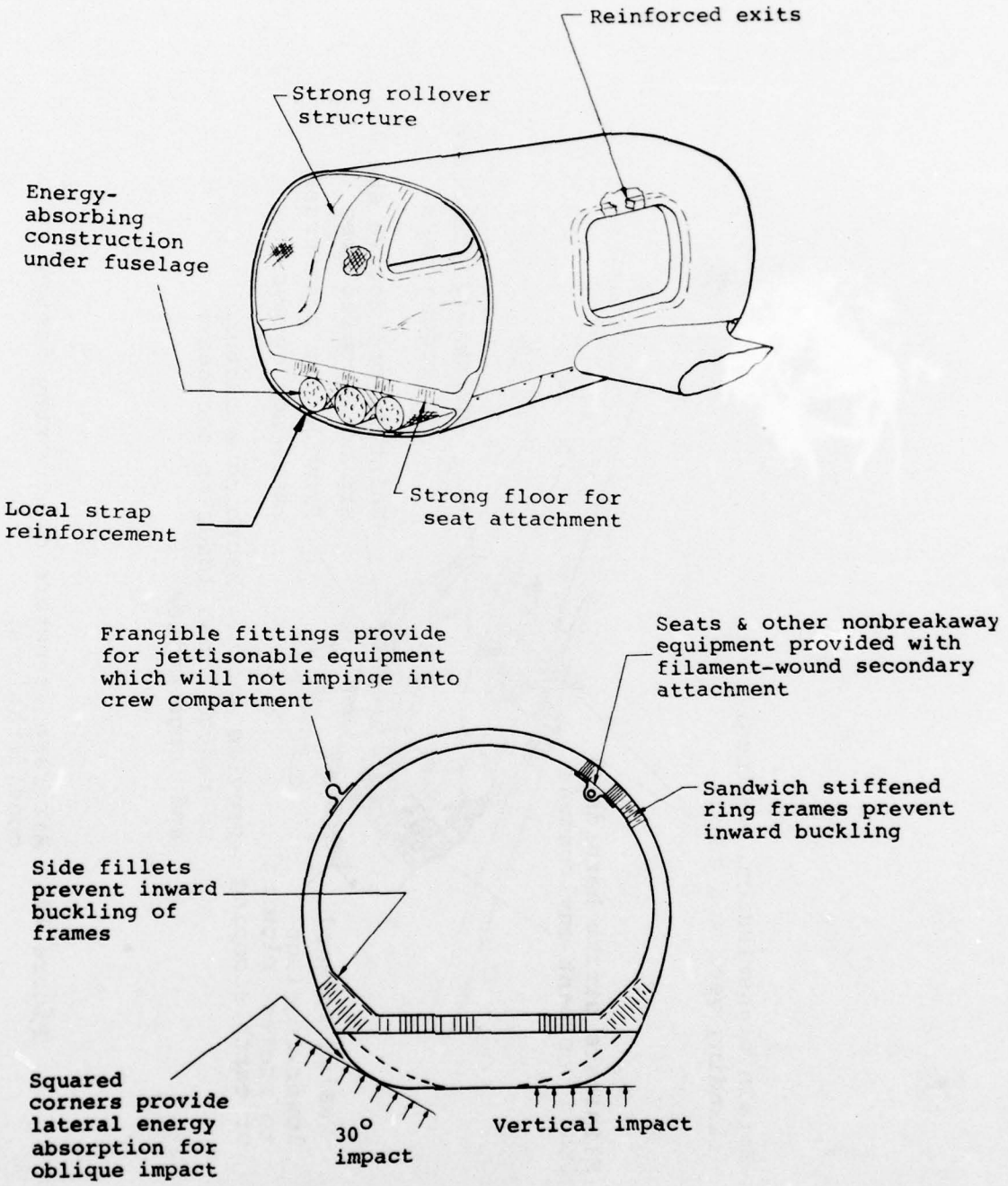

Figure 30. Overall fuselage concepts.

of the emergency exits. It is proposed to reinforce the hatches with a filament-wound composite tube that will provide the strength and stiffness required to prevent the distortion of the hatch region. This local reinforcement can also serve as a framing member that will redistribute the airloads around the cutouts. Local details, such as seat attachment points in the floor or cabin roof, need to be in areas where the airframe distortion during crash impact will not adversely affect the operation of the seat stroking mechanism or the seat belts. Consequently, reinforcements in the form of a higher density core in the sandwich construction or a filament-wound lug are shown in a typical application.

3.3 COMPOSITE MATERIAL CONCEPTS FOR VERTICAL IMPACT

In order to reduce the inertia forces experienced by the occupant in a crash, energy-absorbing material must be placed between the ground and the floor of the cabin. Normally, this location is occupied by controls, wires, and life-support systems; consequently, the overall design must take this into account.

There are three basic characteristics of energy absorbers that will serve as criteria for these concepts. As shown in Figure 31, an energy absorber must first be able to distribute the ground impact forces into the fuselage in a manner that will not overstress the floor or sidewalls. Secondly, both the magnitude of the load and the onset rate must be controlled so that the total force does not exceed the allowable loads for either the structure or the occupants, and so that the rate at which the load is applied is within human tolerance. Finally, an energy absorber should not be rate sensitive and should approach the ideal rectangular shape for the load-deflection curve, since this represents the maximum efficiency.

The beam and bulkhead concepts shown in Figure 32 are designed to react the vertical, longitudinal, and lateral impact loads; however, the most efficient direction for providing a progressive collapse is vertically. In each of the four concepts shown, it is assumed that the floor structure will also be designed to react the crash-impact forces without failure. The concepts shown are directly applicable to many current fixed-and rotary-wing aircraft because their structural arrangement is similar. The first and second concepts will promote progressive crushing by stratifying the core and skins using the less-dense core and the less-stiff skin at the lower ends. The variation of skin stiffness will be accomplished by deleting plys. The stratification will have two effects: It will promote the crushing at the lower surface, and it will provide

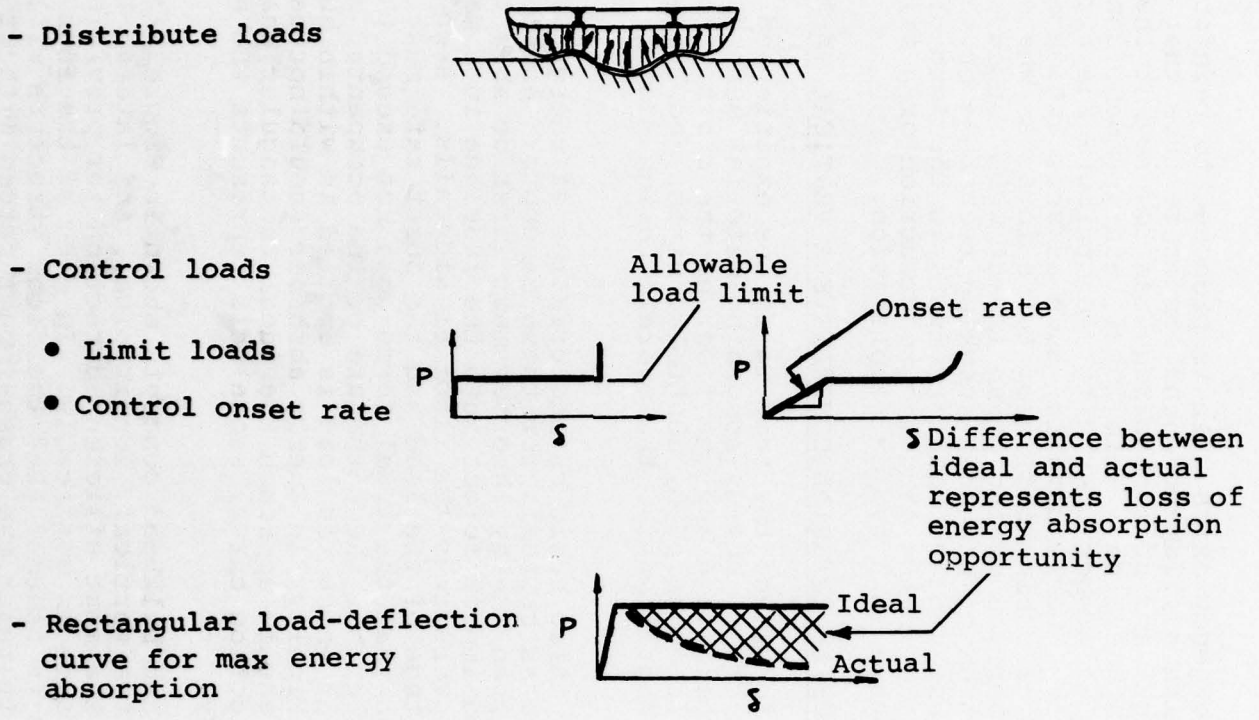

Figure 31. Characteristics of energy-absorbing material.

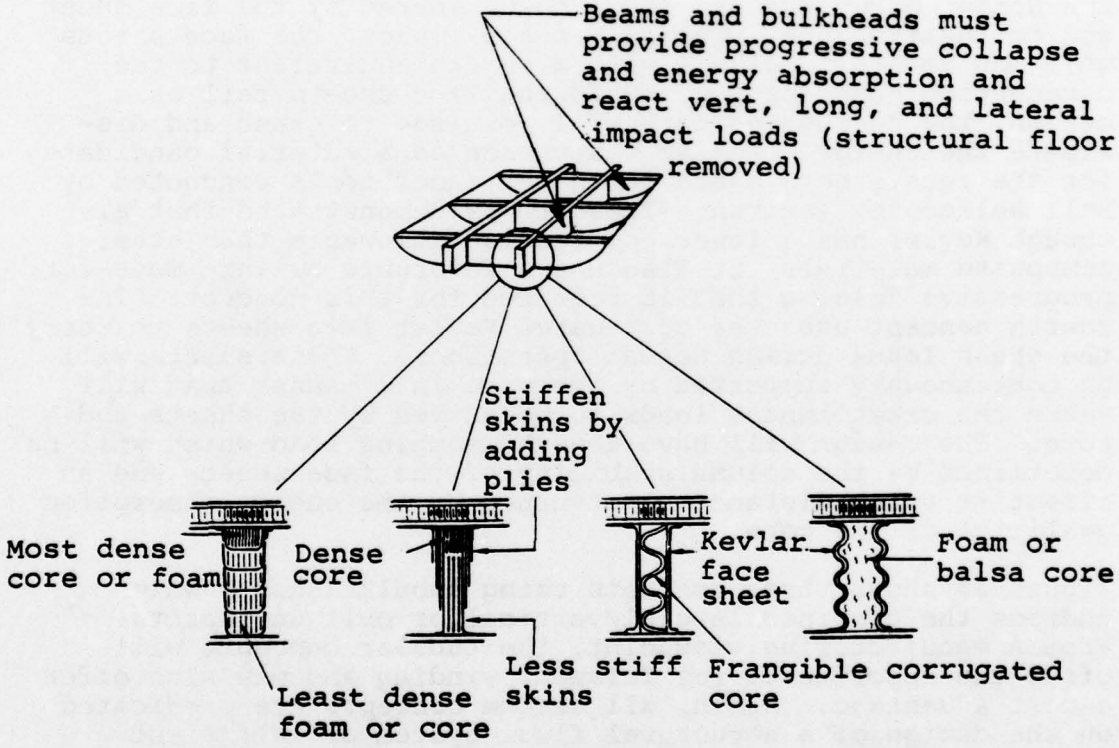

Figure 32. Energy absorption concepts - beams and bulkheads - vertical impact.

the increased strength of the core and skin adjacent to the floor where it is needed for the local reinforcements, or the seat or equipment attachments. Design support tests can be used to select the material, fiber orientations, etc.; however, a promising candidate for fulfilling both the airworthiness and crashworthiness criteria is graphite because of its high specific-energy absorption and its good strength and stiffness.

The third concept features a frangible corrugated core that is bonded to the face sheets at the nodes. This concept requires the normal airworthiness loads to be shared by the face sheet and corrugated core. During a crash impact, the face sheets will act as short columns with a length equivalent to the corrugation node spacing. When the face sheets fail as a column, the corrugated core will continue to crush and dissipate the energy. Kevlar was chosen as a material candidate for the face sheets based on the cylinder tests conducted by Bell Helicopter Textron. These tests demonstrated that although Kevlar has a lower compression allowable than other composite materials, it also has a favorable failure mode for progressive folding that is required for this concept. The fourth concept uses the corrugated Kevlar face sheets to carry the shear loads during normal operations. These sheets will be continuously supported by the core in a manner that will cause the crash-impact loads to be shared by the sheets and core. The design will have a peak crushing load which will be determined by the column stability of the face sheets and an effective crush distance as governed by the energy absorption qualities of the core.

Figure 33 shows three concepts using tubular shapes which address the combined lateral/vertical or oblique impacts. From a manufacturing viewpoint, the tubular concepts will offer the opportunity for filament winding and may also offer a cost advantage. Again, all of the concepts are predicated on the design of a structural floor system of sufficient strength and stiffness to react the crash-impact forces. The heavy hatched area in the floor represents local reinforcement for seat or cargo attachments that coincide with the tube reaction points.

In these concepts, the energy-absorbing agent is the foam or honeycomb structure. In the first concept, Figure 33a, the vertical forces are dissipated by the foam and reacted directly by the floor structure. For the oblique impact, the Kevlar straps will restrain the tendency of the outer tubes to roll by reacting the side forces with a truss action. The straps will also replace the normal subfloor bulkheads to react the normal flight loads. The truss is used instead of

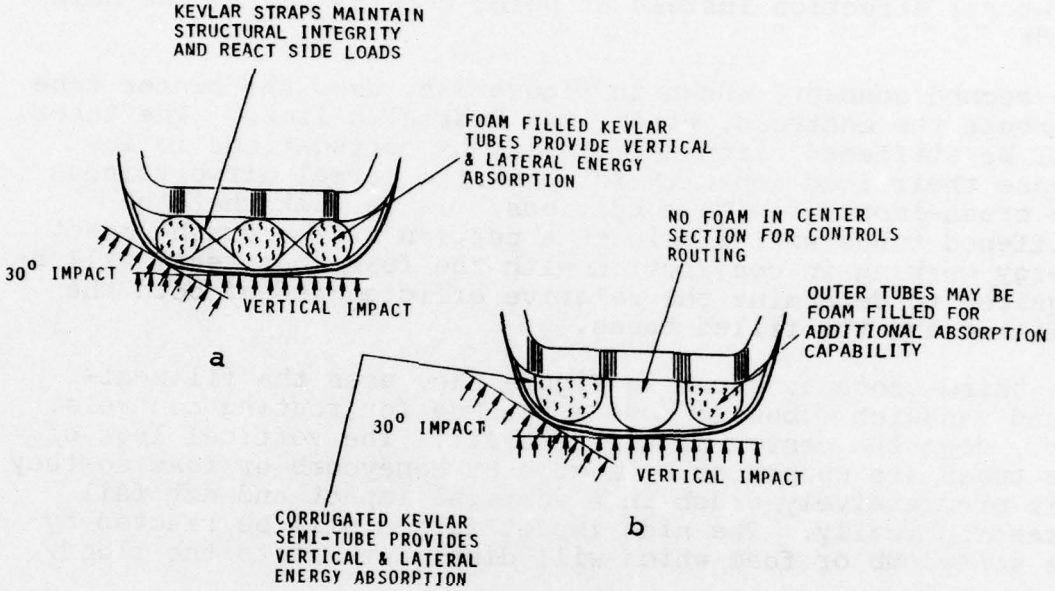

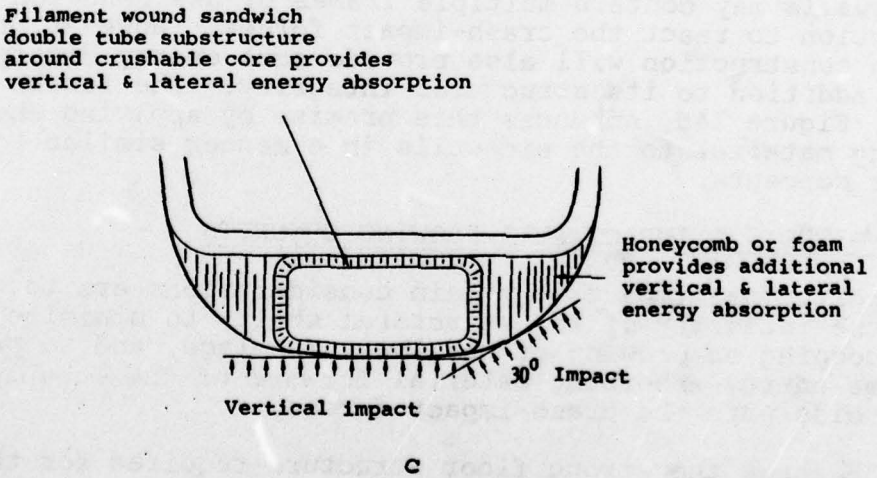

Figure 33. Energy absorption concepts - tubular construction (oblique vertical impact).

the bulkheads because it permits the tubes to expand freely in a lateral direction instead of being constrained by the bulkheads.

The second concept, shown in Figure 33b, uses the center tube to route the controls, wires, and hydraulic lines. The tubes will be stiffened circumferentially by corrugations to increase their load capacity for both the normal airworthiness and crash-impact design conditions. It is felt that the stiffened tubes will dissipate a portion of the crash-impact energy working in conjunction with the foam, but tests will be required to determine the relative efficiencies of both the unfilled and the filled tubes.

The third concept, shown in Figure 33c, uses the filament-wound sandwich tubes to form a housing for routing controls, etc., down the center of the aircraft. The vertical legs of the tubes are supported by a core of honeycomb or foam so they will progressively crush in a vertical impact and not fail catastrophically. The side impact forces will be reacted by the honeycomb or foam which will distribute it to the floor.

3.4 FUSELAGE SIDEWALL CONCEPTS

The fuselage sidewall concepts shown in Figure 34 are essentially designs which are intended to preserve the protective shell. Concepts a through c make use of the geometrical advantage of a circular cross section to reduce load concentrations while providing a strong sidewall to prevent failure. The sidewalls may contain multiple frames or use sandwich construction to react the crash-impact forces. However, the sandwich construction will also provide some energy dissipation in addition to its structural integrity. The fourth concept, Figure 34d, enhances this premise by applying energy-absorbing material to the sidewalls in a manner similar to the subfloor concepts.

3.5 LONGITUDINAL IMPACT ANTI-PLOWING CONCEPTS

In a longitudinal impact, the main considerations are to ensure the integrity of the structural shell, to minimize earth scooping or plowing of the lower fuselage, and to provide some energy-absorbing material forward of the occupied area to dissipate the crash-impact forces.

Figure 35 shows the strong floor structure required for the lateral and vertical impact conditions fairing into a sled-like nose that will act as a landing skid and as a backup structure to react the longitudinal impact forces. The current functions for the nose structure are to house electronic

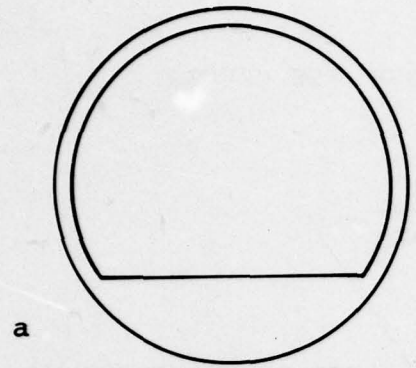

a

Circular cross section to reduce rollover loads

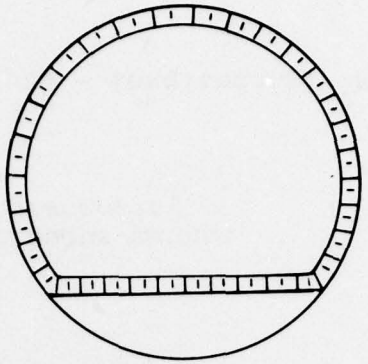

b

Strong sidewall to prevent protective shell failure

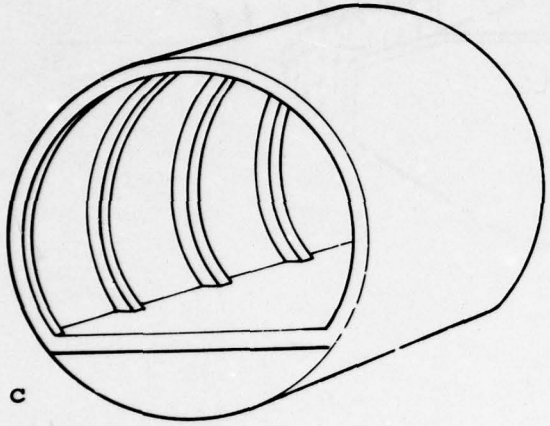

c

Redundant sidewall frames for rollover loads

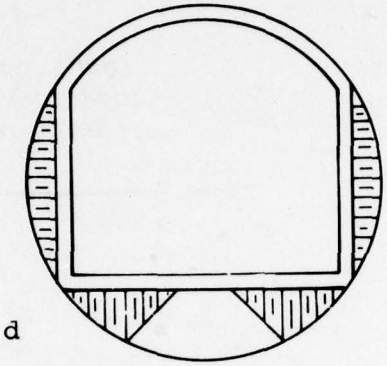

d

Crushable material for load control and distribution

Figure 34. Fuselage sidewall concepts - lateral impact.

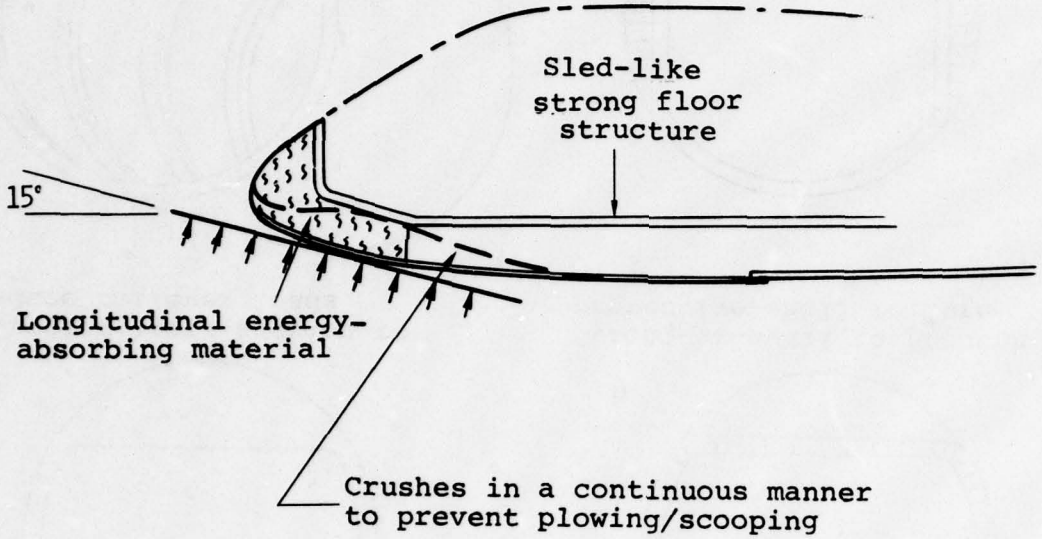

Figure 35. Antiplowing concepts - longitudinal impact.

equipment, batteries, radar units, and ballast, and to act as a storage location for the nose gear. This design concept must be modified to satisfy these requirements while also integrating crushable energy-absorbing material to react the impact force. The belly skin will be fabricated in one section, similar to a large bathtub, to minimize joints that could fail and present a protrusion gouging into the earth's surface. This method of construction eliminates parts and has been suggested as a means for reducing cost of composite components. A sandwich construction using Kevlar face sheets is a material choice that offers strength in shear and a resistance to tearing or puncture. All panels and hatches will be designed to have a leading edge that laps under the skin so that it will not act as a scoop during the large deformations that occur in a crash. The one-piece skins in conjunction with the energy absorbers, which could be a foam-filled Kevlar tube, will be encouraged to collapse in a continuous manner by including longitudinal straps under the absorbers to add bending strength and to act as a skid.

3.6 JOINT CONCEPTS

The joints and attachment fittings of a crashworthy airframe structure must be able to do the following:

- Withstand large deflections without failure in those areas where large deformations are anticipated.

- Connect the large overhead mass items to the fuselage such that failure or separation of the major structural members supporting the items occurs before the joint fails.

Of the two considerations, the first imposes the most constraint on a joint constructed of composite materials or, for that matter, on a metallic fitting manufactured from a casting or a forging since they generally have a lower strain to failure than a sheet-metal-type joint. The composite joint concepts have sought to have redundant or back-up load paths to satisfy the above considerations while relying on the airframe structure to absorb the energy and redistribute crash loads. Most of them contain some metal and therefore are considered hybrids.

In the concept shown in Figure 36a, the primary load path is the bolted connection between the fitting and the bulkhead. The filaments around the bolts will be designed such that they will not begin to accept any load until the primary load path in the joint has yielded.

The joint concept shown in Figure 36b uses a primary load path through the attachment hole and the bondline between the fitting and the skin. A secondary load path exists between the filaments that are wound in a "racetrack" fashion around the fitting and the skin.

The concept shown in Figure 36c depends upon the bond joint between the fitting and the skin for its primary load transfer. The secondary load path uses the mechanical connection provided by the rivets to transfer the load from the fitting to the metallic backup plate to the composite face sheets. The rivets also provide a tension capability to resist peeling forces which are present due to the eccentric load paths.

The flattened filament-wound cone concept shown in Figure 36d provides a progressive failure mode which causes the joint to contract circumferentially as it elongates longitudinally. After the matrix has failed, the joint will still retain some residual cable strength due to the fibers contracting around the metal insert.

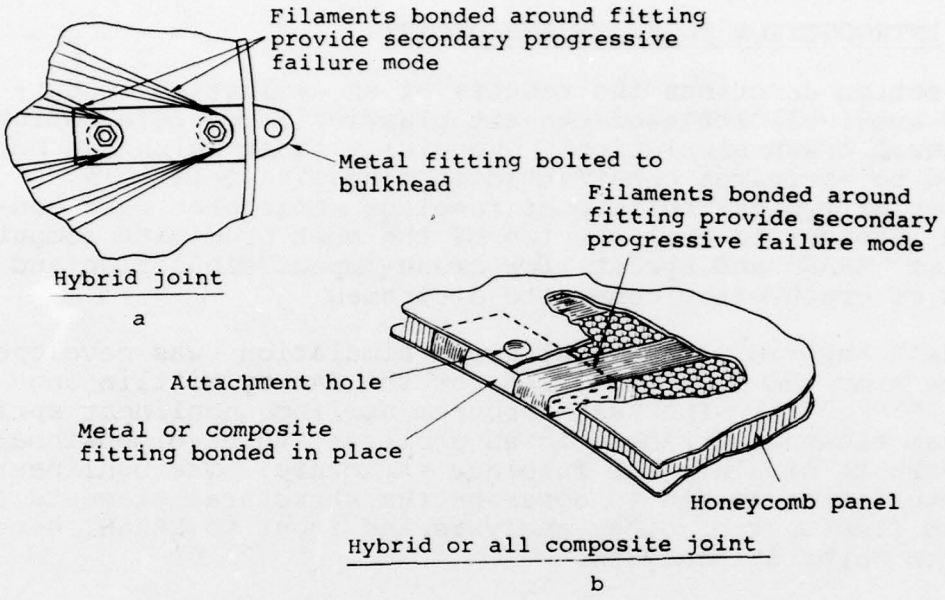

Figure 36. Crashworthy joint concepts.

4. EVALUATION OF STATE-OF-THE-ART STRUCTURAL CRASH SIMULATIONS

4.1 INTRODUCTION TO KRASH AND DYCAST

This section describes the results of an evaluation of currently available state-of-the-art plastic, large-deformation structural crash simulations, especially those which can be applied to airframes constructed of composite materials. Analyses of typical helicopter fuselage structures were conducted in order to evaluate two of the most promising computer programs, KRASH and Dycast, for crash-impact simulation and design of crashworthy composite airframes.

The KRASH "hybrid" structural crash simulation was developed for the Army and later modified for the FAA by Wittlin and Gamon.[48] [49] [50] [51] The KRASH program utilizes nonlinear spring and beam elements arranged in an arbitrary three-dimensional framework to simulate the fuselage structure. The nonlinear characteristics needed to describe the structural elements are derived from test or other analysis and input to KRASH; hence the term "hybrid" analysis.

---

[48] G. Wittlin and M. A. Gamon, EXPERIMENTAL PROGRAM FOR THE DEVELOPMENT OF IMPROVED HELICOPTER STRUCTURAL CRASHWORTHINESS ANALYTICAL AND DESIGN TECHNIQUES, Lockheed California Company, USAAMRDL Technical Report 72-72, 2 Vols, Eustis Directorate, U.S. Army Air Mobility Research and Development Laboratory, Fort Eustis, Virginia, May 1973, AD 764985, AD 764986.

[49] G. Wittlin and K. C. Park, DEVELOPMENT AND EXPERIMENTAL VERIFICATION OF PROCEDURES TO DETERMINE NONLINEAR LOAD-DEFLECTION CHARACTERISTICS OF HELICOPTER SUBSTRUCTURES SUBJECTED TO CRASH FORCES, USAAMRDL Technical Report 74-12, 2 Vols, Eustis Directorate, U.S. Army Air Mobility Research and Development Laboratory, Fort Eustis, Virginia, May 1974, AD 784191, AD 784192.

[50] G. Wittlin and M. A. Gamon, A METHOD OF ANALYSIS FOR GENERAL AVIATION AIRPLANE STRUCTURAL CRASHWORTHINESS, DOT Report No. FAA-RD-76-123, U.S. Department of Transportation, Federal Aviation Administration, Systems Research and Development Service, Washington, D.C., September 1976.

[51] G. Wittlin and M. A. Gamon, GENERAL AVIATION AIRPLANE STRUCTURAL CRASHWORTHINESS USER'S MANUAL, 3 Vols, DOT Report No. FAA-RD-77-189, U.S. Department of Transportation, Federal Aviation Administration, Systems Research and Development Service, Washington, D.C., February 1978.

A KRASH model of a troop transport helicopter airframe used in the study is shown in Figure 37.

The second program evaluated was the DYCAST structural crash simulation developed for NASA by Pifko, et al.[46 47] The DYCAST computer program is a detailed finite-element code which has the capability of modeling stringers, beams, and structural surfaces such as skins and bulkheads and can also idealize structures constructed of orthotropic material. A typical section of a troop transport helicopter that was chosen for analysis with DYCAST is shown in Figure 38. A conventional metal section and a composite section incorporating a crashworthy design concept were modeled and comparable crash impacts simulated. This analysis exercised the capability of DYCAST to represent a typical helicopter section of structure and determined whether a composite structure, properly configured, could be designed to be crashworthy.

The hybrid and finite-element types of analysis have important differences in capability and the manner in which they are used. A flow diagram of each type of analysis is shown in Figure 39. Note that the detailed finite-element analysis has the potential for determining the structure crash-impact response using information obtained directly from design drawings. The hybrid analysis, on the other hand, requires inputs from test or a separate analysis of large structure sections in order to define the nonlinear properties of the spring and beam elements.

For a crash simulation using a hybrid-type analysis, the structural inputs could have been derived from a composite structure, a metal structure, or a structure of practically any type of material. The hybrid analysis itself will require no added special capability for treatment of composites. The major effort in a crash analysis using a hybrid method will be involved in developing the inputs to the analysis. The detailed finite-element analysis, on the other hand, being mathematically more complete, does require special treatment of composites relative to metals.

4.2 KRASH ANALYSIS

4.2.1 Approach

In order to evaluate the KRASH program, the following approach was taken:

1. Using the UH-1 KRASH analysis described in Reference 48, plus BHT's in-house structural analysis programs, a metal

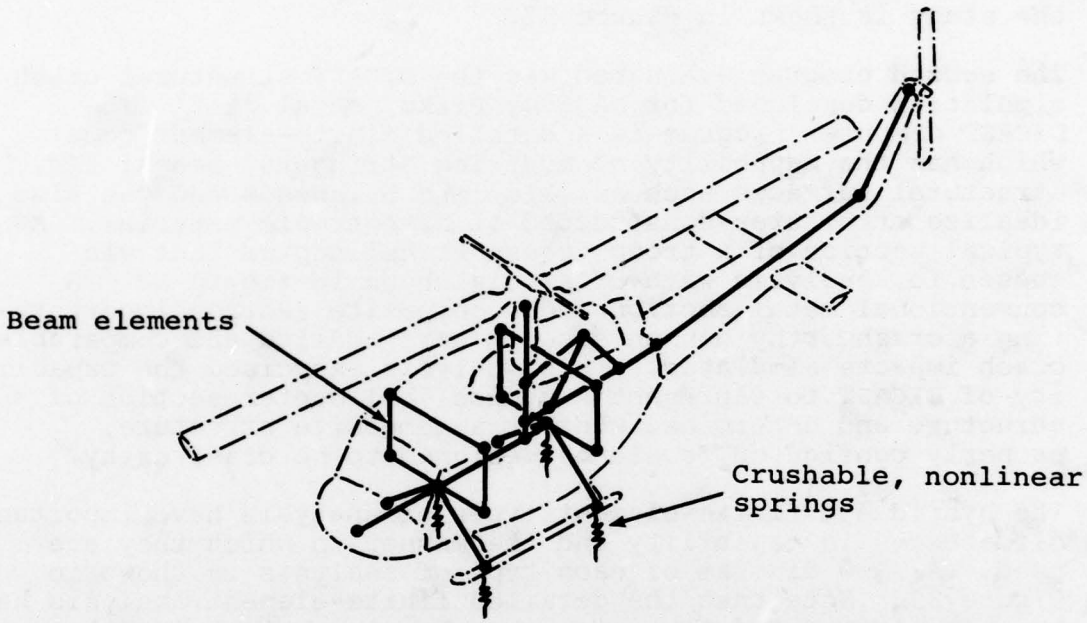

Figure 37. Model of UH-1 helicopter used for "KRASH" analysis.

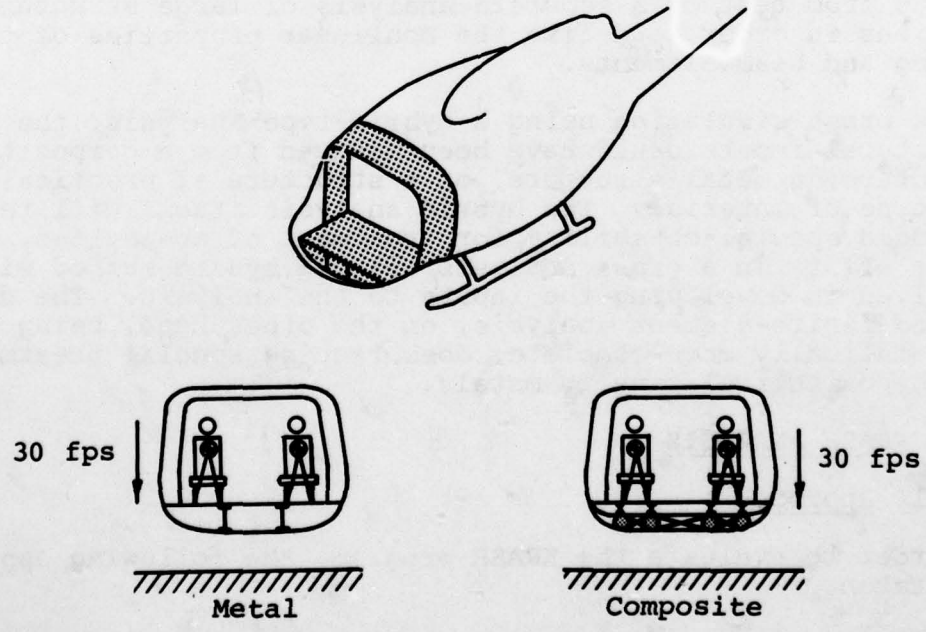

Figure 38. Section of helicopter used for "DYCAST" analysis.

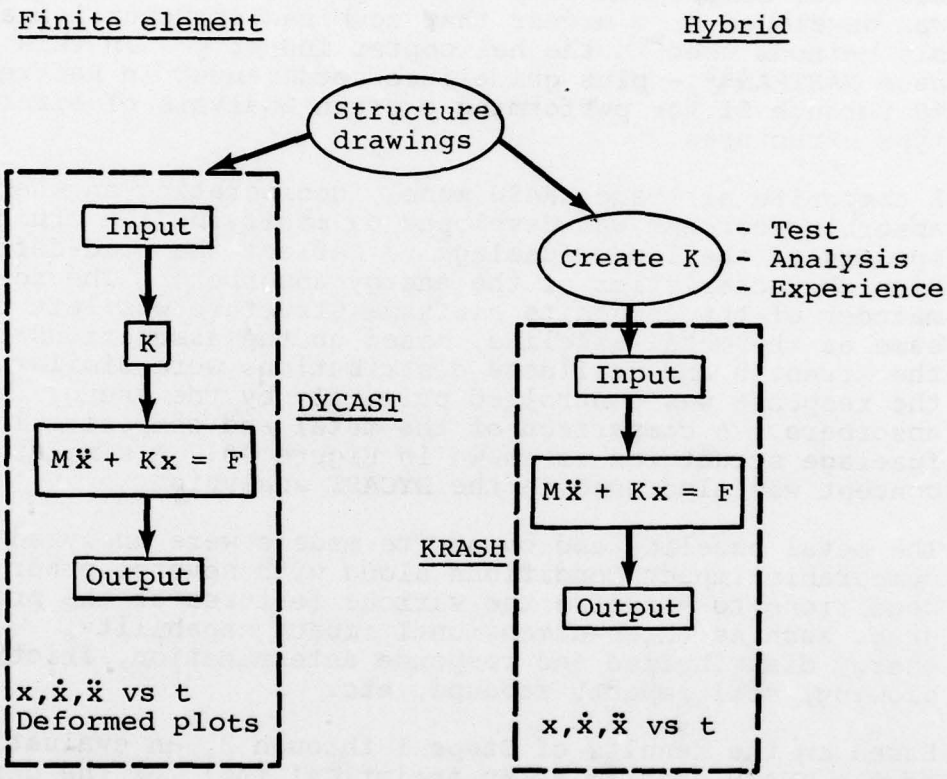

Figure 39. Hybrid/finite-element structure crash simulation comparison.

baseline troop transport helicopter KRASH model was established. A complete description of the model and explanation of how it was developed are presented in Appendix A. The metal baseline helicopter was used as a basis for comparison with the composite model. The model was developed in a manner that combines structural analysis methods used in the helicopter industry - in this case NASTRAN[52] - plus guidelines recommended in References 48 through 51 for performing a crash analysis of aircraft-type structures.

2. A composite airframe KRASH model incorporating an energy-absorbing concept was developed by modifying the crushing springs of the lower fuselage to reflect the load-deflection characteristics of the energy absorbers. The remainder of the composite airframe structure was left the same as the metal baseline, based on the assumptions that the strength and stiffness distributions were similar and the response was controlled primarily by the energy absorbers. A comparison of the metal and composite lower fuselage structures is shown in Figure 40. A similar concept was also used in the DYCAST analysis.

3. The metal baseline and composite models were analyzed for comparable impact conditions along with several other conditions to exercise the various features of the program, such as three-dimensional impact capability, energy distribution and response determination, friction, plowing, soil impact, rebound, etc.

4. Based on the results of Steps 1 through 3, an evaluation of the KRASH program as an analytical tool for the design of crashworthy composite, as well as metal helicopter structures, was made.

4.2.2 KRASH Program Features and Output

A summary of the features of the KRASH program important to the engineering user are the following:

- Lumped mass representation.

---

[52] THE NASTRAN USER'S MANUAL, NASA SP-222(03), National Aeronautics and Space Administration, Washington, D.C., July 1976.

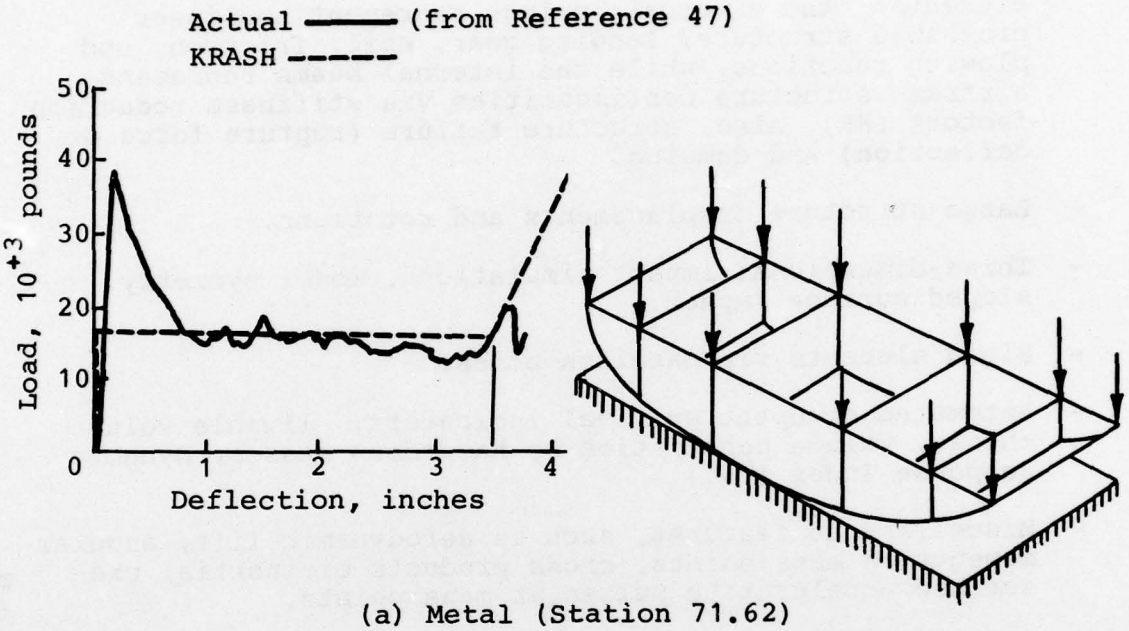

(a) Metal (Station 71.62)

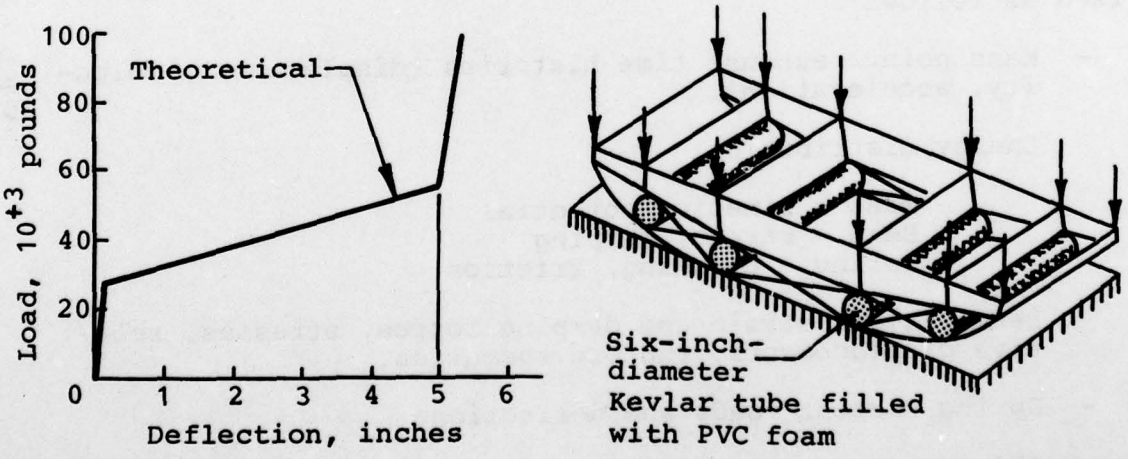

(b) Composite (Station 71.62)

Figure 40. Typical load-deflection curves used to represent lower fuselage crushing in metal and composite KRASH models.

- Nonlinear external spring and internal beam structural elements: the external springs represent nonlinear crushable structure, landing gear, soil, friction, and plowing reactions, while the internal beams represent airframe structure nonlinearities via stiffness reduction factors (KR), also, structure failure (rupture force or deflection) and damping.

- Large structure displacements and rotations.

- Three-dimensional impact simulations, model symmetry, sloped surface impact.

- Rigid elements via massless nodes.

- Automated occupant survival indicators: livable volume change, volume penetration by hazardous masses, Dynamic Response Index (DRI).

- Miscellaneous features, such as aerodynamic lift, angular moments as mass points, cross products of inertia, prescribed acceleration pulses at mass points.

- Restart.

Output parameters available in the KRASH program are summarized as follows:

- Mass point response time histories (displacement, velocity, acceleration).

- Energy distribution:

  Mass - kinetic, potential
  Beam - strain, damping
  Spring - crushing, friction

- Beam element strain and damping forces, stresses, relative displacements, rupture summaries.

- Spring element loads and deflections.

- DRI response, cg velocity, volume change/penetration.

- Print and plot of responses, element data.

- Energy summaries.

Very comprehensive documentation and correlation of the KRASH analysis is available in References 48 through 51.

4.2.3 KRASH Analysis Results

In order to evaluate the usefulness of the KRASH analysis for crash simulation of metal as well as composite airframe structures, a variety of cases were run using three KRASH models: the UH-1 model documented in Reference 48, a metal baseline model, and a composite model. The seven impact conditions that were analyzed are summarized in Figures 41(a) through (g). These conditions were designed to exercise most of the features found in KRASH, such as analysis of three-dimensional impacts, load-deflection stiffness parameters from metal or composite structures, soil deformation, friction, and plowing. The analysis results are described here and in Appendix A.

The responses of the TR 72-72[48] model and the metal baseline model were compared for condition (a) of Figure 41 which simulates a test documented in TR 72-72. Comparisons were made between the two models and the test results to validate and calibrate the metal baseline KRASH model. The results of this comparison are shown in Figure 42 in the form of a bar chart showing peak accelerations and corresponding times. The metal baseline model generally shows higher peak accelerations than the TR 72-72 results, which may be due in part to the higher gross weight of 9500 pounds for the metal baseline as compared to 8500 pounds for the TR 72-72 case. This would give the metal baseline helicopter almost 12 percent higher initial kinetic energy for the same impact velocity. When choosing the acceleration values for Figure 42, there was often some question as to which peaks in the time histories to select for comparison. Sometimes two values had to be chosen, as shown in Figure 43, for the test values of crew floor acceleration. Note that for the metal baseline model there are two values shown for the main rotor lateral transmission response. This is because the main rotor transmission was modeled with two lumped masses, one at the rotor hub and one at the transmission cg, whereas the TR 72-72 model used only one lumped mass.

Energy distribution versus time curves are shown in Figure 44 for the comparable metal and composite impact conditions, Figures 41(c) and (d). Energy distribution curves for all of the impact conditions analyzed are given in Appendix A. The energy distribution curves allow the engineer to readily determine how the energy is managed by the structure during the crash sequence and evaluate the roles of crushable structure, strain in the internal structure, friction, and damping in absorbing the initial kinetic energy of the aircraft. Also, the amount of energy being stored in the structure and later returned to the aircraft in the form of kinetic energy can easily be seen when rebound occurs.

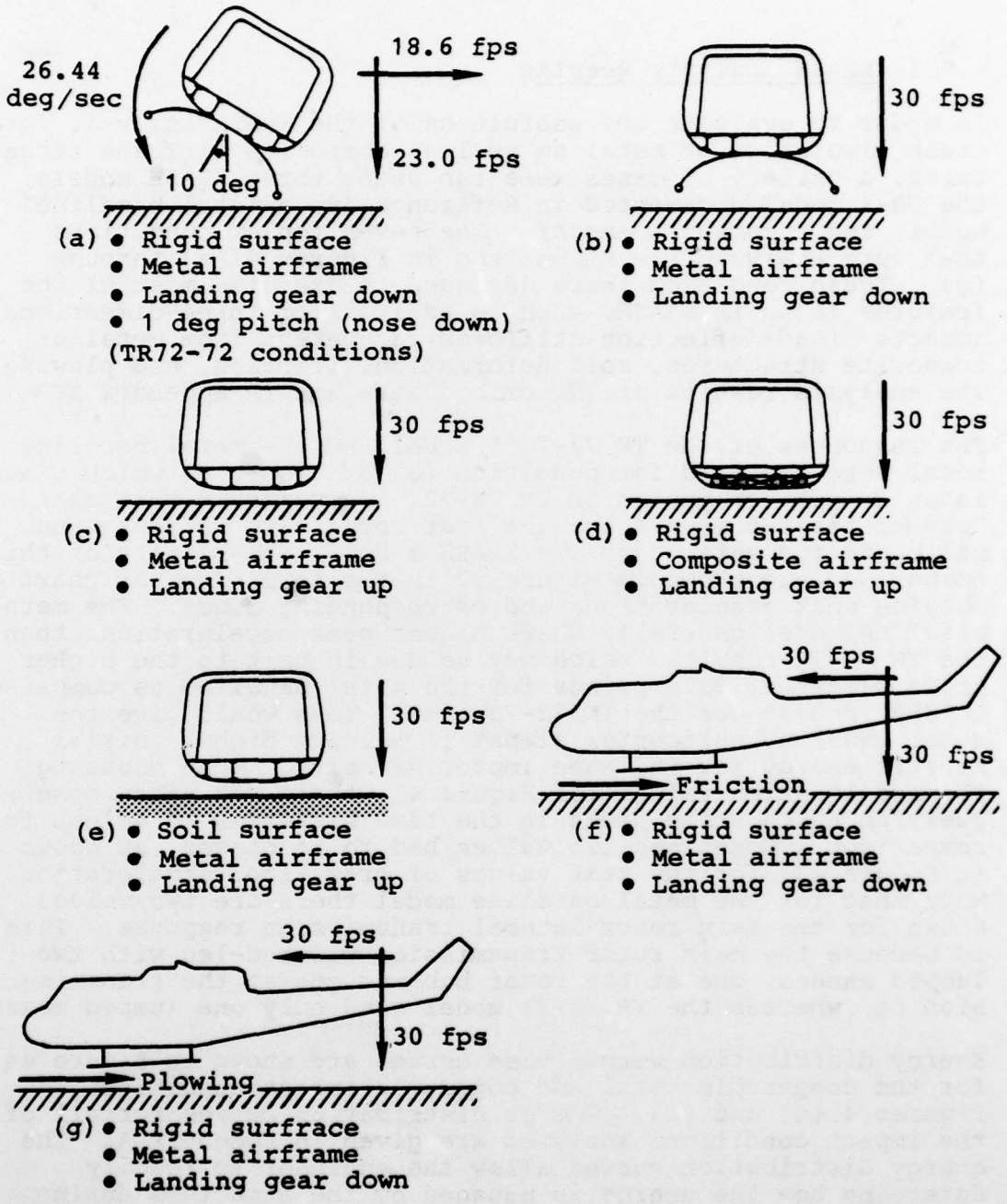

Figure 41. Impact conditions used for KRASH analysis of troop transport helicopter.

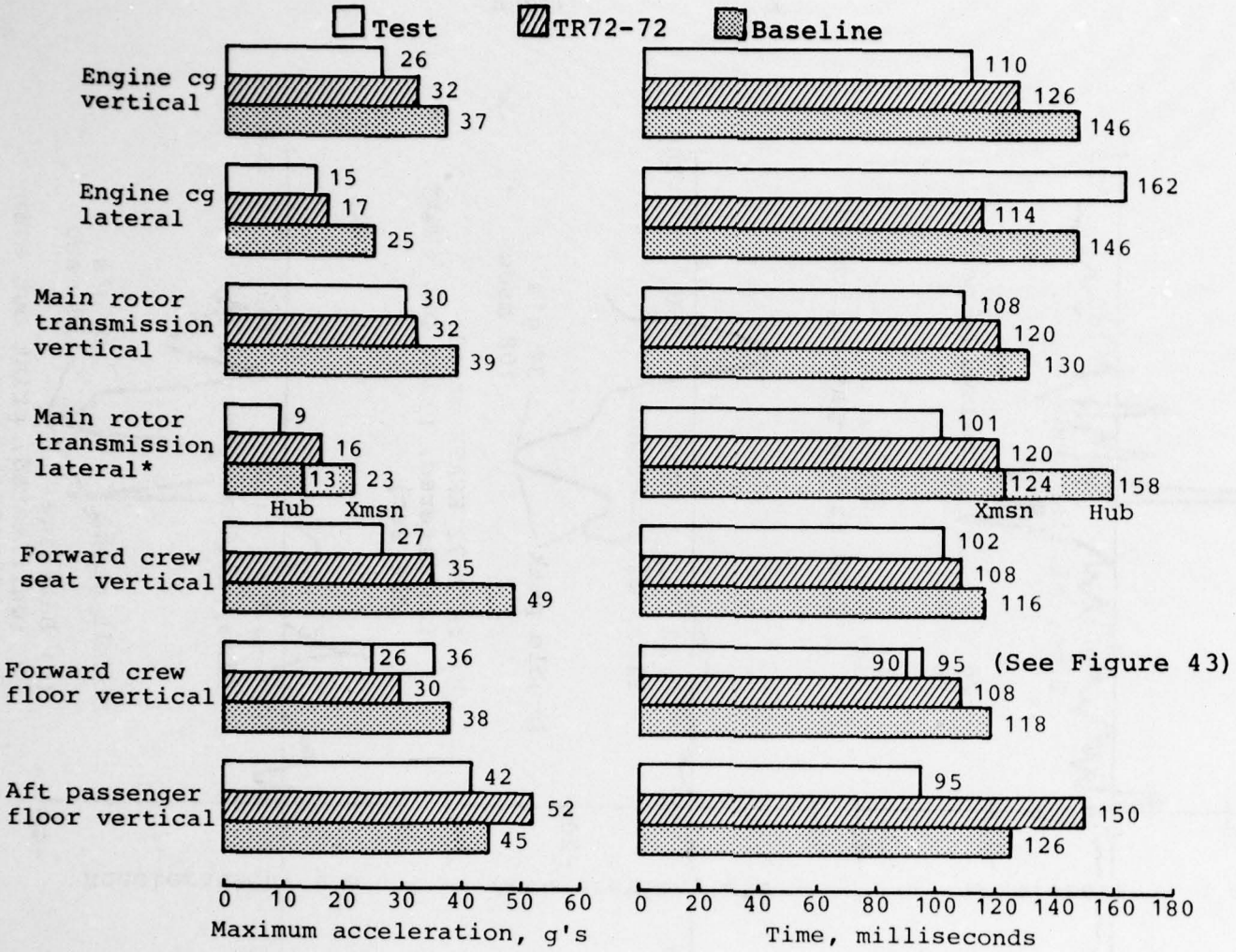

* Baseline model has separate transmission and rotor hub masses instead of single lumped mass of TR72-72 model.

Figure 42. Comparison of TR72-72 test data with original UH-1 KRASH model and baseline model.

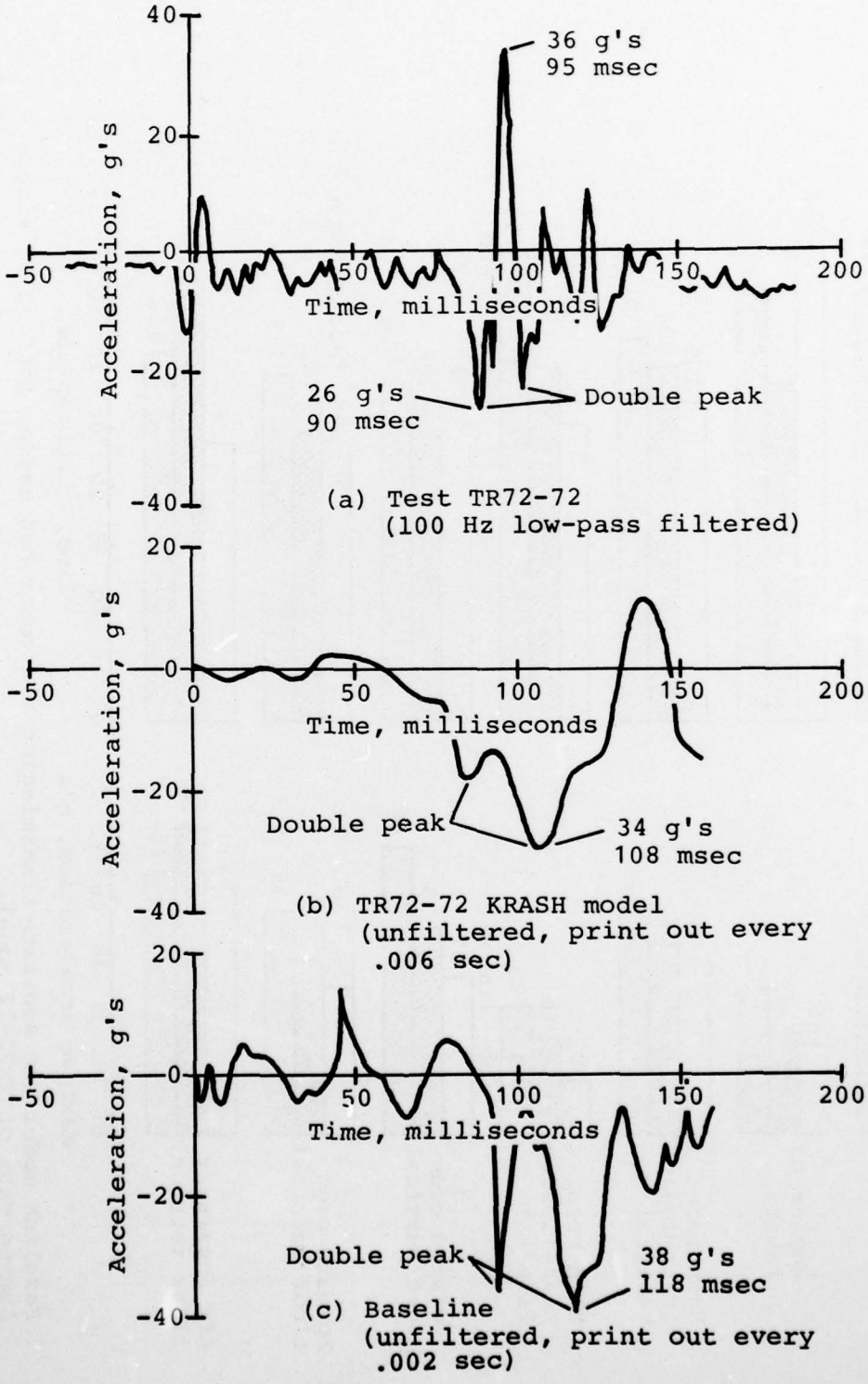

Figure 43. Comparisons of forward crew floor (mass point 16) vertical response for TR72-72 impact conditions.

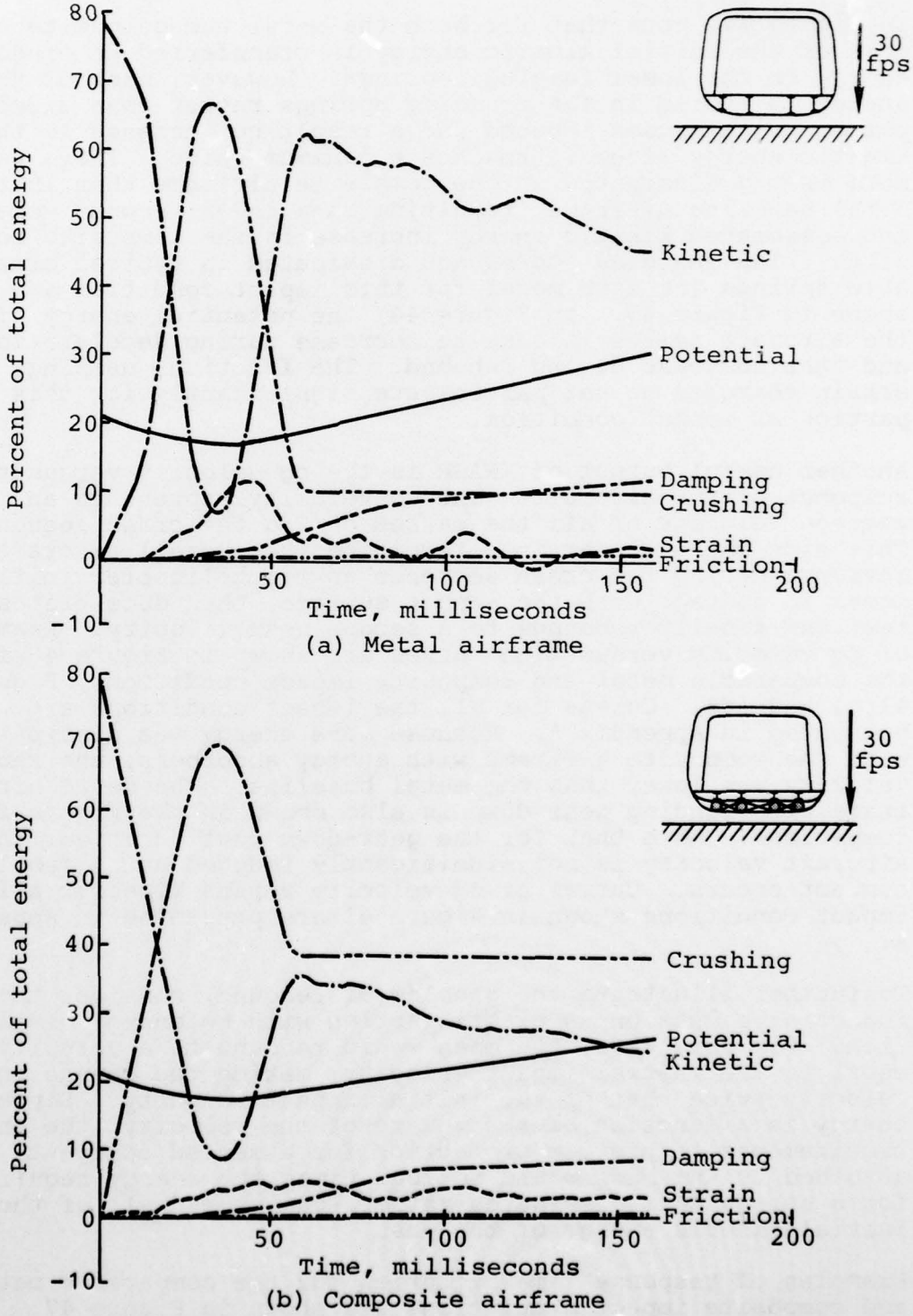

Figure 44. Comparison of metal and composite airframe energy distributions for 30 fps vertical impact on rigid surface with landing gear up.

AD-A075 163 BELL HELICOPTER TEXTRON FORT WORTH TX F/G 1/3
INVESTIGATION OF THE CRASH-IMPACT CHARACTERISTICS OF ADVANCED A--ETC(U)
SEP 79 J D CRONKHITE, T J HAAS, V L BERRY DAAJ02-77-C-0062
UNCLASSIFIED USARTL-TR-79-11 NL

2 OF 3
AD
A075163

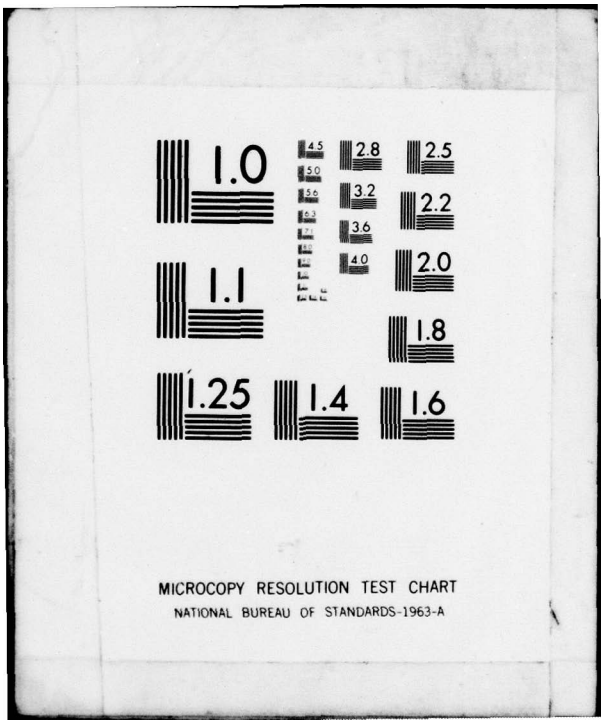
1.0
1.1
1.25
1.4
1.6
1.8
2.0
2.2
2.5
2.8
3.2
3.6
4.0
4.5
5.0
5.6
6.3
MICROCOPY RESOLUTION TEST CHART
NATIONAL BUREAU OF STANDARDS-1963-A

In Figure 44, note that for both the metal and composite cases most of the initial kinetic energy is transferred to crushing energy in the lower fuselage springs. However, much of the energy is stored in the crushing springs rather than dissipated, which causes rebound and a resulting increase in the kinetic energy after it reaches a minimum value. There was more energy dissipated in the composite airframe than in the metal baseline airframe, resulting in a lower rebound velocity and associated kinetic energy increase in the composite results. The energies stored and dissipated in typical crushable springs for each model for this impact condition are shown in Figure 45. In Figure 44, the potential energy of all the aircraft masses is seen to decrease during deceleration and then increase during rebound. The friction, damping, and strain energies do not participate significantly for this particular impact condition.

Another useful output of KRASH is the cg velocity versus time response of the aircraft. The cg velocity represents an average velocity of all the masses during the crash sequence. This aids the engineer in determining the overall aircraft response during the crash sequence as the helicopter initially comes in contact with the impact surface, then decelerates to rest and finally rebounds to a second peak velocity. Examples of cg velocity versus time curves are shown in Figure 46 for the comparable metal and composite impact conditions, Figures 41(c) and (d). Curves for all the impact conditions are presented in Appendix A. Because more energy was dissipated with the composite airframe with energy absorbers, the rebound velocity was lower than the metal baseline. The metal airframe with landing gear down is also shown in the figure for comparison. Note that for the gear-down configuration, the aircraft velocity is not significantly reduced until fuselage contact occurs. Curves of cg velocity versus time for all the impact conditions shown in Figure 41 are presented in Appendix A.

To further illustrate the problem of rebound, consider the impact of a mass on an elastic spring with no energy dissipation. For this case, the mass would rebound to a velocity equal to the initial impact velocity, making the change in velocity twice that of the initial impact velocity. Since energy is a function of the square of the velocity, the energy requirements to provide protection for a seated occupant attached to the mass would be four times the energy required for a spring that dissipated rather than stored all of the initial kinetic energy of the mass.

Examples of response time histories for the comparable metal and composite impact simulations are shown in Figure 47.

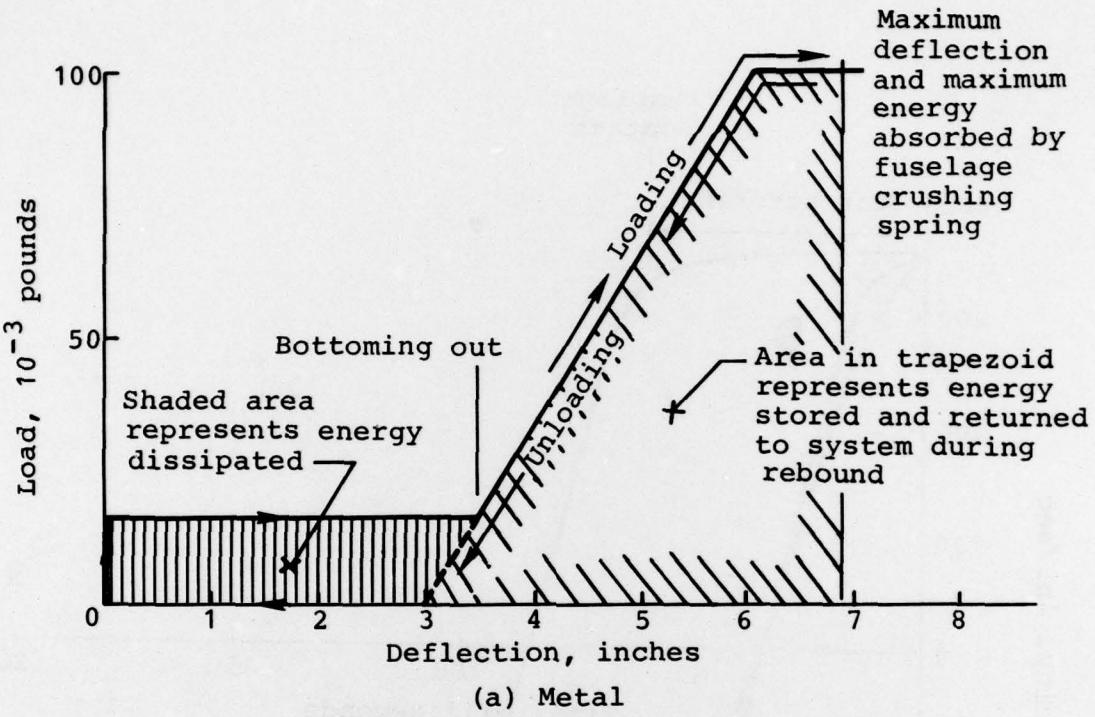

Figure 45. Energy stored and dissipated during fuselage crushing for metal and composite structures.

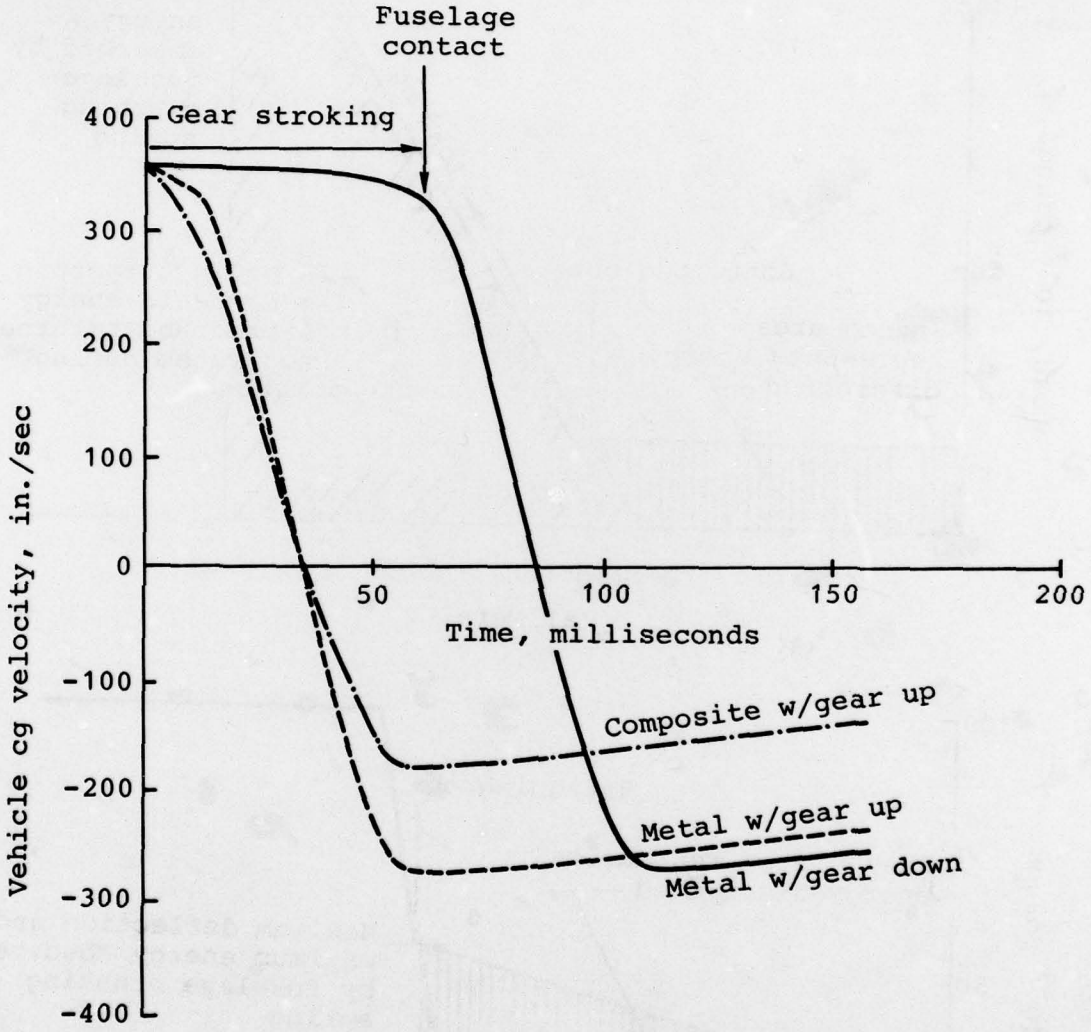

Figure 46. Comparison of vehicle cg velocity for 30 fps vertical impact on rigid surface.

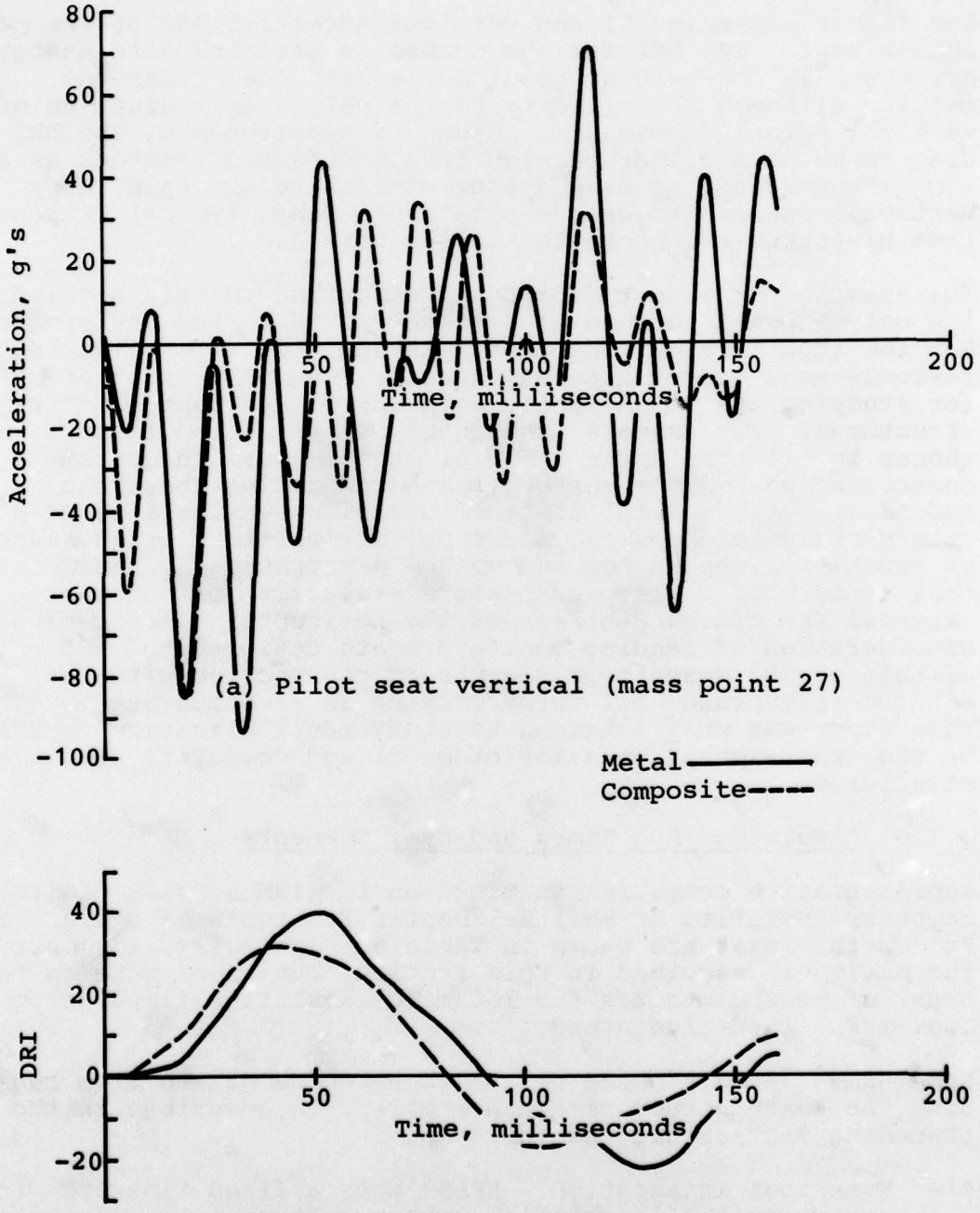

(a) Pilot seat vertical (mass point 27)

(b) Pilot seat DRI (mass point 31)

Figure 47. Comparisons of pilot seat response and DRI for metal and composite airframes.

The figure shows in DRI and vertical accelerations of the passenger seat. The DRI for the composite airframe with energy absorbers is shown to be about 20 percent lower than the metal. Although the validity of the DRI as an indication of vertical spinal compression injury is questionable, the DRI does serve as a filter of high frequencies and responds as a low frequency spring mass system similar to the upper body vertical response to seat excitation. Other typical response time histories are presented in Appendix A.

The examples of output from KRASH described in this section are only a small portion of available output from the program. For the impact conditions that were analyzed, typical output features were selected to demonstrate the application of KRASH for studying the crash-impact behavior of helicopter airframe structures. For example, the energy distribution feature was chosen to illustrate the value of this feature in quickly understanding how the energy is managed during the crash sequence. Other useful features are also available to help determine the chances for occupant survival in a crash, such as livable volume change and volume penetration by hazardous mass items. Of course, a complete evaluation of occupant survival and crashworthiness of the helicopter also involves consideration of landing gear and seats designed to meet certain crash-impact requirements in conjunction with the airframe structure - all three working as an integrated system. This study was only intended to study the application of KRASH to the crash-impact behavior of metal and composite airframe structures.

4.2.4 Simulation Run Times and User Comments

Representative computer run times on the IBM 370/168 digital computer installed at Bell Helicopter Textron's main plant in Ft. Worth, Texas, are shown in Table 5. Typically, for most of the analyses described in this section, run times were on the order of 30 CPU minutes for 160 msec simulation times using .001 msec fixed-time steps.

Some user comments based on the experiences gained from running the KRASH structure crash simulations described in the preceding section are the following:

- Numerical integration - KRASH uses a fixed time step in its numerical integration scheme. It would be easier and more efficient to use a variable time step determined by the program as it proceeds through the simulation. Smaller time steps could be used when rapid changes in response are occurring and larger time steps as the response becomes smoother.

TABLE 5. COMPARISON OF IBM 370/168 COMPUTER RUN TIMES FOR KRASH ANALYSIS CASES

Case	CPU Time (Min)
Baseline, Δt = .010 msec, t_{max} = 160 msec, dp/dt* = 200, w/64 printer plots	28.50
Baseline, Δt = .015 msec, t_{max} = 160 msec, dp/dt = 400, w/64 printer plots	17.58
Baseline, Δt = .010 msec, t_{max} = 160 msec, dp/dt = 200, w/o printer plots	26.58

dp/dt is print interval

- A stable solution was difficult to obtain for some cases when the following occurred:
  - Severe impact conditions at velocities in excess of 30 fps where bottoming out occurred quickly and the structure became very stiff.
  - There was a lack of sufficient energy absorption via external crushing springs. Energy-absorbing structure allows the structure to be slowed down over a longer period of time with lower accelerations. Lack of energy-absorbing structure is similar to having structure that is too stiff.
  - Incompatible off-diagonal stiffness matrix terms in critical areas of the model. A clue to this problem is when negative strain energies occur.
  - Structural elements are too stiff. An indication of this is when the element frequencies exceed 1000 Hz.

- Some FORTRAN coding errors that were discovered are the following:

  - The printer plot routine contained array dimensioning errors that occurred randomly when plotting element loads and relative deflections.

  - No input for external crushing springs caused all material properties to be zeroed out.

  - Maximum external spring load after bottoming out was internally set to ten times the load just prior to bottoming out which in some cases did not slow the vehicle down. This has since been fixed by making the cutoff load ten times the maximum load used before bottoming out.

  - The damping coefficient for beam elements remains a constant value even though the element stiffness has been reduced by the stiffness reduction factor KR. The damping should also be reduced by the same factor as the stiffness.

- For engineers accustomed to user-oriented structural analysis digital computer codes, such as NASTRAN, the input to KRASH seems cumbersome. A preprocessor to help convert NASTRAN input data to KRASH input may partially solve this problem. This would also facilitate user training on the KRASH program.

As a final comment on the use of the KRASH structure crash simulation, the most difficult problem found was that of deriving the nonlinear properties of the crushable springs and deformable beam elements. This part of the analysis requires the art and experience to know what is important in accurately representing the crash-impact behavior of the actual structure. Wittlin in References 48 through 51 has attempted to describe techniques for determining the nonlinear characteristics of aircraft-type structures. These reports should be reviewed by all engineers working in the area of structure crash simulation, whether the KRASH analysis is being used or not. Wittlin's guidelines, examples, and analysis techniques at least provide a good background for analyzing one's own particular structure. However, some testing will inevitably be required for each structure analyzed until a data bank of typical structure sections has been developed and experience has been developed sufficiently to accurately predict structure crash-impact behavior. In the future, structure inputs may be provided by detailed structure analyses such as DYCAST, but these techniques need validation.

4.2.5 Conclusions

4.2.5.1 Evaluation of KRASH

- The KRASH analysis was found to be a useful tool for studying effects of various impact conditions and parameter variations on the overall crash-impact response of the airframe, whether the airframe is of metal or composite construction.

- Excellent documentation and correlation of the KRASH program are found in References 48 through 51. These documents should be useful to anyone working in the area of structure crashworthiness and simulation, whether or not the KRASH program itself is used.

- KRASH has many useful built-in crashworthiness features, such as:

  - Energy summaries
  - Occupiable volume change and penetration
  - Automatic rupture of elements
  - DRI and man model
  - Friction and plowing
  - Soil
  - Sloped surface impact

- Because of the coarse mathematical representation of the structure, the major problem with performing a KRASH analysis is involved in the 'art' of modeling and obtaining structure inputs to the program.

4.2.5.2 Recommended Improvements to KRASH

- Because the airframe structure often fails locally at a weak spot, a plastic hinge element for the internal structure modeling is needed. Also, scalar springs would be useful for modeling seats and main rotor pylons.

- The user should be allowed to apply arbitrary boundary conditions to the model.

- A 12 by 12 direct input matrix option would essentially allow substructuring.

- KRASH now uses a fixed-time step integrator. A variable time step procedure should be employed to improve run times. Also, an implicit integrator such as the Newmark-Beta method should reduce run times as well as improve numerical stability.

- A rigid body motion analysis for impacts such as rollover where no significant structure response occurs for long periods of time would greatly reduce solution times.

- Damping should be added to the external springs.

- The stiffness reduction features (KR) should apply to element damping as well as stiffness.

- Input improvements

  · Add descriptive names to identify data types

  · Allow arbitrary mass point numbering by user

  · Develop a NASTRAN to KRASH imput preprocessor

- Add structure plotting capability - deformed and undeformed.

4.3 DYCAST ANALYSIS

The results of two mathematical crash simulations using the DYCAST[46] [47] finite-element computer code are described in this section. The two cases studied were on an all-composite helicopter fuselage cockpit section with energy absorbers and a conventional metal cockpit section that provided a baseline of comparison. Both were subjected to a vertical impact at 30 fps, in a level attitude, onto a rigid horizontal surface.

The purposes of this investigation were to:

- Demonstrate the use of a finite-element method for detailed simulation of structural crash behavior

- Compare the crash responses of the particular composite and baseline sections.

- Evaluate DYCAST as a design analysis tool for composite airframes.

A general description of the analysis is given here. Geometric details of the idealized structures are presented in Appendix B. Since nonlinear finite-element crash simulations

in general -- and DYCAST in particular -- are still in the development stage, it was decided to limit the study to a detailed model of the crew compartment fuselage structure only. No attempt was made to perform a full crashworthiness evaluation of the aircraft. Even so, the fuselage sections modeled were among the largest nonlinear crash models analyzed so far, with 144 nodes, 422 elements, and 471 degrees of freedom.

4.3.1 DYCAST Features

The major DYCAST features of importance to the engineering user are:

- Nonlinear spring, stringer, beam, and orthotropic thin sheet elements.
- Plasticity.
- Very large deformations.
- Variable problem size.
- Restart (stop, review, and continue).
- Deletion of failed members.
- Four different numerical solution methods, three with internally varied time steps.
- Modular formulation.

The basic element library of stringers (axial stiffness only), beams (axial, two shears, torsion, and two bending stiffnesses), and orthotropic membrane skin triangles (in-plane normal and shear stiffnesses) allows the convenient modeling of aircraft-type structures built up from such components. The nonlinear spring element is a general-purpose axial stiffness unit with a user-specified force-displacement curve.

The changing stiffnesses in the structure are accounted for by plasticity (material nonlinearity) and very large deflections (geometric nonlinearities). The plasticity enters the model through the nonlinear stress-strain curve for each element. The geometric nonlinearities are modeled by reforming the structure into its new shape after small time increments, while accumulating deformations, strains, stresses, and forces. In this way, the progressive crushing and folding of structural elements can be followed. The nonlinearities due to combined loadings (such as beam-column effects) are maintained, and the stiffness of the elements can vary depending on the combination of loads imposed on them.

The restart feature allows for a large problem, or one of long event duration, to be run in small time sequences. This minimizes the tie-up of computer facilities, allows the user to examine the response as it progresses, permits the ending of a simulation if a critical damage occurs, or permits the deletion of elements that appear to have failed as indicated by the stress and strain output.

The numerical time-integrators available are fixed-step central difference, modified Adams, Newmark Beta, and Wilson Theta. The last three have variable time steps, controlled internally by a solution convergence error measurement. Thus, the time steps increase and decrease as required during the simulation.

The modular formulation allows for easier addition of new elements, material types, time-integrations, etc. by structuring the program in well-defined modules with a minimum of interfaces with other modules.

The overall accuracy and computational cost of the simulation will depend on the quantity of elements used (fineness of the geometric model). The finer the model, the greater the accuracy and cost.

A user-oriented input/output format is utilized. The primary input data groups are:

- Numerical controls and options.
- Geometry (nodes and elements).
- Motion constraints (and impact surface).
- Initial conditions.
- Rigid masses.
- Material properties.
- Element cross-section geometries.
- Applied dynamic loads (if any).

The output data are in the form of:

- Printed displacement, velocities, accelerations, strains, stresses, and forces.
- Plotted histories of displacement, velocity, and acceleration at chosen nodes.

- Time-sequenced drawings of deforming structure or portions from any viewing angle.

4.3.2 Actual Fuselage Sections

The fuselage sections to be modeled were defined by Bell Helicopter Textron and idealized and analyzed by Grumman Aerospace Corporation. Both the conventional metal section and the all-composite section with energy absorbers were impacted vertically into a rigid horizontal surface at 30 fps. This impact speed was derived by assuming that an initial speed of 42 fps, specified in MIL-STD-1290, would be attenuated by the landing struts to 30 fps before the fuselage bottom contacted the ground.

The baseline metal section was taken from a representative troop-carrying helicopter, as shown in Figure 38, and the composite section was designed by Bell to replace it. The two cockpit sections therefore had the same overall dimensions indicated in Figure 48 and were designed for comparable flight loads. They both carried two 150-pound point-masses representing crew members on rigid weightless seats with four legs attached to seat rails. Their floor structures were composed mainly of four longitudinal beams, four transverse bulkheads, an outer belly skin, and a floor panel covering. The longitudinal beams were located at 14 and 30 inches from the centerline, while the three rearward bulkheads were located at 15, 26, and 37 inches aft of the front bulkhead. The forward doorpost and roof frame surrounding the crew carried four simulated equipment masses on the roof totaling 40 pounds, as shown in Figure 48, positioned 14 inches from the centerline. Note that only the central section between the two inboard main beams is in initial contact with the ground surface. The outboard fuselage is above the ground at impact.

The crew masses were 22 inches above the floor surface, directly above the third bulkhead, midway between the inboard and outboard beams. The seat rails were fastened to the top caps of the main beams, with the seat leg attachments positioned midway between the adjacent bulkheads, just above the vertical stiffeners on the beam webs. Vertical web stiffeners are shown as dashed lines.

The conventional metal section (Figure 48a) had full-depth webs on the beams and bulkheads. In the composite section (Figure 48b), the lower portions of the longitudinal beams were replaced by energy-absorbing crushable tubes and the lower parts of the bulkheads were replaced by diagonal tension straps and transverse formers attached to the skin.

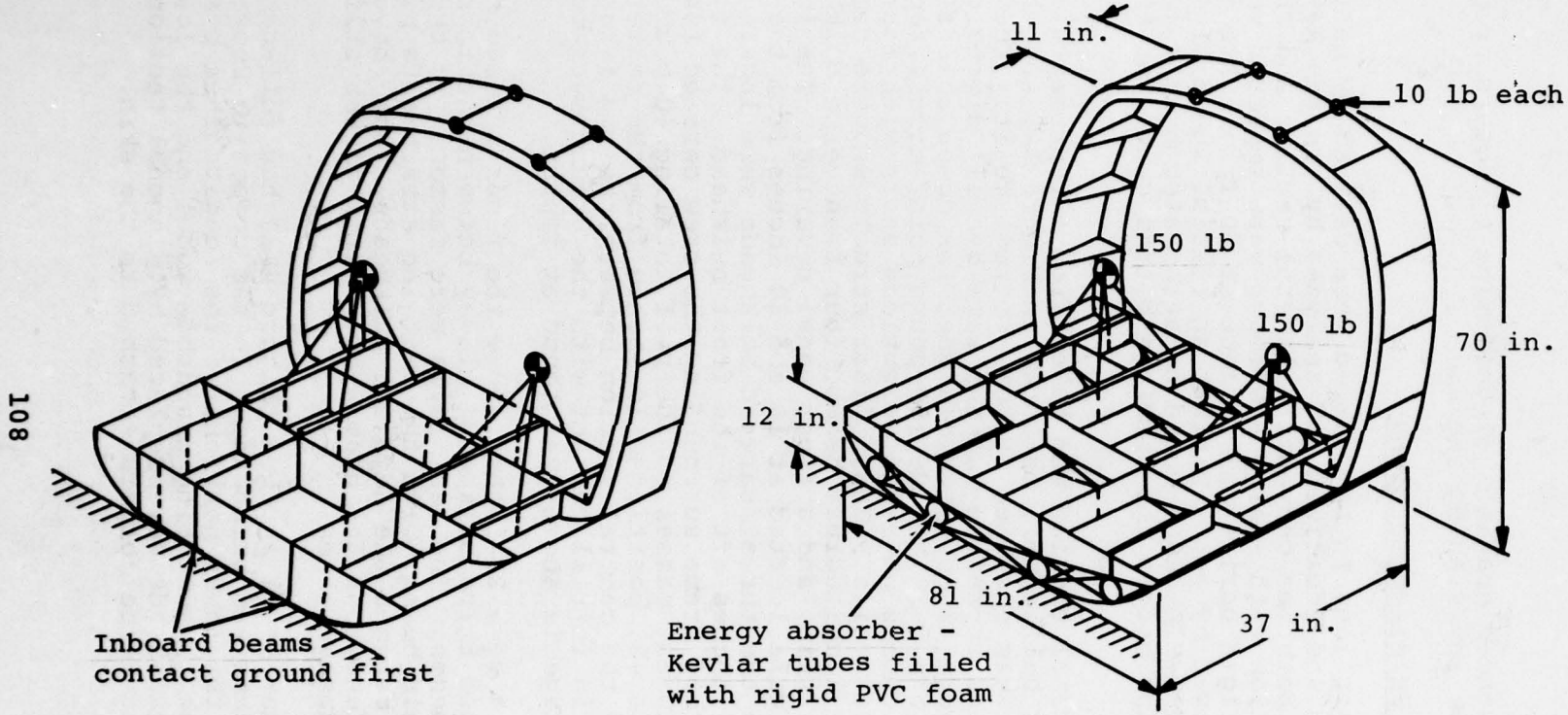

a. Metal section.

b. Composite section.

Figure 48. Original fuselage sections, floor panel removed.

The metal baseline section had titanium seat rails, 7075-T6 aluminum longitudinal beam caps, and all remaining structure 2024-T3 aluminum. The composite section had the same seat rails; ±45° Kevlar/epoxy laminate for the beam webs, bulkhead webs, energy-absorbing tube walls, and doorpost webs; and 0°/90° Kevlar/epoxy laminate for the belly skin and floor cover panels. A multidirectional graphite/epoxy laminate was used for the longitudinal beam caps and transverse skin formers, while unidirectional graphite/epoxy reinforced the bulkhead caps and formed the corner angles for the doorposts and roof frame. The energy-absorbing tubes were filled with PVC foam and were braced by the transverse diagonal tension straps of unidirectional Kevlar/epoxy.

4.3.3 Idealized Fuselage Sections

The idealized fuselage sections are shown in Figure 48. For this analysis, only the left half of each section was modeled because of symmetry. Each fuselage section was broken down into its natural structural components: beam webs and caps, bulkhead webs and caps, skin panels, and energy-absorbing tubes. Each of these was further divided into elements using stringers, beams, membrane triangles, and nonlinear springs. In Figure 49, beams are drawn as double or thick lines, stringers and nonlinear springs as single or thin lines. Membrane triangles are easily identified, with diagonal lines between triangles representing only their common boundaries, not stringer elements.

A general description of each idealized section follows, while further geometric details are given in Appendix B.

4.3.3.1 Metal Baseline Section Model. In the metal baseline model, the bulkheads and longitudinal beams were generally idealized using isotropic membrane triangles for the webs and beam elements for the seat rails, web caps, and vertical stiffeners. The exception was forward of the second bulkhead, where the beam elements were replaced by stringers. This was done because local bending of caps and stiffeners was assumed to be important only near the seat and doorpost attachments. Generally, less modeling detail was used forward of the second bulkhead (as apparent in Figure 49a), since less load and deformation was expected there.

The floor structure contained several large unstiffened web and skin panels that were expected to deform transversely under in-plane compression loads. They were the four rectangular skin panels, inboard and rearmost in Figure 49a, and the inboard web panels on the three rearmost bulkheads. The membrane triangles alone had no initial transverse stiffness to approximate any out-of-plane vibration, buckling, or collapse.

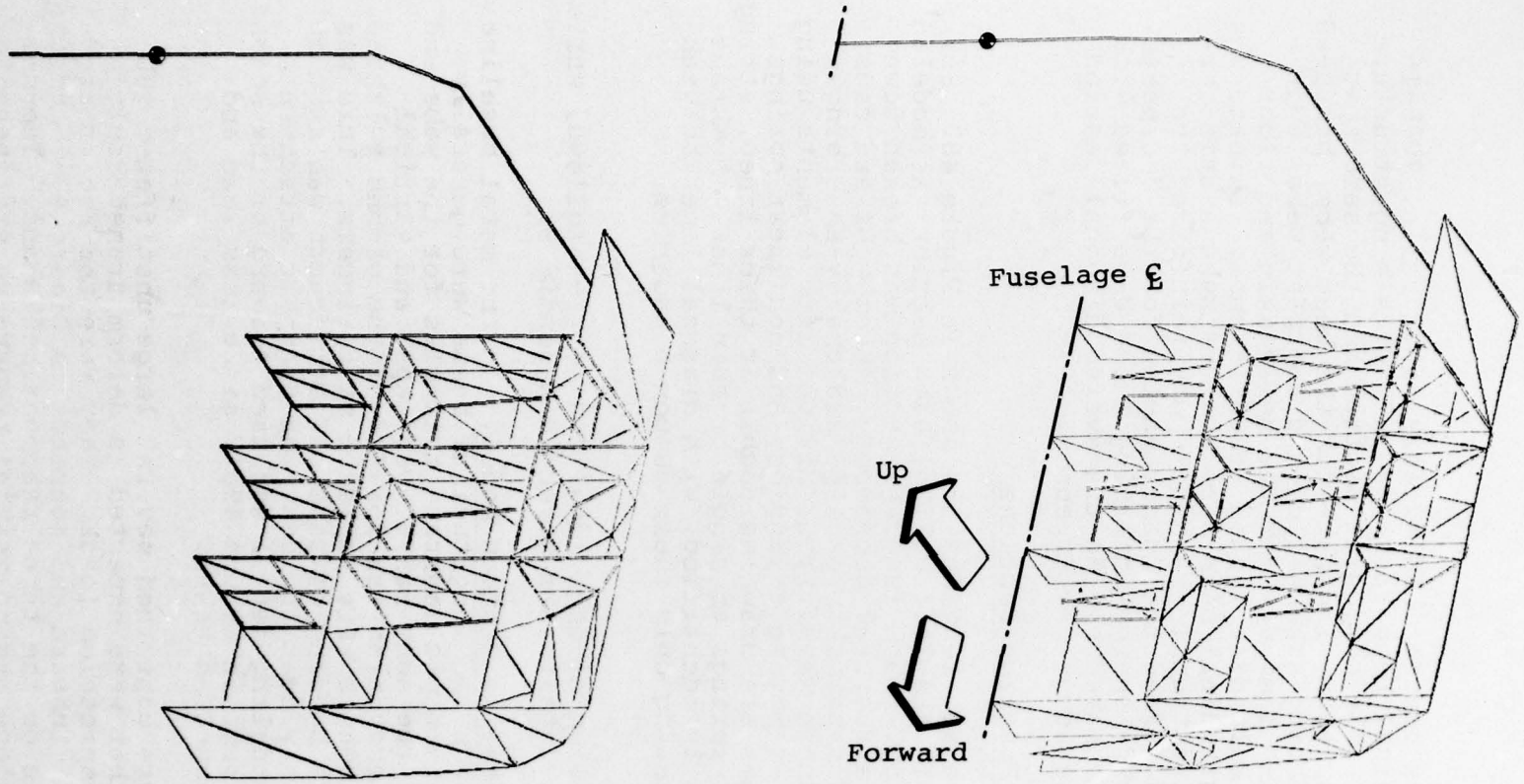

a. Baseline metal section.

b. Composite section with energy absorbers.

Figure 49. Idealized fuselage cockpit sections, floor panels and seat removed.

Therefore, false beams were added in a cross-grid meeting in the center of each panel and visible on the three inboard bulkhead web panels in Figure 49a. These beams were of thin rectangular cross section, with the same thickness as the web sheet and having half the panel width. In this way, the out-of-plane bending stiffness of these panels was approximated.

The intersection of the bulkheads and longitudinal beams was formed by four angle stiffeners connecting the webs, forming a vertical beam of cruciform cross section. That cross section was not in the DYCAST element library at that time, so the cruciform beams were modeled by two tee-section beams back-to-back, with the same combined elastic stiffnesses as the cruciform.

The roof frames and doorpost were specified as channel beams built up from thin webs and angles. These were modeled with a single arch of beam elements, as shown in Figure 49, except for the lower part of the doorpost. This lower part was modeled in more detail, using triangles for the outer skin panel and beam elements for the frames to distribute the roof loads more evenly into the floor edge. The two 10-pound equipment masses on the roof were replaced by a single 20-pound mass with the proper value of rotary inertia.

The belly skin panels and floor cover panels were represented by membrane triangles. The floor cover is deleted from Figure 49 to more clearly show the subfloor structure. Since the outer part of the floor structure was cantilevered above the ground, a downward bending motion was expected, imposing a compressive load on the belly skin panels which would thereby buckle them. Therefore, a false beam grid was added to the belly skin to account for vertical buckling.

The material behavior of the aluminum and titanium used in the metal baseline section was represented by elastic-perfectly plastic stress-strain curves, with appropriate Young's moduli, Poisson's ratios, and yield stresses for each material, as specified in Table 6.

The metal section model had 111 nodes, 348 elements, and 419 degrees of freedom (unknown displacements).

4.3.3.2 Composite Section Model. The composite section (Figure 49b) was idealized in the same way as the metal section, except that orthotropic membrane triangles represented all the webs, skins, and tube walls. Furthermore, the lower portion of the subfloor was quite different, as described above under "Actual Fuselage Sections." The bending, shear, and axial stiffnesses of the tubes were modeled by using orthotropic membrane triangles to form hollow, square, diamond tube walls

TABLE 6. MATERIAL PROPERTIES FOR METAL BASELINE SECTION

Material	Weight Density (lb/in^3)	Compression Data			Tension Ultimate Strain	Applicable Components
		Modulus (10^6 psi)	Poisson's Ratio	Yield Stress (10^3 psi)		
Titanium -6AL-4V(STA) Extrusion	0.160	16.0	0.31	180	0.08	Seat Rails
Aluminum 7075-T6 Extrusion	0.101	10.5	0.33	92	0.07	Main Beam Caps
Aluminum 2024-T3 Sheet and Extrusion	0.100	10.7	0.33	50	0.18	All Except Seat Rails and Beam Caps

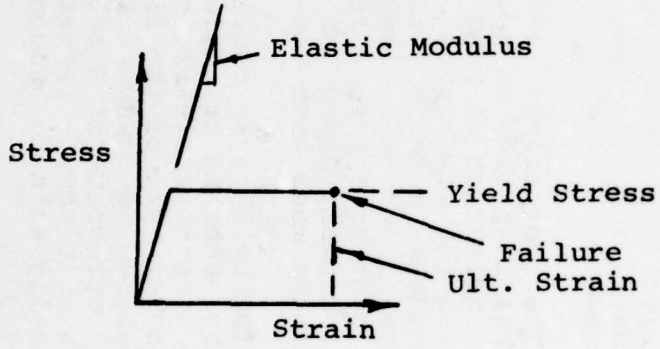

that could flatten as the tube crushed. The vertical crushing behavior of each energy-absorbing tube was represented by seven vertical nonlinear springs having known force-displacement curves. The load-deflection curve of the vertical crush springs is shown in Figure 50 for a unit length of tube. During rebound, the unloading from any peak load proceeded along the initial slope, as shown by the dashed line. The diagonal tension straps below each bulkhead were modeled by nonlinear springs having no compression load capacity; that is, they were treated as cables that would go slack when compressed.

The material behavior of the composite laminates was represented by a linear elastic stress-strain curve up to the failure stress. Thus, these materials were assumed to be completely brittle, with no plastic deformation before failure. Their material properties are displayed in Table 7. The failure criterion used for these materials was to assume that brittle failure would occur in an element whenever a calculated strain component exceeded its specified failure level. In the current version of DYCAST such failures are determined by scanning the element strain printout data. The failed element's stiffness can then be removed from the simulation at the next convenient point in time by restarting with a "delete" specified for that element. In practice, it was not feasible to print out the strain data for all the elements, so only those elements near the seat attachments and on the roof and door frames were examined for failure.

The composite model contained 144 nodes, 422 elements, and 471 degrees of freedom.

4.3.4 Simulation Results

The output data for each simulation consisted of printed data at intervals varying from 2 to 4 time increments (20 to 320 μsec) and a tape of the complete motions at all the nodes at every time increment. From each tape, approximately 30 traces of displacement, velocity, and acceleration histories were automatically machine-plotted for certain selected nodes, including the crew and equipment masses, those on the roof and door frames, and those under the crew seat attachments. From the same tapes, approximately 100 machine drawings were generated showing the deformed state of each structure at many time intervals for different views. These views included several of the entire structure, plus one each of the major subsections (bulkheads, main beams, skin panels, etc.). In this way, a comprehensive qualitative and quantitative display of the structural response was available for both simulations. The data reported here are necessarily restricted to a small part of the total.

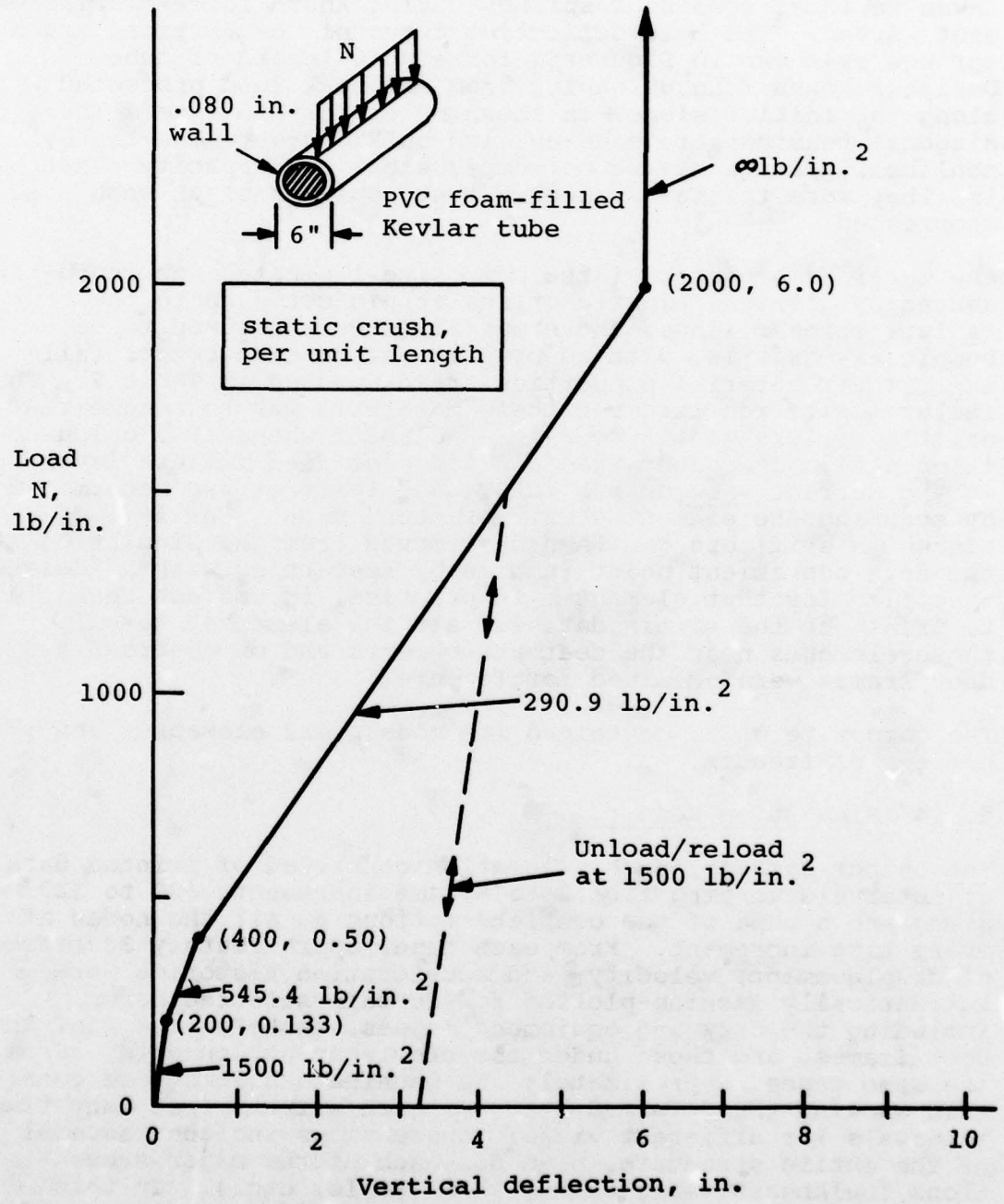

Figure 50. Energy absorber characteristics.

TABLE 7. MATERIAL PROPERTIES FOR COMPOSITE SECTION

Material	Weight Density (lb/in.^{3})	Elastic Moduli (10^6 psi)	Poisson's Ratio	Yield Stress (10^3 psi)	Ultimate Stresses (10^3 psi)	Ultimate Strains	Applicable Components
Titanium -6Al-4V(Sta) Extrusion	0.160	16 (compr) 6.1(shear)	0.31	180 (compr)	180 (compr)	0.08 (tens)	Seat Rails
Kevlar 49/Epoxy, 181 Cloth 0°/90° Symmetric Balanced Laminates	0.048	4.3(T,C;0°,90°)* 0.3(S;0°/90°)	0.34	---	70(T;0°,90°) 25(C;0°,90°) 7.0(S;0°/90°)	0.163(T;0°,90°) 0.0058(C;0°,90°) 0.0233(S;0°/90°)	Belly Skin Panels (.040 in.) Floor Cover Panels (.055 in.)**
		1.1(T;C;±45°) 1.6(S;±45°)	0.83	---	14(T;±45°) 14(C;±45°) 18.6(S;±45°)	0.0127(T;±45°) 0.0127(C;±45°) 0.0116(S;±45°)	Main Beam Webs (.080 in.) Bulkhead Webs (.080 in.) Doorpost Webs (.040 in.) Tube Walls (.080 in.) Blkhd-to-Beam Angles(.080 in.)
Kevlar/Epoxy Unidirectional Laminate	0.048	11(T,C;0°) 0.3(S;0°/90°)	0.34	---	160(T;0°) 40(C;0°) 7.0(S;0°/90°)	0.0145(T;0°) 0.0036(C;0°) 0.0233(S;0°/90°)	Diagonal Tension Straps (.260 in.)
Graphite/Epoxy T300/5209, $[0_4/\pm 45\ /90]_s$ Laminate	0.058	13.1(T,C;0°) 5.44(T,C;90°) 2.15(S;0°/90°)	0.30	---	100(T,C;0°) 50(T,C;90°) 24(S;0°/90°)	0.0076(T,C;0°) 0.0038(T,C;90°) 0.0112(S;0°/90°)	Main Beam Caps (.076 in.) Skin Formers (.076 in.)
Graphite/Epoxy T300/5209 Unidirectional Laminate	0.058	20(T,C;0°) 0.93(S;0°/90°)	0.30	---	170(T,C;0°) 13.8(S;0°/90°)	0.0085(T,C;0°) 0.0148(S;0°/90°)	Bulkhead Flanges (.045 in.) Doorpost Beams (.015 in.)

* T = Tension, C = Compression, S = Shear

** Floor cover panels were sandwiched, with .040 in. top skin, .015 in. bottom skin, and .75 in. Nomex core.

The metal baseline simulation covered 10 msec of event time, with 71 time steps, using 19 minutes of computer time (CPU). The composite model simulation covered 30 msec, with 197 time steps, using 56 minutes of CPU time. The Newmark Beta numerical time integrator option with variable time steps was used in both cases.

4.3.4.1 Metal Baseline Section Results. The most significant events during the impact simulation for the metal baseline section were:

- 0.1 msec: plastic compression in main beam under inboard seat legs.
- 0.5 msec: crew mass peak acceleration 1122 g, plastic bending in seat rail under inboard legs.
- 1.3 msec: crew mass maximum downward displacement 0.23 inch, plastic bending in upper door post.
- 2.0 msec: slight plastic buckle of belly skin panels, plastic tension of floor cover panels, vertical oscillations of equipment mass begin.
- 2.4 msec: plastic bending in roof frame at equipment mass.
- 7.4 msec: doorpost buckle begins.
- 7.9 msec: upper doorpost local bending failure.
- 10.0 msec: end simulation.

The deformed structure of the baseline metal section is shown in Figure 51 with the seat and floor panels removed at the beginning and end of the simulation. Very little deformation of the subfloor structure can be seen, but the roof beam has deformed downward while the vertical doorpost has buckled outward. There is also a slight forward buckle of the middle web on the aft bulkhead. Figure 52 shows only the main beams and the belly skin. Note that the skin panels buckled slightly, while under the inboard seat legs the stiffened webs on the inboard longitudinal beam also buckled slightly.

The vertical motion histories of the 150-pound crew mass are given in Figure 53. The crew mass on its rigid seat was subjected to a peak upward acceleration of 1122 g at 0.5 msec

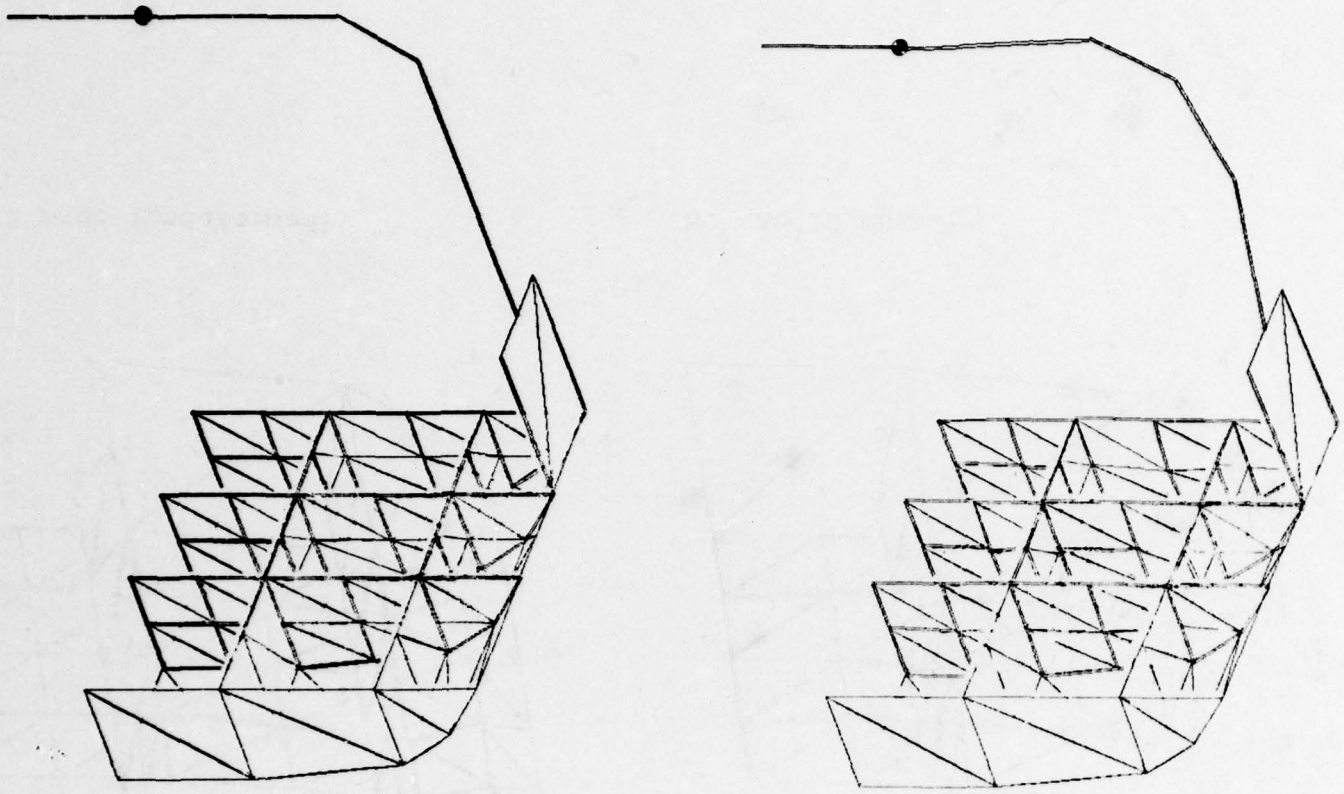

a. At 0 msec (undeformed).

b. At 10 msec.

Figure 51. Baseline metal section deformations, floor panels and seat removed.

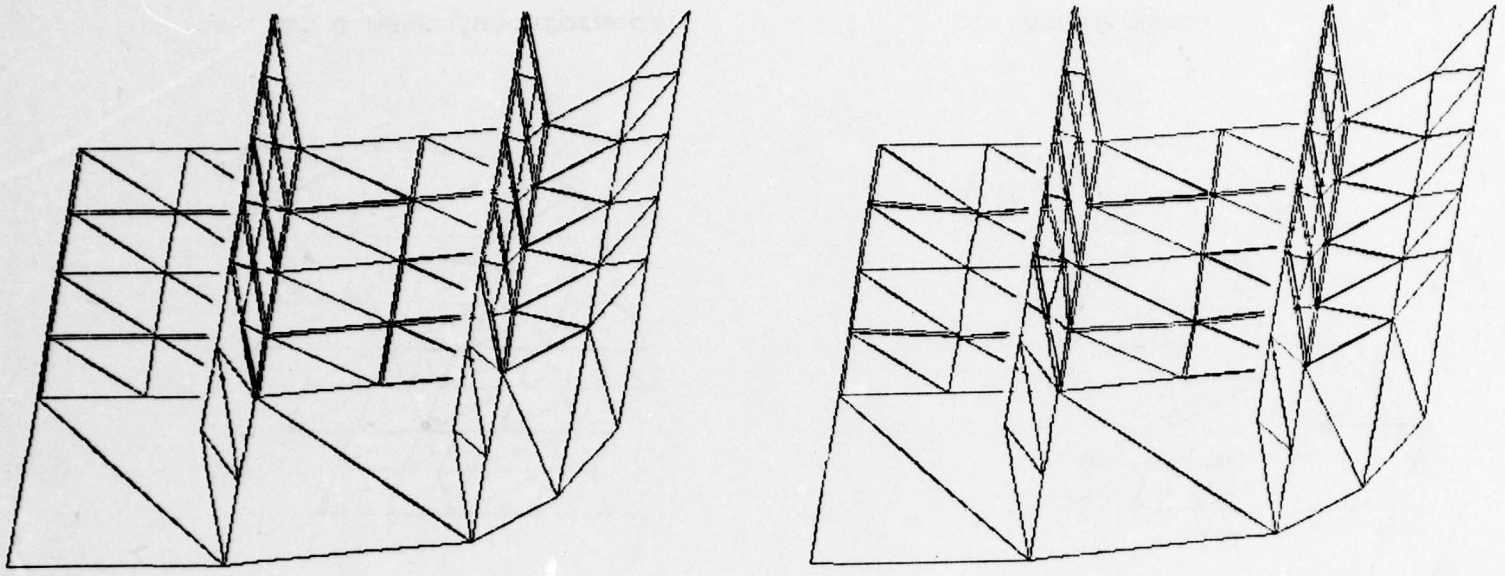

a. At 0 msec (undeformed).

b. At 10 msec.

Figure 52. Metal baseline section skin and beam deformations.

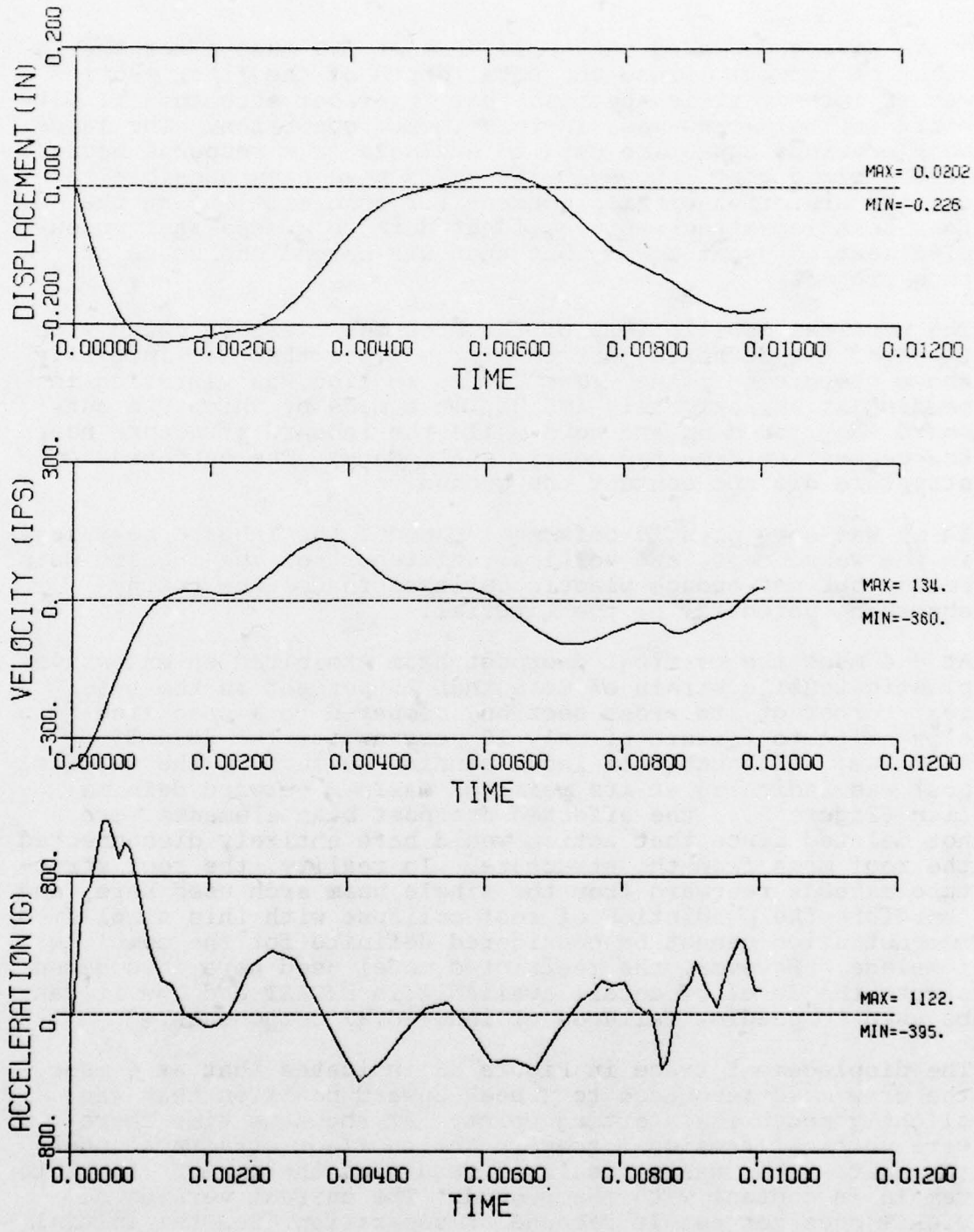

Figure 53. Vertical motion histories of crew mass in metal baseline section.

while moving downward only 0.23 inch at 1.3 msec after the instant of impact. Since the total depth of the floor section was 12 inches, it is apparent that the floor structure is very stiff for this crew mass in this impact condition. The large accelerations cannot be used to evaluate crew response because of the rigid seat. However, it could have been possible to use the histories of displacement (or acceleration) at the four seat leg attachments as input data to a separate, uncoupled seat/occupant model, but that was beyond the scope of this project.

The vertical oscillations of the crew mass were in phase with those of the outboard portion of the floor that was initially above the ground plane. The entire section was vibrating in bending at approximately 125 Hz, in a mode by which the outboard edge moved up and down while the inboard structure near the centerline remained nearly stationary. The outboard structure did not contact the ground.

There was some plastic deformation under the inboard seat legs in the webs, caps, and vertical stiffeners of the inboard main beams, but not enough plastic collapse to use the energy-absorbing potential of the material.

At 8.4 msec the vertical doorpost beam exhibited an excessive plastic tensile strain of more than 25 percent in the outer rear corner of its cross section, compared to a specified elongation-to-failure of only 18 percent for the 2024-T3 aluminum. Although this local bending failure of the vertical post was indicated at its point of maximum outward deformation (Figure 51), the affected doorpost beam elements were not deleted since that action would have entirely disconnected the roof mass from the structure. In reality, the roof structure extends rearward from the single beam arch used here, and therefore the prediction of roof collapse with this simplified demonstration cannot be considered definite for the complete fuselage. However, the restricted model used here does demonstrate the level of detail available in DYCAST and how it can be used to predict failures of individual components.

The displacement trace in Figure 53 indicates that at 6 msec, the crew mass rebounded to a peak upward position that was slightly above its starting point. At the same time there were vertical tension forces in the subfloor structure under the seat. This was a result of requiring the impact points to remain in contact with the ground. The current version of DYCAST does not permit rebound or separation from the initial impact surface. Therefore, after 4 msec, when the upward moving crew mass starts to pull up on the subfloor, the crew motions would have been somewhat different had the rebound been allowed. However, the peak motions had already passed,

and it is not likely that the subsequent accelerations with rebound would have been greater than the initial peak shown here at 0.5 msec.

The vertical motions of the 20-pound equipment mass on the roof frame are shown in Figure 54. The roof mass bulged downward 2.5 inches and had not yet reached its maximum deflection when the simulation was ended because of the earlier collapse of the doorpost. The accelerations of this mass oscillated rapidly with peaks at ±1100 g prior to the doorpost collapse, after which the oscillation amplitude increased.

4.3.4.2 Composite Section with Energy Absorbers. The significant events for the composite section were:

- 4.9 msec: local bending overstress in top cap of inboard main beam under seat legs.
- 5.0 msec: slight buckle of belly skin panels.
- 8.0 msec: crew mass peak acceleration 183 g.
- 8.4 msec: maximum 1.67 in. downward displacement of crew mass and floor structure, maximum crush of inboard tube, outer tube barely contacts ground, slight forward buckle of bulkheads under seat.
- 10.2 msec: bending failure in roof frame.
- 15.4 msec: maximum 4.1 in. downward displacement of overhead equipment mass.
- 30.0 msec: end simulation.

A set of views of the deformed structure without seat and floor cover is shown in Figure 55 at impact and near the moments of maximum downward displacement of the crew and equipment masses. The deformed belly skin, energy-absorbing tubes, and main beams are shown in Figure 56 at the same times. There is visible deformation of the roof beam, belly skin panels, bulkheads between inner and outer main beams, and the inboard energy-absorbing tube. The inboard tube maximum crush varied from 0.9 inch at the front to 1.8 inches at the rear, at 8.4 msec. At the same time, the rearmost point on the outboard tube just barely penetrated the ground plane by 0.11 inch. A provision could have been made in the idealization for this secondary impact by the use of a very stiff nonlinear spring with an initial "gap." However, this isolated slight barrier penetration was ignored as being not significant enough to justify the revision effort.

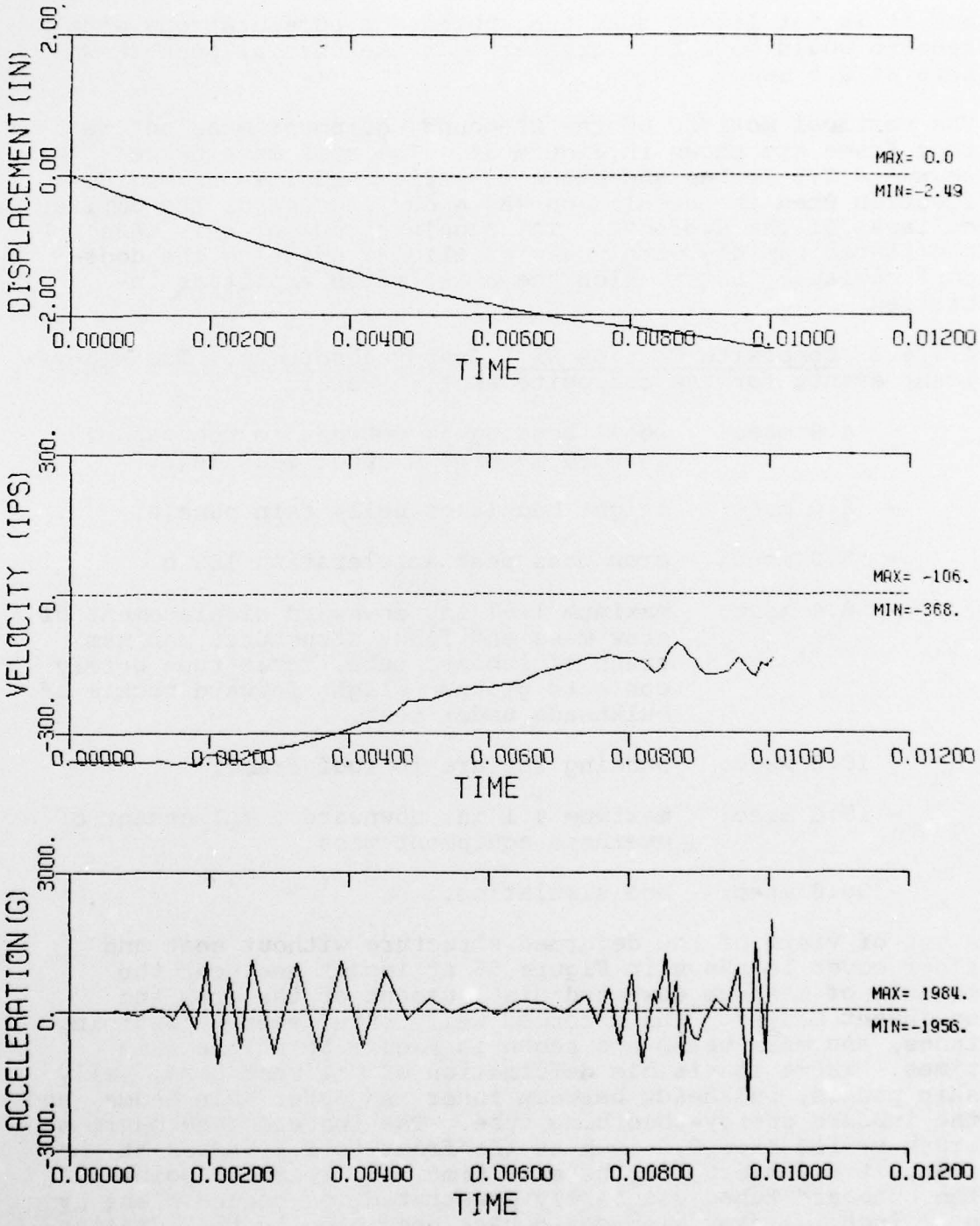

Figure 54. Vertical motion histories of the overhead equipment mass in the metal baseline section.

The inboard tube can be seen to be slightly flattened in Figure 55b, while the outboard tube remains undeformed. Most of the diagonal tension straps were slack all the time except for those extending from the top of the inboard tube downward to the bottom of the outboard tube.

The floor structure above the crash tubes remained intact except for local bending failures of the graphite/epoxy inboard main beam top caps directly under the inboard seat legs. At those points the extreme fiber tension stress exceeded its failure level. However, the beams were held together by the inboard titanium seat rail. Evidently, the vertical web stiffeners under the seat legs, formed by an offset of the web laminate, were insufficiently stiff and transmitted only a small share of the vertical load from the seat legs. This caused too much vertical load to be carried by bending of the longitudinal beam cap and seat rail. The addition of separate vertical web stiffeners at these positions should eliminate the beam cap failures.

A slight fore-and-aft deformation of the lower edge of the three aft transverse bulkheads can be seen in Figure 55 between the inner and outer main beams. Slight vertical buckling of the belly skin panels is visible in Figure 56.

The horizontal roof frame was subjected to bending overstresses along its entire length, and its collapse was therefore indicated. However, it must be noted, as in the case of the metal section, that the unmodeled fuselage structure aft of the front doorpost might have strengthened the doorpost and roof frame. While failure here may not occur in a more complete idealization of the fuselage, it does demonstrate the capability of the DYCAST code to predict failures.

An exterior left-side view of the idealized composite section appears in Figure 57. Responses are shown at the same times as in the two previous figures. These views show the downward deformation of the lower floor structure and subsequent upward rebound. The rearward mass distribution caused a slightly greater downward motion at the rear than at the front.

Figure 58 shows a set of left side views of the inboard main beam and tube assembly, with attached inboard seat legs and crew mass. The peak crush state of the inboard tube appears in Figure 58b. The vertical crush of the tube increased linearly from 0.9 inch at the front to 1.8 inches at the rear, out of an initial undeformed depth of 6.0 inches. This deformation can be clearly seen in Figure 58c, in which the deformed and undeformed views are superimposed relative to the common ground surface. In Figure 58d, the same two views are superimposed so that the main beam webs coincide. This shows

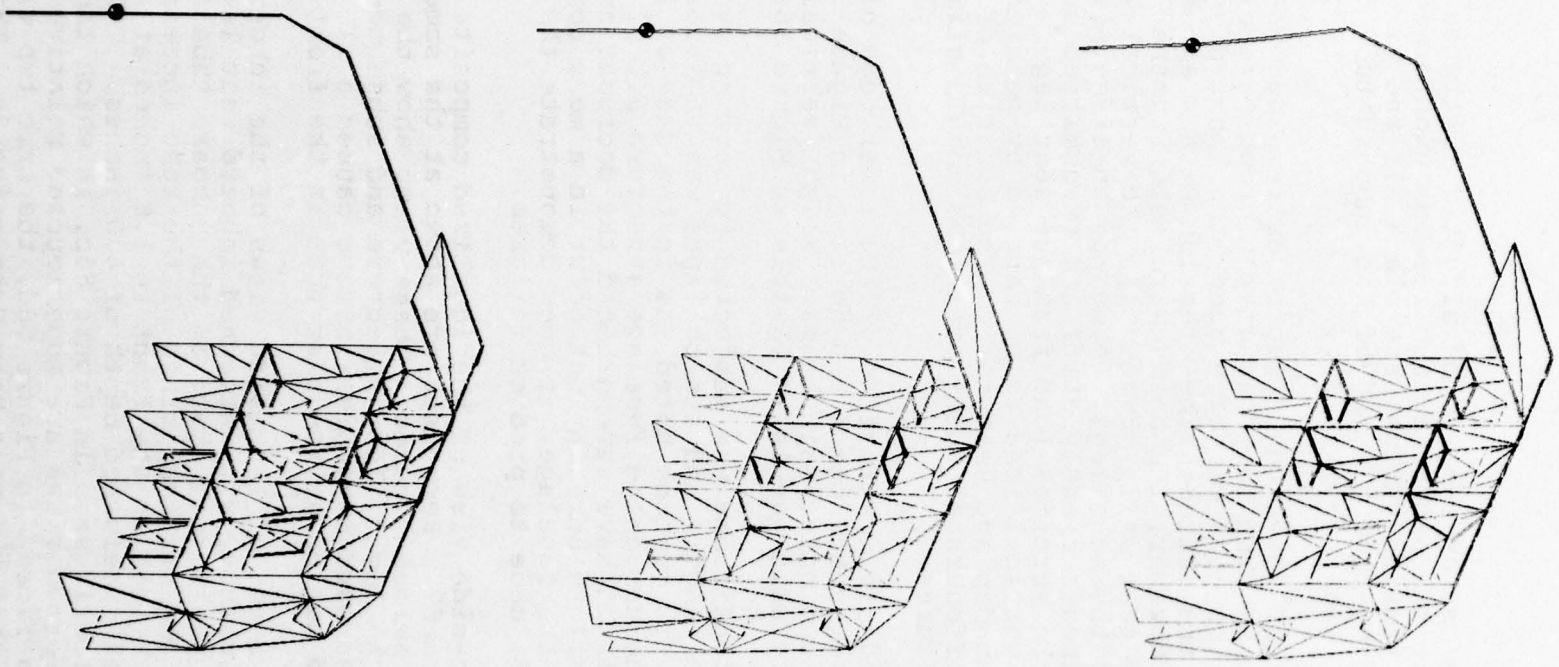

a. At 0 msec (undeformed).

b. At 8.2 msec (near peak crew displacement).

c. At 14.6 msec (near peak equipment displacement).

Figure 55. Composite section deformations, floor panels and seat removed.

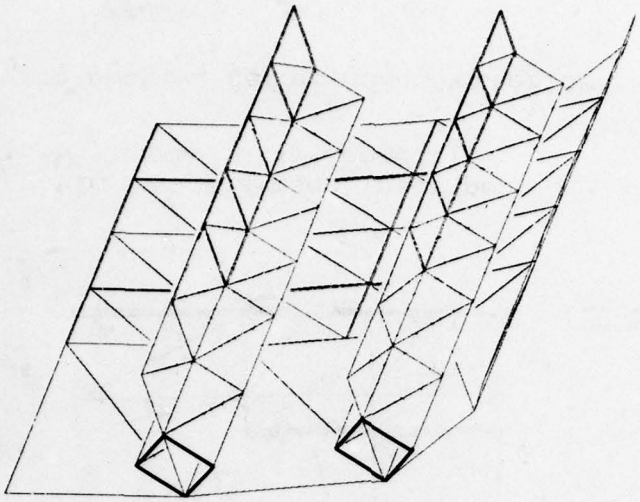

a. At 0 msec (undeformed).

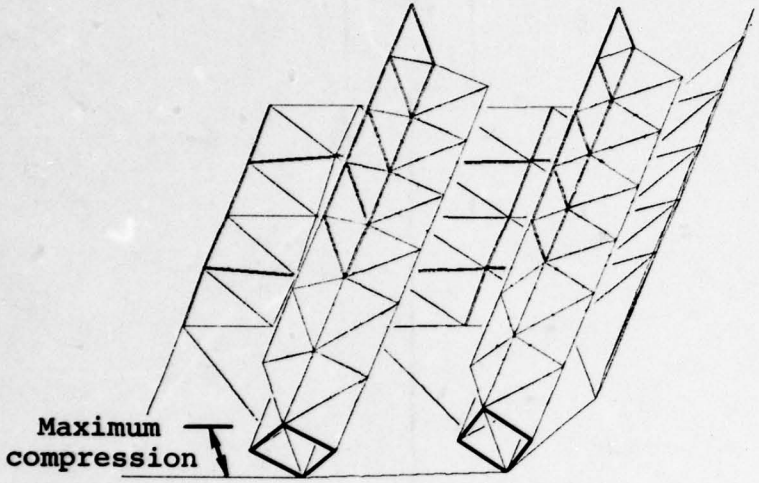

b. At 8.2 msec (near peak crew displacement).

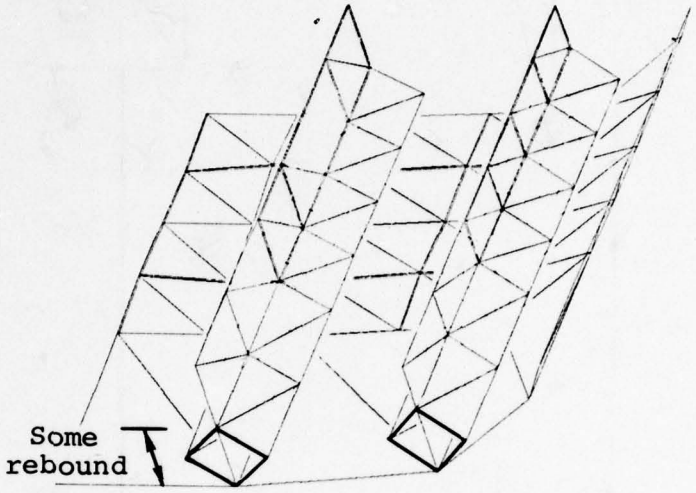

c. At 14.7 msec (near peak equipment displacement).

Figure 56. Composite section skin, beam, and tube deformations.

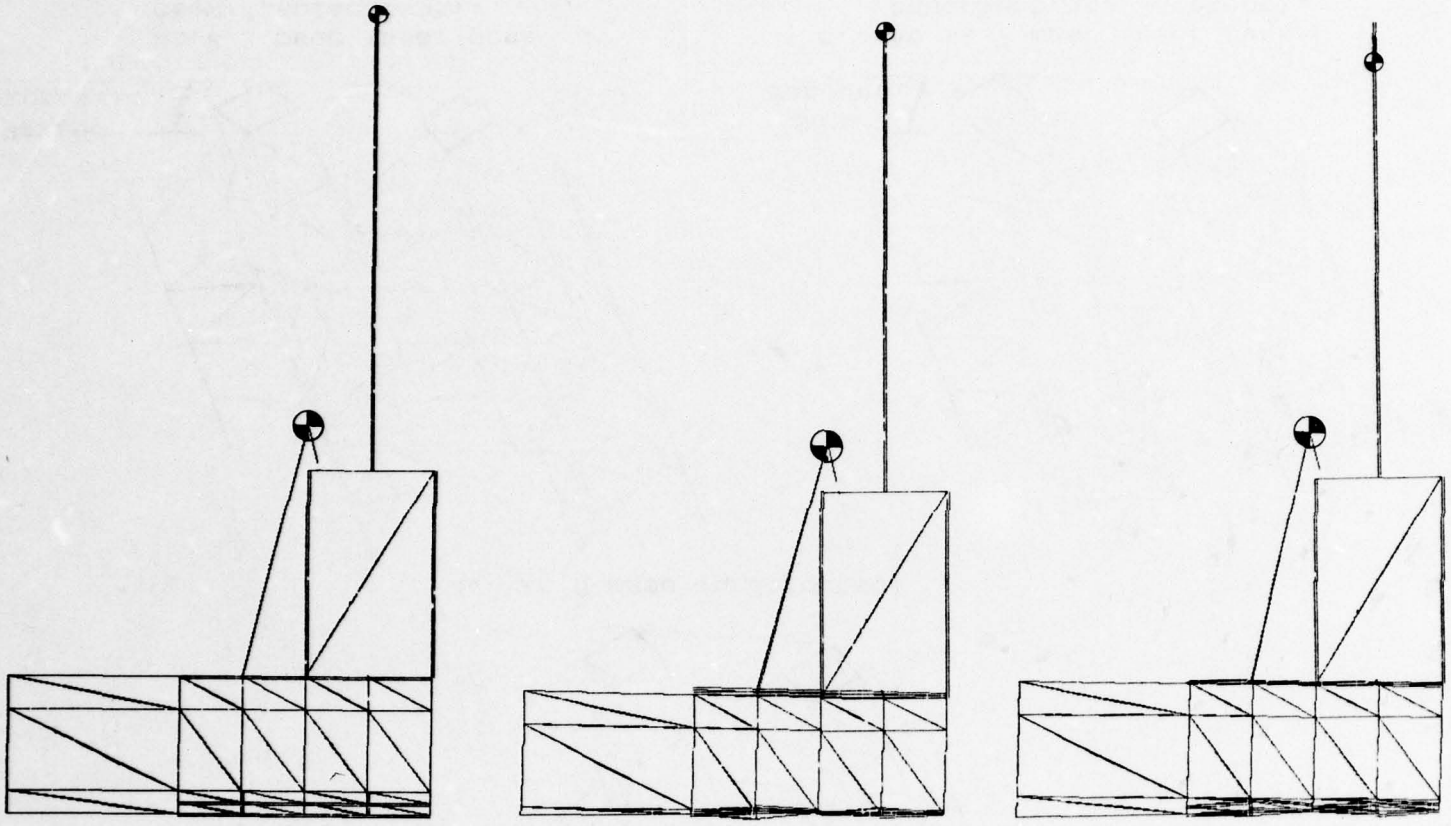

a. At 0 msec (undeformed). b. At 8.2 msec (near peak crew displacement). c. At 14.7 msec (near peak equipment displacement).

Figure 57. Composite section deformation, exterior side view.

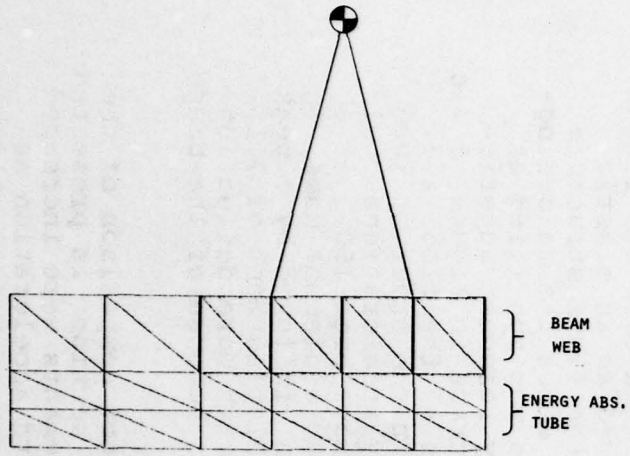

a. At 0 msec (undeformed).

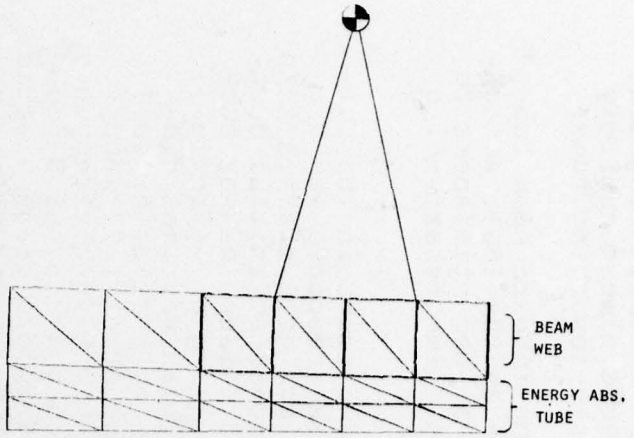

b. At 8.2 msec (near peak crew displacement).

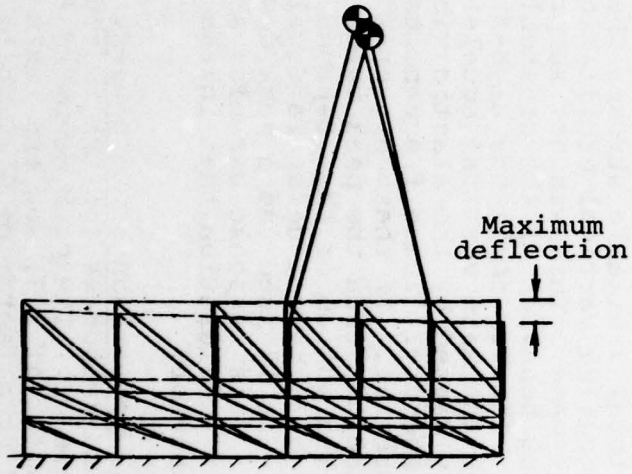

c. 8.2 msec and 0 msec superimposed at ground.

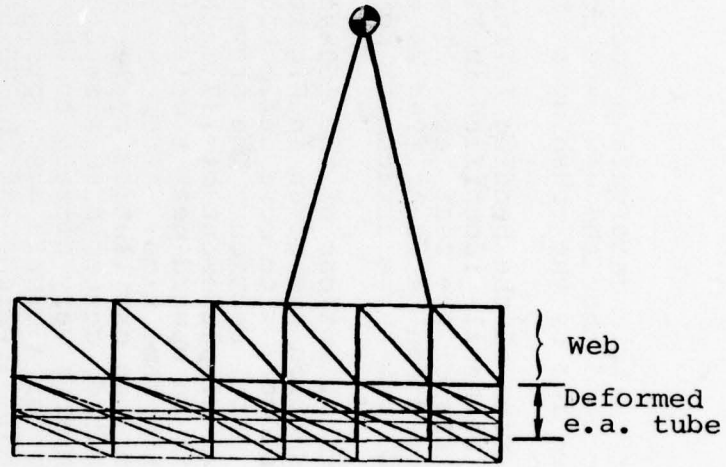

d. 8.2 msec and 0 msec superimposed at beam web.

Figure 58. Composite inboard beam and tube deformations.

that very little deformation took place in the main longitudinal beam, and that the downward motions were almost entirely accounted for by the crushing of the energy-absorbing tube.

The location of the bending failure of the inboard beam top cap can be easily identified in Figure 58 as the lower attachment points of the seat legs. The vertical web stiffeners to be improved can be identified as the beam elements extending downward from those attachment points.

The vertical motions of the 150-pound crew masses in the composite section are given in Figure 59. The response was generally slower, with more deflection and less acceleration than for the metal section. The crew mass reached an initial downward peak displacement of 1.7 inches at 8.4 msec and was subjected to an upward peak acceleration of 183 g at approximately the same time. After the initial peak vertical displacement, an oscillation cycle of 20.5 msec period (or 48.8 Hz) appeared, centered on a mean displacement of 1.02 inches. This compares very closely to the calculated natural frequency of 51 Hz for a simple mass-spring model, using the 208.5-pound total vehicle weight and the 55,500-pound/inch average elastic spring constant of the energy-absorbing tube in its unloading-reloading mode.

Thus, it seems that the upper floor structure moved in a nearly rigid manner. The inboard energy-absorbing tube initially crushed less than 23 percent (averaged over its length) of its total available stroke, then behaved as an elastic spring causing vertical oscillations on the floor structure and seat mass. This was not surprising, since the unloading-reloading behavior of the crushable tubes was specified as linear. The low-amplitude high-frequency response superimposed on the main vertical acceleration trace in Figure 59 was probably caused by the elastic vibrations of the floor and roof structure. These frequencies were in the order of 1000 Hz or greater. If these higher frequency accelerations could be neglected, then the peak value would have been 150 g at 6 msec. The motion of the 20-pound overhead equipment mass (Figure 60) shows a delay in deceleration, followed by a peak of 207 g at 17 msec and a peak downward displacement of 4.1 inches. This response was also slower, with more deflection and less acceleration that in the section because of the brush tube behavior.

4.3.4.3 Comparison of Responses. A direct comparison of the crew mass responses for the two fuselage sections is presented in Figure 61. The peak downward displacements were increased by a factor of 7.3, and the maximum upward acceleration as reduced by a factor of 6.1, while the response was greatly

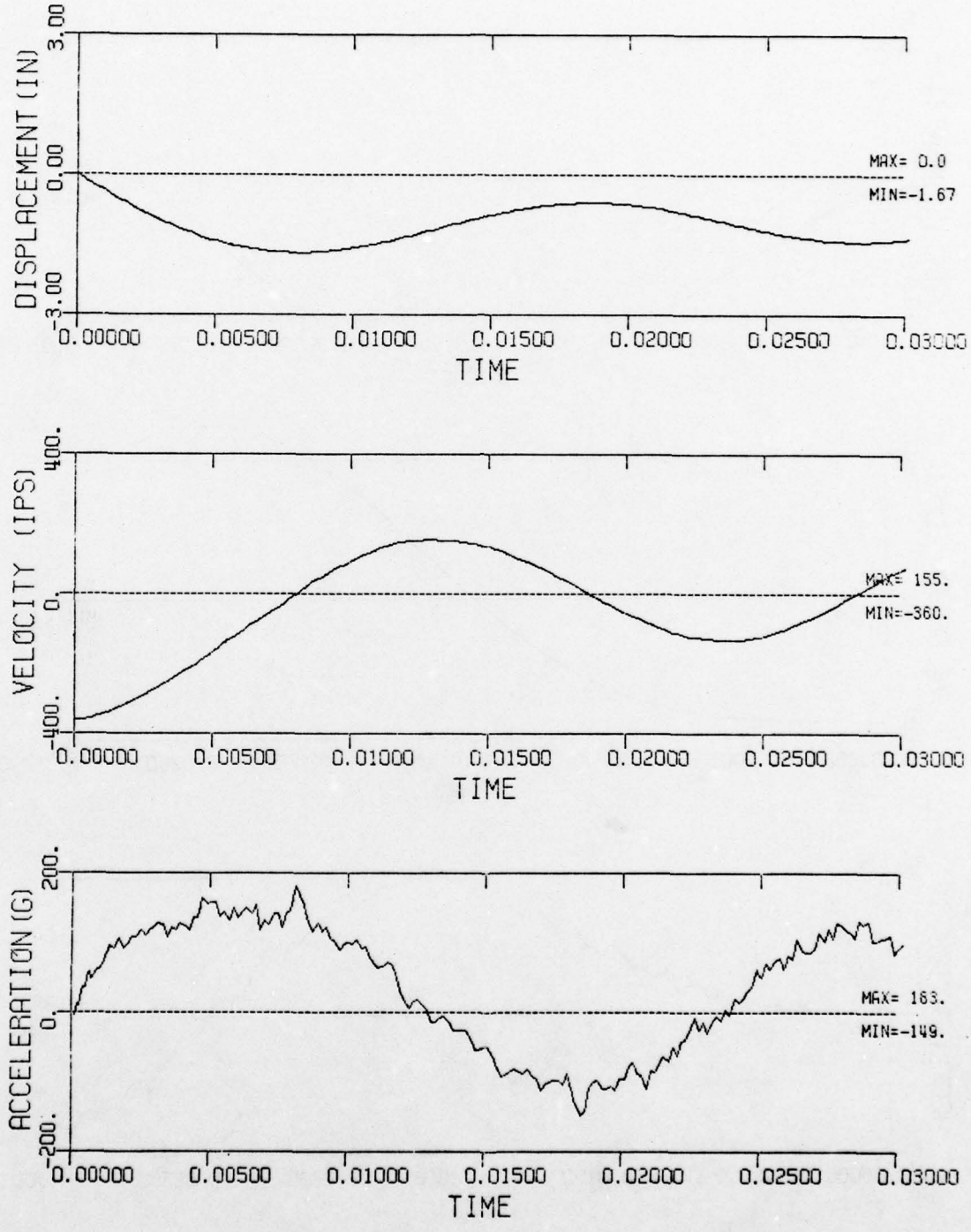

Figure 59. Vertical motion histories of crew mass in composite section.

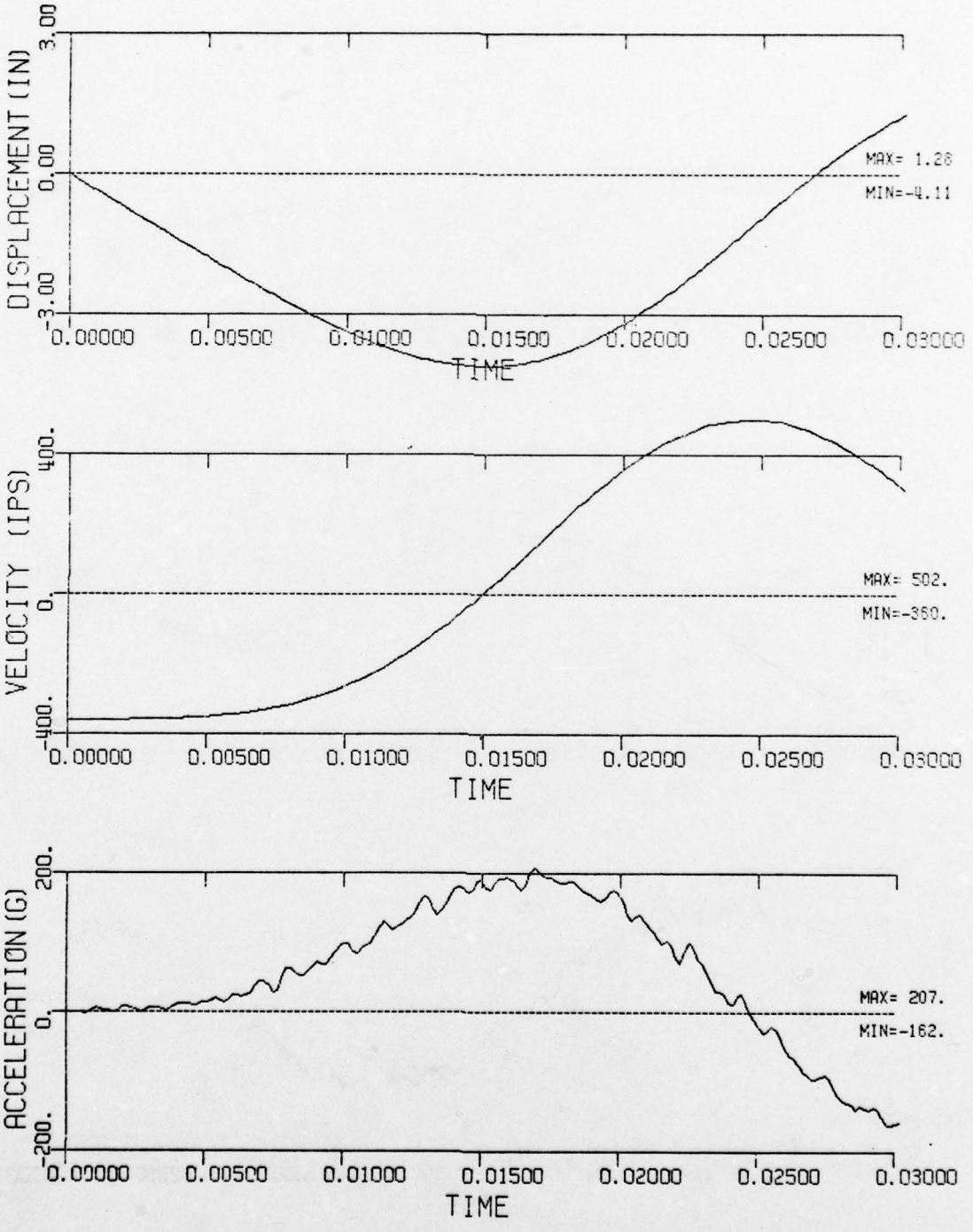

Figure 60. Vertical motion histories of the overhead equipment mass in the composite section.

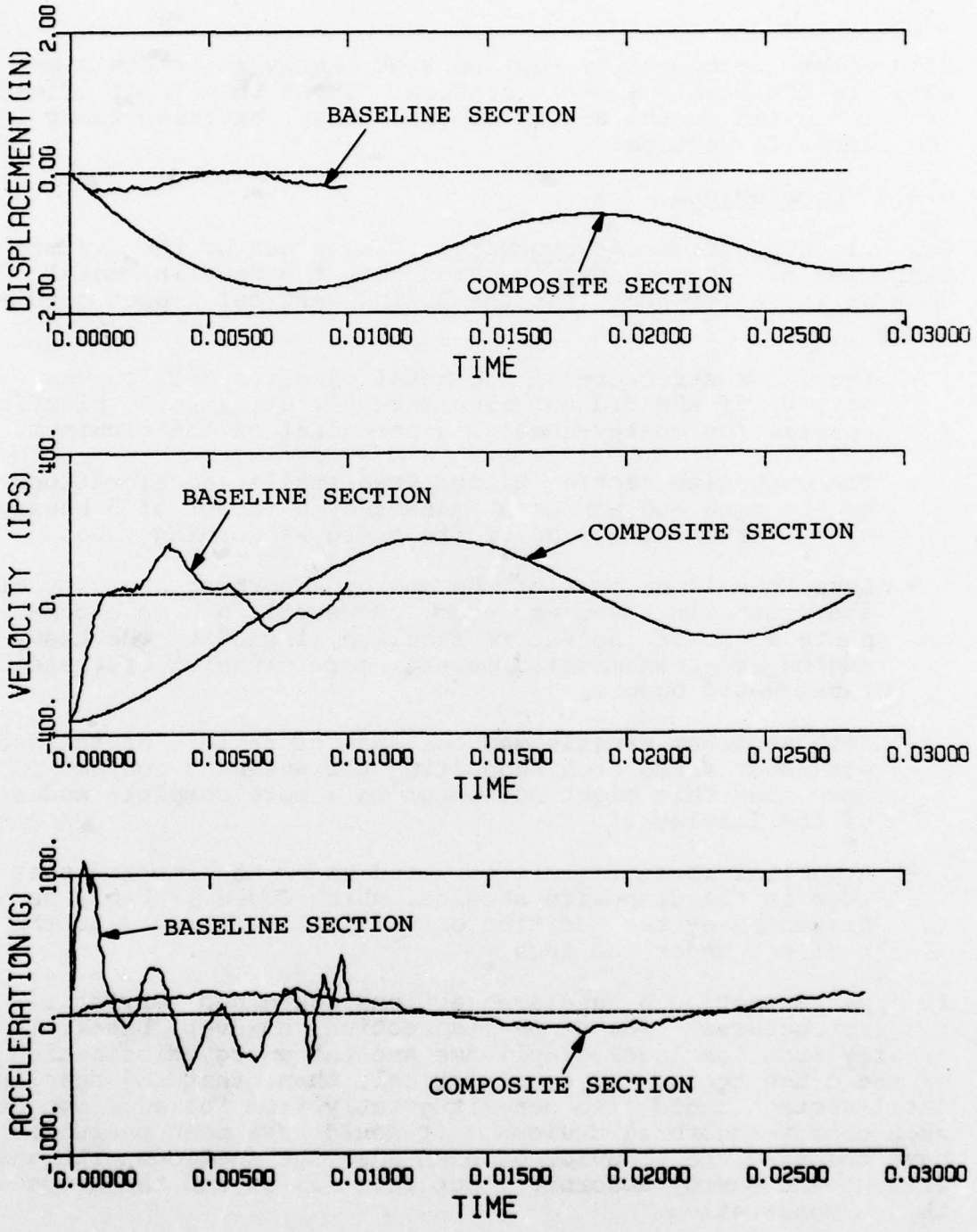

Figure 61. Comparison of vertical motion histories of the crew masses.

slowed for the composite section with energy absorbers compared to the baseline metal section. These beneficial effects are attributed to the action of the energy-absorbing tubes in the composite section.

4.3.5 Conclusions

4.3.5.1 Evaluation of Responses. Comparison of the dynamic responses of the composite section with the baseline metal section indicated that, for the 30 fps vertical impact condition:

- The floor structure of the metal baseline section was very stiff and did not significantly utilize the plastic deformation energy-absorbing potential of the aluminum.

- The composite section transmitted smaller accelerations to the crew and equipment masses by a factor of 6 because of the crushing action of its energy-absorbing tubes.

- Less than 13 percent of the energy-absorbing capacity of the crushable tubes was used. However, in a more complete model of the entire fuselage, including the heavy engine and transmission masses, more crushing of these tubes would occur.

- Both sections experienced collapse or failure of the doorpost/roof frame arch supporting the overhead equipment mass, but this might not occur in a more complete model of the fuselage.

- A partial local failure occurred under the inboard seat legs in the composite section, which could probably be prevented by the addition of vertical stiffeners to the beam web under the legs.

It appears that both fuselage sections contained very stiff floor structures. The composite section, however, benefitted greatly from the lower compliance and the energy dissipation of the crush tubes. It seems logical, then, that the baseline metal section could also benefit greatly from the addition of such energy-absorbing devices. It would have been useful to have compared the behavior of both fuselage sections with and without the energy absorbers, but that was beyond the scope of this demonstration.

Finally, these results lead to the speculation that an all-composite helicopter fuselage structure need not be less crashworthy than a conventional metallic one, in spite of the more brittle nature of the composite material. More precisely stated, this investigation indicates that the use of advanced composite materials in helicopter fuselages should not prevent improvements in the crashworthiness of the structure with innovative energy-absorbing concepts.

Other important aspects such as relative cost, flammability, and toxicity of composite structures compared to metallics were not considered here, but might be important factors in the crashworthy design of future helicopters.

4.3.5.2 Evaluation of DYCAST. This demonstration of DYCAST as a crashworthiness design analysis tool pointed out its usefulness while indicating some need for improvement. The main items in this assessment are:

- Gross dynamic behavior was displayed, including overall structural deformation and motions of critical masses.

- Detailed dynamic response was shown in the deformations, strains, stresses, and loads on individual structural components for metals and orthotropic composites.

- Detailed structural modifications were indicated by noting overloaded components and equipment attachment points and showing action of the energy absorbers.

- Computational costs were acceptably moderate, using 1.9 CPU minutes per msec for 471 degrees of freedom, while the restart feature permitted small time segments to be run in sequence without tying up the computer.

- Immediate improvements needed are rebound from the barrier surface and automatic failure criteria, which are now being implemented.

- Future developments needed are the addition of a core-sandwich plate element (for honeycomb and other cored structural components), output of occupant decelerative injury parameters, and calculation of energy consumption and distribution.

- Test verification is a very important need to explore the range of applicability and accuracy.

5. CONCLUSIONS

Conclusions that can be drawn from this investigation of the crash-impact behavior of composite materials are as follows:

- Very little pertinent data exist on the crash-impact behavior of composites. The pertinent information that was found can be summarized as follows:

  The automotive work done by the Budd Company indicates that composite structures can be crashworthy if proper emphasis is placed on crashworthiness early in the design process. Also, foam sandwich construction improves the energy absorption compared to solid laminate construction.

  Preliminary tests by the Army indicate that when composite structures are constructed in a manner similar to metals, they exhibit lower energy absorption, more fractures, peeling, and splintering.

  The BHT and automotive studies indicate that composites progressively crushed exhibit good energy absorption characteristics.

- There are considerable data on basic strength, projectile impact, and foreign object damage (FOD) of composite materials, but these data do not pertain to crash impact.

- Computer analysis methods are still being verified for metal structures, while composites will need special treatment because of their low strain-to-failure characteristics. At present, both the hybrid (KRASH) and finite-element (DYCAST) structure crash analysis methods are needed. The hybrid type of analysis is useful for preliminary design analysis and for parametric studies of the entire airframe. The finite-element analysis method has the potential for detailed structure analysis directly from drawings and may be used to develop inputs to the hybrid type of analysis. The main problem with a hybrid method is obtaining structure inputs to the coarse math model. Finite-element methods, being a complete analysis, need validation by test.

- There is some research in progress by the Army, NASA, and BHT directed toward investigating the crashworthiness of composite aircraft type structures.

- Although some of the composite material properties and impact behavior of composites on a structural element level are apparently not favorable to crashworthiness, there is evidence that crashworthy helicopter structures constructed from composites are feasible through innovative design.

6. RECOMMENDATIONS

6.1 RECOMMENDATIONS AND GOALS FOR FUTURE RESEARCH

The following are recommendations for future research on the application, analysis, and characterization of advanced airframe structures in a crash environment and of the effects of composite materials on meeting current Army crashworthiness requirements.

- In evaluating composite materials in a crash environment, comparisons should be made with metal structures. These comparisons are needed to evaluate how well conventional airframe designs using composite materials compare with conventional designs using metals. This is important to know in determining the effect on composite designs in meeting current crash requirements that are based on experience with metal structures.

- Improved crashworthy design concepts should be investigated with the objective of serving a dual purpose, that is, serving as part of the primary structure under normal operating conditions and serving to absorb energy in a crash. The weight penalty may be too high to consider strictly add-on energy-attenuating devices such as energy-absorbing bumpers in automobiles. There is considerable design information on energy-attenuating devices for crashworthy design concepts that can be applied to the airframe structure.

- A well organized research program should be planned with investigations conducted in a step-by-step manner, building from simple structure elements and joints to structure assemblies and finally to the entire airframe. Information from design studies, tests, and analyses should be closely integrated during the development of each. In addition, crashworthiness requirements need continuous reevaluation as more is learned of structure behavior in the crash environment.

- Goals of this research investigation would be as follows:

  Design information on the characteristics of composite materials and concepts investigated; also, guidelines for design of the airframe structures in a crash environment (possibly via updating the "Crash Survival Design Guide," TR 79-22)[24].

Analysis tools in the form of methods and computer programs.

Updated crashworthiness requirements.

6.2 RESEARCH REQUIREMENTS FOR CRASHWORTHY AIRFRAME STRUCTURES

Problem areas needing research that apply to the basic airframe structure design in a crash environment are listed below. Following this list, a list of related areas needing research is given.

6.2.1 Material, Structural, and Analytical Research Requirements

- Characterize the crash-impact behavior of composite materials including:

  Post-buckling behavior and energy absorption

  Failure modes and mechanisms

  Crushing behavior - cores, concepts

  New materials - thermoplastics

  Strain rates and combined loading effects - thermosets, thermoplastics, metal matrix, cores

- Investigate local effects at joints, hardpoints and cutouts with emphasis on strength for impact loading.

- Develop analytical tools in the following general areas:

  Analysis of basic properties of structure elements and joints - experimental data are needed.

  Analysis of aircraft-type structure assemblies (DYCAST needs improvements and validation for analysis of composite materials).

  Response analysis of the total aircraft system including landing gear, airframe structure and seating system - KRASH and DYCAST programs need to be validated.

- Evaluate crashworthy design concepts mentioned in this report along with others that can be integrated into future composite airframe designs.

6.2.2 Related Research Requirements

Related areas of research needed that are not specifically involved with the application of composites to airframe design are the following:

- Develop analytical tools for determining pylon loads. The analysis methods should include the effects of blade strike and rotor dynamics on pylon loads in a crash environment. Also, innovative pylon restraint concepts should be developed and evaluated.

- Energy-absorbing seat concepts are currently being developed and evaluated. The seat development programs should be tied into the airframe research in order to evaluate the total aircraft system crashworthiness. Various seat designs should be considered for the verification testing. Integrated airframe and seat structure concepts should be investigated.

- The landing gear is an important part of the energy management system of the aircraft and needs to be included in the evaluation of the airframe crashworthiness and in tradeoff studies. Introduction of landing loads into the airframe structure needs investigation.

- The effects on crashworthiness requirements of what is learned in the research program need to be evaluated continuously. Requirements should be updated periodically as it becomes apparent that the requirements need change or improvement from results of the investigations.

6.3 LONG-RANGE RESEARCH PROGRAM

The proposed long-range research program can be outlined as follows:

- **Set goals**

  Design crashworthy composite helicopter airframe

  Need: Design data, analytical tools, requirements

- **Standardize testing methods**

- **Develop firm and reliable data base - Compare composites to metals**

- **Develop analytical tools**

- Integrate with related developments: Environment, seats, rotor, landing gear

- Use Design Guide for documenting results

- Industry/Government advisory group to encourage participation

The research program, shown schematically in Figure 62 and Table 8, demonstrates the interaction necessary for a comprehensive evaluation of composites under crash loadings. This evaluation should compare the performance of composites to equivalent metallic designs by means of dynamic tests in typical structural elements and assemblies.

This program also contains needed research in other areas, such as landing gear and seat design technology, analysis of rotors, defining the crash environment, and crash requirements, which are needed to perform in-depth trade studies. The culmination of these trade studies and subsequent verification tests should be a supplement to the design guide.

Two other comments on planning the program:

- Composite data are needed on a timely basis to ensure proper implementation in imminent future composite designs.

- Industry-wide participation is essential to ensure that the data obtained gets wide dissemination and that the results of the program are accepted by industry.

Industry participation with this program will also provide a diversity of thought and ideas that is important for the successful completion of the program.

Industry participation can be direct involvement in investigations or as a member of an industry/Government advisory committee. This committee should be established to monitor the program, to determine overall program guidelines, and to standardize procedures to be followed. This committee will ensure that the original program goals are met in an unprejudiced manner.

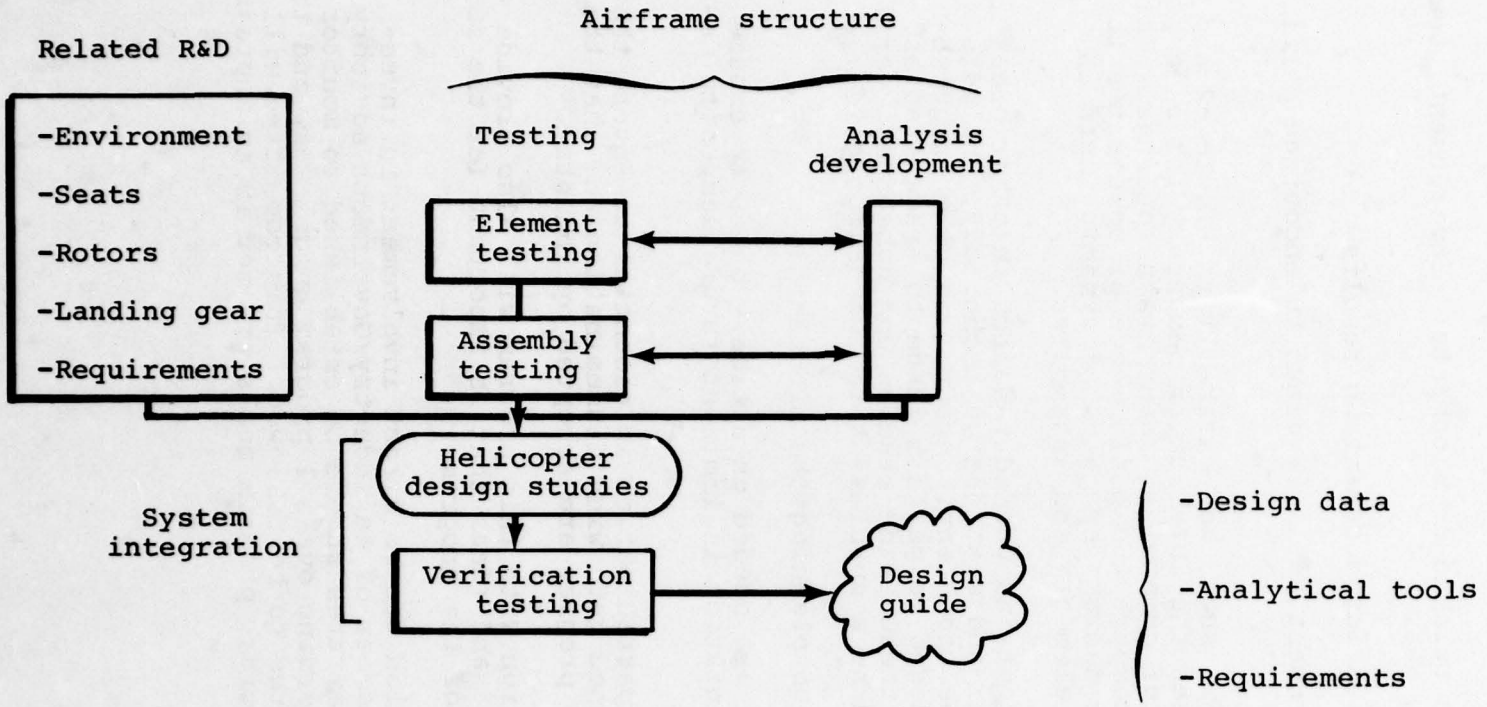

Figure 62. Proposed research program.

TABLE 8. PROPOSED RESEARCH PROGRAM, ELEMENT AND ASSEMBLY INVESTIGATIONS

Manufacturing method	Categories	Specimens	Loading
Element investigation			
Lab (ideal)	1. Energy-absorbing concepts	-Laminates	-Static
Factory	2. Conventional structure	-Panels	-Dynamic
	3. Concentrated loads, attachments, cutouts	-Joints, sections	-Combined
		-Fittings, hardpoints	
Assembly investigation			
Lab	1. C/W design concepts	Typical aircraft sections:	-Static
Factory	2. Conventional structures		-Dynamic
	3. Innovative designs and manufacturing methods	-Floor	-Combined
		-Frame	
		-Stiffened cylinder (load radial and axial)	
		-Monocoque	

REFERENCES

1. Turnbow, J., Carroll, D., Haley, J., Reed, W., and Robertson, S., CRASH SURVIVAL DESIGN GUIDE, Dynamic Science, USAAMRDL Technical Report 71-22, Eustis Directorate, U.S. Army Air Mobility Research and Development Laboratory, Fort Eustis, Virginia, October 1971, AD-733358.

2. LIGHT FIXED- AND ROTARY-WING AIRCRAFT CRASHWORTHINESS, MIL-STD-1290(AV), Eustis Directorate, U.S. Army Air Mobility Research and Development Laboratory, Fort Eustis, Virginia, January 1974.

3. Greer, D. L., Breeden, J. J., and Heid, T. L., CRASHWORTHY DESIGN PRINCIPLES, General Dynamics-Convair, FAA Technical Report ADS-24, Department of Transportation, Federal Aviation Administration, Washington, D.C., September 1964.

4. Reed, W.H., and Avery, J. P., PRINCIPLES FOR IMPROVING STRUCTURAL CRASHWORTHINESS FOR STOL AND CTOL AIRCRAFT, Aviation Safety Engineering and Research, USAAVLABS Technical Report 66-39, Eustis Directorate, U.S. Army Air Mobility Research and Development Laboratory, Fort Eustis, Virginia, June 1966, AD-637 133.

5. Greer, D. L., Heid, T. L., and Weber, J. D., DESIGN STUDY AND MODEL STRUCTURES TEST PROGRAM TO IMPROVE FUSELAGE CRASHWORTHINESS, General Dynamics-Convair, FAA Technical Report DS-67-20, Department of Transportation, Federal Aviation Administration, Washington, D.C., October 1967, AD-666 816.

6. Kimball, C. E., and DeHart, R. C., ENERGY ABSORBING MATERIALS FOR IMPROVING HELICOPTER CRASHWORTHINESS, Southwest Research Institute, Office of Naval Research, Department of the Navy, Arlington, Virginia, March 1976, AD-A023 006.

7. Brooks, J. D., and Rey, L. G., POLYSTYRENE-URETHANE COMPOSITE FOAM FOR CRASH PADDING APPLICATIONS, Dow Chemical of Canada, Presented at the 3rd International Cell Plastic Conference, Montreal, Quebec, September 1972, EI 1731154583.

8. Hoffstedt, D. J., and Swatton, S., ADVANCED HELICOPTER STRUCTURAL DESIGN INVESTIGATION, Boeing-Vertol Company, USAAMRDL Technical Report 75-56A & B, Eustis Directorate, U.S. Army Mobility Research and Development Laboratory, Fort Eustis, Virginia, March 1976. AD 024662, AD 024478.

REFERENCES (Continued)

9. Rich, M. J., INVESTIGATION OF ADVANCED HELICOPTER STRUCTURAL DESIGNS, Sikorsky Aircraft Division, USAAMRDL Technical Report 75-59, Eustis Directorate, U.S. Army Mobility Research and Development Laboratory, Fort Eustis, Virginia, May 1976, AD-A026 246.

10. Riddell, Robert M., MOLDED FIBERGLASS NARROW MEDIAN BARRIER, Rockwell International, FHWA RD 75 25, Federal Highway Administration, Washington, D:C., December 1974, DB-242555.

11. Langston, E. D., and Swearingen, J. J., EVALUATION OF A FIBERGLASS GLARE SHIELD FOR PROTECTION AGAINST HEAD INJURY, FAA Civil Aeromedical Institute, FAA AM-72-7, Office of Aviation Medicine, Federal Aviation Administration, Washington, D.C., February 1972, AD-740732.

12. Raschbichler, H. G., TECHNICAL AND ECONOMIC ASPECTS CONCERNING THE APPLICATION OF THE SELF-SUPPORTING PLASTIC SANDWICH CONSTRUCTION TO ELECTRIC TRANSPORT VEHICLES, Messerschmitt-Boelkow Blohm, Presented at the 3rd International Electric Vehicle Symposium and Exposition, Washington, D.C., February 1974, EI 1750962776.

13. Jahnle, H. A., FEASIBILITY STUDY OF PLASTIC AUTOMOTIVE STRUCTURE, Budd Company, DOT HS-801-771, U.S. Department of Transportation, National Highway Traffic Safety Administration, Washington, D.C., December 1975, PB 248354.

14. Gallant, R. A., X898 - A PASSENGER VEHICLE OF UNITIZED BODY - CHASSIS STRUCTURE OF RP/C, Presented at the 29th Annual Conference of the Reinforced Plastics/Composite Institute, Washington, D.C., February 1974.

15. Raschbichler, H. G., VEHICLE CHASSIS OF SANDWICH CONSTRUCTION, Modern Plastics, Volume 50, No. 7, July 1973, pp. 76-79, EI 730946605.

16. Shimamura, S., and Ishine, K., A CONTRIBUTION TO THE SAFETY DESIGN OF THE FRP CAR, Presented at the Reinforced Plastics Congress, Brighton, England, November 1974.

17. Millman, R. S., and Morley, J. G., ENERGY ABSORPTION AT HIGH RATES OF DEFORMATION IN FIBROUS COMPOSITES WITH NON-FRACTURING REINFORCING ELEMENTS, University of Nottingham (GCBA, Britain), Materials Science and Engineering, Volume 23, No. 1, April 1976, pp. 1-10, EI 1761065436.

REFERENCES (Continued)

18. Jones, B. H., DESIGN AND PRODUCTION OF ECONOMICAL FRP ENERGY ABSORBING SYSTEMS FOR TRANSPORTATION APPLICATIONS, Goldsworthy Engineering Inc., Presented at the SPE National Technical Conference: Plastic in Surface Transportation, Detroit, Michigan, November 1974, EI 1751176050.

19. Eshelman, R. H., FUTURE BUMPER MATERIALS UP FOR GRABS, Automotive Industry, Volume 147, No. 11, December 1, 1972, pp. 45-47, EI 1730205811.

20. Newton, D. A., DUNLOP COMPOSITE ENERGY ABSORBING BUMPER SYSTEMS, Dunlop LTD., Leicester, England, SAE Prepr. No. 750010, EI 1750635832.

21. Lifshitz, J. M., IMPACT STRENGTH OF ANGLE PLY FIBER REINFORCED MATERIALS, Journal of Composite Materials, Volume 10, January 1976, pp. 92-100, EI 760529620.

22. Eaton, G. A., BALLISTIC DAMAGE OF GRAPHITE/EPOXY PLATES, Naval Post Graduate School, Monterey, California, Master's Thesis, June 1977, AD-A042 29614ST.

23. Spier, E. E., and Klouman, F. L., POST BUCKLING BEHAVIOR OF GRAPHITE/EPOXY LAMINATED PLATES AND CHANNELS, Presented at Army Symposium on Solid Mechanics, Cape Cod, Mass., September 1976, EI 770534416.

24. CRASH SURVIVAL DESIGN GUIDE, USARTL Technical Report 79-22, The Applied Technology Laboratory, U.S. Army Research and Technology Laboratory (AVRADCOM), Fort Eustis, Virginia (To be published).

25. Smith, H. G., DESIGNING HELICOPTERS FOR IMPROVED CRASH SURVIVABILITY, Presented at the Agard/NATO Aerospace Medical Panel Specialist's Meeting, Oporto, Portugal, June 1977.

26. Ezra, A. A., and Fay, R. J., AN ASSESSMENT OF ENERGY ABSORBING DEVICES FOR PROSPECTIVE USE IN AIRCRAFT IMPACT SITUATIONS, Dynamic Response of Structures, Pergamon Press, N. Y., 1972, pp. 225-246.

27. Thomson, R. G., and Goetz, R. C., NASA/FAA GENERAL AVIATION CRASH DYNAMICS PROGRAM-A STATUS REPORT, Presented at the AIAA/ASME/ASCE/AHS 20th Structures, Structural Dynamics, and Materials Conference, St. Louis, Missouri, April 4-6, 1979.

28. Saczalski, K. J., MODELLING AND ANALYSIS TECHNIQUES FOR PREDICTION OF STRUCTURAL AND BIODYNAMIC CRASH IMPACT RESPONSE, Finite Element Analysis of Transient Nonlinear Structural Behavior, ASME, New York, Publication AMD Vol. 14, 1975, pp. 99-117.

29. McIvor, I. K., Wineman, A. S., Yang, W. H., and Bowman, B., MODELLING, SIMULATION, AND VERIFICATION OF IMPACT DYNAMICS, VOL. 2, STATE OF ART, COMPUTER SIMULATIONS OF VEHICLE IMPACT, DOT Report HS-800-997, U.S. Department of Transportation, Washington, D. C., February 1974.

30. Kamat, M. P., SURVEY OF COMPUTER PROGRAMS FOR PREDICTION OF CRASH RESPONSE AND ITS EXPERIMENTAL VALIDATION, Measurement and Prediction of Structural and Biodynamic Crash Impact Response, ASME, New York, 1976, pp. 33-48.

31. Emori, R. I., ANALYTICAL APPROACH TO AUTOMOBILE COLLISION, SAE Paper 680016, January 1968.

32. Miura, N., and Kawamura, K., ANALYSIS OF DEFORMATION MECHANISMS IN HEAD-ON COLLISIONS, SAE Paper 680484, May 1968.

33. Tani, M., and Emori, R. I., A STUDY ON AUTOMOBILE CRASHWORTHINESS, SAE Paper 700175, January 1970.

34. Kamal, M. M., ANALYSIS AND SIMULATION OF VEHICLE-TO-BARRIER IMPACT, SAE Paper 700414, May 1970.

35. Herridge, J. T., and Mitchell, R. K., DEVELOPMENT OF A COMPUTER SIMULATION PROGRAM FOR COLLINEAR CAR/CAR AND CAR/BARRIER COLLISIONS, Battelle Columbus Laboratory for Department of Transportation, Report DOT-HS-800-645, U.S. Department of Transportation, Washington, D.C., January 1975.

36. Gatlin, C. I., Goebel, D. E., and Larsen, S. E., ANALYSIS OF HELICOPTER STRUCTURE CRASHWORTHINESS, USAAVLABS Technical Report 70-71A and B, Eustis Directorate, U. S. Army Air Mobility Research and Development Laboratory, Fort Eustis, Virginia, January 1971, AD 880680, AD 88678.

37. Gamon, M. A., and Wittlin, G., ANALYTICAL TECHNIQUES FOR PREDICTING VEHICLE CRASH RESPONSE, Aircraft Crashworthiness, University Press of Virginia, Charlottesville, 1975, pp. 605-622.

38. Wittlin, G., and Gamon, M. A., A METHOD OF ANALYSIS FOR GENERAL AVIATION STRUCTURE CRASHWORTHINESS, Measurement and Prediction of Structural and Biodynamic Crash Impact Response, ASME, New York, 1976, pp. 63-81.

39. Shieh, R. C., BASIC RESEARCH IN CRASHWORTHINESS II - LARGE DEFLECTION DYNAMIC ANALYSIS OF PLANE ELASTO-PLASTIC FRAME STRUCTURES, Calspan Corporation, Report YB-2987-V-7, August 1972.

40. Young, J. W., CRASH: A COMPUTER SIMULATOR OF NONLINEAR TRANSIENT RESPONSE OF STRUCTURES, DOT Report HS-091-1-125B, U.S. Department of Transportation, Washington, D.C., 1972.

41. Melosh, R. J., CAR-BARRIER IMPACT RESPONSE OF COMPUTER-SIMULATED MUSTANG, DOT Report HS-800-999, U.S. Department of Transportation, Washington, D.C., 1972.

42. McIvor, I. K., Wineman, A. S., Anderson, W. J., and Wang, H. C., MODELLING, SIMULATION AND VERIFICATION OF IMPACT DYNAMICS - VOL. 4, THREE DIMENSIONAL PLASTIC HINGE FRAME SIMULATION MODULE, DOT Report HS-800-999, U.S. Department of Transportation, Washington, D.C., February 1974.

43. Belytschko, T. B., WHAM USER'S MANUAL, University of Illinois, Report 74-B2, 1974.

44. Welch, R. E., Bruce, R. W., and Belytschko, T. B., DYNAMIC RESPONSE OF AUTOMOTIVE SHEET METAL UNDER CRASH LOADINGS, AIAA Paper 75-793, May 1975.

45. Melosh, R. J., and Kamat, M. P., COMPUTER SIMULATION OF A LIGHT AIRCRAFT CRASH, Journal of Aircraft, Vol. 14, No. 10, October 1977, pp. 1009-1014.

46. Armen, H., Pifko, A., and Levin, H., NONLINEAR FINITE ELEMENT TECHNIQUES FOR AIRCRAFT CRASH ANALYSIS, Aircraft Crashworthiness, University Press of Virginia, Charlottesville, 1975, pp. 517-548.

47. Winter, R., Pifko, A. B., and Armen, H., CRASH SIMULATION OF SKIN-FRAME STRUCTURE USING A FINITE ELEMENT CODE, SAE Paper 770484, April 1977.

48. Wittlin, G., and Gamon, M. A., EXPERIMENTAL PROGRAM FOR THE DEVELOPMENT OF IMPROVED HELICOPTER STRUCTURAL CRASHWORTHINESS ANALYTICAL AND DESIGN TECHNIQUES, USAAMRDL Technical Report 72-72, 2 Vols., Eustis Directorate, U.S.

Army Air Mobility Research and Development Laboratory, Fort Eustis, Virginia, May 1973, AD 7864985, AD 764986.

49. Wittlin, G., and Park, K. C., DEVELOPMENT AND EXPERIMENTAL VERIFICATION OF PROCEDURES TO DETERMINE NONLINEAR LOAD-DEFLECTION CHARACTERISTICS OF HELICOPTER SUBSTRUCTURES SUBJECTED TO CRASH FORCES, USAAMRDL Technical Report 74-12, 2 Vols., Eustis Directorate, U.S. Army Air Mobility Research and Development Laboratory, Fort Eustis, Virginia, May 1974, AD 784191, AD 784192.

50. Wittlin, G., and Gamon, M. A., A METHOD OF ANALYSIS FOR GENERAL AVIATION AIRPLANE STRUCTURAL CRASHWORTHINESS, DOT Report Number FAA-RD-76-123, U.S. Department of Transportation, Federal Aviation Administration, Systems Research and Development Service, Washington, D. C., September 1976.

51. Whittlin, G., and Gamon, M. A., GENERAL AVIATION AIRPLANE STRUCTURAL CRASHWORTHINESS USER'S MANUAL, 3 Vols., DOT Report Number FAA-RD-77-189, U.S. Department of Transportation, Federal Aviation Administration, Systems Research and Development Service, Washington, D. C., February 1978.

52. THE NASTRAN USER'S MANUAL, NASA SP-222(03) National Aeronautics and Space Administration, Washington, D. C., July 1976.

53. Cronkhite, J. D., Berry, V. L., and Brunken, J. E., A NASTRAN VIBRATION MODEL OF THE AH-1G HELICOPTER AIRFRAME, U.S. Army Armament Command Report No. R-TR-64-45, Research Directorate, Gen. Thomas J. Rodman Laboratory, Rock Island Arsenal, Rock Island, Illinois, 61201, June 1974.

APPENDIX A

KRASH ANALYSIS

KRASH MODEL DESCRIPTION

The development of the KRASH models of the metal baseline airframe and composite airframe with energy absorbers for a troop transport helicopter relied heavily on the UH-1 data presented in TR 72-72[48]. For example, the mass point numbering scheme and most of the nonlinear beam and crushable spring element properties were retained. The linear mass and elastic stiffness characteristics were modified based on BHT's available in-house NASTRAN analysis of the UH-1 helicopter. This was done in order to develop the KRASH math model consistent with structural analysis practices used in the helicopter industry.

The description of the KRASH model is discussed in the following order:

1. Elastic Stiffness and Mass Modeling
2. Fuselage
3. Tailboom
4. Main Rotor Pylon
5. Engine on Mounts
6. Landing Gear
7. Occupant/Seat
8. KRASH Input Data

Elastic Stiffness and Mass Modeling

The procedure for determining elastic stiffness properties for the simplified KRASH model was based on an existing NASTRAN finite-element model of a UH-1 helicopter configured to a gross weight of 9500 lb. First, a FORTRAN preprocessor was developed to convert KRASH input data to NASTRAN format. Then to verify the elastic stiffness properties of the simplified model, a NASTRAN normal modes analysis was performed on the idealized KRASH model. Table A-1 lists the resulting elastic stiffness properties of the beam elements for the KRASH model and Figure A-1 shows the comparison of natural frequencies between the coarse KRASH model idealization and the detailed finite-

TABLE A-1. BEAM ELEMENT ELASTIC STIFFNESS PROPERTIES

Mass Points		Section Properties					Material Properties	
End A	End B	A (In^2)	J (In^4)	I_{11} (In^4)	I_{22} (In^4)	Damping Ratio	E (10^6 Lb/In^2)	G (10^6 Lb/In^2)
Fuselage								
3	4	9.520	1727.140	658.250	658.250	0.04	10.5	4.0
4	5	9.520	1796.990	807.270	731.990	0.04	10.5	4.0
5	6	4.760	2591.550	1316.150	987.380	0.04	10.5	4.0
10	11	4.760	2591.550	1316.150	987.380	0.04	10.5	4.0
11	16	9.520	1271.000	645.670	484.230	0.04	10.5	4.0
16	19	9.520	218.580	45.720	82.130	0.04	10.5	4.0
12	16	7.620	12.004	15.353	92.192	0.04	10.5	4.0
13	16	7.620	12.004	15.353	92.192	0.04	10.5	4.0
12	24	0.762	4.024	92.195	6.762	0.04	10.5	4.0
13	25	0.762	4.024	92.195	6.762	0.04	10.5	4.0
24	25	7.620	1.474	1.762	23.036	0.04	10.5	4.0
10	22	0.381	0.0	95.241	16.191	0.04	10.5	0.0
10	23	0.381	0.0	95.241	16.191	0.04	10.5	0.0
20	22	0.381	0.0	16.191	95.246	0.04	10.5	0.0
21	23	0.381	0.0	16.191	95.246	0.04	10.5	0.0
20	21	0.381	0.0	95.271	16.195	0.04	10.5	0.0
5	20	0.893	0.0	83.877	0.0	0.04	10.5	0.0
5	21	0.893	0.0	83.877	0.0	0.04	10.5	0.0
5	22	0.801	0.0	67.918	0.0	0.04	10.5	0.0
5	23	0.801	0.0	67.918	0.0	0.04	10.5	0.0
20	24	3.258	0.0	0.0	0.0	0.04	10.5	4.0
21	25	3.258	0.0	0.0	0.0	0.04	10.5	4.0
6	11	0.762	33.998	12.096	14.934	0.04	10.5	4.0
6	33	8.283	183.104	60.847	74.982	0.04	10.5	4.0
Tailboom								
1	2	9.520	154.520	58.860	44.150	0.04	10.5	4.0
2	34	9.520	556.460	212.110	212.110	0.04	10.5	4.0
3	34	9.520	1226.670	467.370	467.370	0.04	10.5	4.0
Main rotor pylon								
9	33	2.570	54.880	4.760	2.620	0.04	10.5	4.0
8	9	9.520	371.430	185.710	185.710	0.04	10.5	4.0
8	32	9.520	22.870	11.440	11.440	0.04	10.5	4.0
Engine								
4	7	0.254	0.0	93.524	93.524	0.04	10.5	0.0
5	7	0.253	0.0	92.384	92.384	0.04	10.5	0.0
7	9	0.0	26.003	0.0	0.0	0.04	10.5	1.0
Landing gear								
10	14	3.387	7.118	3.559	3.559	0.04	10.5	4.0
10	15	3.387	7.118	3.559	3.559	0.04	10.5	4.0
16	17	1.963	3.099	1.549	1.549	0.04	10.5	4.0
16	18	1.963	3.099	1.549	1.549	0.04	10.5	4.0
14	17	1.165	4.446	2.223	2.223	0.04	10.5	4.0
15	18	1.165	4.446	2.223	2.223	0.04	10.5	4.0
Occupant/seat								
16	27	0.029	2.500	0.873	0.873	0.04	10.5	4.0
27	29	1.000	0.01227	0.300	0.0075	0.814	1.0	0.3
27	31	1.000	0.007855	0.300	0.0048	0.597	1.0	0.3
10	26	0.010	2.500	0.873	0.873	0.04	10.5	4.0
26	28	1.000	0.01227	0.300	0.0075	0.955	1.0	0.3
26	30	1.000	0.007855	0.300	0.0048	0.700	1.0	0.3

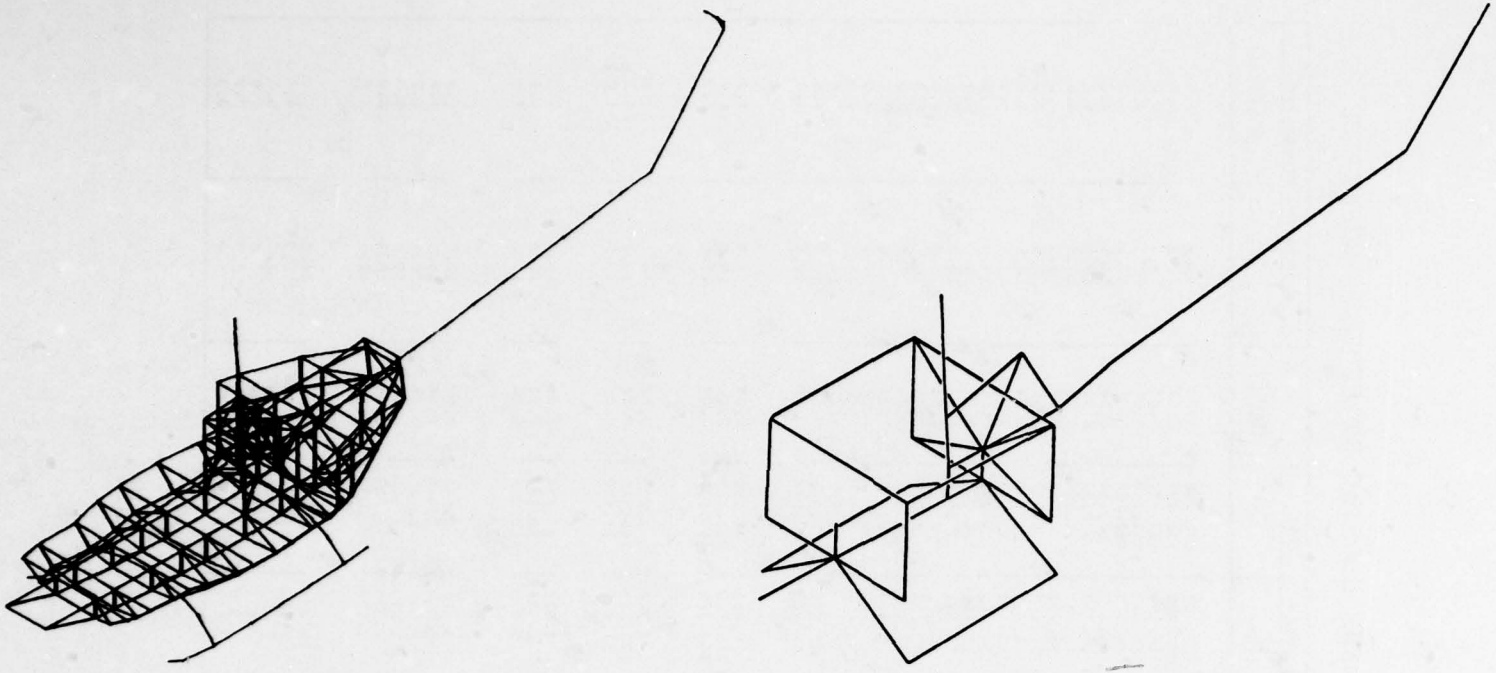

(a) NASTRAN model

(b) KRASH model

Mode	Natural frequency, Hz	
	NASTRAN	KRASH
Main rotor pylon pitch	2.98	2.97
Main rotor pylon roll	3.12	3.73
First fuselage lateral bending	6.33	6.28
First fuselage vertical bending	6.77	6.59
Second fuselage vertical bending	14.30	14.96
Second fuselage lateral bending	14.50	16.19

Figure A-1. Comparison of NASTRAN and KRASH analytical models of troop transport helicopter airframe.

element model. The results of the comparison show good agreement between the two elastic models. This indicates that the dynamics of the detailed model have been preserved in the simplification process.

The mass point data for the 9500-lb troop transport helicopter configuration was determined by using an in-house computer program, SDSN02[53], that distributes the detailed helicopter weights information on a weights data file to the mass points of the KRASH model. In addition to the lumped weights, mass moments of inertia including cross products were obtained for the mass points from the SDSN02 output. Table A-2 contains the revised mass point geometry, weights, and mass moments of inertia.

Fuselage

The fuselage idealization of the troop transport helicopter KRASH model is shown in Figure A-2. The fuselage structure forward of the tailboom junction at Station 241.44 that is considered effective for stiffness consists of the following:

1. Main beams extending from nose (Station 23) to the tailboom junction
2. Honeycomb panel floor (WL 22) and engine deck (WL 55)
3. All lower contour skins
4. Outer contour skin aft of Station 166
5. Cabin roof and doorposts

Structure not considered as effective includes nonstructural items such as cowlings, doors, windows, fairings, etc.

For the metal baseline airframe, the external crushing spring nonlinear parameters were obtained from report TR 74-12A[49] which extensively details the determination of the crushing characteristics for the UH-1.

Since the composite model employed an energy-absorbing concept for the lower fuselage, new crushing characteristics had to

---

[53] J.D. Cronkhite, V.L. Berry, and J.E. Brunken, A NASTRAN VIBRATION MODEL OF THE AH-1G HELICOPTER AIRFRAME, U. S. Army Armament Command Report No. R-TR-64-045, Research Directorate, Gen. Thomas J. Rodman Laboratory, Rock Island Arsenal, Rock Island, Ill., 61201, June 1974.

TABLE A-2. MASS POINT GEOMETRY, WEIGHTS, AND MASS MOMENTS OF INERTIA

Mass Point Number	Coordinates (In)			Weight (Lb)	Mass Moments of Inertia (In-Lb-Sec^2)					
	Station	Buttline	Waterline		I_{xx}	I_{yy}	I_{zz}	I_{xy}	I_{yz}	I_{xz}
1	478.10	0.0	131.96	74.50	11.92	10.98	12.88	0.802	1.311	-4.833
2	428.14	0.0	74.39	71.86	17.02	62.23	47.59	0.306	-0.027	-6.797
3	241.44	0.0	46.31	135.35	120.37	332.03	289.39	-1.080	-3.468	-25.896
4	211.06	0.0	38.45	285.79	238.77	190.14	175.35	-3.422	-8.299	-1.558
5	163.00	0.0	38.45	613.08	380.84	248.81	241.88	72.268	-5.882	16.239
6	141.00	0.0	38.45	862.94	583.69	801.18	625.08	82.603	4.614	107.510
7	186.83	0.0	79.17	536.90	139.21	328.49	322.81	0.0	0.0	0.0
8	136.90	0.0	98.00	248.97	32.28	38.24	7.03	-0.080	0.110	3.970
9	139.60	0.0	67.00	314.75	56.29	138.07	88.37	-0.440	-0.550	42.220
10	163.00	0.0	22.0	357.52	344.01	231.78	216.40	73.656	-5.032	17.656
11	141.00	0.0	22.00	771.08	535.86	724.87	566.98	84.240	4.758	99.093
12	71.62	-45.00	22.00	332.28	247.99	361.25	308.38	22.790	1.484	35.859
13	71.62	45.00	22.00	429.65	277.32	394.31	349.06	-17.411	7.396	20.630
14	165.03	-48.00	-6.65	30.30	24.00	14.00	26.40	-4.420	-7.390	-3.580
15	165.03	48.00	-6.65	30.30	24.00	14.00	26.40	4.420	7.390	-3.580
16	71.62	0.0	22.00	585.92	539.45	772.63	671.54	6.886	10.440	58.388
17	72.71	-48.00	-11.25	27.90	20.40	13.90	24.90	5.360	-6.930	2.640
18	72.71	48.00	-11.25	27.90	20.40	13.90	24.90	-5.360	6.930	2.640
19	23.00	0.0	22.00	651.63	326.85	306.47	302.66	-10.463	-10.455	2.642
20	163.00	-45.00	76.00	122.43	54.51	128.20	157.38	-12.484	-3.877	-1.035
21	163.00	45.00	76.00	142.16	59.72	119.42	150.25	13.122	7.581	-3.042
22	163.00	-45.00	22.00	241.04	151.21	101.63	87.72	61.090	-2.986	21.695
23	163.00	45.00	22.00	235.84	166.39	125.71	105.32	8.283	-0.325	-6.455
24	71.62	-45.00	76.00	94.55	54.93	123.93	168.21	-13.349	-4.883	-1.020
25	71.62	45.00	76.00	151.03	70.74	146.74	198.63	10.639	9.787	-0.873
26	163.00	0.0	32.00	55.00	180.00	180.00	180.00	0.0	0.0	0.0
27	71.62	0.0	32.00	70.00	180.00	180.00	180.00	0.0	0.0	0.0
28	163.00	0.0	42.00	120.00	180.00	180.00	180.00	0.0	0.0	0.0
29	71.62	0.0	42.00	120.00	180.00	180.00	180.00	0.0	0.0	0.0
30	163.00	0.0	42.00	120.00	180.00	180.00	180.00	0.0	0.0	0.0
31	71.62	0.0	42.00	120.00	180.00	180.00	180.00	0.0	0.0	0.0
32	133.51	0.0	136.52	839.25	16.76	17.03	0.29	0.0	0.0	1.410
33	139.60	0.0	57.00	599.85	410.79	669.82	559.43	2.195	5.182	77.986
34	365.95	0.0	65.04	94.15	81.80	208.88	246.61	2.265	0.945	-23.149

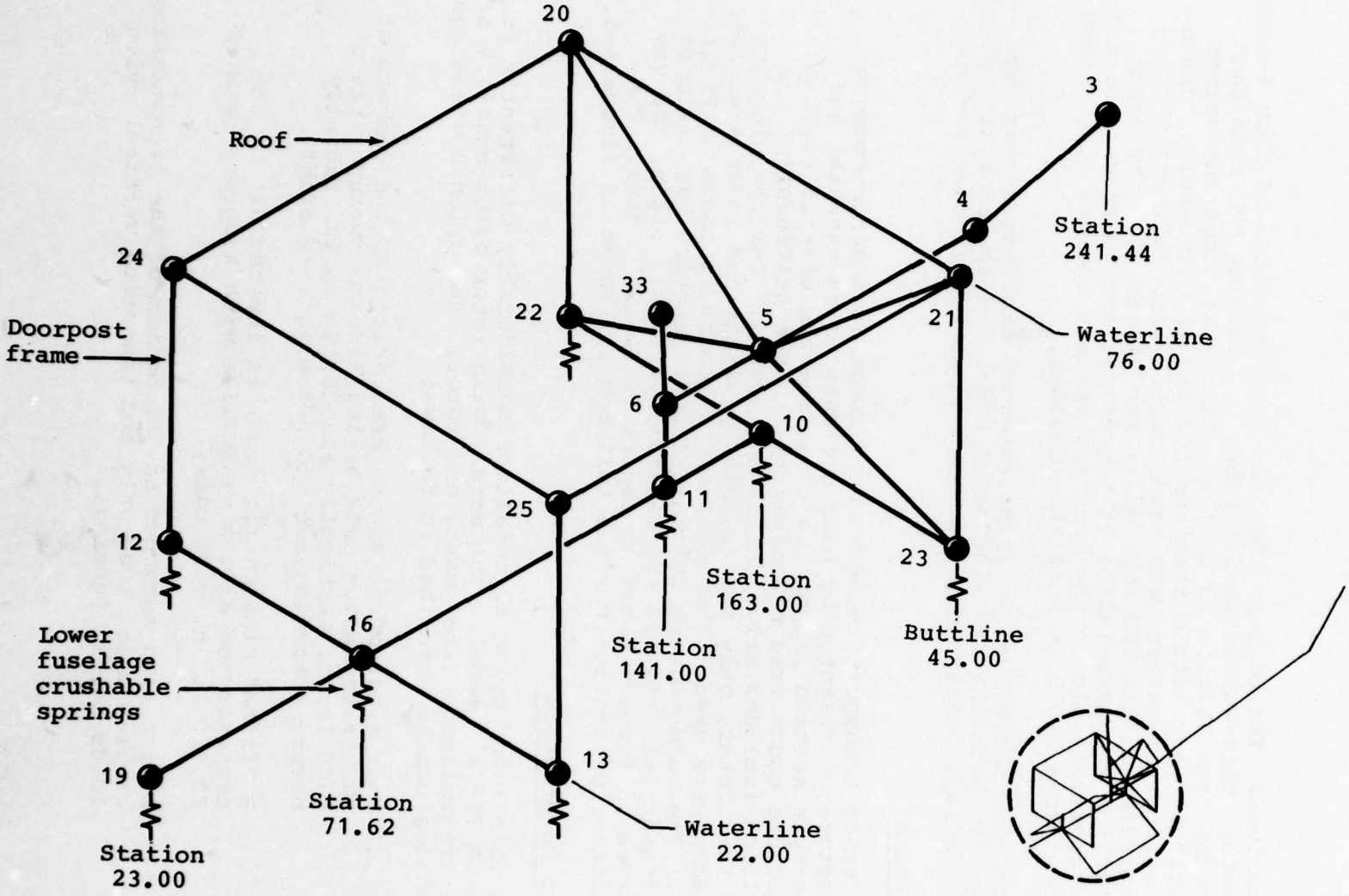

Figure A-2. KRASH model of troop transport helicopter fuselage.

be derived. The concept that was used consisted of four 6-inch-diameter, thin-walled Kevlar tubes filled with PVC foam that extended from Station 23 to 163. Since the tubes themselves contribute very little reaction for radial compression, crushing spring parameters were based on the load-deflection characteristics of the PVC foam only; see Figure 40. The load-deflection characteristics of the energy absorbers were distributed geometrically to the crushing springs located at the mass points along the bottom of the fuselage.

Figure A-3 shows the nonlinear external crushing spring parameters for both the baseline metal model and the composite model. The fuselage idealization contains no nonlinear beam elements.

Tailboom

The troop transport helicopter tailboom is a semimonocoque structure represented by beam elements using material and structure section properties to define the elastic stiffness. Structure considered not effective in the stiffness of the tailboom includes drive shafts and covers. For the elevator and tail rotor, only the rigid body weight and inertia effects of each were used. The idealized tailboom is shown in Figure A-4. The beam element at the tailboom junction was assigned nonlinear stiffness in the lateral, vertical, pitch, and yaw degrees of freedom based on report TR 74-12A[49] data. The nonlinear properties for the tailboom are shown in Figure A-5.

Main Rotor Pylon

The main rotor pylon is idealized considerably differently from the TR 72-72[48] model. The actual main rotor pylon consists of the transmission case, mast, and rotor. The pylon-to-fuselage mounting can be described as follows:

1. Four elastomeric mounts are located at the corners of the transmission case having elastic spring rates of 4500 lb/in. vertically and 28,125 lb/in. radially before bottoming out and becoming very stiff.

2. A "fifth" elastomeric mount is located aft of the transmission on the centerline with a spring rate of 20,000 lb/in. vertically.

3. A lift link attached to the bottom of the transmission carries axial load only and transmits vertical pylon loads to the fuselage.

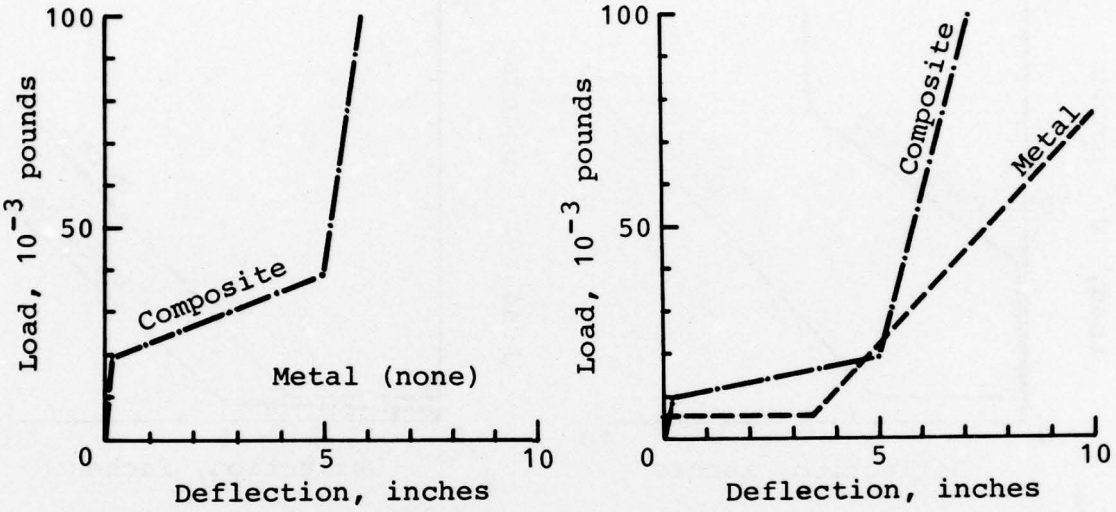

(a) Mass point: 19
Degree-of-freedom: 3

(b) Mass point: 12
Degree-of-freedom: 3

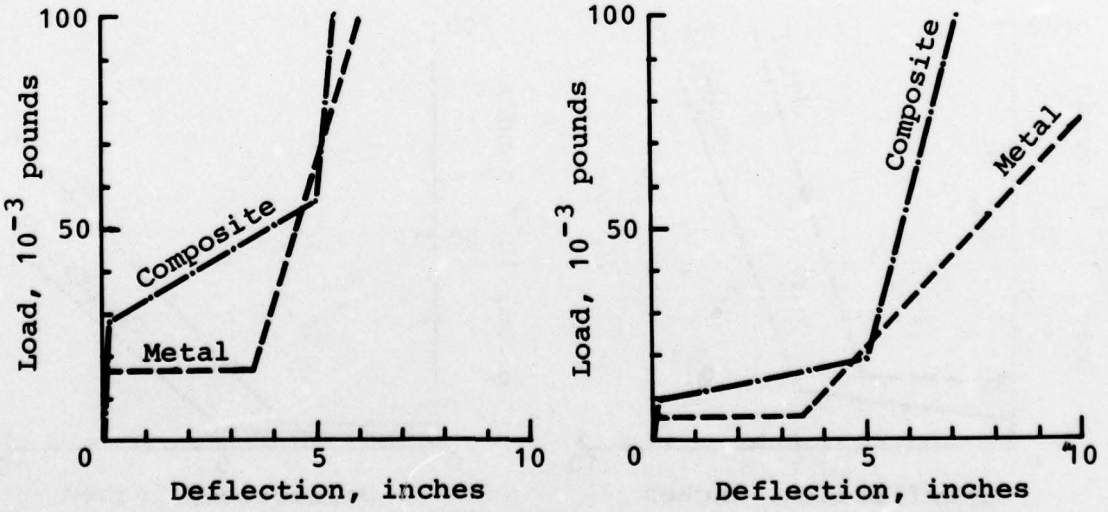

(c) Mass point: 16
Degree-of-freedom: 3

(d) Mass point: 13
Degree-of-freedom: 3

Figure A-3. KRASH model external crushing spring data for metal and composite airframes.

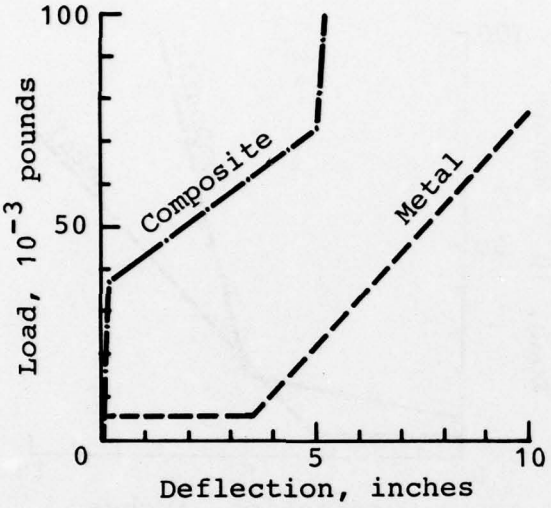

(e) Mass point: 11
Degree-of-freedom: 3

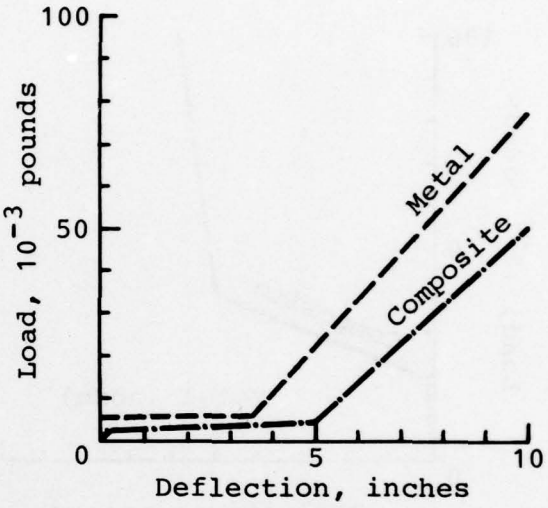

(f) Mass point: 22
Degree-of-freedom: 3

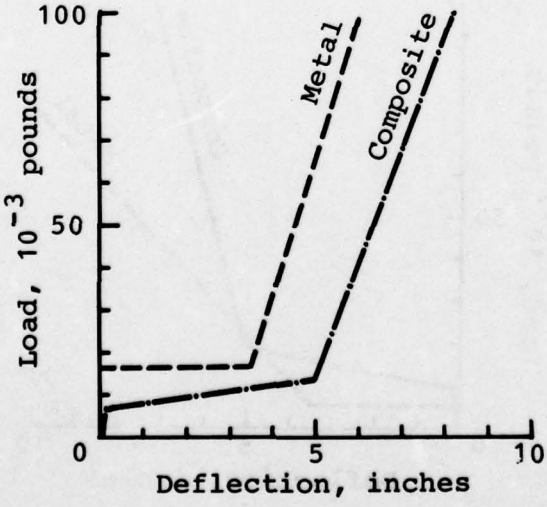

(g) Mass point: 10
Degree-of-freedom: 3

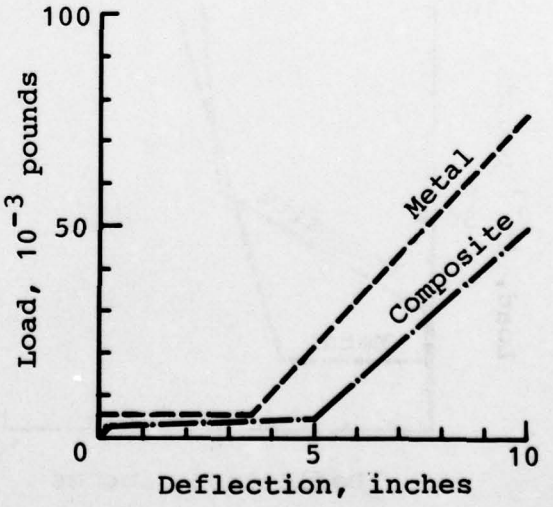

(h) Mass point: 23
Degree-of-freedom: 3

Figure A-3 (concluded).

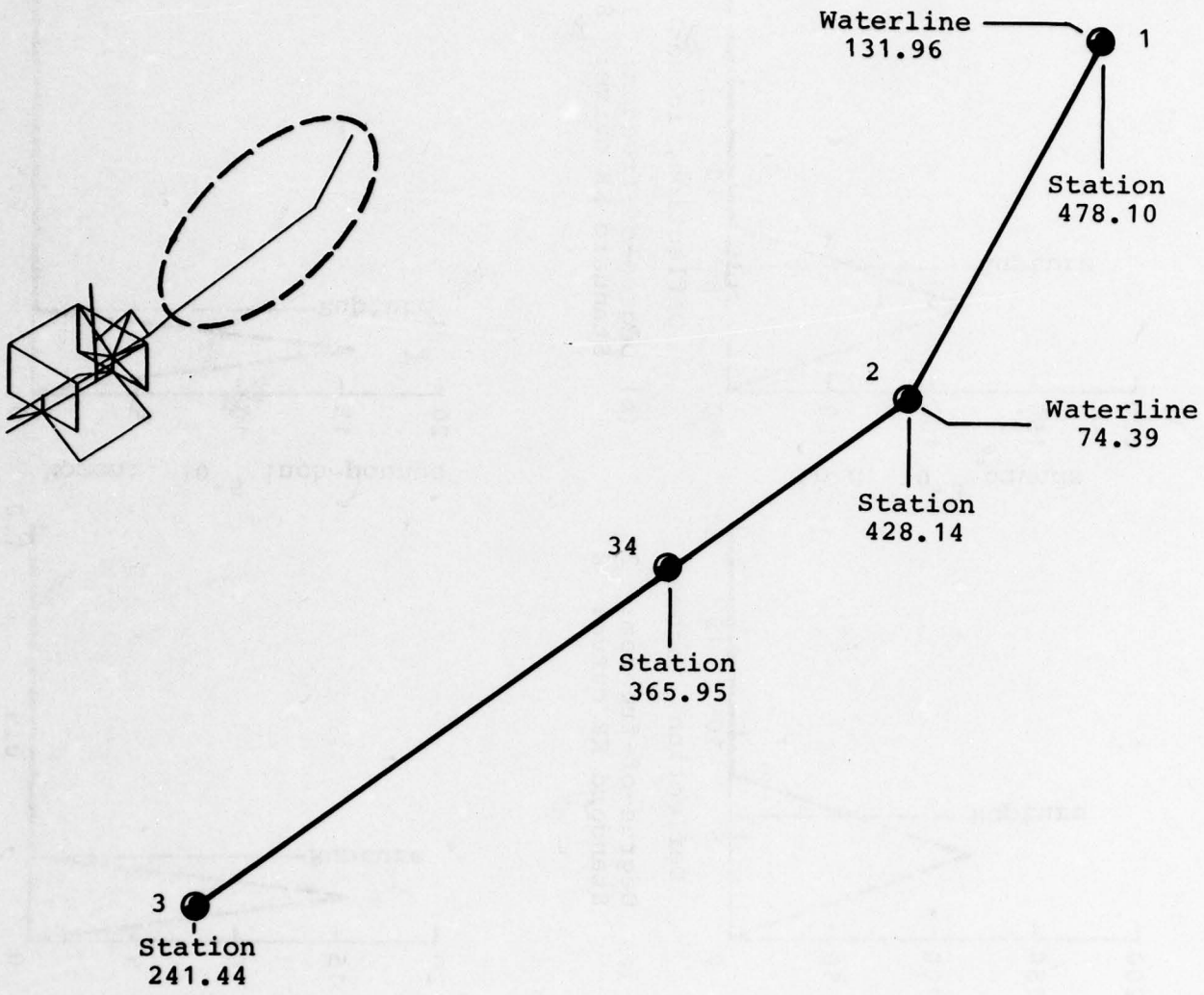

Figure A-4. KRASH model of troop transport helicopter tailboom.

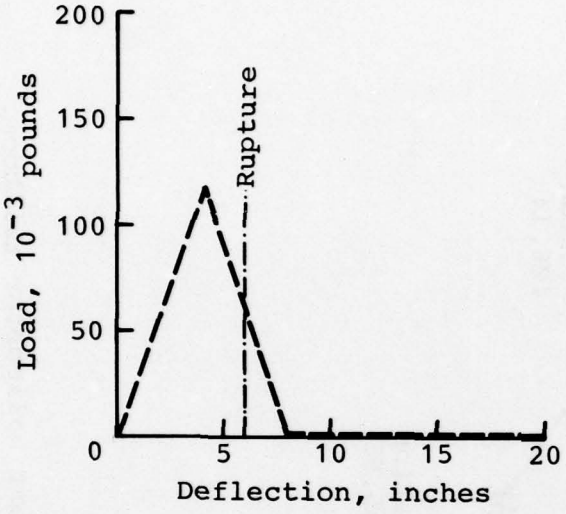

(a) Degree-of-freedom: 2
Standard KR curve: 8

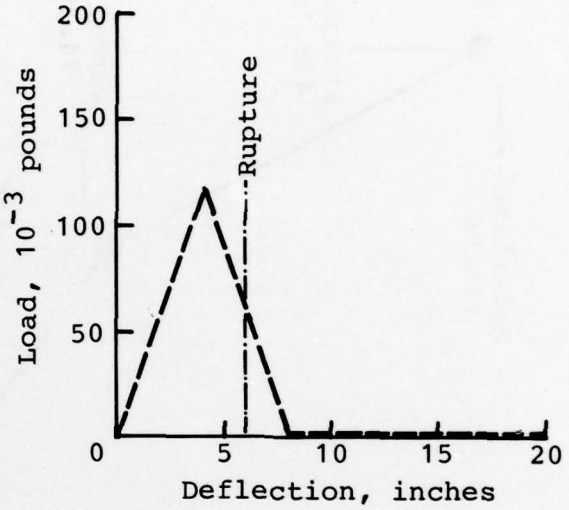

(b) Degree-of-freedom: 3
Standard KR curve: 8

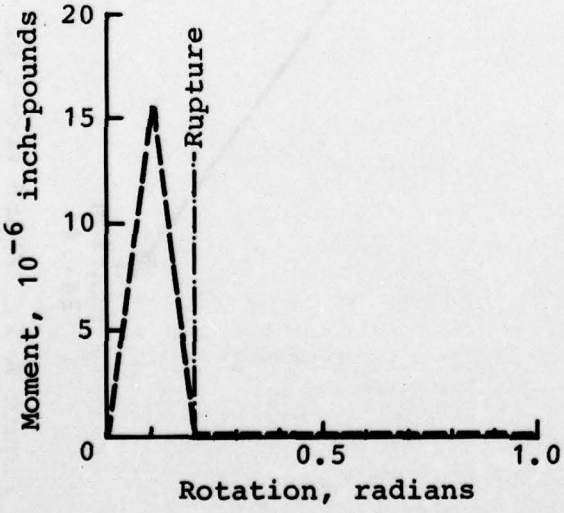

(c) Degree-of-freedom: 5
Standard KR curve: 8

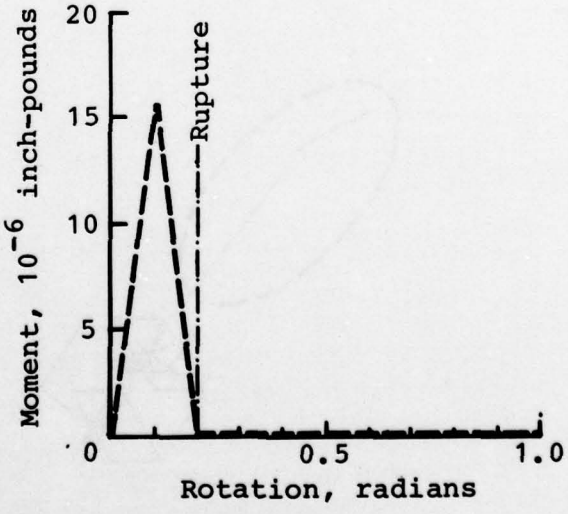

(d) Degree-of-freedom: 6
Standard KR curve: 8

Figure A-5. KRASH model nonlinear beam properties for tailboom (element 3-34).

The pylon is idealized with beam elements as shown in Figure A-6. The mass points have the proper weights and inertia distribution; however, the rotational mass inertia of the blades is not included.

The beam element (9-33) representing the main rotor pylon mounting has nonlinear stiffness properties in the pitch and roll degrees of freedom which are shown in Figure A-7. The beam element elastic stiffness gives the correct pylon rocking mode natural frequencies. The mounts bottom out when the pylon pitch or roll angular motions exceed ±2.9 degrees. The maximum load at failure was based on the static criteria of 8g for the pylon in the fore-and-aft and lateral directions. The moment in the mount beam element at failure was calculated by summing the "weight x 8g x length" terms for each mass point about the mounting plane waterline. No failure or nonlinear stiffness properties were calculated for the other degrees of freedom.

Engine and Mounts

The Lycoming T53-L-13 engine is modeled as a rigid lumped mass. The mass point weight and inertia data include the basic engine plus BHT-installed engine-supported weight items such as residual fluids, starter-generator, and tailpipe. The engine mounting scheme employs pinned tubes arranged as follows:

1. Aft right bipod
2. Left aft tripod
3. Forward right monopod
4. Forward left monopod (effective only in the event of failure of right side monopod)

The mounts are modeled with two beam elements having nonlinear stiffness properties. The engine-to-transmission driveshaft is modeled with a beam element having only torsional stiffness. The idealized KRASH model is shown in Figure A-8.

The engine mounting idealization including the nonlinear stiffness parameters presented in Figures A-9 and A-10 were taken directly from TR 72-72[48]. More information on the modeling techniques can also be found in TR 74-12A[49].

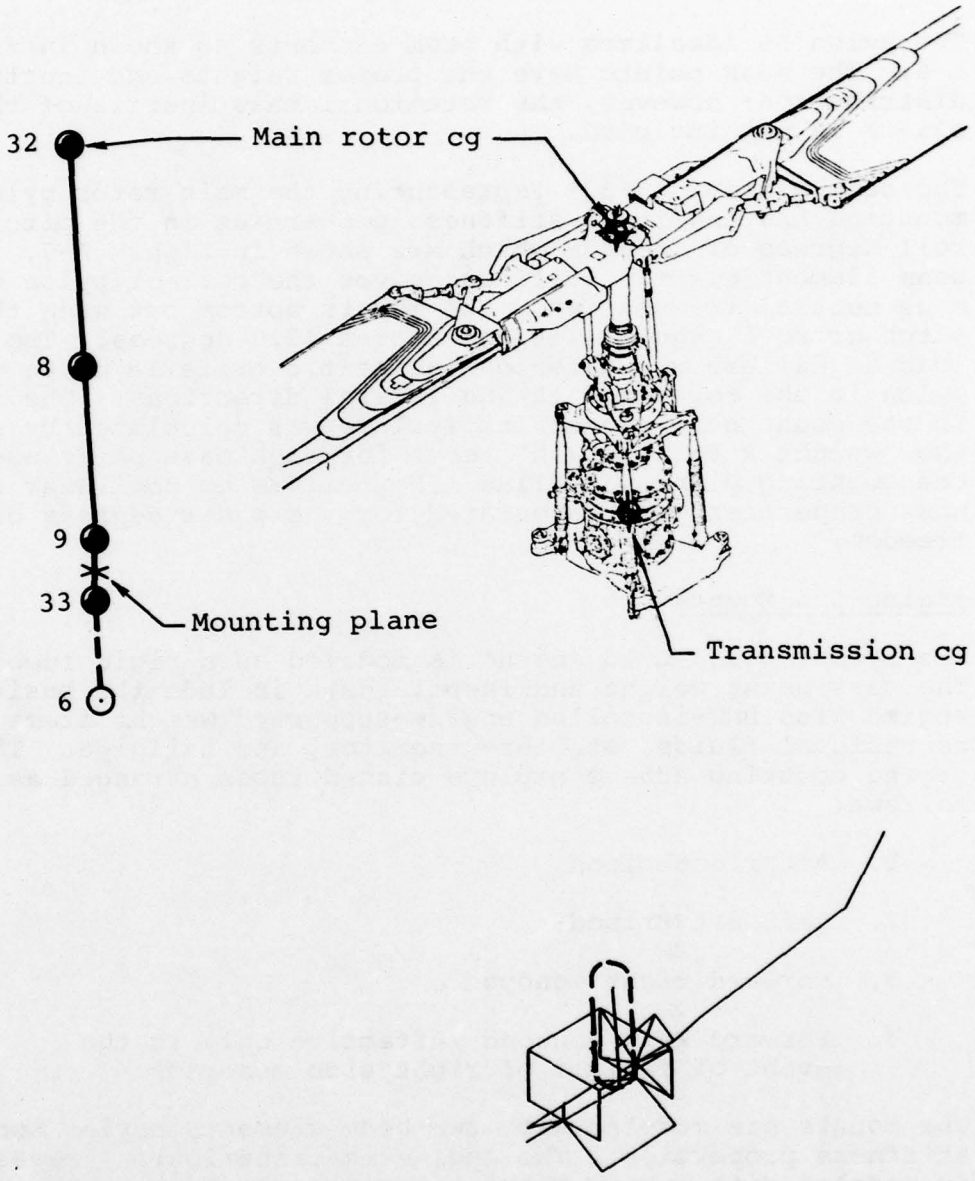

Figure A-6. KRASH model of troop transport helicopter main rotor pylon.

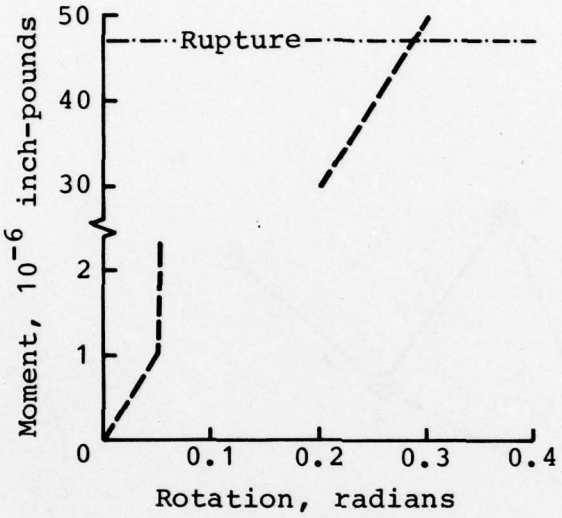

(a) Degree-of-freedom: 5
Nonstandard KR curve: 10

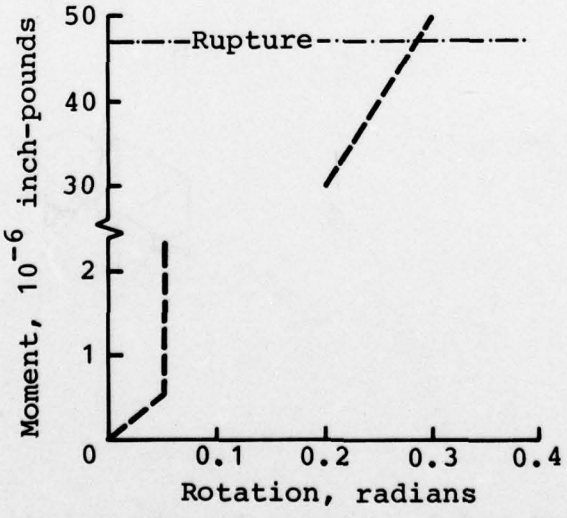

(b) Degree-of-freedom: 6
Nonstandard KR curve: 10

Figure A-7. KRASH model nonlinear beam properties for main rotor pylon soft mounting (element 9-33).

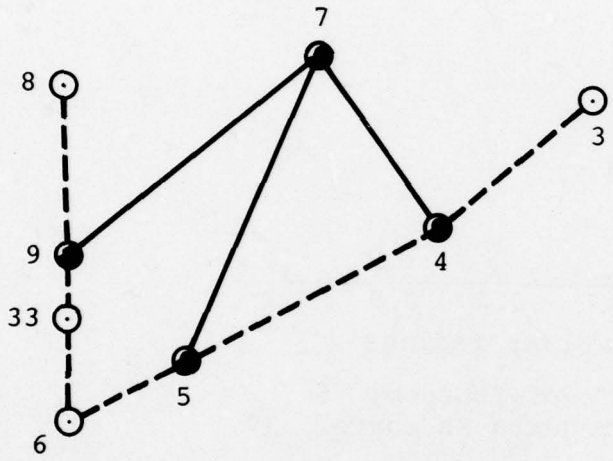

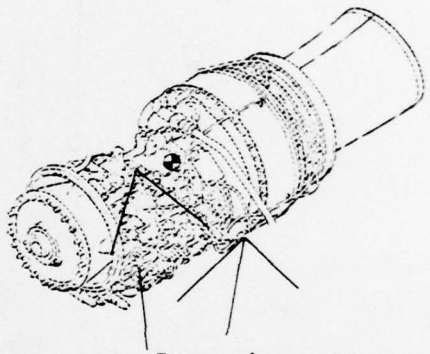

Lycoming T53-L-13
engine mounting

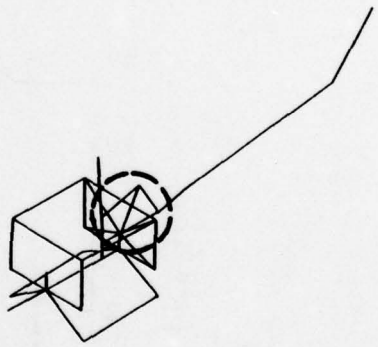

Figure A-8. KRASH model of troop transport helicopter engine and mounts.

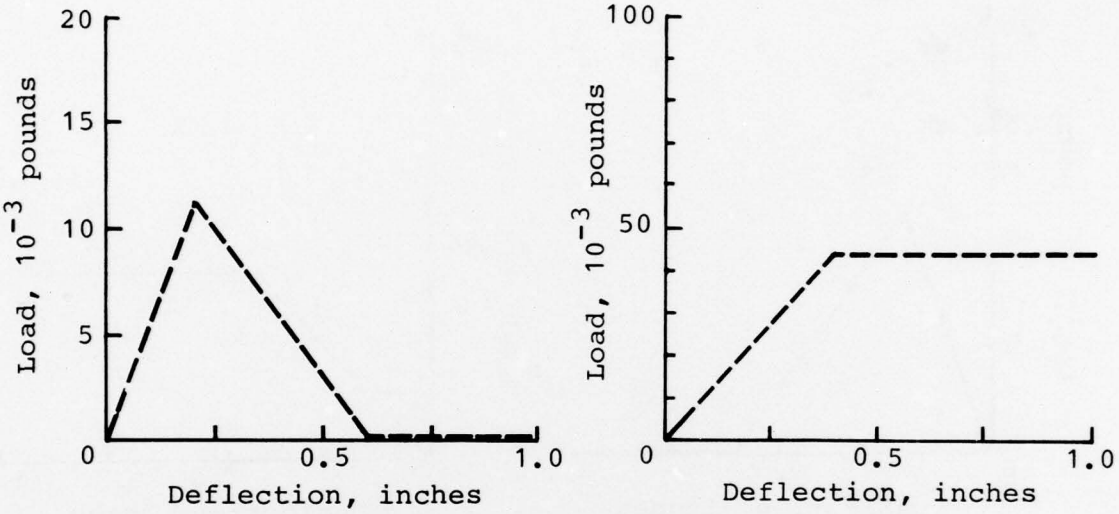

(a) Degree-of-freedom: 1
Standard KR curve: 7

(b) Degree-of-freedom: 2
Standard KR curve: 5

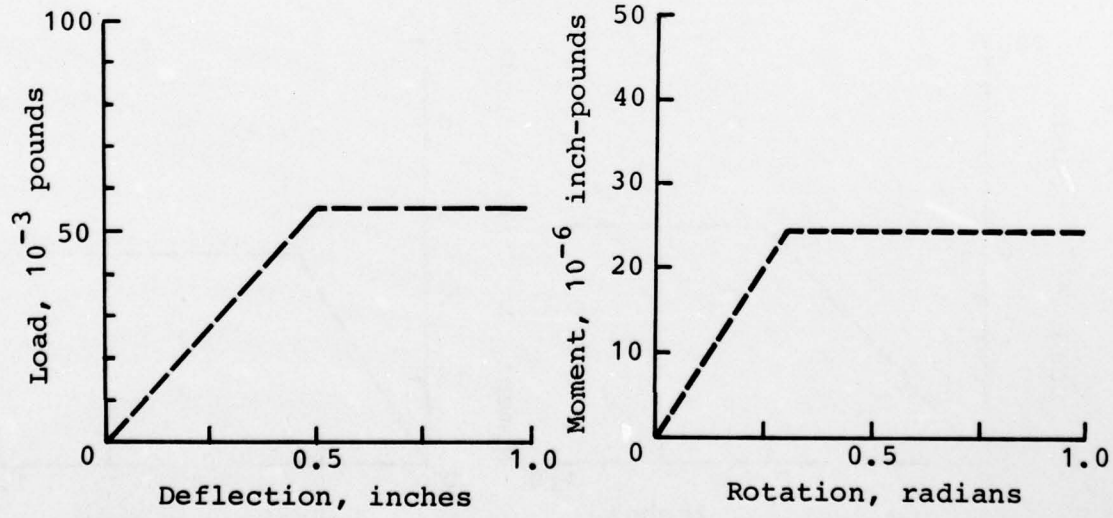

(c) Degree-of-freedom: 3
Standard KR curve: 5

(d) Degree-of-freedom: 5,6
Standard KR curve: 5

Figure A-9. KRASH model nonlinear beam properties for forward engine mount (element 5-7).

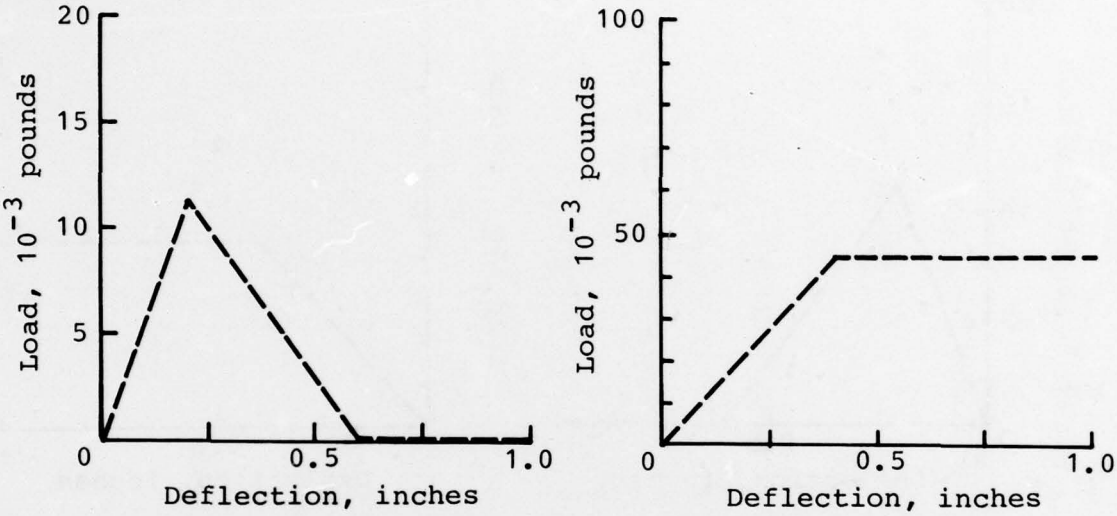

(a) Degree-of-freedom: 1
Standard KR curve: 7

(b) Degree-of-freedom: 2
Standard KR curve: 5

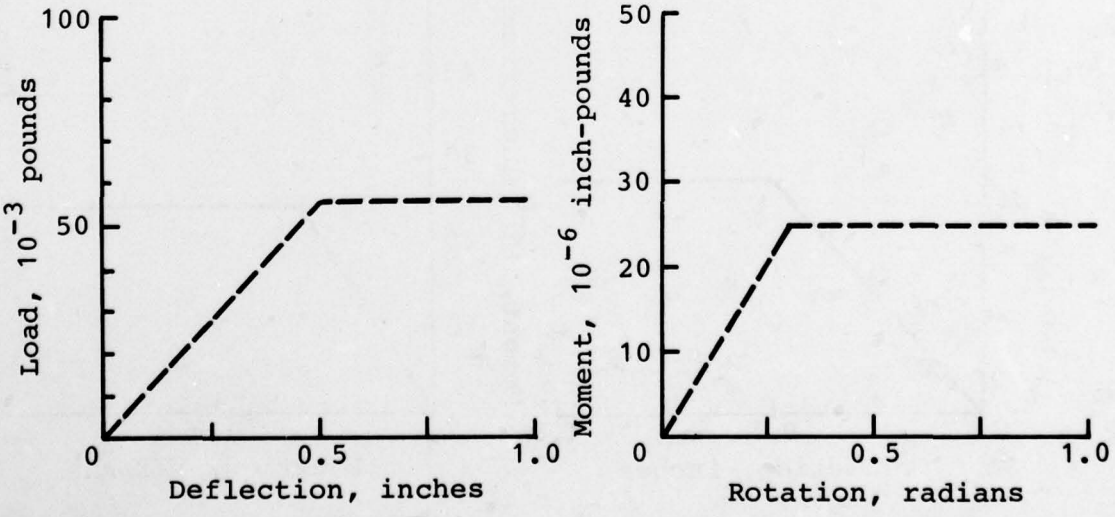

(c) Degree-of-freedom: 3
Standard KR curve: 5

(d) Degree-of-freedom: 5,6
Standard KR curve: 5

Figure A-10. KRASH model nonlinear beam properties for aft engine mount (element 4-7).

Landing Gear

The troop transport helicopter landing gear is of tubular construction. The forward and aft cross tubes are tied together with longitudinal skid tubes.

The cross tubes are pin-connected to the lower fuselage structure at four points. The skid tube to cross tube attachments can be assumed as welded joints.

The KRASH model idealization is shown in Figure A-11. The external crushing spring data are shown in Figure A-12 and the nonlinear beam element stiffness characteristics of the cross tubes are shown in Figures A-13 and A-14. These were taken from TR 72-72[48]. Report TR 74-12A[49] also provides information on the modeling techniques involved in the idealization.

Occupant/Seat

The occupant/seat models for the forward crew and aft passenger are shown in Figure A-15. The troop transport helicopter was analyzed using standard, nonstroking seats. As shown in Figure A-16, the two occupant/seat weights are the seat plus lower torso at the lower point and the upper torso at the upper point.

The weight for the Dynamic Response Index (DRI) beam element is that of the upper torso also. Although the helicopter model weights distribution includes a full load of crew and passengers, only one crew and one passenger are modeled in detail. The other masses are lumped to the bottom fuselage mass points. A DRI element is also connected to the seat mass point but does not actually apply loads to the seat.

The beam element stiffnesses for the occupants are selected to give 10 and 8 Hz natural frequencies for the man and DRI, respectively. With the FAA version of KRASH, this is done automatically using special material codes.

KRASH Input Data Listing

The input data for the metal baseline KRASH model is listed in Table A-3. The listing is annotated for quick reference.

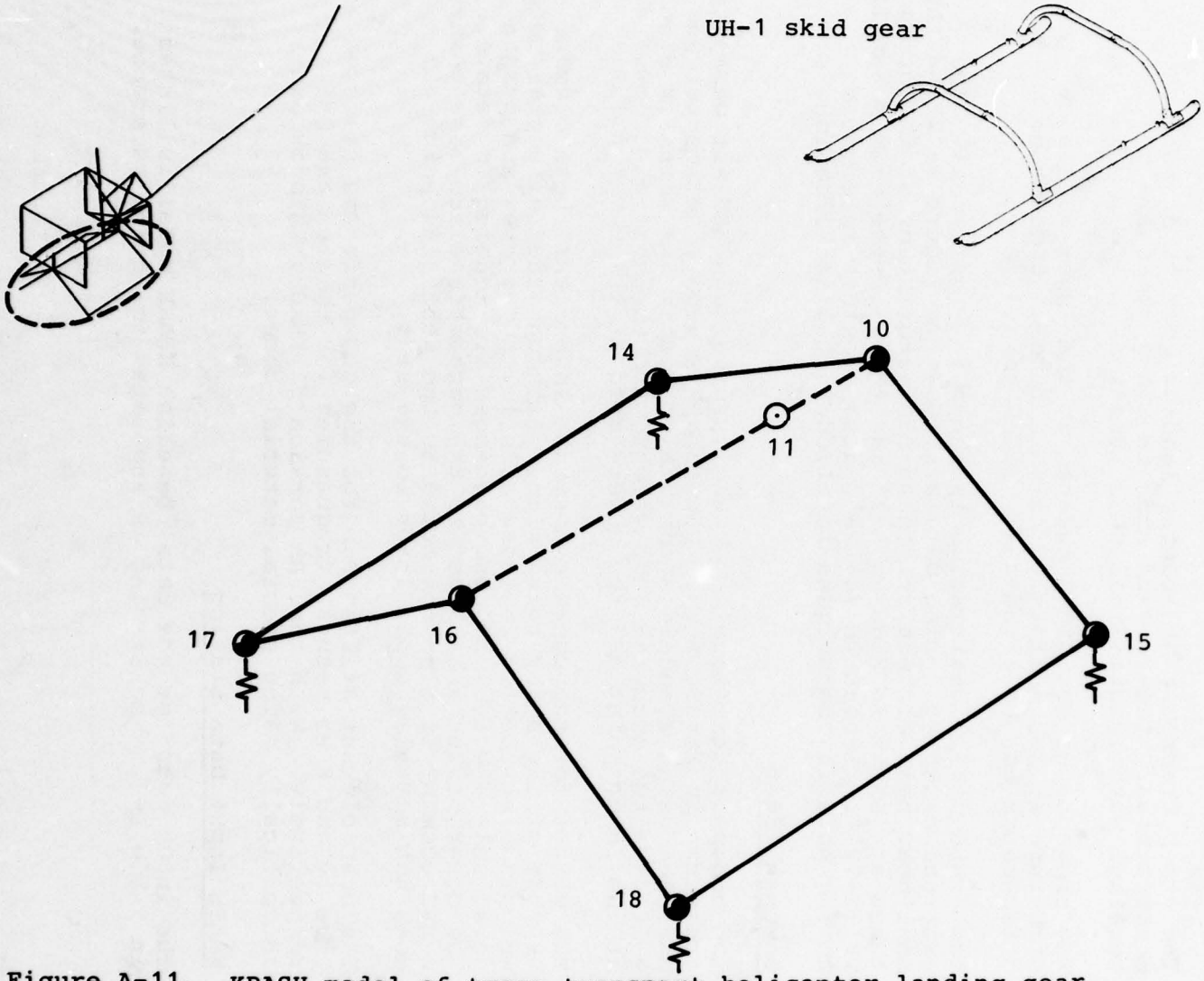

Figure A-11. KRASH model of troop transport helicopter landing gear.

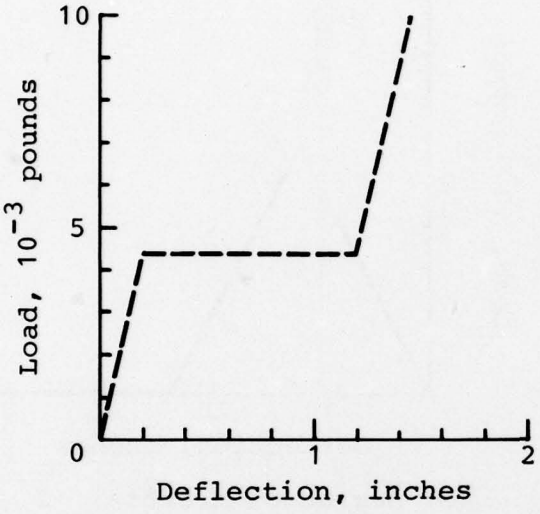

(a) Mass point: 17
Degree-of-freedom: 3

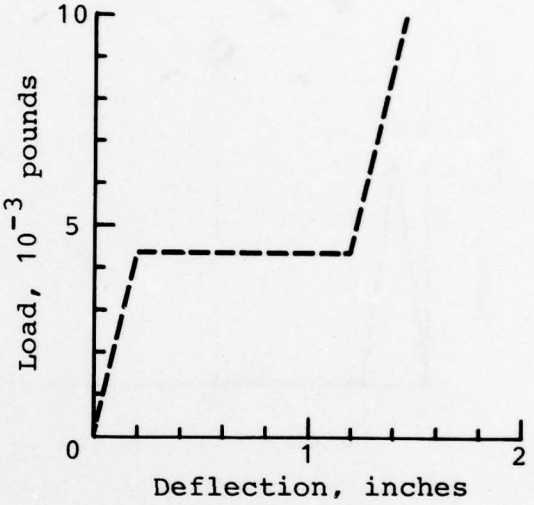

(b) Mass point: 18
Degree-of-freedom: 3

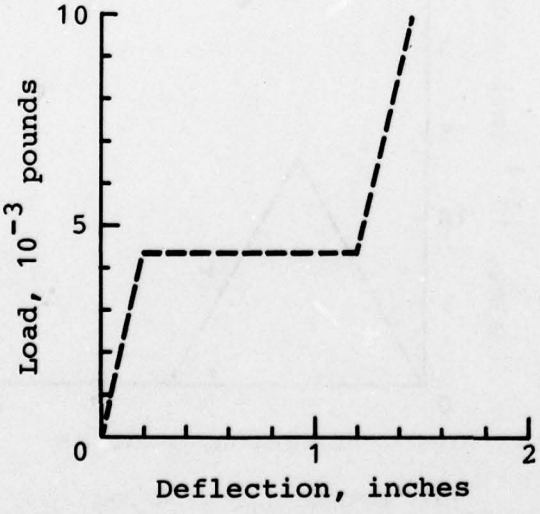

(c) Mass point: 14
Degree-of-freedom: 3

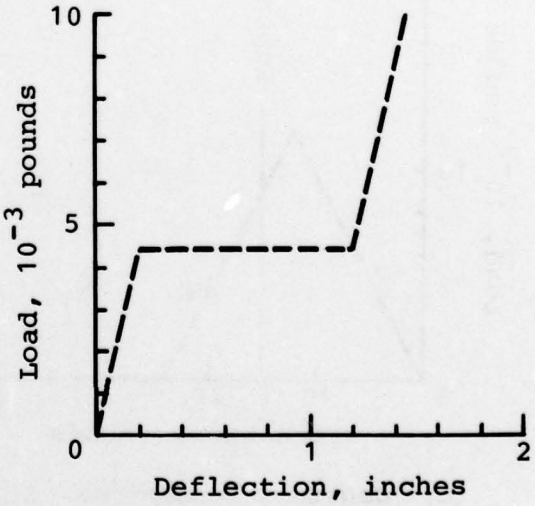

(d) Mass point: 15
Degree-of-freedom: 3

Figure A-12. KRASH model external crushing spring data for landing gear.

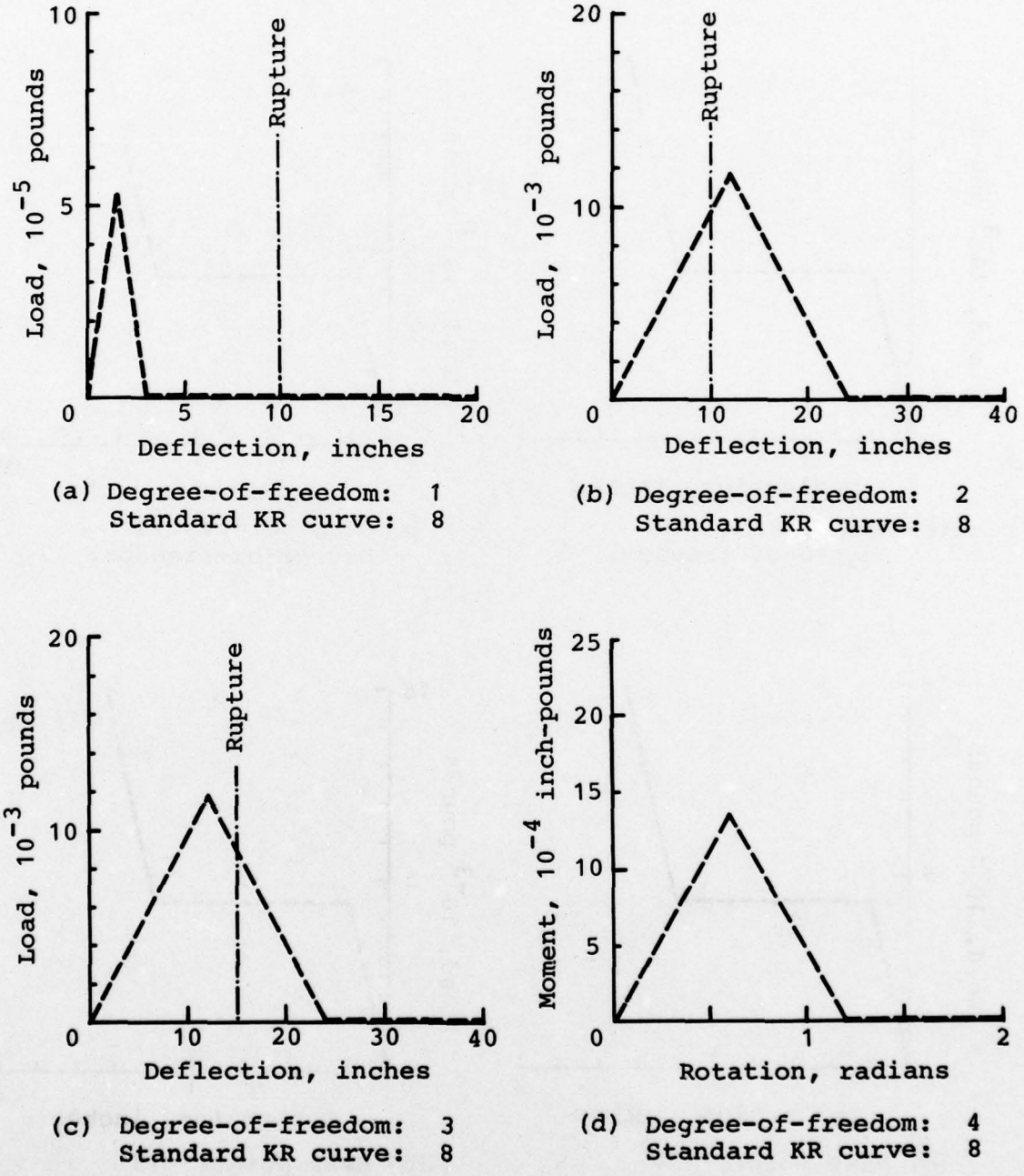

(a) Degree-of-freedom: 1
Standard KR curve: 8

(b) Degree-of-freedom: 2
Standard KR curve: 8

(c) Degree-of-freedom: 3
Standard KR curve: 8

(d) Degree-of-freedom: 4
Standard KR curve: 8

Figure A-13. KRASH model nonlinear beam properties for forward cross tubes (elements 16-17, 16-18).

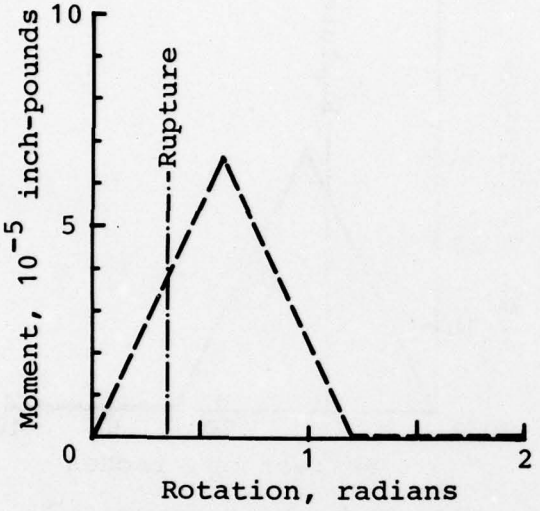

(e) Degree-of-freedom: 5
Standard KR curve: 8

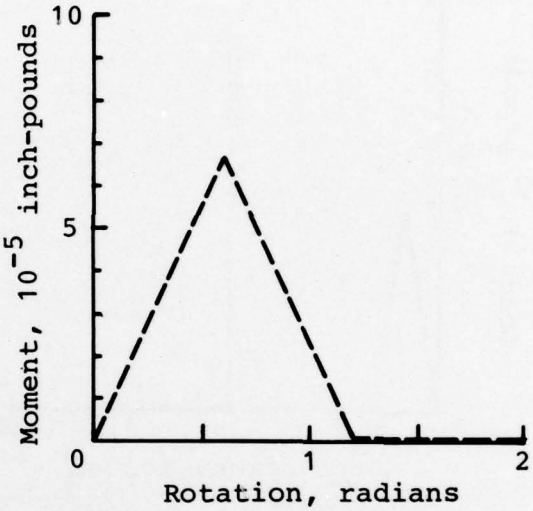

(f) Degree-of-freedom: 6
Standard KR curve: 8

Figure A-13 (concluded).

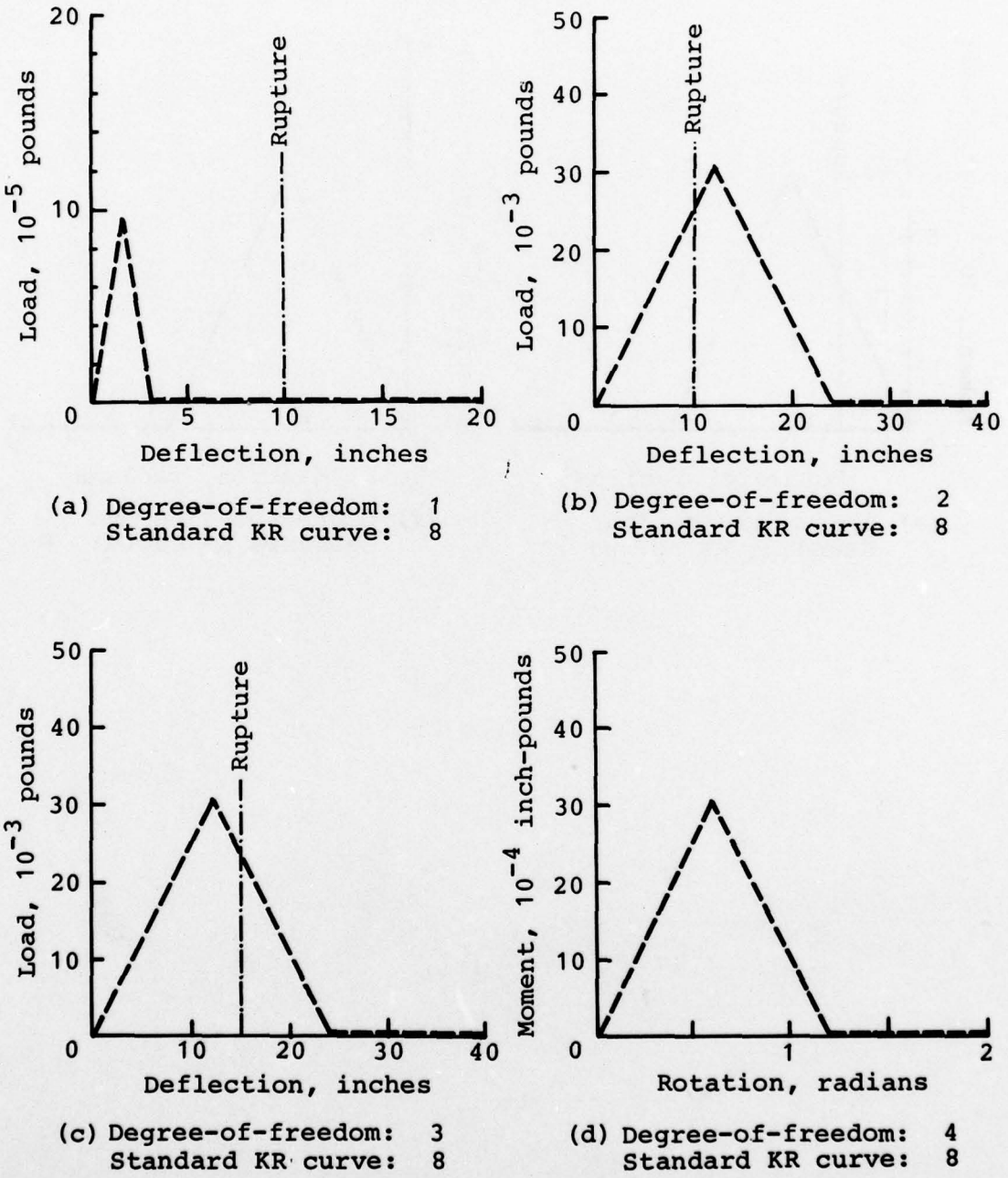

(a) Degree-of-freedom: 1
Standard KR curve: 8

(b) Degree-of-freedom: 2
Standard KR curve: 8

(c) Degree-of-freedom: 3
Standard KR curve: 8

(d) Degree-of-freedom: 4
Standard KR curve: 8

Figure A-14. KRASH model nonlinear beam properties for aft cross tubes (elements 10-14, 10-15).

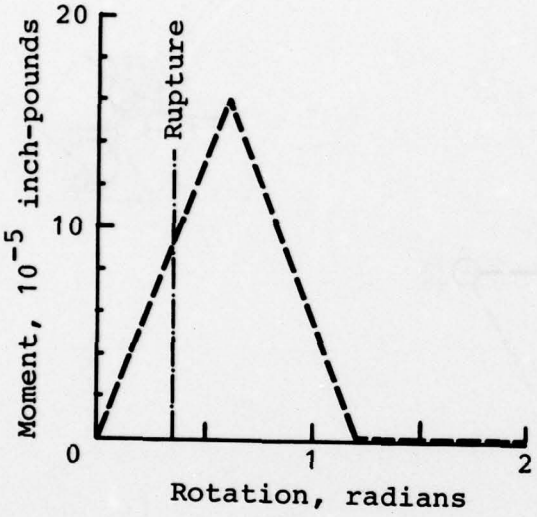

(e) Degree-of-freedom: 5
Standard KR curve: 8

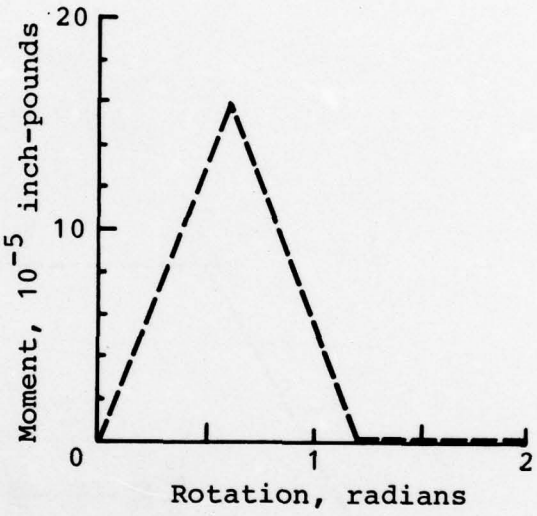

(f) Degree-of-freedom: 6
Standard KR curve: 8

Figure A-14 (concluded).

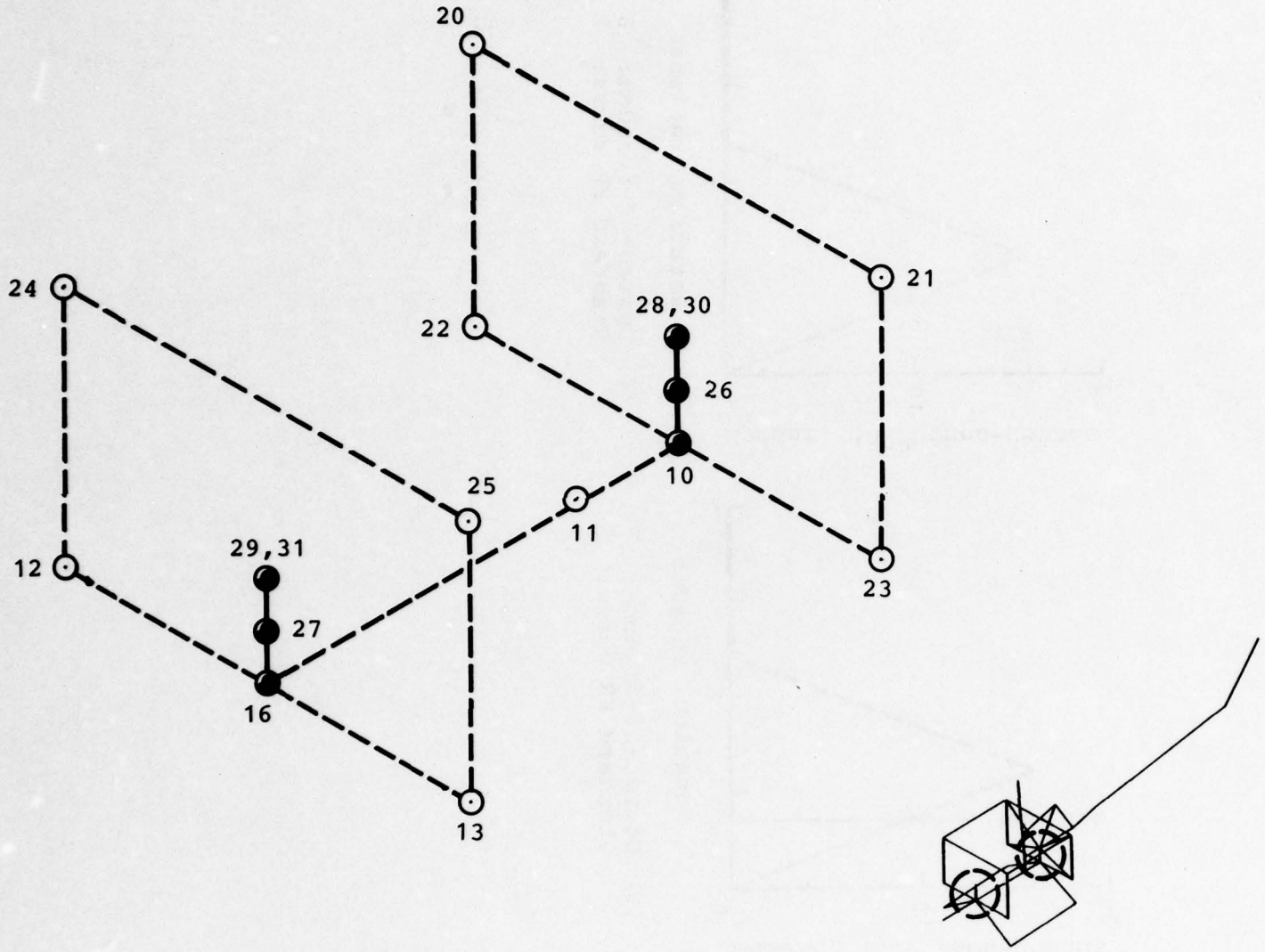

Figure A-15. KRASH occupant/seat models.

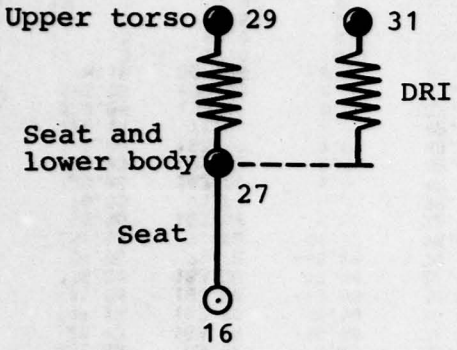

(a) Forward occupant/seat model
(pilot)

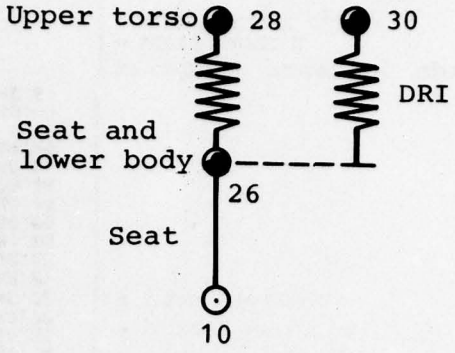

(b) Aft occupant/seat model
(aft passenger)

Forward occupant/seat weight distribution
120 pounds at mass point 29
120 pounds at mass point 31
70 pounds at mass point 27
586 pounds at mass point 16

Aft occupant/seat weight distribution
120 pounds at mass point 28
120 pounds at mass point 30
55 pounds at mass point 26
358 pounds at mass point 10

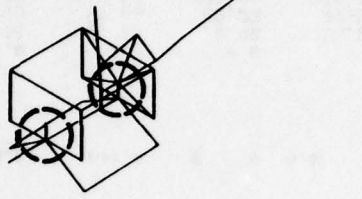

Figure A-16. Detail of KRASH occupant/seat models.

TABLE A-3. ANNOTATED KRASH INPUT DATA DECK

```
00010 METAL BASELINE KRASH MODEL - 9500 LB GROSS WEIGHT
00020 INITIAL CONDITIONS:  TR72-72 REPORT
00030 123456789012345678901234567890123456789012345678901234567890123456789012
00040   34   11   45   42   27    0    1    2    1    0   44    1    0    4
00050
00060
00070       200  0.000010      0.16       0.0      100.0    0    0  0.0    0
00080
00090    1    1    1    1    1    0    1
00100   13    0   10   10    0   11    2
00110        0.0     -223.2     276.0
00120     0.4615        0.0       0.0
00130    -0.1746    -0.01746       0.0        0.0        0.0        0.0
00140      74.50      478.10       0.0     131.96      11.92      10.98      12.88
00150      71.86      428.14       0.0      74.39      17.02      62.23      47.59
00160     135.36      241.44       0.0      46.31     120.37     332.03     289.39
00170     285.79      211.86       0.0      38.45     238.77     190.14     175.35
00180     613.08      163.00       0.0      38.45     380.84     248.81     241.88
00190     862.94      141.00       0.0      38.45     583.69     801.18     625.08
00200     536.90      186.83       0.0      79.17     139.21     328.49     322.81
00210     248.97      136.90       0.0      98.00      32.28      38.24       7.03
00220     314.76      139.60       0.0      67.00      56.29     138.07      88.37
00230     357.52      163.00       0.0      22.00     344.01     231.78     216.40
00240     771.08      141.00       0.0      22.00     535.86     724.87     566.98
00250     332.28       71.62     -45.00     22.00     247.99     361.25     308.38
00260     429.65       71.62      45.00     22.00     277.32     394.31     349.06
00270       30.3      165.03     -48.00     -6.65       24.0       14.0       26.4
00280       30.3      165.03      48.00     -6.65       24.0       14.0       26.4
00290     585.92       71.62       0.0      22.00     539.45     772.63     671.54
00300       27.9       72.71     -48.00     -11.25       20.4       13.9       24.9
00310       27.9       72.71      48.00     -11.25       20.4       13.9       24.9
00320     651.63       23.00       0.0      22.00     326.85     306.47     302.66
00330     122.43      163.00     -45.00      76.00      54.51     128.20     157.38
00340     142.16      163.00      45.00      76.00      59.72     119.42     150.25
00350     241.04      163.00     -45.00      22.00     151.21     101.63      87.72
00360     235.84      163.00      45.00      22.00     166.39     125.71     105.32
00370      94.55       71.62     -45.00      76.00      54.93     123.93     168.21
00380     151.03       71.62      45.00      76.00      70.74     146.74     198.63
00390      95.00      163.00       0.0       32.00     180.00     180.00     180.00
00400      70.00       71.62       0.0       32.00     180.00     180.00     180.00
00410     180.00      163.00       0.0       42.00     180.00     180.00     180.00
00420     120.00       71.62       0.0       42.00     180.00     180.00     180.00
00430     180.00      163.00       0.0       42.00     180.00     180.00     180.00
00440     120.00       71.62       0.0       42.00     180.00     180.00     180.00
00450     839.85      133.51       0.0     136.52      16.76      17.03       0.28
00460     598.85      139.60       0.0      57.00     410.79     669.82     559.43
00470      94.15      366.95       0.0      65.04      81.88     208.88     246.61
00480   10    3      17.0         0.3   33000.0        0.0        0.0
00490   11    3      17.0         0.3   11000.0        0.0        0.0
00500   12    3      17.0         0.3   11000.0        0.0        0.0
00510   13    3      17.0         0.3   11000.0        0.0        0.0
00520   14    3      8.25         0.3   22000.0        0.0        0.0
00530   15    3      8.25         0.3   22000.0        0.0        0.0
00540   16    3      17.0         0.3   33000.0        0.0        0.0
00550   17    3      8.25         0.3   22000.0        0.0        0.0
00560   18    3      8.25         0.3   22000.0        0.0        0.0
00570   22    3      17.0         0.3   11000.0        0.0        0.0
00580   23    3      17.0         0.3   11000.0        0.0        0.0
```

Title cards

Control cards

Initial conditions

Mass point data
- weight
- station
- buttline
- waterline
- roll inertia
- pitch inertia
- yaw inertia

External crushing spring data
- mass point
- degree-of-freedom
- free length of spring
- bottoming out spring rate
- plowing force
- soil flexibility coefficient

TABLE A-3 (CONTINUED).

00590	0.001	1.0	2.0	3.5	16500.0	16500.0		
00600	0.001	1.0	2.0	3.5	5500.0	5500.0		
00610	0.001	1.0	2.0	3.5	5500.0	5500.0		
00620	0.001	1.0	2.0	3.5	5500.0	5500.0		
00630	0.2	0.4	0.6	1.2	4400.0	4400.0		
00640	0.2	0.4	0.6	1.2	4400.0	4400.0		
00650	0.001	1.0	2.0	3.5	16500.0	16500.0		
00660	0.2	0.4	0.6	1.2	4400.0	4400.0		
00670	0.2	0.4	0.6	1.2	4400.0	4400.0		
00680	0.001	1.0	2.0	3.5	5500.0	5500.0		
00690	0.001	1.0	2.0	3.5	5500.0	5500.0		
00700	1 2	9.520	154.520	58.860	44.150		4	
00710	2 34	9.520	556.460	212.110	212.110		4	
00720	3 34	9.520	1226.670	467.370	467.370		4	
00730	3 4	9.520	1727.140	658.250	658.250		4	
00740	4 5	9.520	1796.990	807.270	731.990		4	
00750	5 6	4.760	2591.550	1316.150	987.380		4	
00760	5 20	0.893	0.0	83.877	0.0		16	
00770	5 21	0.893	0.0	83.877	0.0		16	
00780	5 22	0.901	0.0	67.918	0.0		16	
00790	5 23	0.901	0.0	67.918	0.0		16	
00800	6 33	8.283	183.104	60.847	74.982		4	
00810	9 33	2.570	54.880	4.760	2.620		4	
00820	6 11	0.7619	33.9880	12.0956	14.9343		4	
00830	4 7	0.254	0.0	93.524	93.524		16	
00840	5 7	0.253	0.0	92.384	92.384		16	
00850	7 9	0.0	26.003	0.0	0.0		4	
00860	8 9	9.520	371.430	185.710	185.710		4	
00870	8 32	9.520	22.870	11.440	11.440		4	
00880	10 11	4.760	2591.550	1316.150	987.380		4	
00890	10 14	3.387	7.118	3.559	3.559		4	
00900	10 15	3.387	7.118	3.559	3.559		4	
00910	10 22	0.381	0.0	95.241	16.191		16	
00920	10 23	0.381	0.0	95.241	16.191		16	
00930	11 16	9.520	1271.000	645.670	484.230		4	
00940	12 16	7.620	12.004	15.353	92.192		4	
00950	12 24	0.762	4.824	92.195	6.762		4	
00960	13 16	7.620	12.004	15.353	92.192		4	
00970	13 25	0.762	4.824	92.195	6.762		4	
00980	20 24	3.258	0.0	0.0	0.0		4	
00990	21 25	3.258	0.0	0.0	0.0		4	
01000	16 17	1.963	3.089	1.549	1.549		4	
01010	16 18	1.963	3.089	1.549	1.549		4	
01020	14 17	1.165	4.446	2.223	2.223		4	
01030	15 18	1.165	4.446	2.223	2.223		4	
01040	16 19	9.520	215.580	46.780	82.130		4	
01050	20 21	0.381	0.0	95.271	16.195		16	
01060	20 22	0.381	0.0	16.191	95.246		16	
01070	21 23	0.381	0.0	16.191	95.246		16	
01080	24 25	7.620	1.474	1.762	23.036		4	
01090	10 26	0.010	2.500	0.873	0.873		4	
01100	16 27	0.020	2.500	0.873	0.873		4	
01110	26 28	1.0	0.01227	0.3	0.0075	0.0075	9	
01120	27 29	1.0	0.01227	0.3	0.0075	0.0075	9	
01130	26 30	1.0	0.007855	0.3	0.0048	0.0048	10	
01140	27 31	1.0	0.007855	0.3	0.0048	0.0048	10	

External crushing spring data
- x_o, x_1, x_2, x_f, F_{0-1}, F_{2-f}

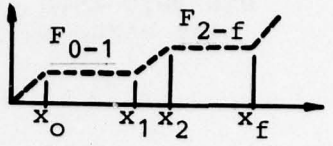

Beam element linear data
- mass point at end A
- mass point at end B
- area
- J } cross-sectional
- Iyy } properties
- Izz
- z } stress recovery
- y
- material id

TABLE A-3 (CONTINUED).

01150	16			10.5E06	0.0	47000.	39000.	0.0	Non-standard material definition
01160		0.04							Standard beam element damping ratio
01170	26	28		0.955					Non-standard beam element damping ratio
01180	27	29		0.814					
01190	26	30		0.700					
01200	27	31		0.597					
01210	3	34	2	8	4.0	0.0			Nonlinear beam element properties • mass point at end A • mass point at end B • degree-of-freedom • standard KR curve id • linear deflection point • linear deflection point for KR=9
01220	3	34	3	8	4.0	0.0			
01230	3	34	5	8	0.1	0.0			
01240	3	34	6	8	0.1	0.0			
01250	4	7	1	7	0.2	0.0			
01260	4	7	2	5	0.4	0.0			
01270	4	7	3	5	0.5	0.0			
01280	4	7	4	5	0.3	0.0			
01290	4	7	5	5	0.3	0.0			
01300	4	7	6	5	0.3	0.0			
01310	5	7	1	7	0.2	0.0			
01320	5	7	2	5	0.4	0.0			
01330	5	7	3	5	0.5	0.0			
01340	5	7	4	5	0.3	0.0			
01350	5	7	5	5	0.3	0.0			
01360	5	7	6	5	0.3	0.0			
01370	9	33	5	10	0.0	0.0			
01380	9	33	6	10	0.0	0.0			
01390	10	14	1	8	1.5	0.0			
01400	10	14	2	8	12.0	0.0			
01410	10	14	3	8	12.0	0.0			
01420	10	14	4	8	0.6	0.0			
01430	10	14	5	8	0.6	0.0			
01440	10	14	6	8	0.6	0.0			
01450	10	15	1	8	1.5	0.0			
01460	10	15	2	8	12.0	0.0			
01470	10	15	3	8	12.0	0.0			
01480	10	15	4	8	0.6	0.0			
01490	10	15	5	8	0.6	0.0			
01500	10	15	6	8	0.6	0.0			
01510	16	17	1	8	1.5	0.0			
01520	16	17	2	8	12.0	0.0			
01530	16	17	3	8	12.0	0.0			
01540	16	17	4	8	0.6	0.0			
01550	16	17	5	8	0.6	0.0			
01560	16	17	6	8	0.6	0.0			
01570	16	18	1	8	1.5	0.0			
01580	16	18	2	8	12.0	0.0			
01590	16	18	3	8	12.0	0.0			
01600	16	18	4	8	0.6	0.0			
01610	16	18	5	8	0.6	0.0			
01620	16	18	6	8	0.6	0.0			
01630		0.0		1.0					Non-standard KR curve data for nonlinear beam elements • deflection • KR value
01640		0.01		1.0					
01650		0.02		1.0					
01660		0.03		1.0					
01670		0.04		1.0					
01680		0.05		1.0					
01690		0.05061		1.0					
01700		0.05062		10.0					
01710		0.10		10.0					

TABLE A-3 (CONTINUED).

```
01720      0.20      10.0
01730       0.0       1.0
01740      0.01       1.0
01750      0.02       1.0
01760      0.03       1.0
01770      0.04       1.0
01780      0.05       1.0
01790   0.050061      1.0
01800   0.060062     10.0
01810       0.10     10.0
01820       0.20     10.0
01830  26   30  27   31
01840  25   24  21   20  13  12  23  22
01850   1    2      10.0    10.0    10.0    10.0    10.0    10.0
01860   2   34      10.0    10.0    10.0    10.0    10.0    10.0
01870   3   34      10.0     6.0     6.0    10.0     0.2     0.2
01880   3    4      10.0    10.0    10.0    10.0    10.0    10.0
01890   4    5      10.0    10.0    10.0    10.0    10.0    10.0
01900   5    6      10.0    10.0    10.0    10.0    10.0    10.0
01910   5   20      10.0    10.0    10.0    10.0    10.0    10.0
01920   5   21      10.0    10.0    10.0    10.0    10.0    10.0
01930   5   22      10.0    10.0    10.0    10.0    10.0    10.0
01940   5   23      10.0    10.0    10.0    10.0    10.0    10.0
01950   6   33      10.0    10.0    10.0    10.0    10.0    10.0
01960   6   11      10.0    10.0    10.0    10.0    10.0    10.0
01970   4    7      10.0    10.0    10.0    10.0    10.0    10.0
01980   5    7      10.0    10.0    10.0    10.0    10.0    10.0
01990   7    9       1.0    10.0    10.0    10.0    10.0    10.0
02000   8    9      10.0    10.0    10.0    10.0    10.0    10.0
02010   8   32      10.0    10.0    10.0    10.0    10.0    10.0
02020  10   11      10.0    10.0    10.0    10.0    10.0    10.0
02030  10   14      10.0    10.0    15.1    10.0   0.349    10.0
02040  10   15      10.0    10.0    15.1    10.0   0.349    10.0
02050  10   22      10.0    10.0    10.0    10.0    10.0    10.0
02060  10   23      10.0    10.0    10.0    10.0    10.0    10.0
02070  11   16      10.0    10.0    10.0    10.0    10.0    10.0
02080  12   16      10.0    10.0    10.0    10.0    10.0    10.0
02090  12   24      10.0    10.0    10.0    10.0    10.0    10.0
02100  13   16      10.0    10.0    10.0    10.0    10.0    10.0
02110  13   25      10.0    10.0    10.0    10.0    10.0    10.0
02120  20   24      10.0    10.0    10.0    10.0    10.0    10.0
02130  21   25      10.0    10.0    10.0    10.0    10.0    10.0
02140  16   17      10.0    10.0    15.1    10.0   0.349    10.0
02150  16   18      10.0    10.0    15.1    10.0   0.349    10.0
02160  14   17      10.0    10.0    10.0    10.0    10.0    10.0
02170  15   18      10.0    10.0    10.0    10.0    10.0    10.0
02180  16   19      10.0    10.0    10.0    10.0    10.0    10.0
02190  20   21      10.0    10.0    10.0    10.0    10.0    10.0
02200  20   22      10.0    10.0    10.0    10.0    10.0    10.0
02210  21   23      10.0    10.0    10.0    10.0    10.0    10.0
02220  24   25      10.0    10.0    10.0    10.0    10.0    10.0
02230  10   25      10.0    10.0    10.0    10.0    10.0    10.0
02240  16   27      10.0    10.0    10.0    10.0    10.0    10.0
02250  26   28      10.0    10.0    10.0    10.0    10.0    10.0
02260  27   29      10.0    10.0    10.0    10.0    10.0    10.0
02270  28   30      10.0    10.0    10.0    10.0    10.0    10.0
02280  27   31      10.0    10.0    10.0    10.0    10.0    10.0
```

Non-standard KR curve data for nonlinear beam elements (cont'd)

DRI element pair definition

Occupiable volume definition

Non-standard maximum beam element deflections for failure

- x, y, z, θx, θy, θz

TABLE A-3 (CONTINUED).

02290	9	33	1.0E10	1.0E10	1.0E10	1.0E10	4.7E07	4.7E07	Non-standard maximum beam element forces for failure • F_x, F_y, F_z, M_x, M_y, M_z
02300	1	0.0	0.0	0.0	0.0	0.802	1.311	-4.833	
02310	2	0.0	0.0	0.0	0.0	0.306	-0.027	-6.797	
02320	3	0.0	0.0	0.0	0.0	-1.080	-3.468	-25.896	
02330	4	0.0	0.0	0.0	0.0	-3.422	-8.299	-1.558	
02340	5	0.0	0.0	0.0	0.0	72.268	-5.882	16.239	
02350	6	0.0	0.0	0.0	0.0	82.603	4.614	107.510	
02360	8	0.0	0.0	0.0	0.0	-0.080	0.110	3.970	
02370	9	0.0	0.0	0.0	0.0	-0.440	-0.550	42.220	
02380	10	0.0	0.0	0.0	0.0	73.656	-5.032	17.656	
02390	11	0.0	0.0	0.0	0.0	84.240	4.758	99.093	
02400	12	0.0	0.0	0.0	0.0	22.790	1.484	35.859	Miscellaneous mass point data • mass point • aerodynamic lift constant • angular momenta of rotating masses • cross product mass moments of inertia
02410	13	0.0	0.0	0.0	0.0	-17.411	7.396	20.630	
02420	14	0.0	0.0	0.0	0.0	-4.420	-7.390	-3.580	
02430	15	0.0	0.0	0.0	0.0	4.420	7.390	-3.580	
02440	16	0.0	0.0	0.0	0.0	6.886	10.440	58.388	
02450	17	0.0	0.0	0.0	0.0	5.360	-6.930	2.640	
02460	18	0.0	0.0	0.0	0.0	-5.360	6.930	2.640	
02470	19	0.0	0.0	0.0	0.0	-10.463	-10.455	2.642	
02480	20	0.0	0.0	0.0	0.0	-12.484	-3.877	-1.035	
02490	21	0.0	0.0	0.0	0.0	13.122	7.581	-3.042	
02500	22	0.0	0.0	0.0	0.0	61.090	-2.986	21.695	
02510	23	0.0	0.0	0.0	0.0	8.283	-0.325	-6.455	
02520	24	0.0	0.0	0.0	0.0	-13.349	-4.883	-1.020	
02530	25	0.0	0.0	0.0	0.0	10.639	9.787	-0.873	
02540	32	0.0	0.0	0.0	0.0	0.000	0.000	1.410	
02550	33	0.0	0.0	0.0	0.0	2.195	5.182	77.986	
02560	34	0.0	0.0	0.0	0.0	2.265	0.945	-23.149	
02570	7	1	0	0	1	0	0		Printer plot control cards
02580	8	1	0	0	1	0	0		
02590	9	1	0	0	1	0	0		
02600	10	1	0	0	1	0	0		
02610	16	1	0	0	1	0	0		
02620	26	1	0	0	1	0	0		
02630	27	1	0	0	1	0	0		
02640	28	1	0	0	1	0	0		
02650	29	1	0	0	1	0	0		
02660	30	1	0	0	1	0	0		
02670	31	1	0	0	1	0	0		
02680	32	1	0	0	1	0	0		
02690	33	1	0	0	1	0	0		
02700	3	0	1	1					
02710	12	0	1	1					
02720	14	0	1	1					
02730	15	0	1	1					
02740	20	0	1	1					
02750	21	0	1	1					
02760	31	0	1	1					
02770	32	0	1	1					
02780	40	0	1	1					
02790	41	1	0	0					
02800	3	1	0	0					
02810	12	1	0	0					
02820	14	1	0	0					
02830	15	1	0	0					
02840	20	1	0	0					
02850	21	1	0	0					

TABLE A-3 (CONCLUDED).

Printer plot control cards (cont'd)

```
$$$$1111111111111111
$$$$111111111111111
11111
31 32 40 41 10 11 12 13 14 15 16 17 18 22 23 30 31
                                                END
```

KRASH ANALYSIS RESULTS

The results presented in this section supplement those described in the KRASH analysis section of the main body of the report. The seven impact conditions that were analyzed are shown in Figure A-17(a) through (g). These conditions were designed to exercise many of the features in KRASH, such as analysis of three-dimensional impact conditions, arbitrary load-deflection input parameters from metal or composite structures, soil deformation, friction, and plowing.

For each case shown in Figure A-17, energy distribution versus time curves are shown in Figures A-18 through A-24. The energy curves allow the engineer to readily determine how the energy is managed during the crash sequence. The cg velocity time history curves for all seven impact conditions are shown in Figures A-25 through A-31. The cg velocity represents an average velocity of all the aircraft masses during the crash sequence and aids the engineer in understanding the overall aircraft response during the crash sequence. Examples of acceleration time history responses available in a KRASH analysis are shown in Figure A-32 through A-34. The accelerations shown in the figures compare responses at various locations for the metal and composite models simulating impact conditions (c) and (d) of Figure A-17. Many other output parameters are also available as explained in the main body of the report.

The methods used for determining the friction, soil, and plowing parameters used in the KRASH analyses are described as follows:

1. Friction

   The ground coefficient of friction used in all seven cases shown in Figure A-17 was 0.3. This value was recommended in TR 72-72[48] as a representative number for a concrete surface; however, in Wittlin's later FAA report[51] a value of 0.4 was suggested. In Reference 49, coefficients of friction with values of between 1.0 and 1.5 were recommended for use with a soil surface. But, to better understand the effect of plowing in condition (g) of Figure A-17, the coefficient of friction was kept at 0.3 in the analyses.

2. Soil

   The KRASH computer program has the capability to analyze impacts onto a flexible soil surface. The metal airframe model with landing gear up was analyzed for 30 fps vertical impacts on rigid and soil surfaces, conditions

(c) and (e) of Figure A-17. A soil flexibility coefficient is input as part of the external crushing spring data. The coefficient used was .0005 in./lb or 2000 lb/in. The energy distributions and vehicle cg velocities from KRASH show that the soil dissipates much of the airframe kinetic energy, resulting in very little rebound. The soil spring acts in series with the fuselage crushing springs. The external springs load up with a slope of 2000 lb/in. due to ground deformation from initial impact to the time the load builds up to the stroking load of the fuselage crushing springs. At that time, the springs start to deflect instead of the ground until the bottoming-out point is reached. After that, the springs load up again at a rate of 2000 lb/in. When the vehicle cg velocity reaches zero, the external springs unload at a constant ground deflection to zero load. For condition (e) of Figure A-17, permanent soil deformations ranged from 10 to 15 in. Wittlin details an iterative procedure for correlating KRASH analysis with test results to determine soil flexibility coefficients in Reference 51.

3. Plowing

To study the effects of plowing forces in the crash sequence of events for the troop transport helicopter, the metal airframe KRASH model was analyzed for a combined 30 fps vertical and 30 fps fore-and-aft impact with and without plowing, conditions (f) and (g) in Figure A-17. The plowing forces were applied to the lower fuselage mass points having external crushing springs. An arbitrary force of six times the weight of each mass point was applied for 160 msec to demonstrate this feature of the KRASH program. As shown in Figure A-31, the plowing force reduces the final vehicle cg fore-and-aft velocity by 44 fps as compared to the no-plowing case shown in Figure A-30. The energy distributions, Figures A-23 and A-24, show that plowing reduces the kinetic energy while increasing the strain energy through more structural deformation. In Reference 51, Wittlin describes a method for determining plowing forces based on conservation of linear momentum.

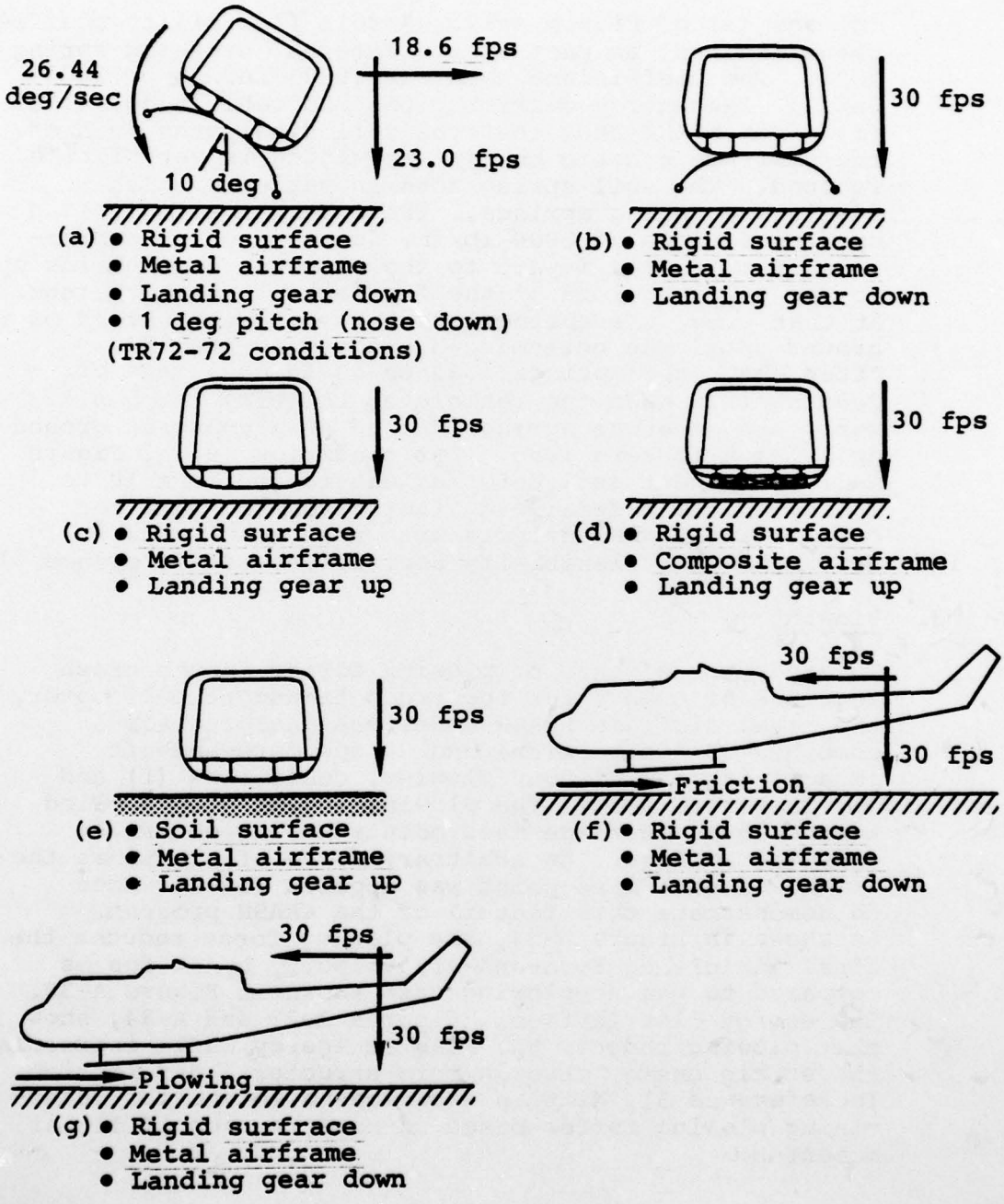

Figure A-17. Impact conditions used for KRASH analysis of troop transport helicopter.

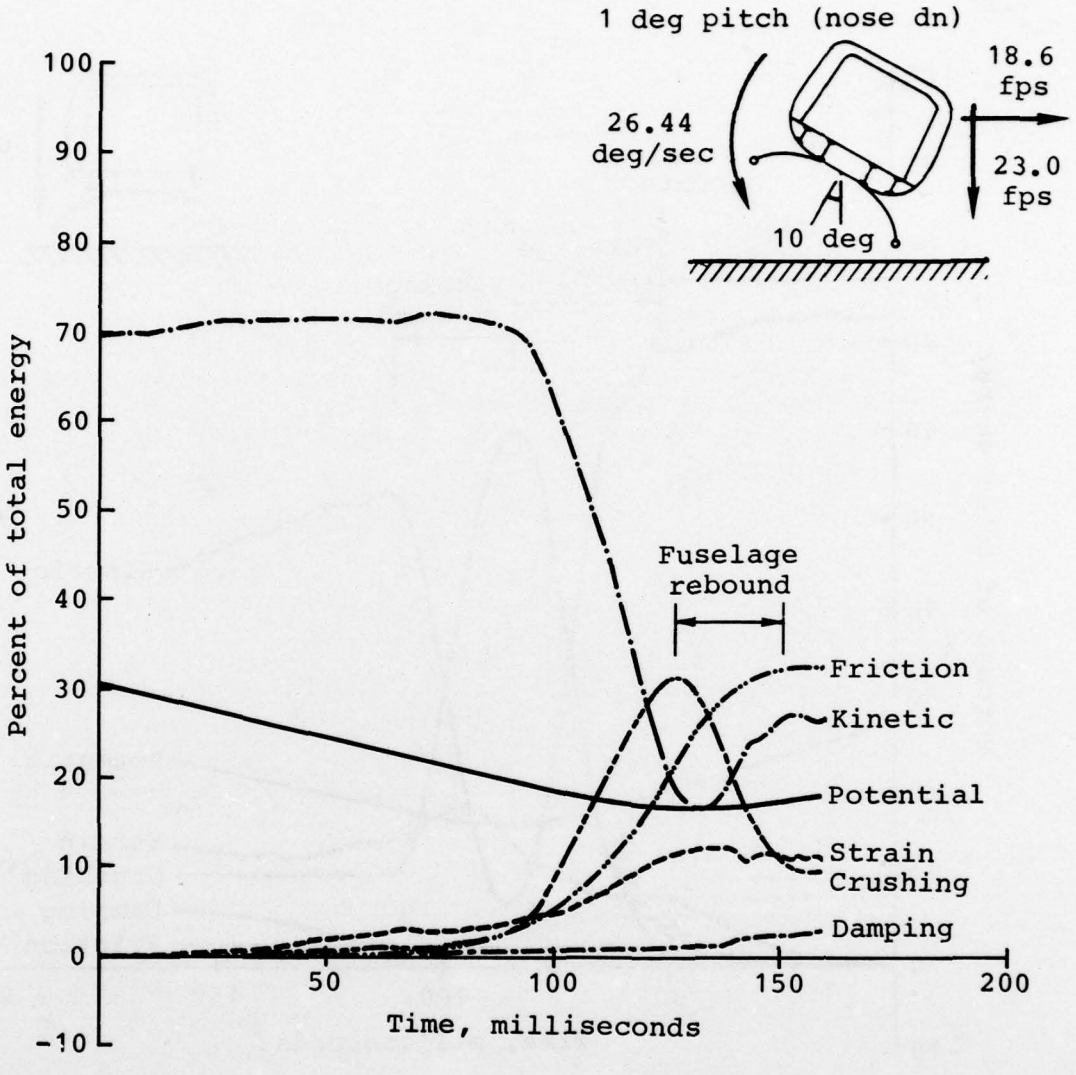

Figure A-18. Energy distribution for TR72-72 impact conditions on rigid surface for metal airframe with landing gear down.

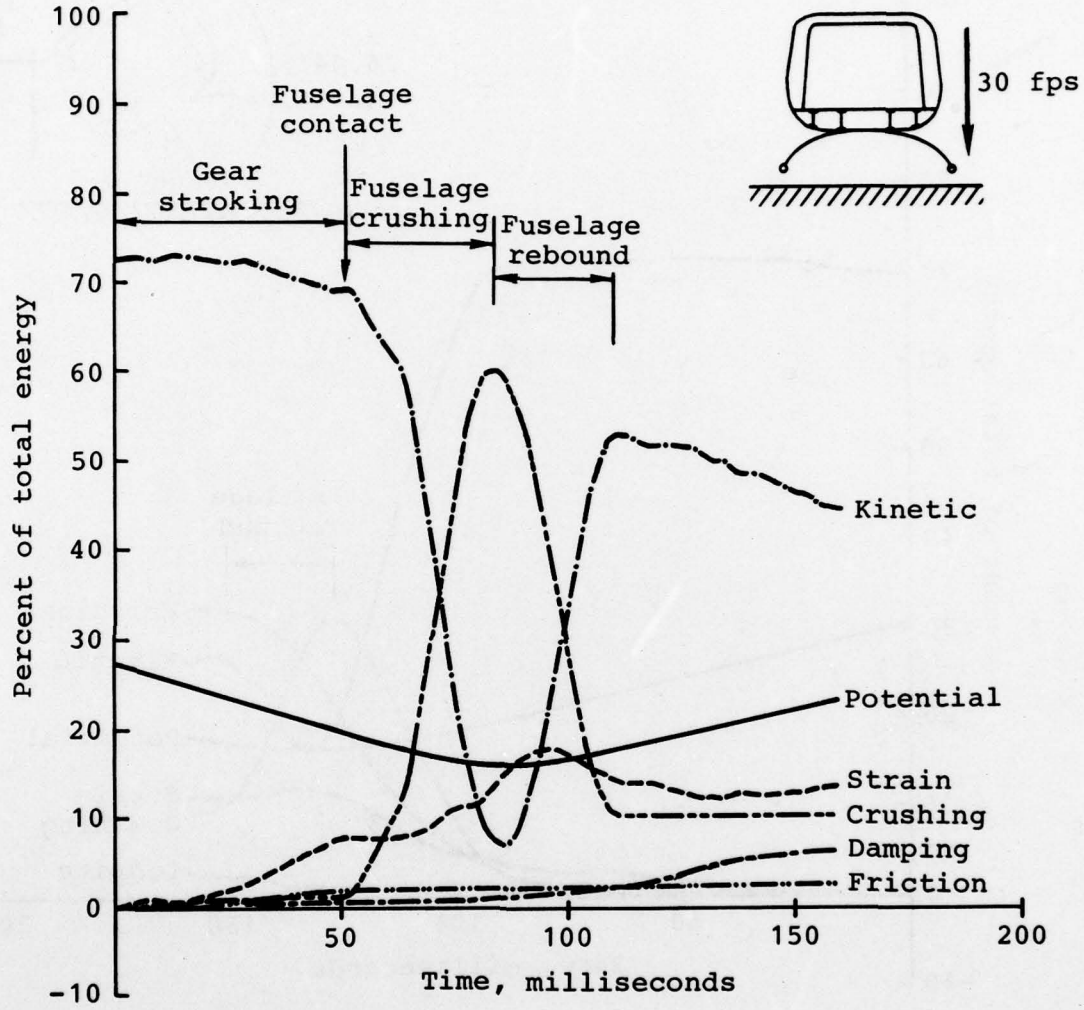

Figure A-19. Energy distribution for 30 fps vertical impact on rigid surface for metal airframe with landing gear down.

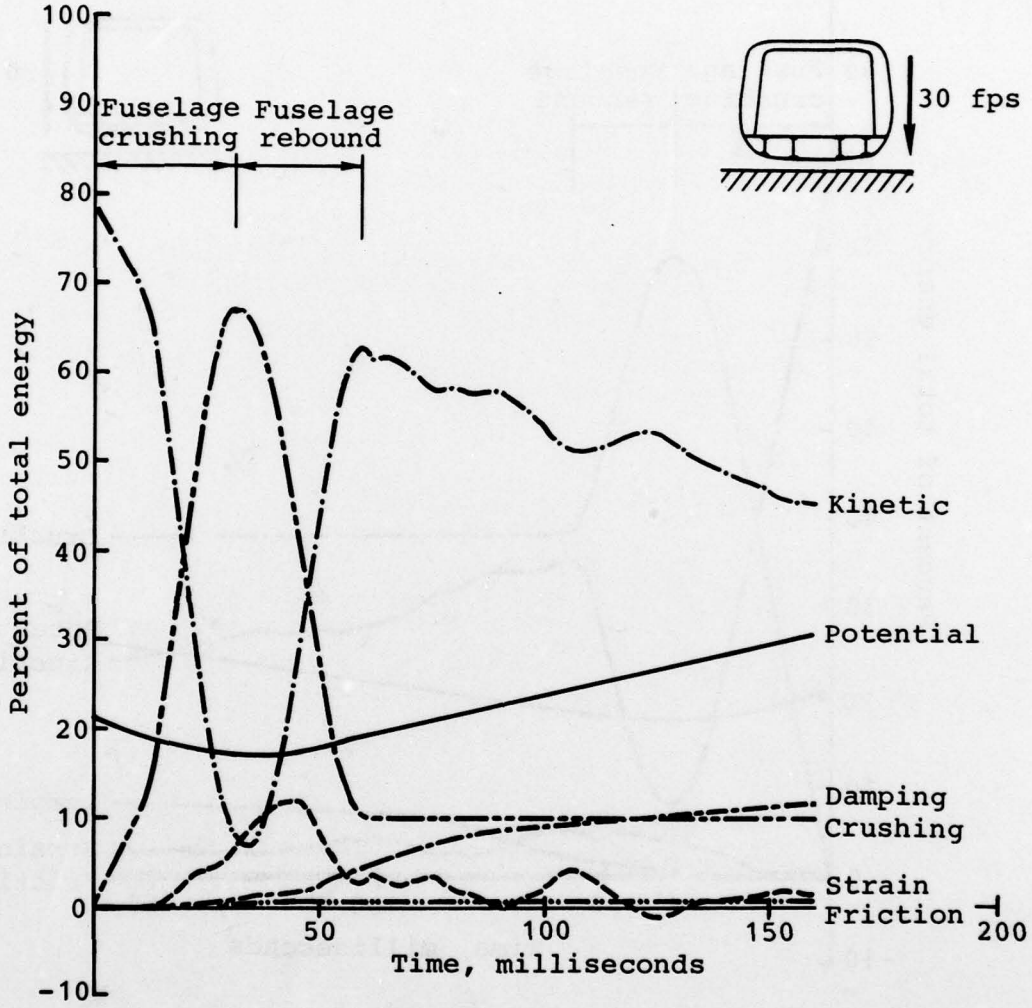

Figure A-20. Energy distribution for 30 fps vertical impact on rigid surface for metal airframe with landing gear up.

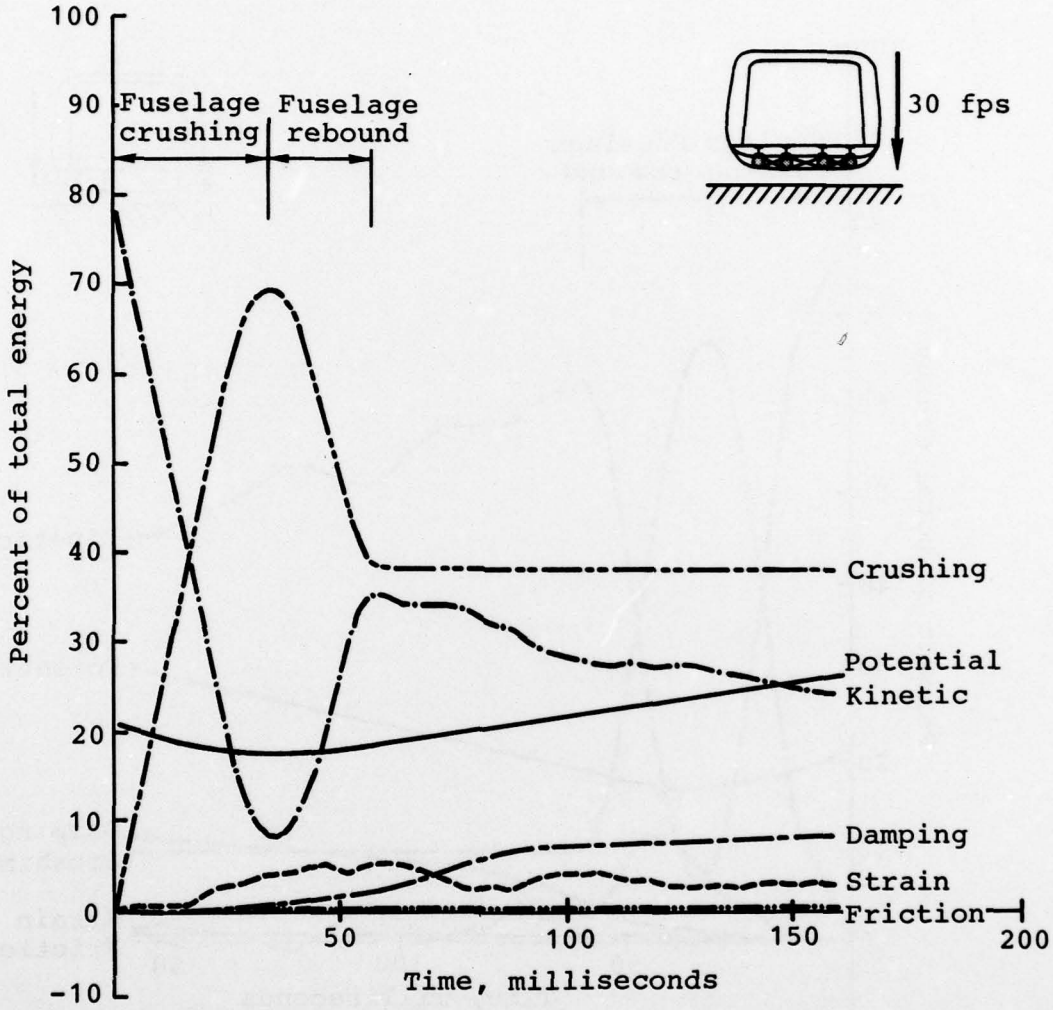

Figure A-21. Energy distribution for 30 fps vertical impact on rigid surface for composite airframe with landing gear up.

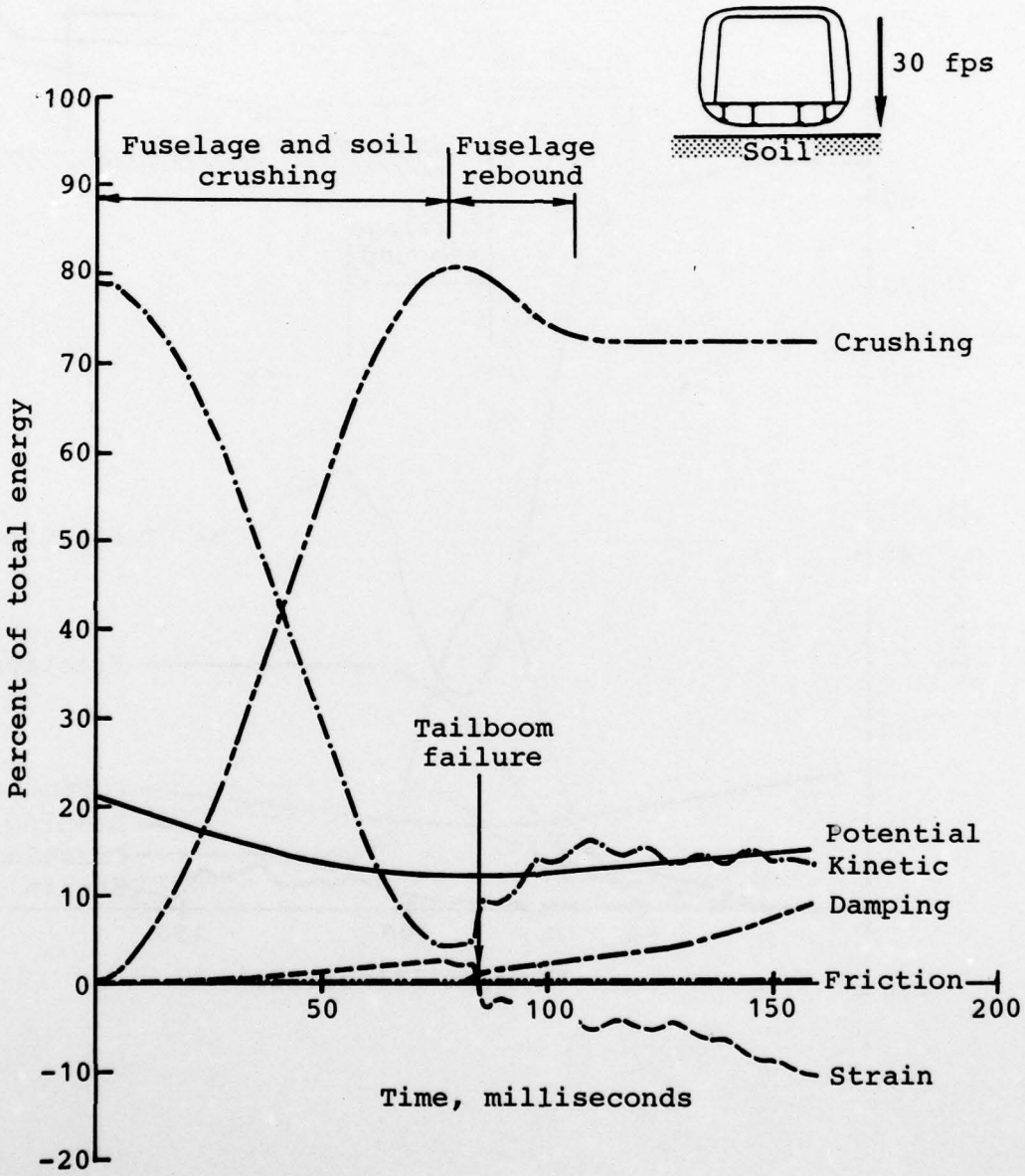

Figure A-22. Energy distribution for 30 fps vertical impact on soil surface for metal airframe with landing gear up.

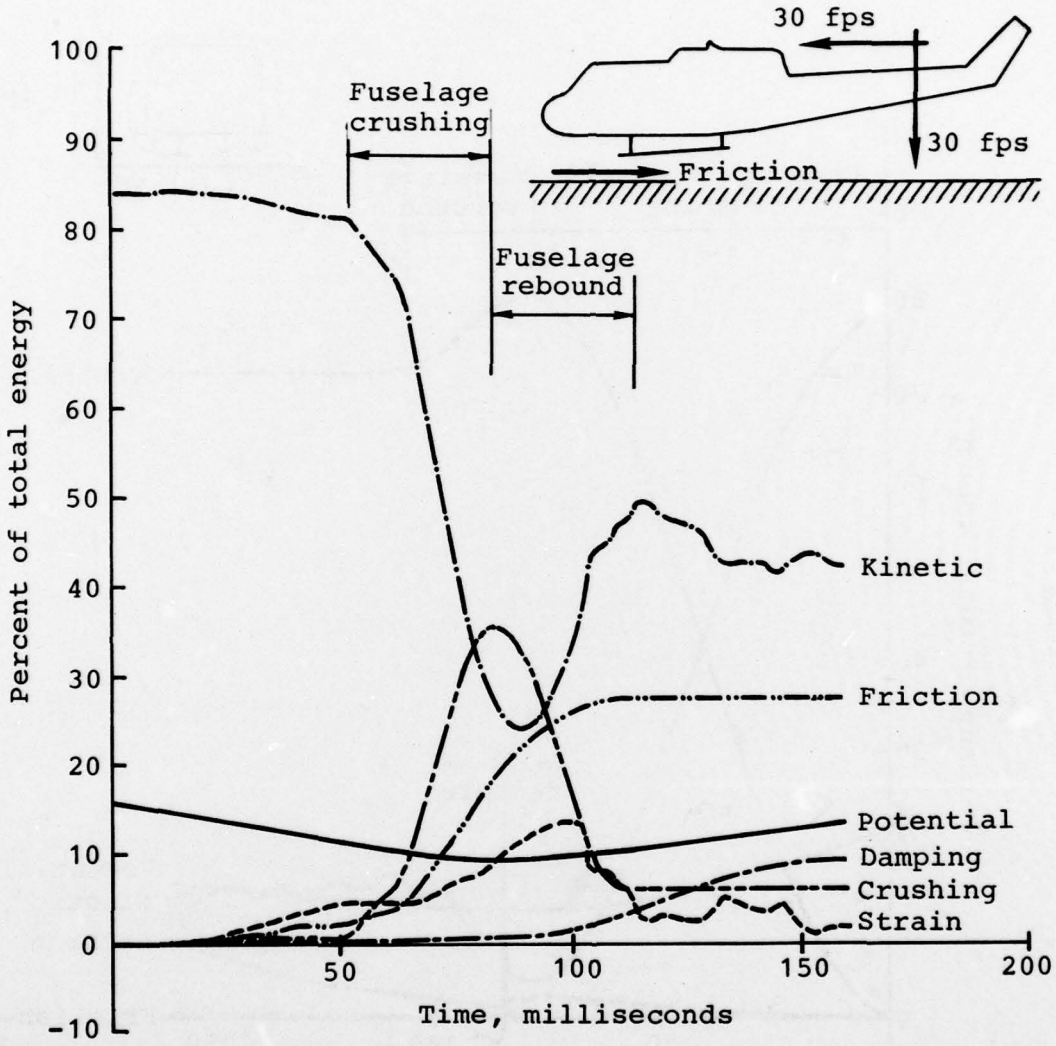

Figure A-23. Energy distribution for 30 fps vertical and fore-and-aft impact on rigid surface for metal airframe with landing gear down.

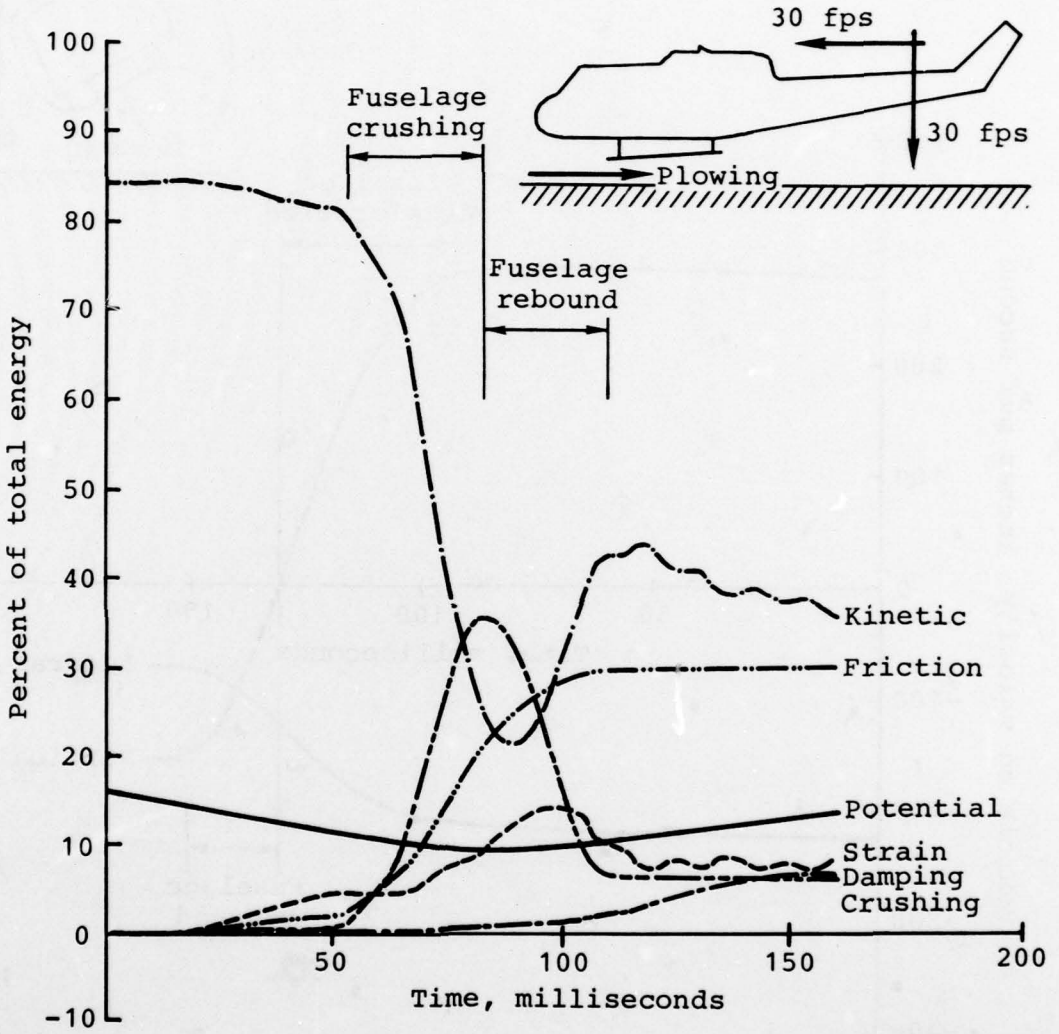

Figure A-24. Energy distribution for 30 fps vertical and fore-and-aft impact on rigid surface with plowing forces for metal airframe with landing gear down.

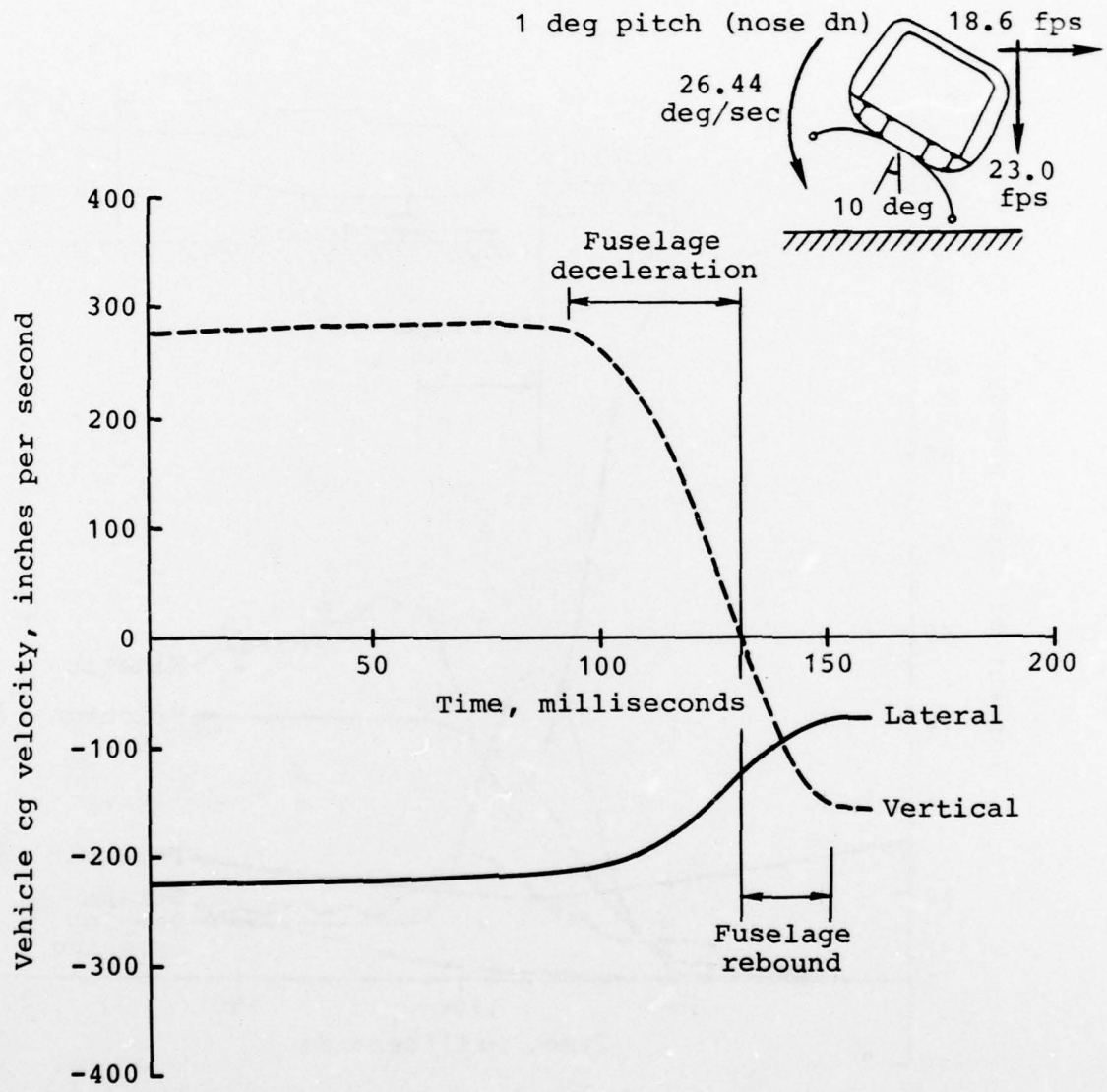

Figure A-25. Vehicle cg velocity for TR72-72 impact conditions on rigid surface for metal airframe with landing gear down.

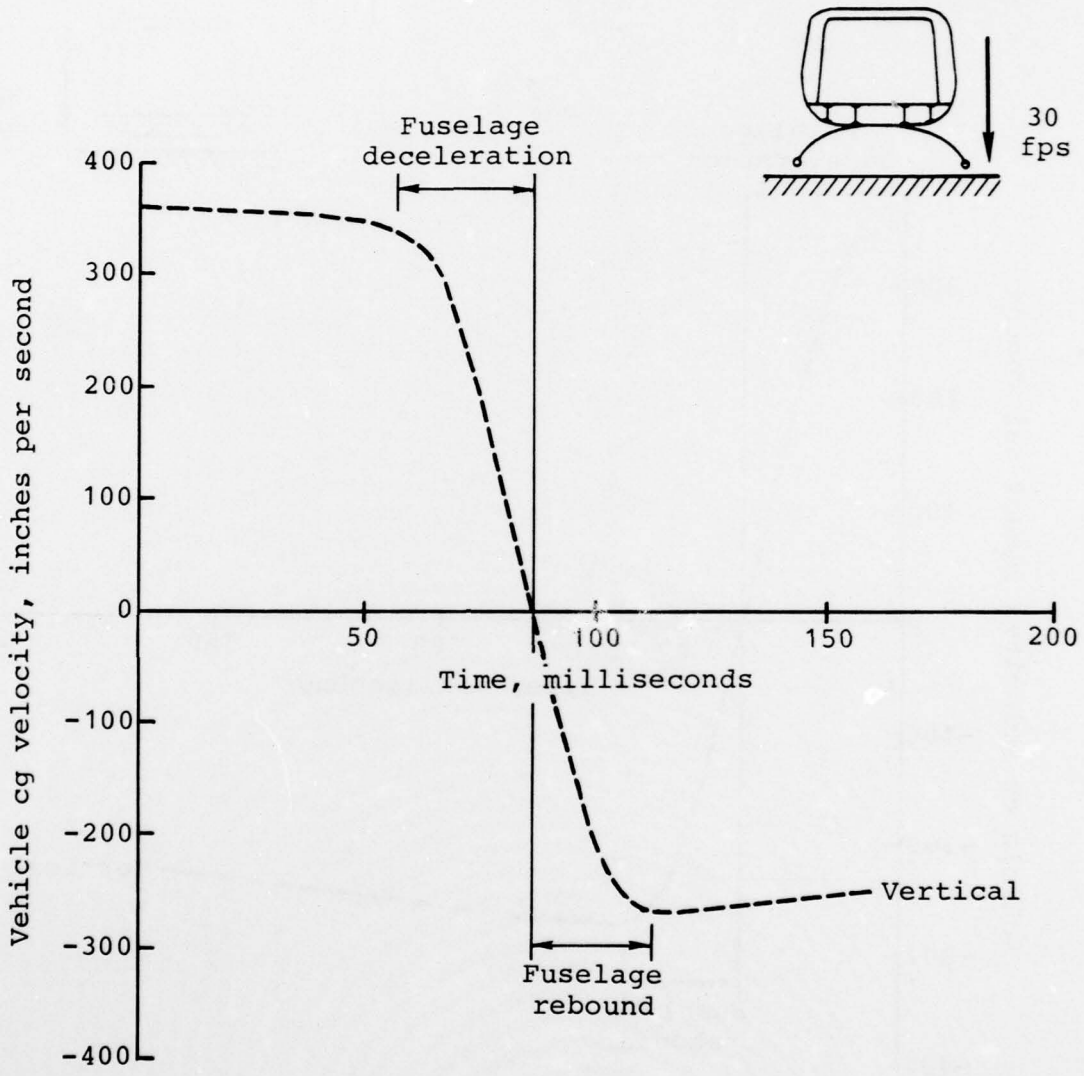

Figure A-26. Vehicle cg vertical velocity for 30 fps vertical impact on rigid surface for metal airframe with landing gear down.

AD-A075 163 BELL HELICOPTER TEXTRON FORT WORTH TX F/G 1/3
INVESTIGATION OF THE CRASH-IMPACT CHARACTERISTICS OF ADVANCED A--ETC(U)
SEP 79 J D CRONKHITE, T J HAAS, V L BERRY DAAJ02-77-C-0062
UNCLASSIFIED USARTL-TR-79-11 NL

3 OF 3
AD
A075183

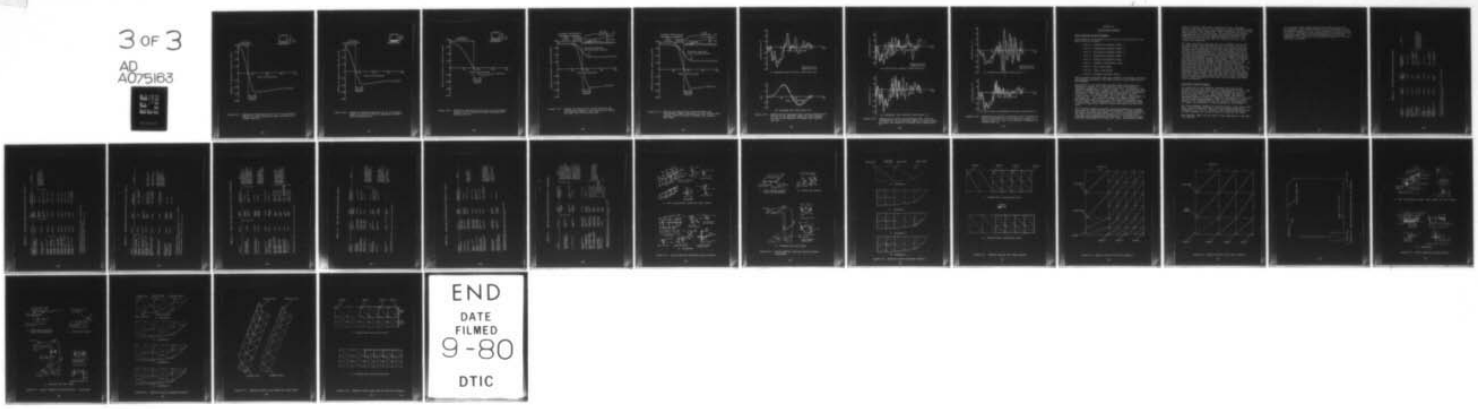

END
DATE
FILMED
9-80
DTIC

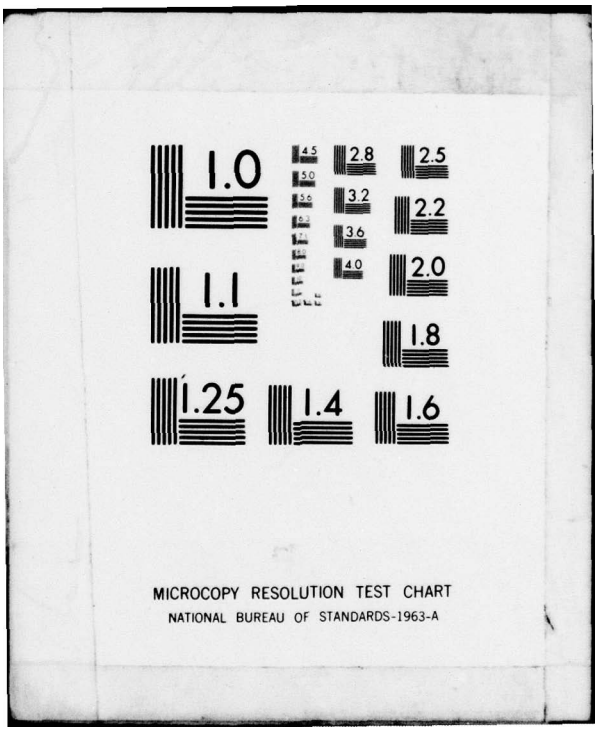
1.0
1.1
1.25
1.4
1.6
1.8
2.0
2.2
2.5
2.8
3.2
3.6
4.0
4.5
5.0
5.6
MICROCOPY RESOLUTION TEST CHART
NATIONAL BUREAU OF STANDARDS-1963-A

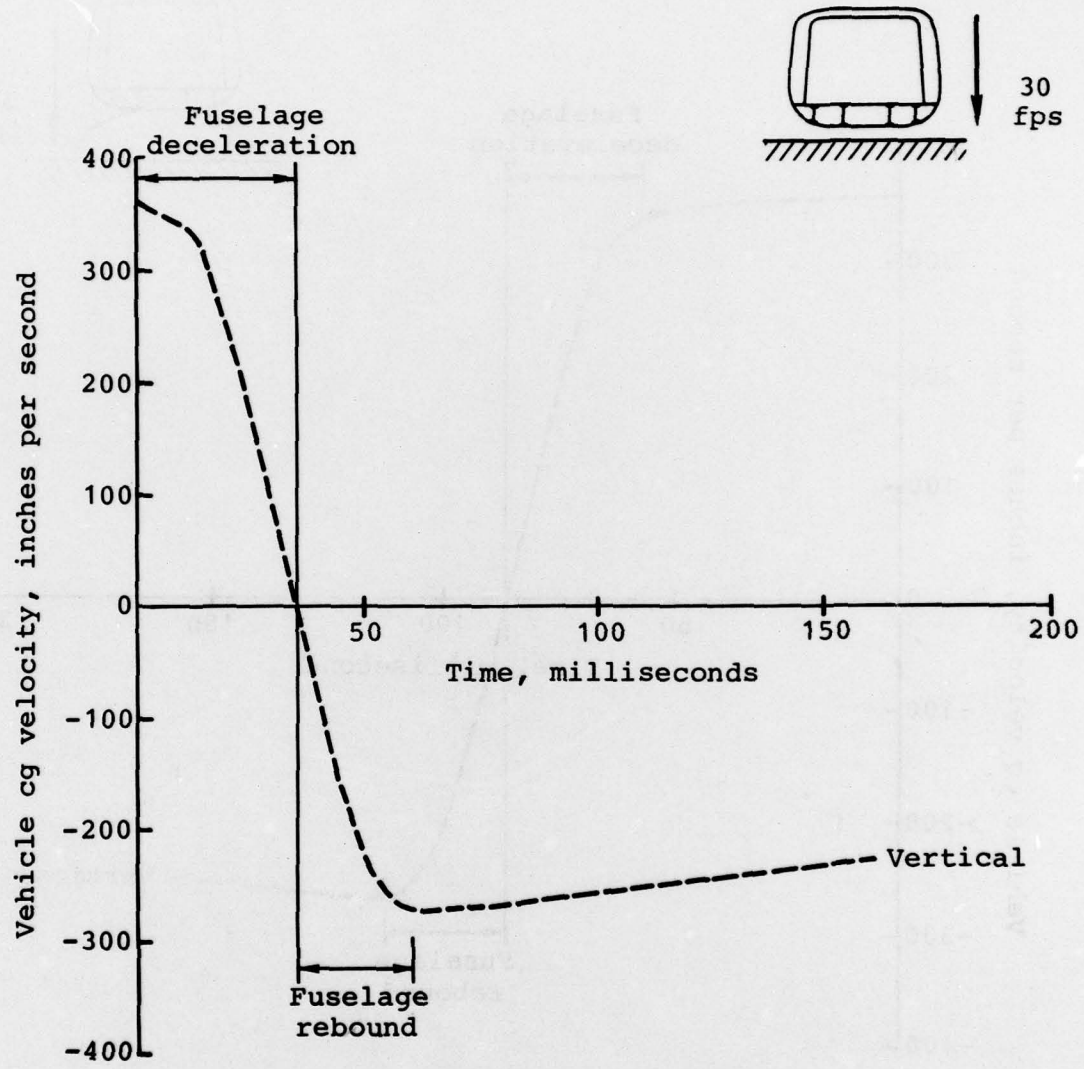

Figure A-27. Vehicle cg vertical velocity for 30 fps vertical impact on rigid surface for metal airframe with landing gear up.

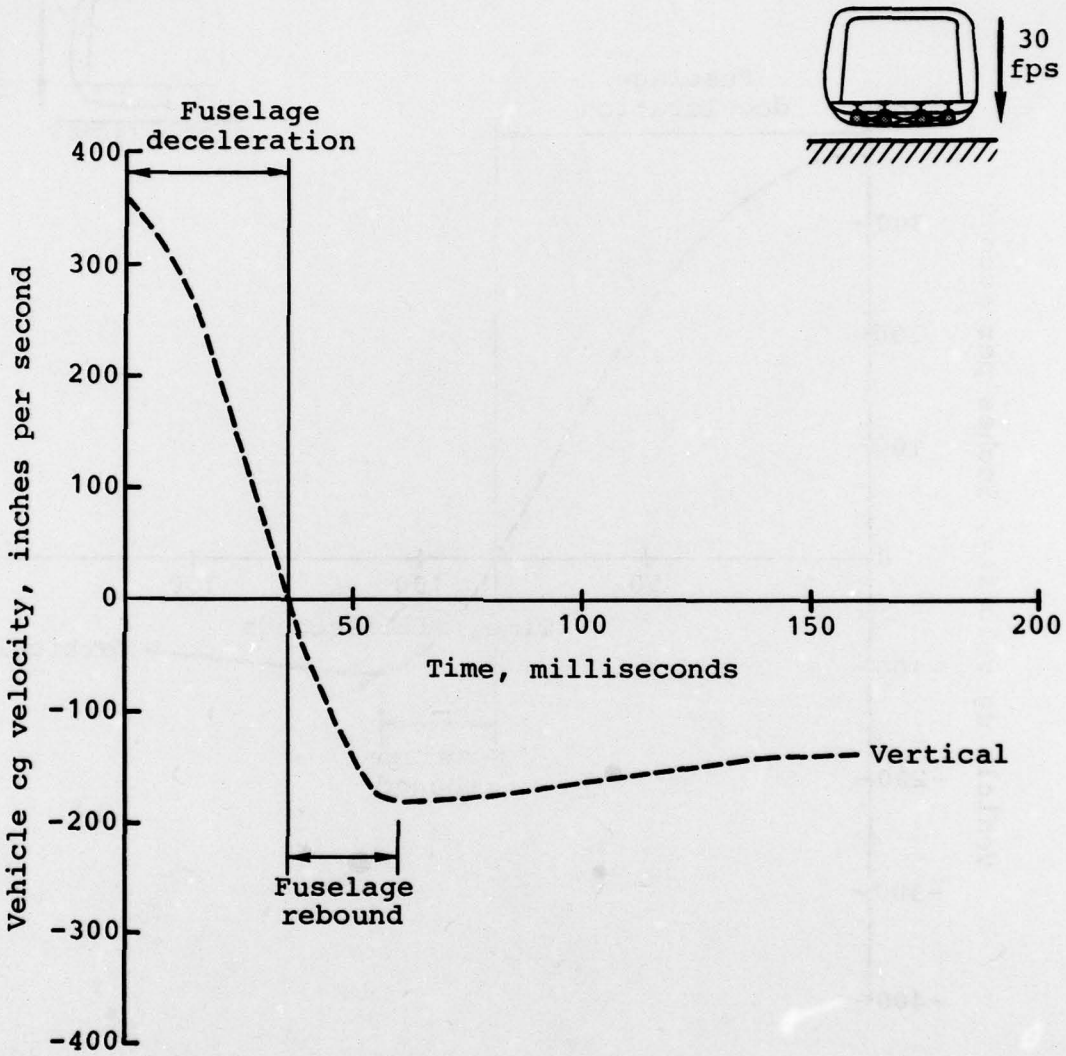

Figure A-28. Vehicle cg vertical velocity for 30 fps vertical impact on rigid surface for composite airframe with landing gear up.

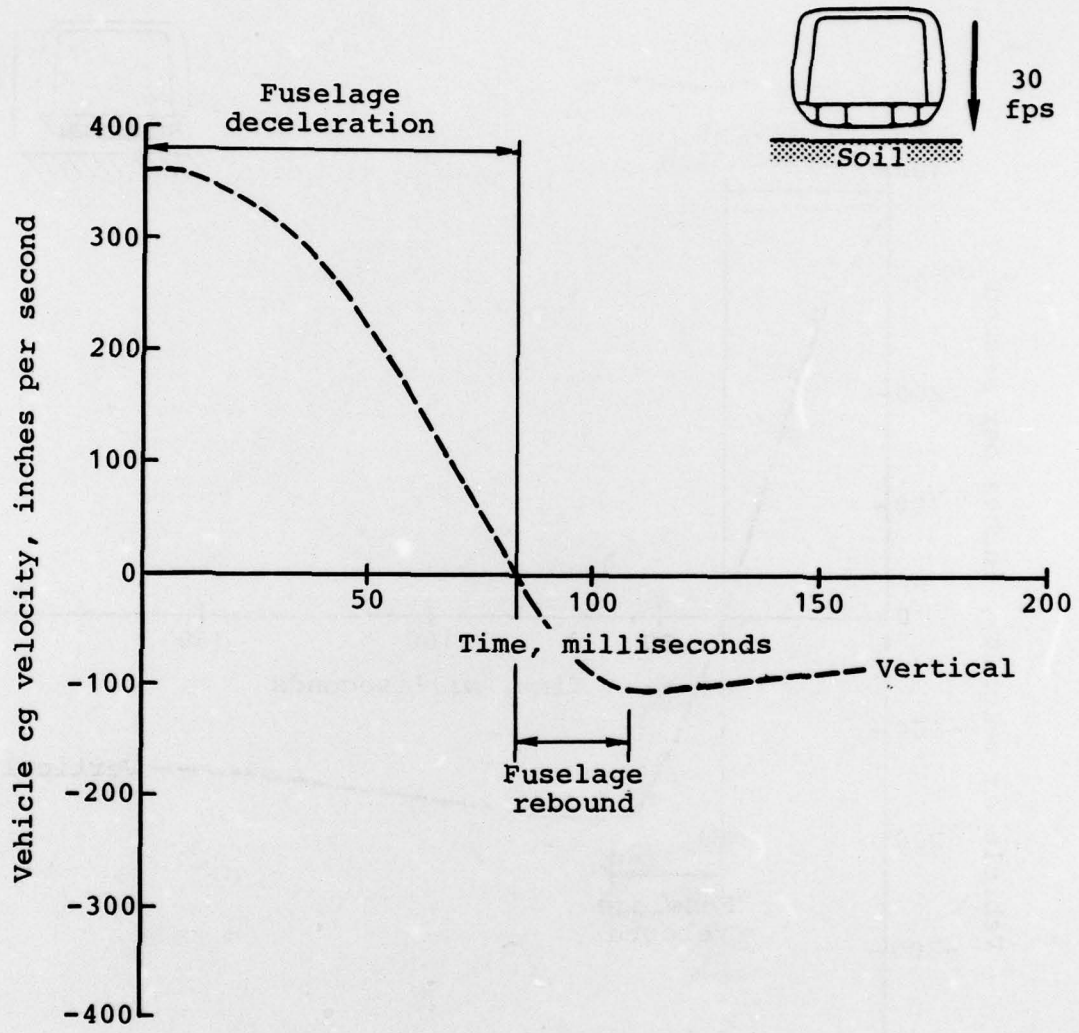

Figure A-29. Vehicle cg vertical velocity for 30 fps vertical impact on soil surface for metal airframe with landing gear up.

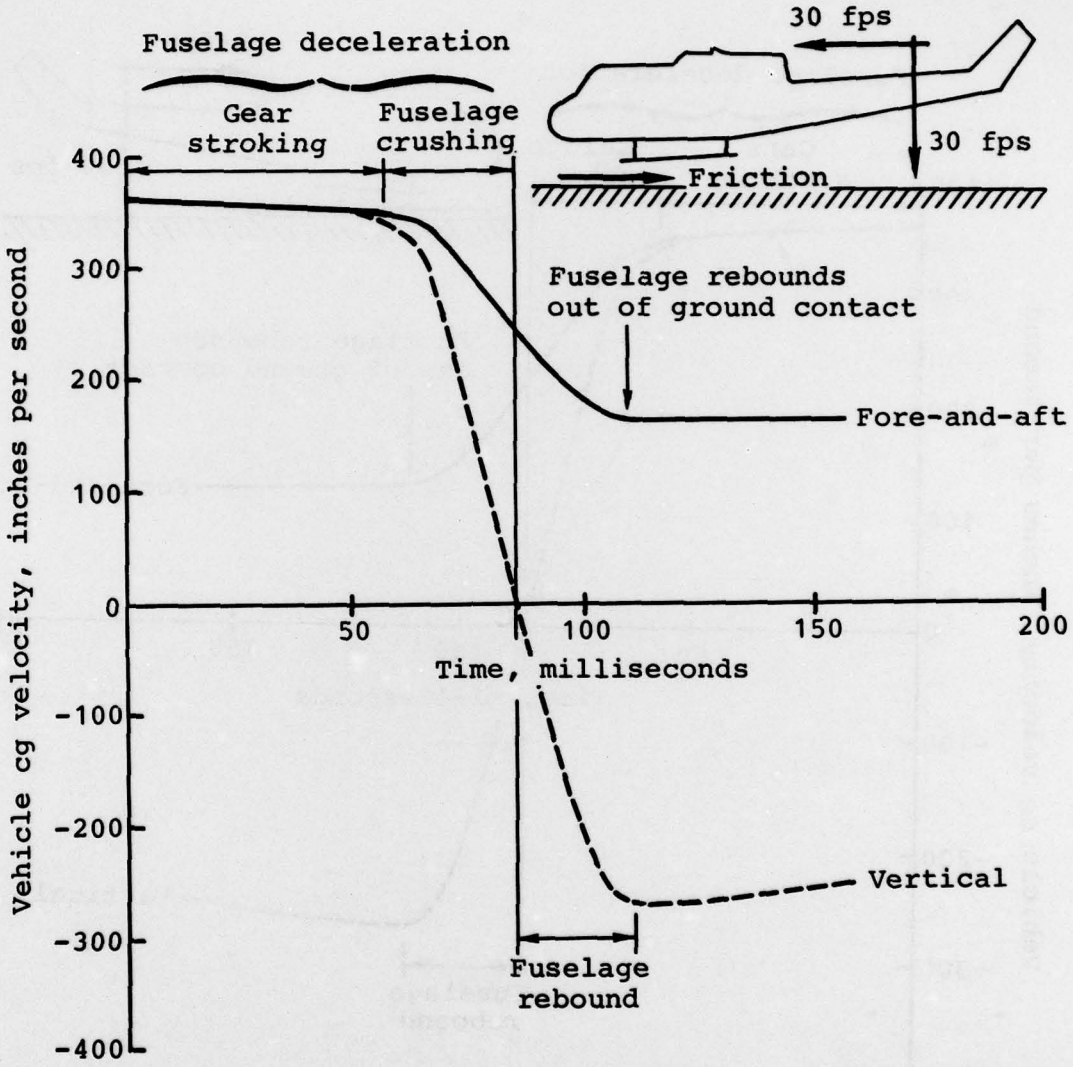

Figure A-30. Vehicle cg velocity for 30 fps vertical and fore-and-aft impact on rigid surface for metal airframe with landing gear down.

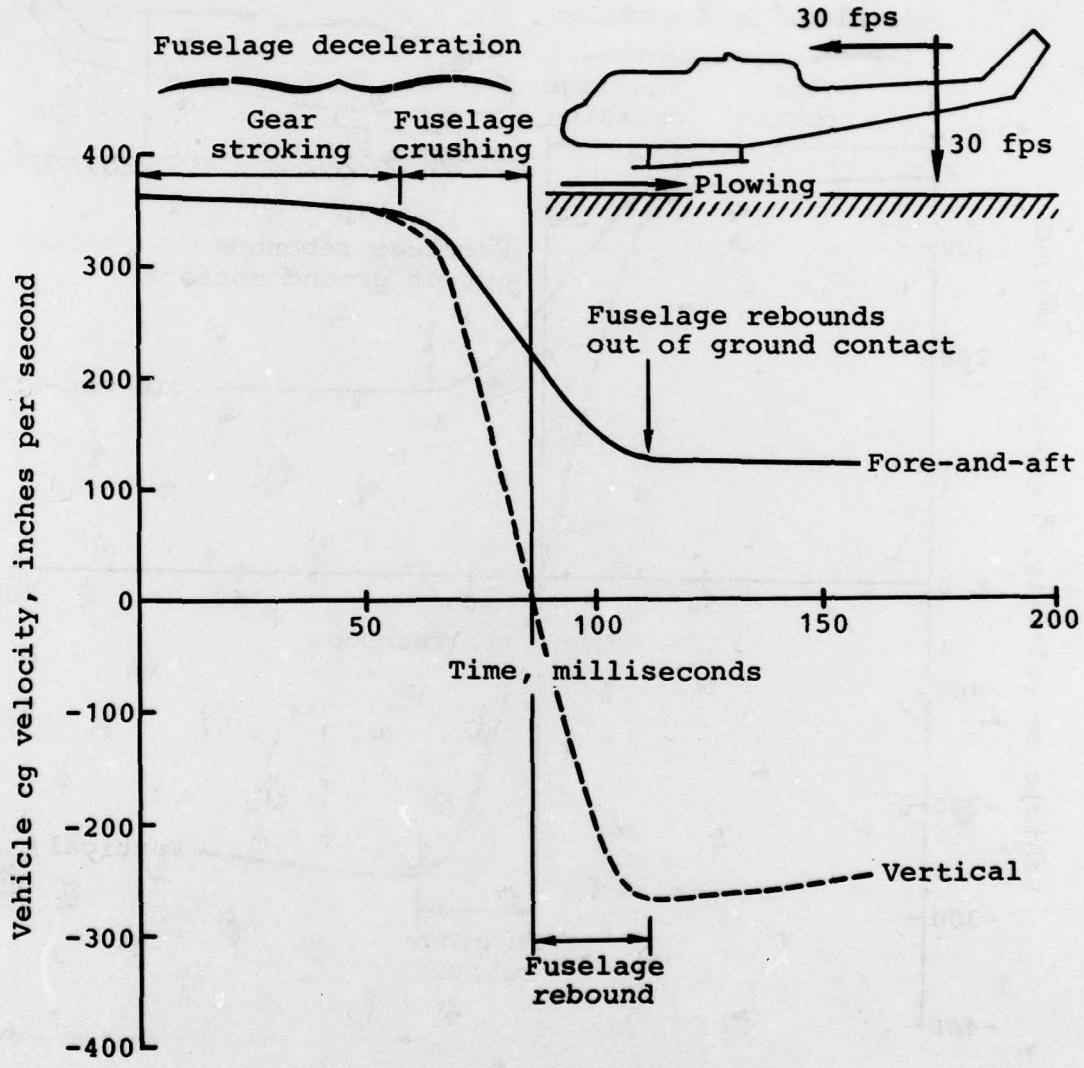

Figure A-31. Vehicle cg velocity for 30 fps vertical and fore-and-aft impact condition on rigid surface with plowing forces for metal airframe with landing gear down.

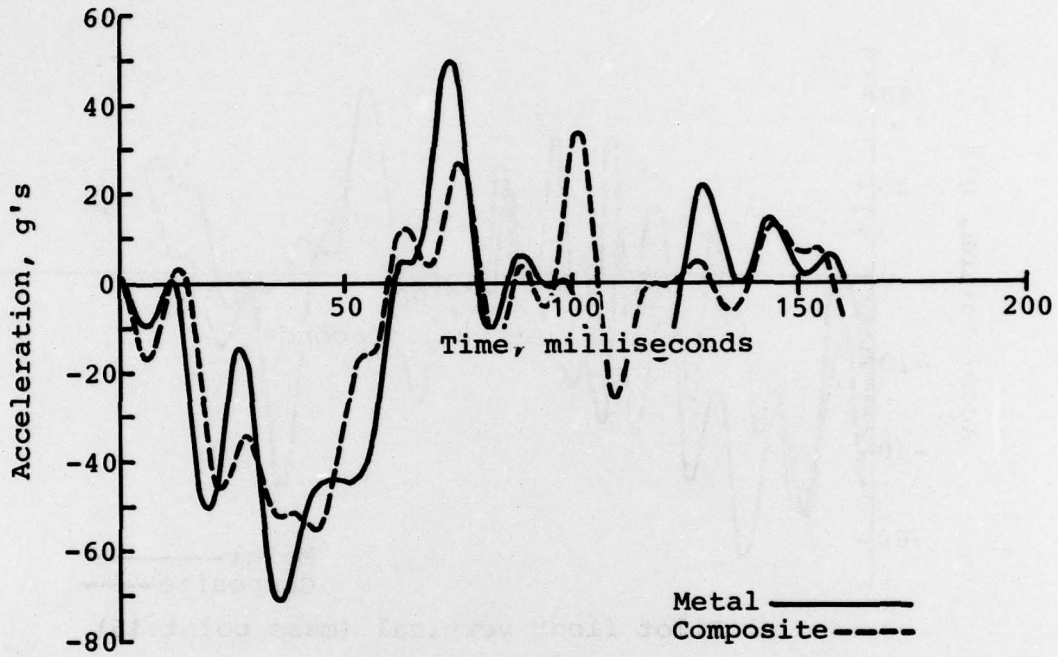

(a) Passenger seat vertical (mass point 26)

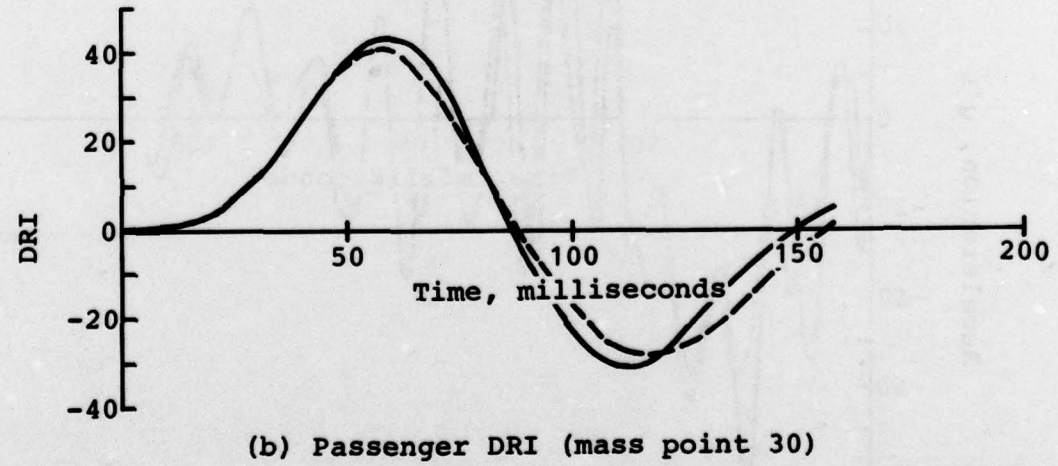

(b) Passenger DRI (mass point 30)

Figure A-32. Comparisons of passenger seat vertical response and DRI for 30 fps vertical impact on rigid surface for metal and composite airframes with landing gear up.

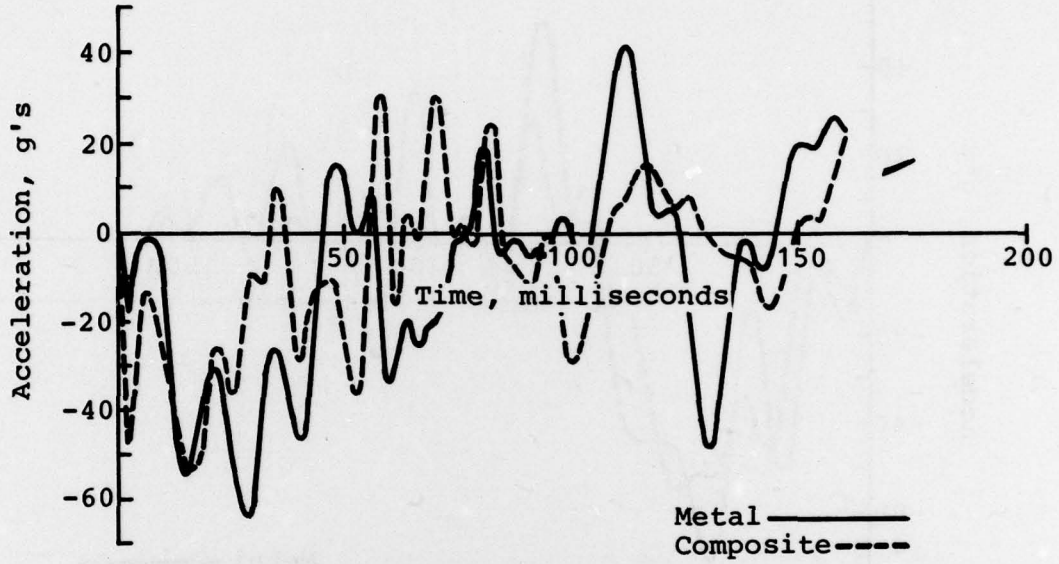

(a) Pilot floor vertical (mass point 16)

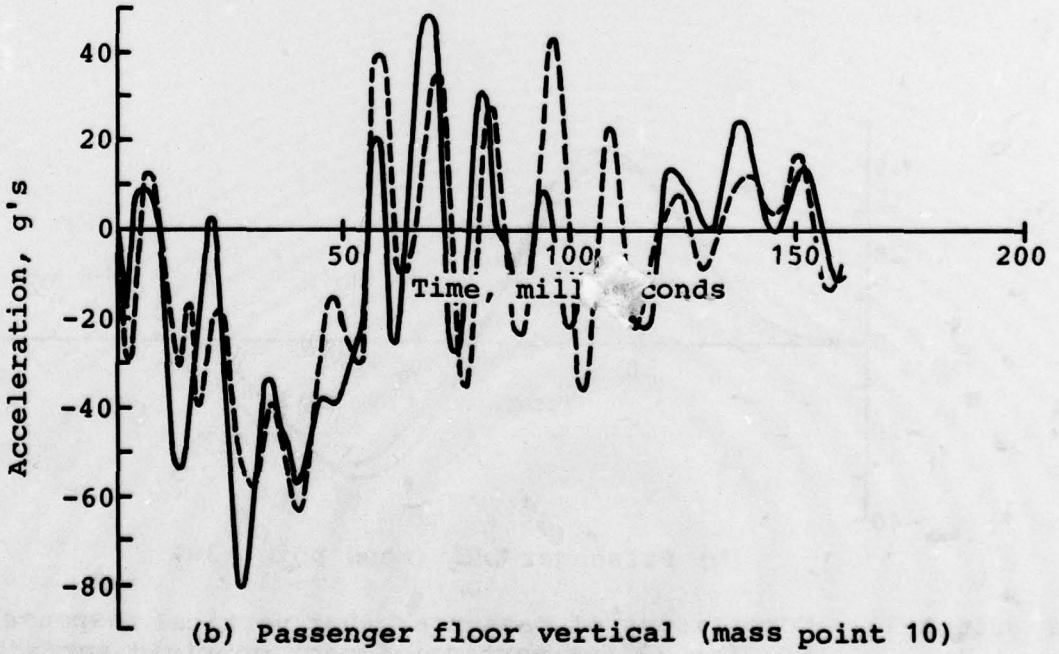

(b) Passenger floor vertical (mass point 10)

Figure A-33. Comparisons of pilot and passenger floor vertical responses for 30 fps vertical impact on rigid surface for metal and composite airframes with landing gear up.

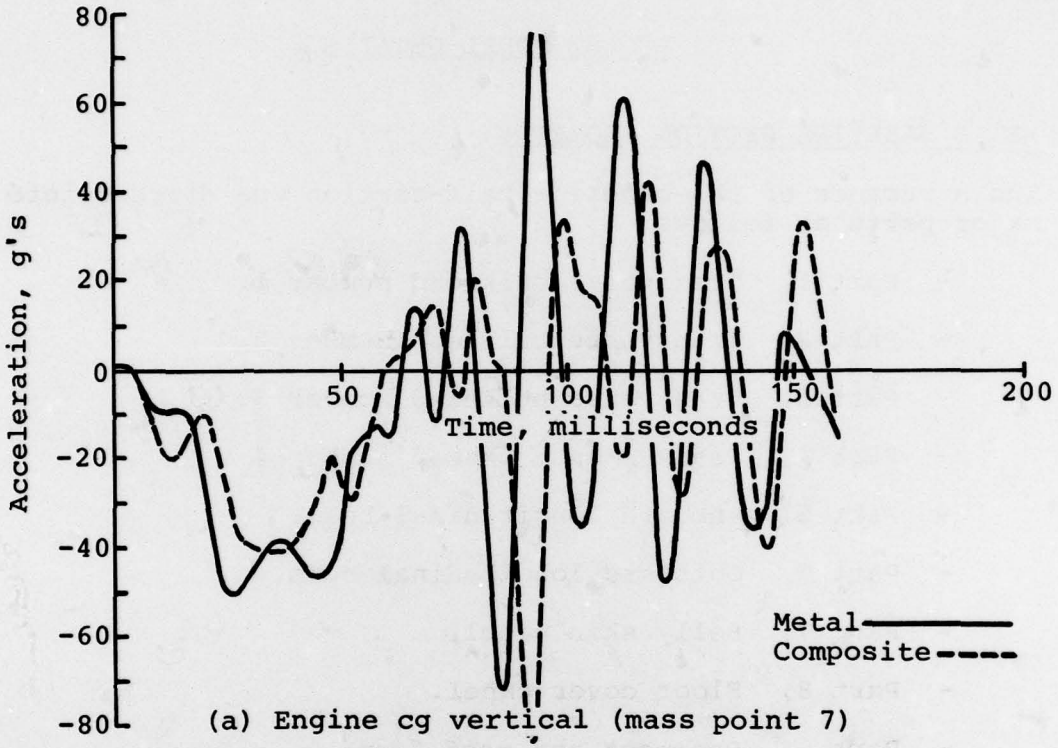

(a) Engine cg vertical (mass point 7)

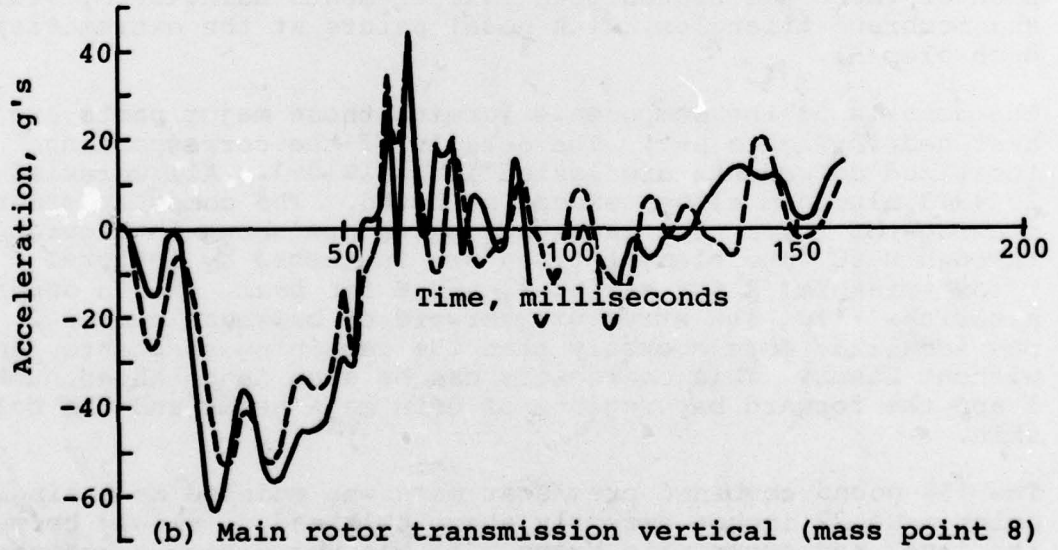

(b) Main rotor transmission vertical (mass point 8)

Figure A-34. Comparisons of engine cg and main rotor transmission vertical responses for 30 fps vertical impact on rigid surface for metal and composite airframes with landing gear up.

APPENDIX B

DYCAST MODEL DETAILS

METAL BASELINE SECTION GEOMETRY

The structure of the baseline half-section was divided into its major parts as follows:

- Part 1, Transverse bulkhead number 1.
- Part 2, Transverse bulkhead number 2.
- Part 3, Transverse bulkhead number 3.
- Part 4, Transverse bulkhead number 4.
- Part 5, Inboard longitudinal beam.
- Part 6, Outboard longitudinal beam.
- Part 7, Belly skin panel.
- Part 8, Floor cover panel.
- Part 9, Doorpost and roof frame.

Each of these was broken down into elements using beam, stringer, and membrane triangles, with nodal points at the extremities of each element.

The details of the components forming these major parts are sketched in Figure B-1. The details of the corresponding idealized components are listed in Table B-1. All material was 2024-T3 aluminum alloy, except as noted. The computer-generated drawings of these nine idealized parts are shown in Figures B-2 through B-6. The element types are indicated by letters: T for triangle, S for stringer, and B for beam. Nodes appear as asterisks (*). The structure forward of bulkhead number 2 was idealized more coarsely than the remaining structure, and without beams. This coarseness can be seen in bulkhead number 1 and the forward bay regions of both main beams and the belly skin.

The 150-pound combined crew/seat mass was modeled as a single-point mass 22 inches directly above bulkhead 3, midway between the inner and outer main beams. It was not directly attached to the floor by any structural elements, but was kinematically attached using dependent motion equations. The crew/seat mass could be visualized at the apex of a rigid, weightless pyramid

whose rectangular base plane connected the four attachment points on the seat rails. An alternative equally correct concept would be four rigid, weightless "legs" connecting the mass to the base rectangle. In either case, the translation and rotation components of this base rectangle completely determined the three translations of the crew/seat mass at the apex. The rotations of the crew mass were not computed, as its rotary inertia was neglected.

The base rectangle connecting the four attachment points was not made rigid. This avoided the error of having the deformations of the relatively stiff floor controlled by the seat. Instead, the translations of the base plane were calculated as the average displacement of the four attachment points in the three coordinate directions. The base rectangle's pitch rotation was calculated as the difference between the average vertical displacement of its front and rear edges divided by the fore-aft distance between those edges. Its roll rotation was determined as the average vertical displacement of the inner and outer edges divided by their lateral separation. The yaw rotations were not included, since the crew mass was directly above the center of the base rectangle, and average yaw rotations would cause no translation of the crew mass. The inertia of the crew mass was equally divided among the four attachment points while retaining the proper eccentric height above the floor surface. In this way, the "seat" transmitted only the average (rigid body) motions of its floor attachment points, while transmitting the crew inertia loads into these floor attachments.

COMPOSITE SECTION GEOMETRY

The structure of the composite fuselage half-section was divided into the same major parts as the baseline section. The details of the actual and idealized components are given in Figure B-7 and Table B-2. The computer-generated drawings of the elements in the bulkheads, main beams, and energy-absorbing tubes are shown in Figures B-8 through B-10. Note that the nonlinear spring elements, used for the diagonal tension straps in the bulkheads and for the vertical crush springs in the tubes, are indicated in these drawings by the letter N.

The finite-element geometry of the belly skin, floor cover, doorpost, and roof were the same as for the baseline section in Figures B-4, -5, and -6. However, the cross-section geometries of these elements as listed in Table B-2 were not the same.

The crew/seat model was the same as that described for the baseline section.

In components where graphite/epoxy was combined with ±45° Kevlar/epoxy, calculations indicated that the graphite would be stressed greater and fail first, because of its much larger stiffness. Therefore, these components were modeled using all graphite/epoxy having the same stiffnesses as the actual component. This applied to the bulkhead flanges and the door-post and roof beams.

TABLE B-1. IDEALIZED BASELINE SECTION DETAILS

Component	Material	Element Type	Cross-Section Dimensions (in.)*	Comments
Beam Webs	Al2024-T3	Membrane Triangle	.063 Thick	
Beam Top & Bottom Caps, Fwd Bay Only	Al7075-T6	Stringer	.2359 in.^{2} Area	
Beam Bottom Cap, Mid & Aft Bays	Al7075-T6	T-Beam	1.25 x .095 Flange,** 1.032x .125 Web**	
Beam Top Caps. Mid & Aft Bays	Al7075-T6	T-Beam	1.25 x .079 Flange,** 1.016x .125 Web**	Top cap and seat track form combined beam for elastic stiffness, but act separately for plastic deformations.
Seat Tracks	Ti-6Al-4V	I-Beam	Figure A-1	
Beam Web Stiffener, Fwd Bay Only	Al2024-T3	Stringer	.1378 in.^{2} Area	
Beam Web Stiffeners, Mid. & Aft Bays	Al2024-T3	T-Beam	1.45 x .125 Flange,** .863 x .063 Web**	
Beam Web Stiffener, Mid. Bay, Inboard Beam	Al2024-T3	Channel Beam	.863 x .063 Flanges,** 2.4 x .125 Web**	

* Beam dimensions are outside, from outer corners to end of segments.

** Includes thickness of attached web or skin.

TABLE B-1. IDEALIZED BASELINE SECTION DETAILS (CONT'D)

Component	Material	Element Type	Cross-Section Dimensions (in.)*	Comments
Bulkhead 1 All Webs, Bulkhead 2,3,4 Webs, Intermed. and Outer Bays	Al2024-T3	Membrane Triangle	.063 Thick	
Bulkhead 2,3,4 Webs, Inner Bays Only	Al2024-T3	Membrane Triangle	.063 Thick	Beams imbedded into each panel, in vert. and lateral directions, to account for local bending of web.
		Rectangular Beam	.063 x Half Panel Width	
Bulkhead 1, Top Cap,*** Inner Bay	Al2024-T3	Stringer	.1598 $in.^2$ Area	
Bulkhead 1, Top Cap, Intermed. & Outer Bays; Bulkhead 1, Bot. Cap, Inner Bay	Al2024-T3	Stringer	.1101 $in.^2$ Area	
Bulkhead 1, Bot. Flange, Intermed. & Outer Bays	Al2024-T3	Stringer	.0510 $in.^2$ Area	
Bulkhead 1, Vert. Stiffener, Inner Bay at Vehicle ℄	Al2024-T3	Stringer	.2201 $in.^2$ Area	
Bulkhead 1, Vert. Stiffener, Intermed. Bay	Al2024-T3	Stringer	.1101 $in.^2$ Area	
Bulkhead 1-to-Main Beams, Intersections	Al2024-T3	Stringer	.7441 $in.^2$ Area	
Bulkheads 2,3,4 Top Cap, Inner Bay	Al2024-T3	T-Beam	1.6 x .063 Flange 1.0 x .125 Web**	

* Beam dimensions are outside, from outer corners to end of segments.

** Includes thickness of attached web or skin.

*** Bulkheads are numbered 1 through 4, from forward to aft.

TABLE B-1. IDEALIZED BASELINE SECTION DETAILS (CONT'D)

Component	Material	Element Type	Cross-Section Dimensions (in.)*	Comments
Bulkheads 2,3,4 Top Cap,*** Intermed. & Outer Bays Bulkheads 2,3,4 Bot. Cap, Inner Bay	Al2024-T3	L-Beam	.873 x .063 Flange** 1.0 x .125 Web**	
Bulkheads 2,3,4 Bot. Flange, Intermed. & Outer Bays	Al2024-T3	Rectangular Beam	.81 x .063	
Bulkheads 2,3,4 Vert. Stiffener, Inner Bay at Vehicle ℄	Al2024-T3	Channel Beam	.873 x .063 Equal Flanges** 2.0 x .125 Web**	Web attached to bulkhead, flanges aft.
Bulkheads 2,3,4 Vert. Stiffeners, Intermed. & Outer Bays	Al2024-T3	L-Beam	.873 x .063 Flange** 1.0 x .125 Web**	Flange aft, web attached to bulkhead.
Bulkheads 2,3,4-to-Main Beam, Intersections	Al2024-T3	T-Beam	2.063x.095 Flange** 1.032x.189 Web**	Two T's back-to-back at flanges combine for form a cruciform section beam for elastic stiffness, but act separately in plastic range.
Belly Skin Panels, Forward Inner & Intermed. Bays	Al2024-T3	Membrane Triangle	.032 Thick	
Belly Skin Panels, Forward Outer Bay	Al2024-T3	Membrane Triangle	.025 Thick	

* Beam dimensions are outside, from outer corners to end of segments.

** Includes thickness of attached web or skin.

*** Bulkheads are numbered 1 through 4, from forward to aft.

TABLE B-1. IDEALIZED BASELINE SECTION DETAILS (CONCLUDED)

Component	Material	Element Type	Cross-Section Dimensions (in.)*	Comments
Belly Skin Panels, Aft of Bulkhead 2, Inboard of Outer Beam	Al2024-T3	Membrane Triangle Rectangular Beam	.016 Thick .032 x Half Panel Width	Beams imbedded into each panel, in fore/aft and lateral directions, account for local bending stiffness of skin. Membrane thickness reduced to half to keep total axial stiffness correct.
Belly Skin Panels, Outboard of Outer Beam	Al2024-T3	Membrane Triangle	.025 Thick	
Floor Cover Panels	Al2024-T3	Membrane Triangle	.016 Thick	Only face sheet of panels included, to account for membrane stiffness only. Transverse bending neglected
Outer Floor Edge Longeron	2024-T3	Stringer	.1260 $in.^2$ Area	
Lower Doorpost Web, to 22 in. Above Floor	2024-T3	Membrane Triangle	.032 Thick	
Lower Doorpost, Forward Edge Frame, to 22 in. Above Floor	2024-T3	Channel Beam	.832 x .056 Equal Flanges, 3.0 x .032 Web	Simple channel beams with elastic stiffnesses set equal to actual values. In plastic range, only the bending stiffness in the vertical-lateral (roll) plane is correct.
Lower Doorpost, Aft Edge Frame, to 22 in. Above Floor	2024-T3	Channel Beam	.832 x .057 Equal Flanges 7.0 x .032 Web	
Upper Vertical Doorpost, from 22 in. Above Floor to Roof	2024-T3	Channel Beam	3.0 x .116 Fwd Flange, 7.0 x .059 Aft Flange, 11.0 x .032 Web	
Horizontal Roof	2024-T3	Channel Beam	3.0 x .098 Equal Flanges, 11.0 x .032 Web	

*Beam dimensions are outside, from outer corners to end of segments.

TABLE B-2. IDEALIZED COMPOSITE SECTION DETAILS

Component	Material	Element Type	Cross-Section Dimensions (in.)*	Comments
Beam Webs	Kevlar/Epoxy ±45°	Membrane Triangle	.080 Thick	
Beam Top & Bottom Caps, Fwd Bay Only	Graphite/Epoxy $[0_4/\pm 45\ /90]_s$	Stringer	.1652 $in.^2$ Area	
Beam Bottom Caps, Middle and Aft Bays	Graphite/Epoxy $[0_4/\pm 45\ /90]_s$	T-Beam	Same as Actual Fig. A-7	
Beam Top Caps, Middle and Aft Bays	Graphite/Epoxy $[0_4/\pm 45\ /90]_s$	T-Beam	Fig. A-7	Top cap and seat track form combined beam for elastic stiffness, but act separately in plastic deformation range of seat track.
Seat Tracks	Ti-6Al-4V	I-Beam	Fig. A-7	
Beam Web Vert. Stiffening Bead.	Kevlar/Epoxy ±45°	Channel Beam	.25 x .080 Equal Flanges, 1.42 x .080 Web	
Tube Walls	Kevlar/Epoxy ±45°	Membrane Triangles	.080 Thick	Forms square tube (on edge) to model longitudinal bending, shear, and axial stiffnesses of tubes as they flatten.
Tube Vert. Crush Stiffness	Load vs. Deflection Curve	Nonlinear Spring	----------	At each bulkhead and mid way between them

*Beam dimensions are outside, from outer corners to end of segments.

TABLE B-2. IDEALIZED COMPOSITE SECTION DETAILS (CONT'D)

Component	Material	Element Type	Cross-Section Dimensions (in.)*	Comments
Tube Wedge Cap	Graphite/Epoxy $[0_4/\pm45\ /90]_s$	Stringer	.067 $in.^2$ Area	
Bulkhead Webs	Kevlar/Epoxy ±45°	Membrane Triangle	.080 Thick	
Bulkhead Flanges	Graphite/Epoxy Unidirectional	Stringer	.0494 $in.^2$ Area	Same stiffness as actual Kevlar/ Graphite Flanges
Bulkhead 1 Skin** Former	Graphite/Epoxy $[0_4/\pm45\ /90]_s$	Stringer	.1371 $in.^2$ Area	
Bulkhead 2,3,4 Skin Formers	Graphite/Epoxy $[0_4/\pm45\ /90]_s$	L-Beam	Same as Actual Fig. A-7	
Bulkhead 1-to-Main Beam Intersections	Kevlar/Epoxy ±45°	Stringer	.6144 $in.^2$ Area	
Bulkhead 2,3,4-to-Main Beam Intersections	Kevlar/Epoxy ±45°	T-Beam	2.08 x .120 Flange, 1.04 x .240 Web	Two T's back-to-back at flanges combine to form cruciform section beam, including thicknesses of bulkhead and beam webs.
Bulkhead Diagonal Tension Straps	Kevlar/Epoxy Unidirectional	Nonlinear Spring	----------	Actual tension stiffness, no compression stiffness.
Belly Skin Panels, Outboard of Outer Beam, also Entire Forward Bay	Kevlar/Epoxy 0°/90°	Membrane Triangles	.040 Thick	

* Beam dimensions are outside, from outer corners to end of segments.
**Bulkheads are numbered from forward to aft, 1 through 4.

TABLE B-2. IDEALIZED COMPOSITE SECTION DETAILS (CONCLUDED)

Component	Material	Element Type	Cross-Section Dimensions (in.)*	Comments
Belly Skin Panels,** Aft of Bulkhead 2, Inboard of Outer Beam	Kevlar/Epoxy 0°/90°	Membrane Triangles	.020 Thick	Beams imbedded into each panel, in fore/aft and lateral directions, account for local bending stiffness of skin. Membrane thickness reduced to keep total axial stiffness correct.
		Rectangular Beam	.040 x Half Panel Width	
Floor Cover Panels	Kevlar/Epoxy 0°/90°	Membrane Triangles	.055 Thick	Upper and lower covers combined into one thickness to account for inplane axial and shear stiffnesses. Bending and transverse shear neglected.
Outer Floor Edge Longeron	Graphite/Epoxy $[0_4/\pm 45/90]_s$	Stringer	.152 $in.^2$ Area	
Lower Doorpost Web, to 22 in. above Floor	Kevlar/Epoxy ±45°	Membrane Triangle	.040 Thick	
Lower Doorpost Forward Frame, to 22 in. Above Floor	Graphite/Epoxy Unidirectional	Channel Beam	.80 x .015 Equal Flanges, 3. x .015 Web	Simple channel beams with all stiffnesses set equal to those of actual Kevlar/Graphite parts.
Lower Doorpost Aft Frame, to 22 in. Above Floor	Graphite/Epoxy Unidirectional	Channel Beam	.80 x .015 Equal Flanges, 7. x .015 Web	
Upper Doorpost, From 22 in. Above Floor to Roof	Graphite/Epoxy Unidirectional	Channel Beam	3 x .016 Fwd Flange, 7 x .016 Aft Flange, 11 x .002 Web	
Horizontal Roof	Graphite	Channel Beam	3 x .016 Equal Flanges, 11 x .016 Web	

* Beam dimensions are outside, from outer corners to end of segments.
** Bulkheads are numbered from forward to aft, 1 through 4.

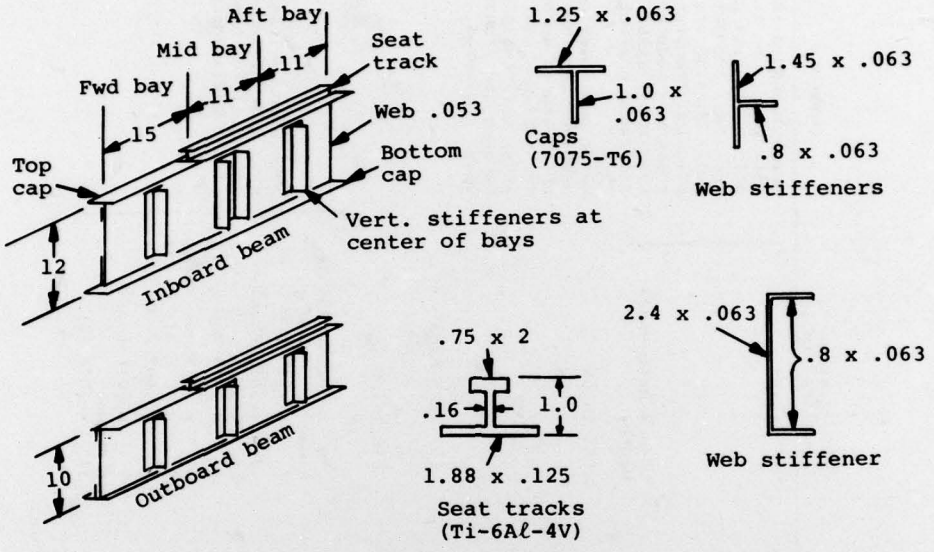

a. Main longitudinal beams and seat tracks.

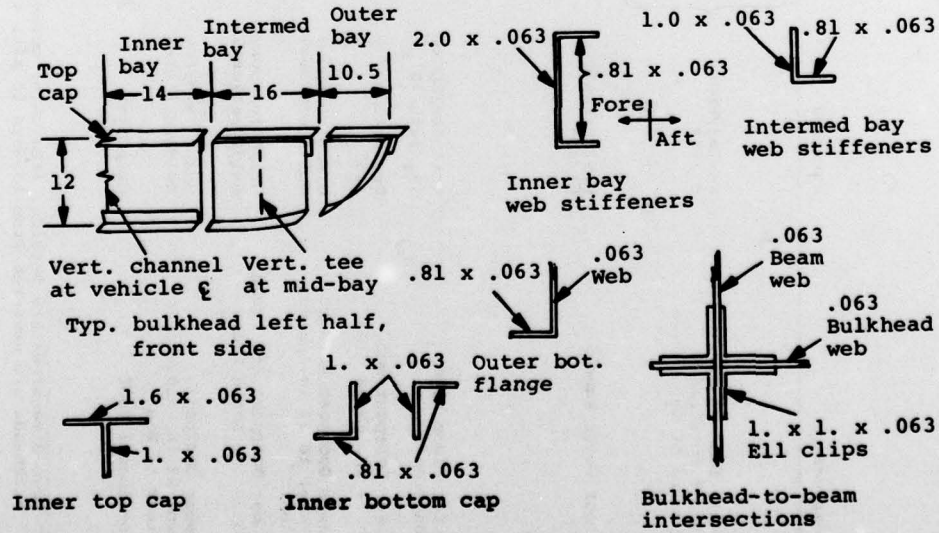

b. Bulkheads.

Figure B-1. Actual baseline fuselage section details.

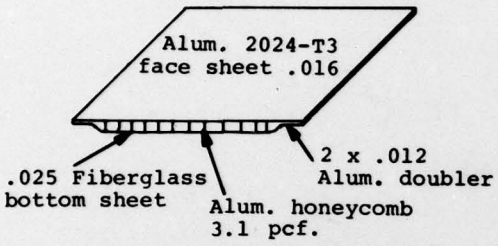

c. Floor panels between beams and bulkheads.

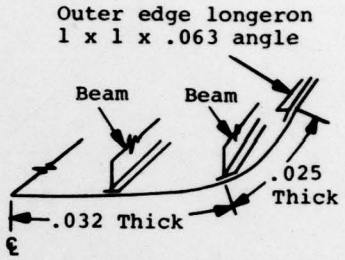

d. Belly skin panels.

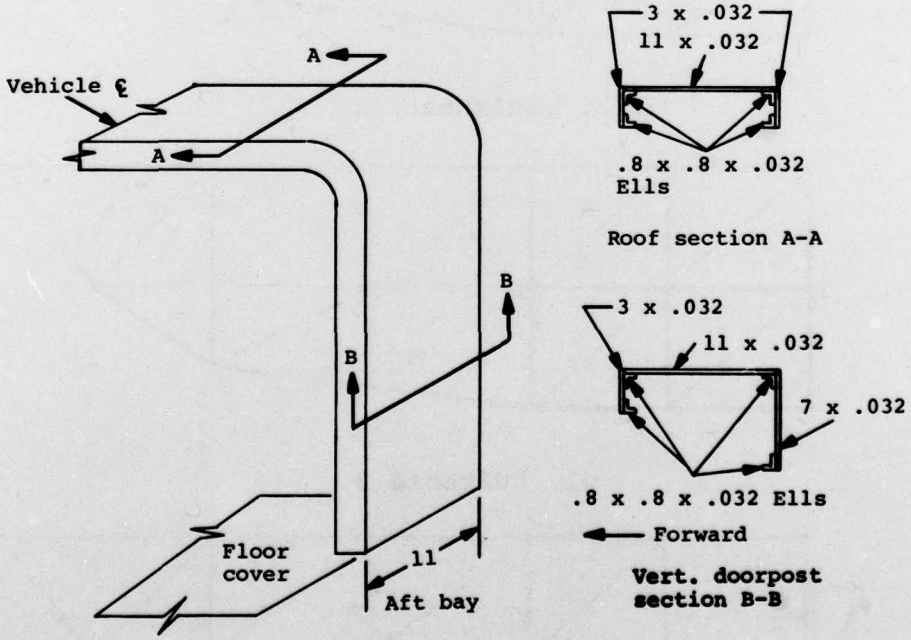

e. Doorpost and roof frame.

Figure B-1. Actual baseline fuselage section details. (Concluded)

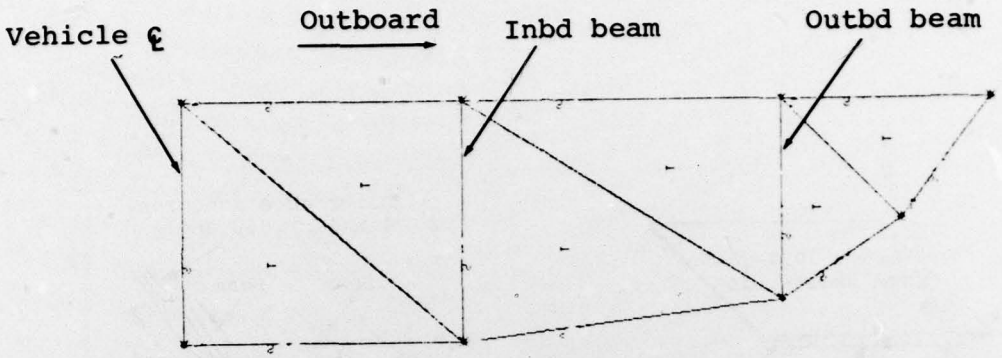

a. Bulkhead 1.

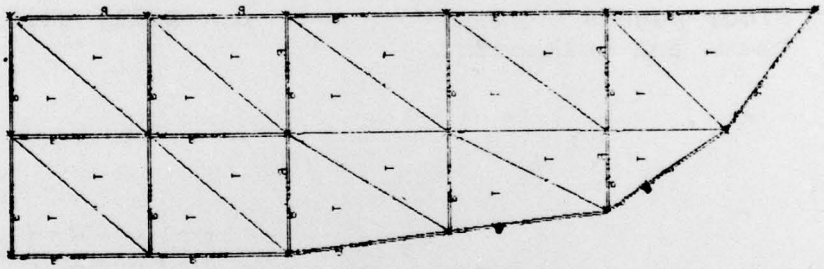

b. Bulkhead 2.

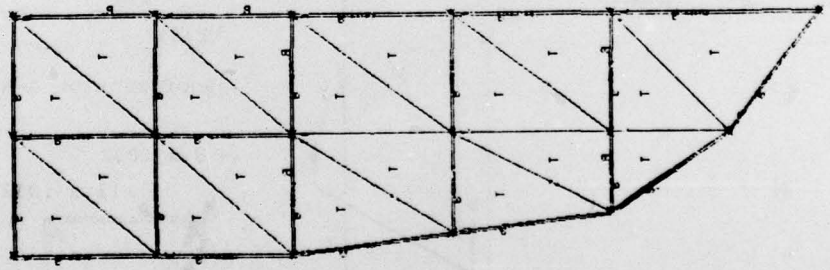

c. Bulkhead 3.

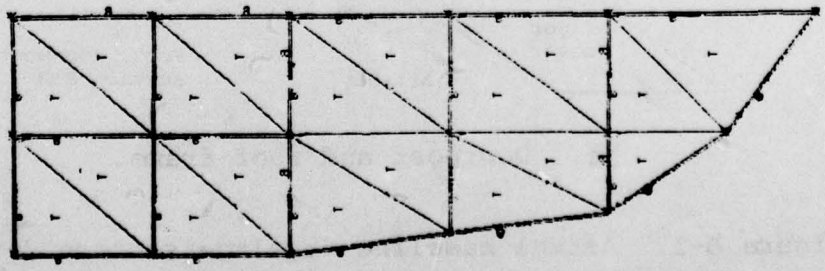

d. Bulkhead 4.

Figure B-2. Baseline section bulkhead elements.

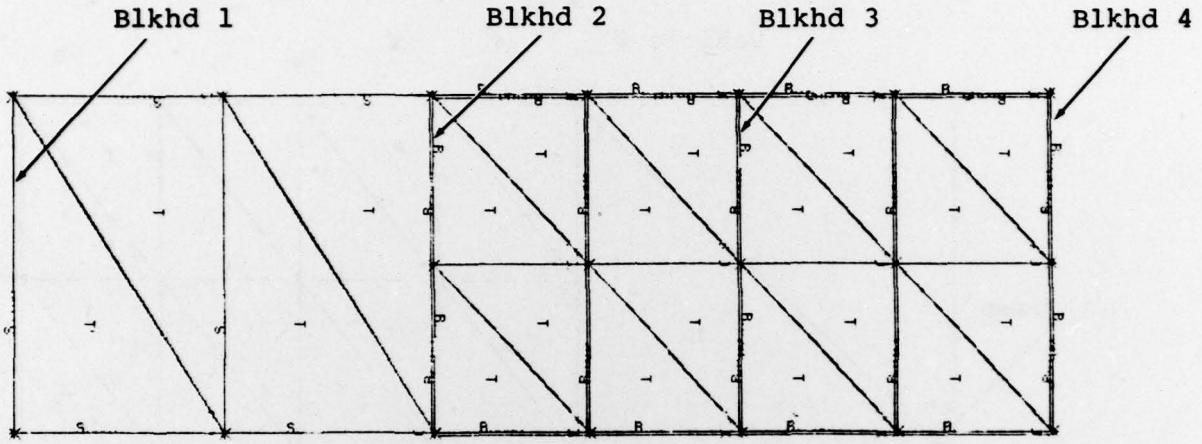

a. Inboard main longitudinal beam.

Forward

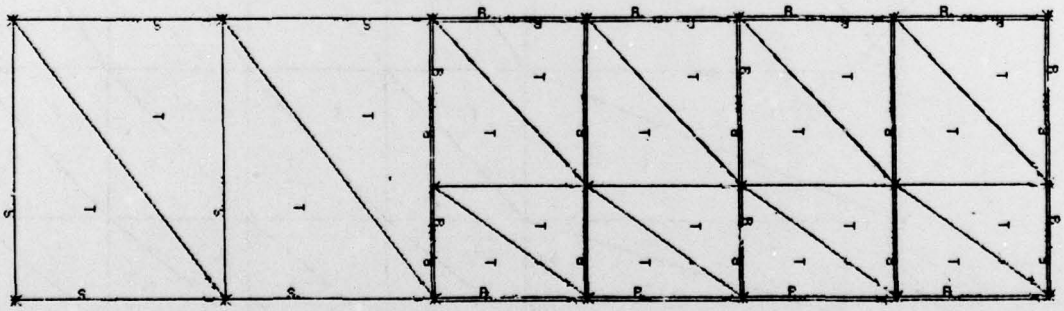

b. Outboard main longitudinal beam.

Figure B-3. Baseline section main beam elements.

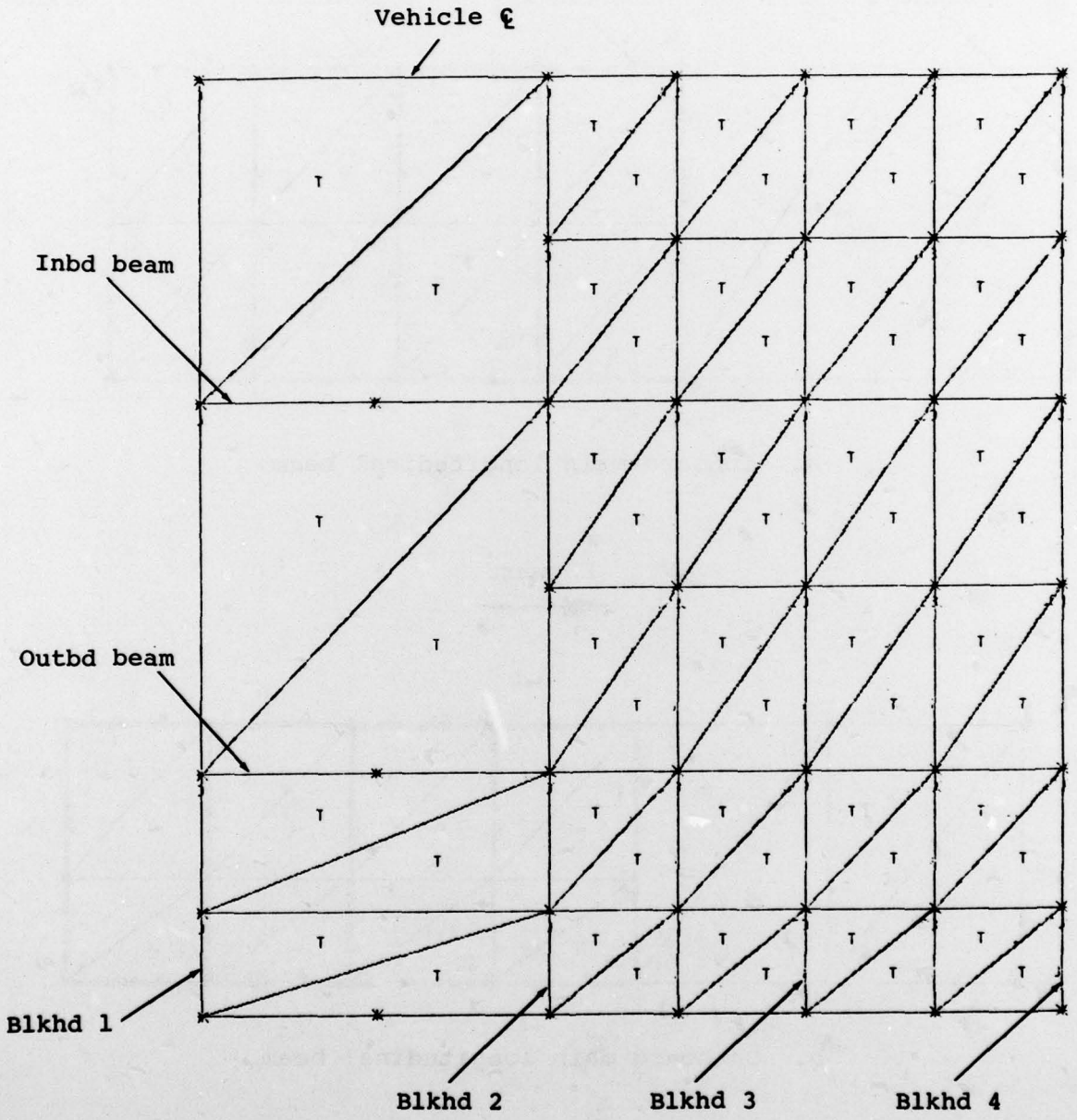

Figure B-4. Baseline section belly skin elements.

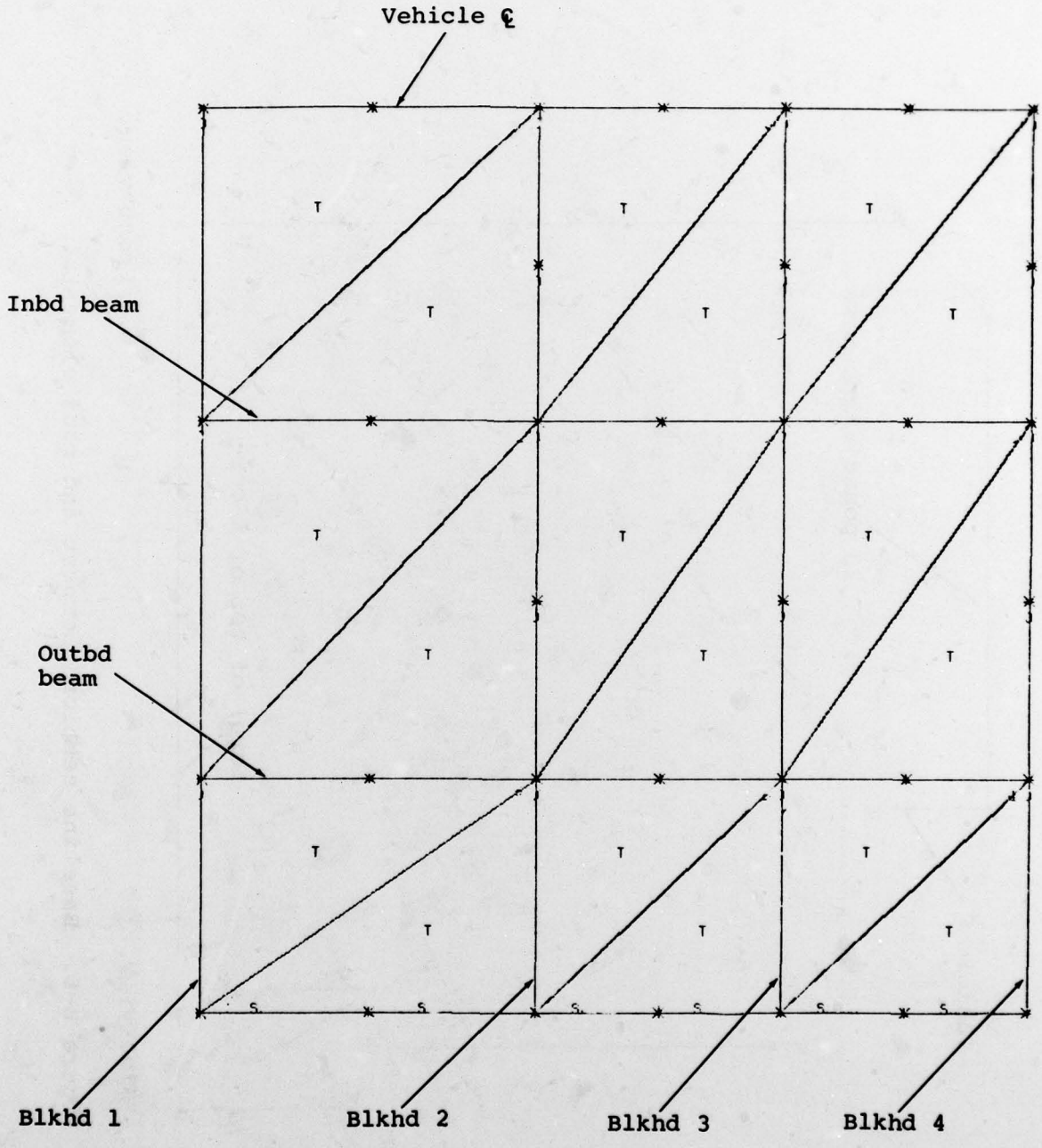

Figure B-5. Baseline section floor cover elements.

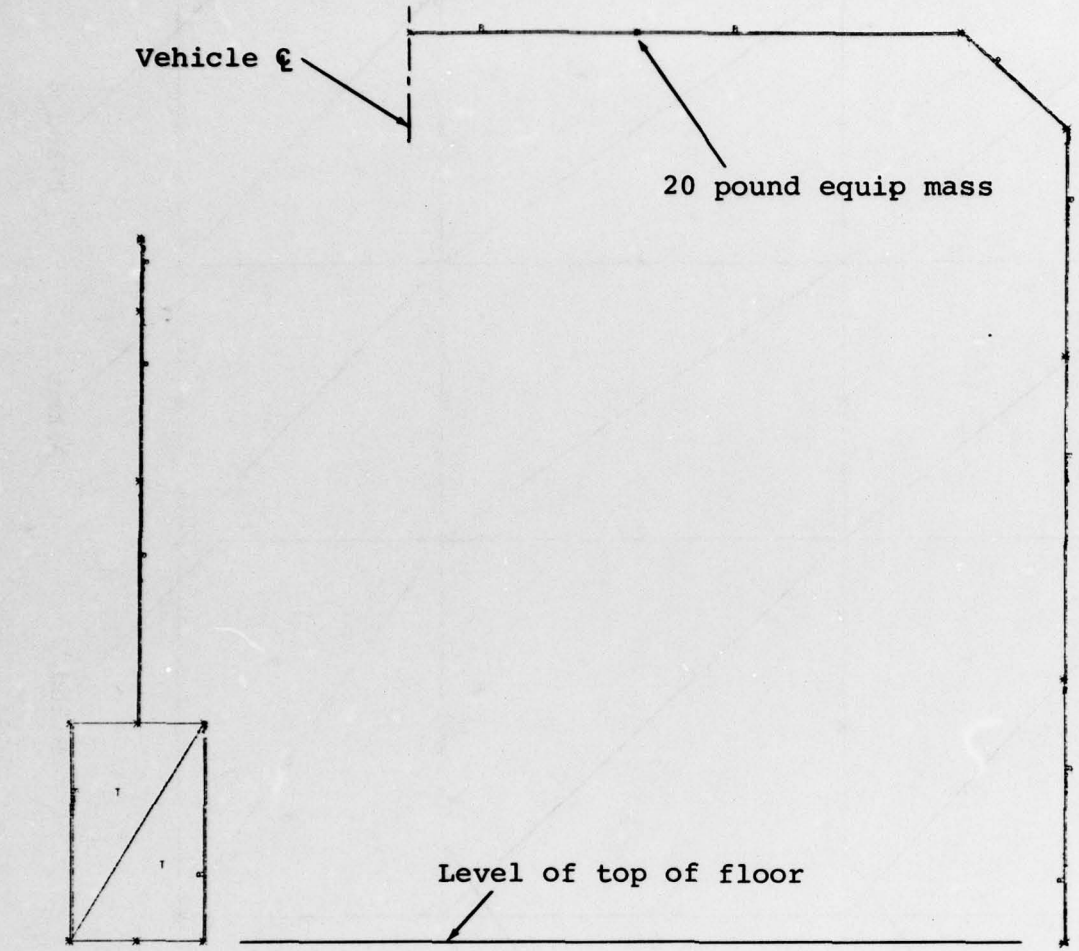

a. Side view. b. Front view.

Figure B-6. Baseline section doorpost and roof elements.

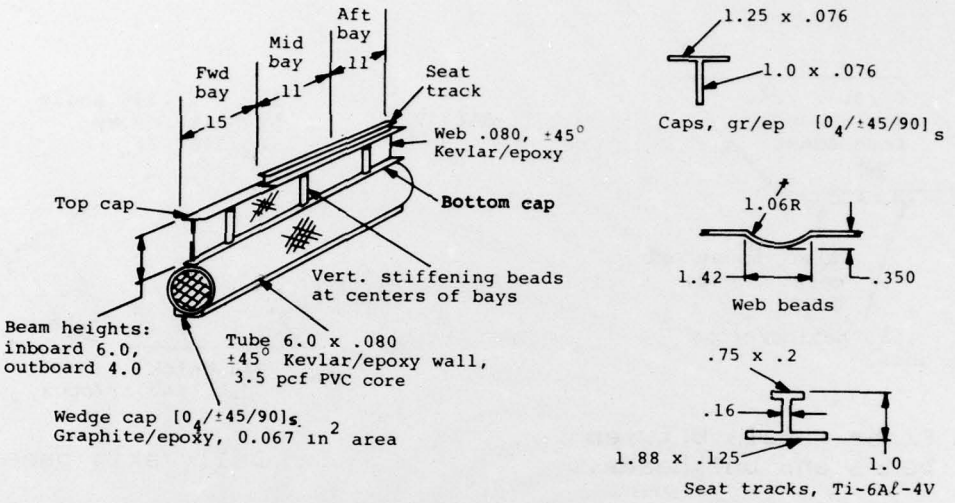

a. Main longitudinal beams, crush tubes, and seat tracks.

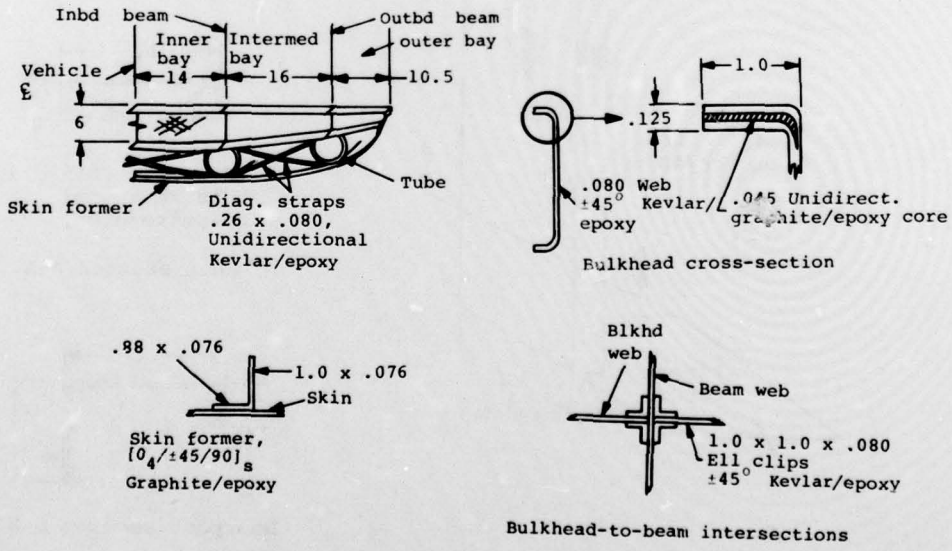

b. Bulkheads.

Figure B-7. Actual composite section details.

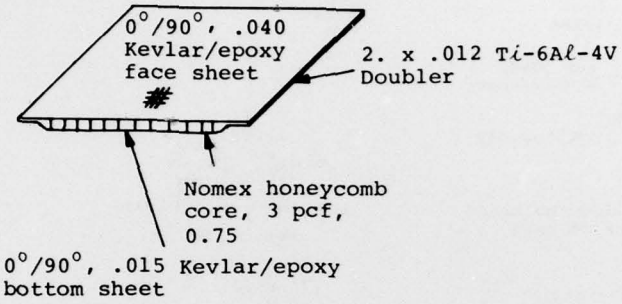

c. Floor panels between beams and bulkheads.

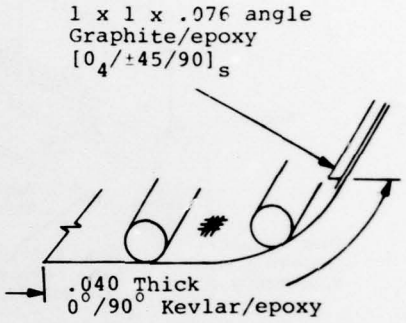

d. Belly skin panels.

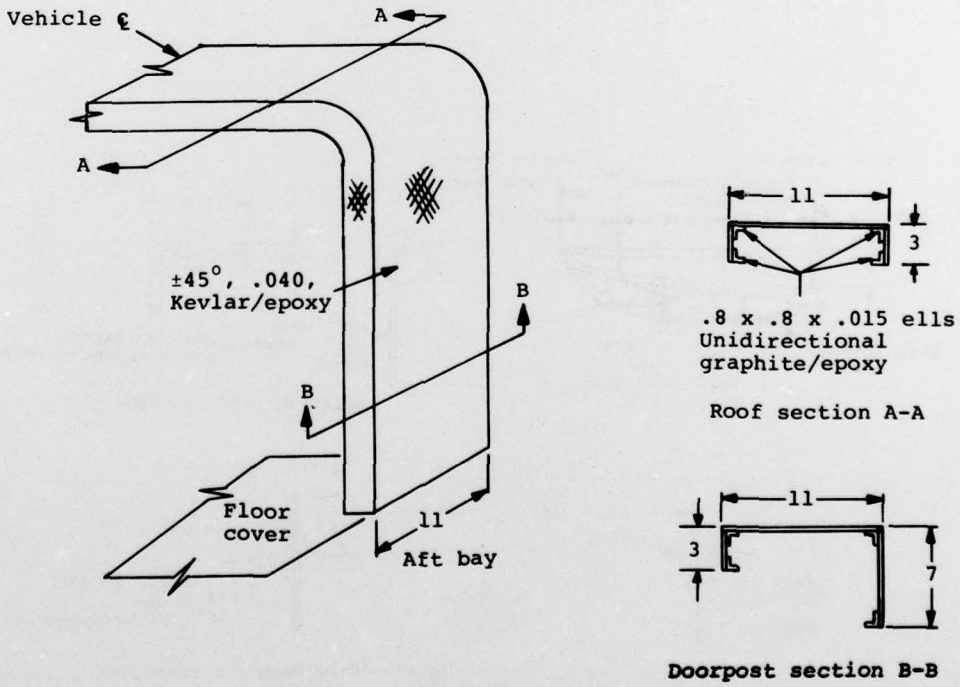

e. Doorpost and roof frame.

Figure B-7. Actual composite section details. (Concluded)

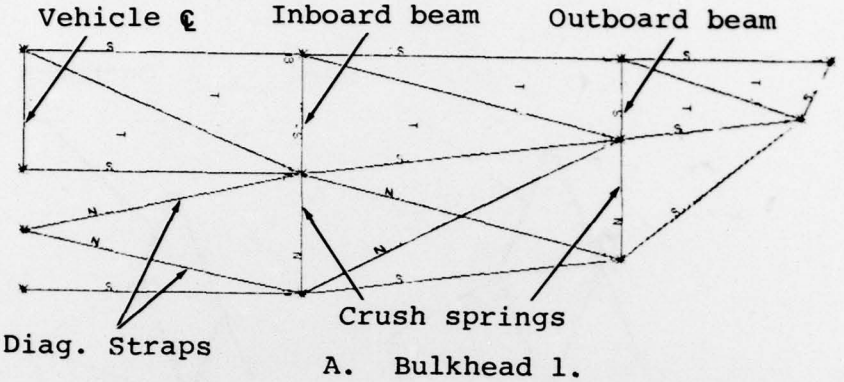

A. Bulkhead 1.

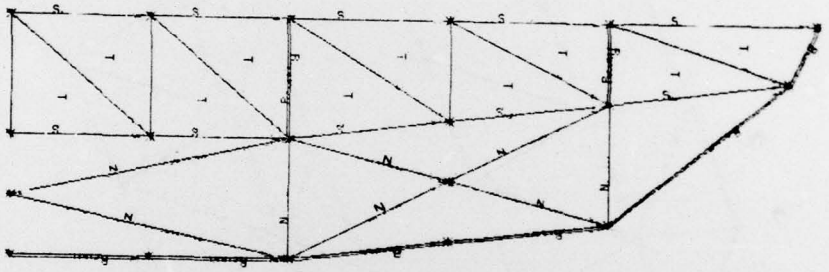

b. Bulkhead 2.

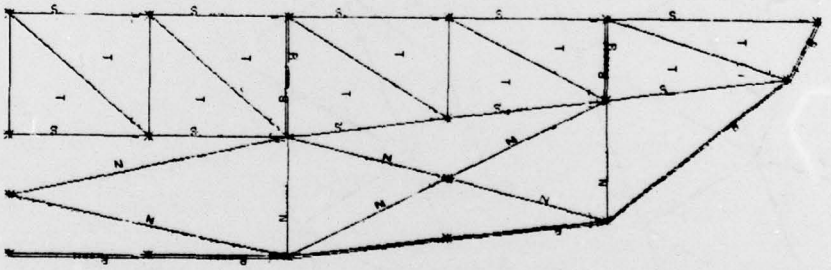

c. Bulkhead 3.

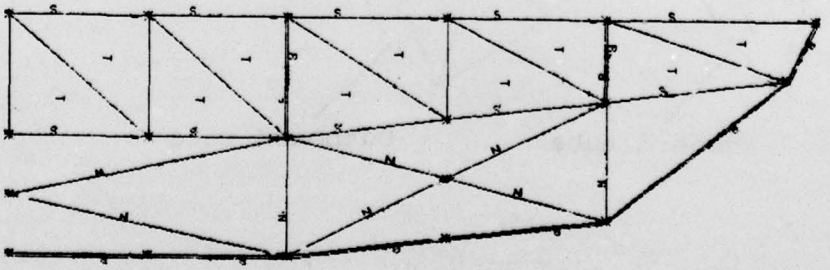

d. Bulkhead 4.

Figure B-8. Composite section bulkhead elements.

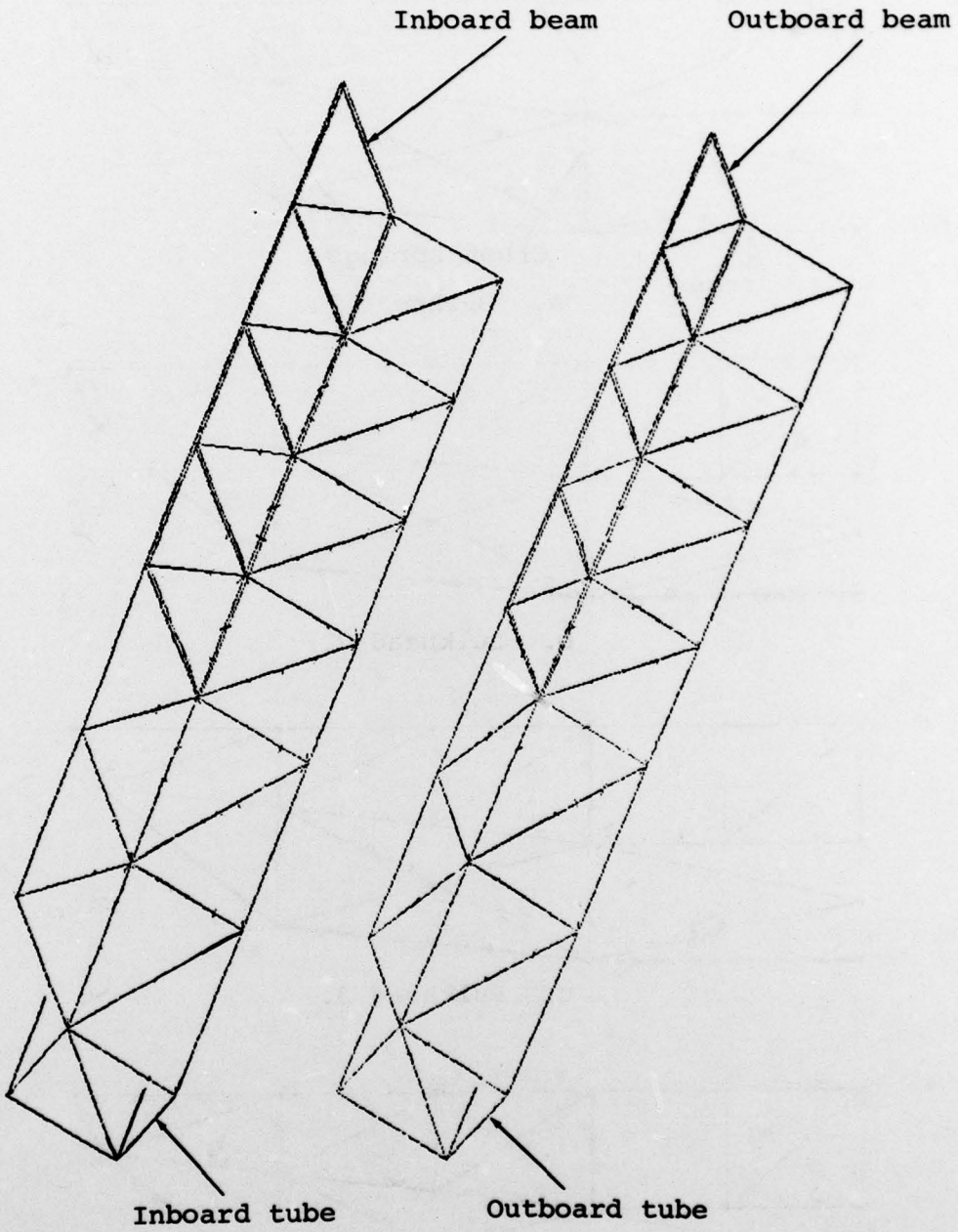

Figure B-9. Composite section main beams and crush tubes.

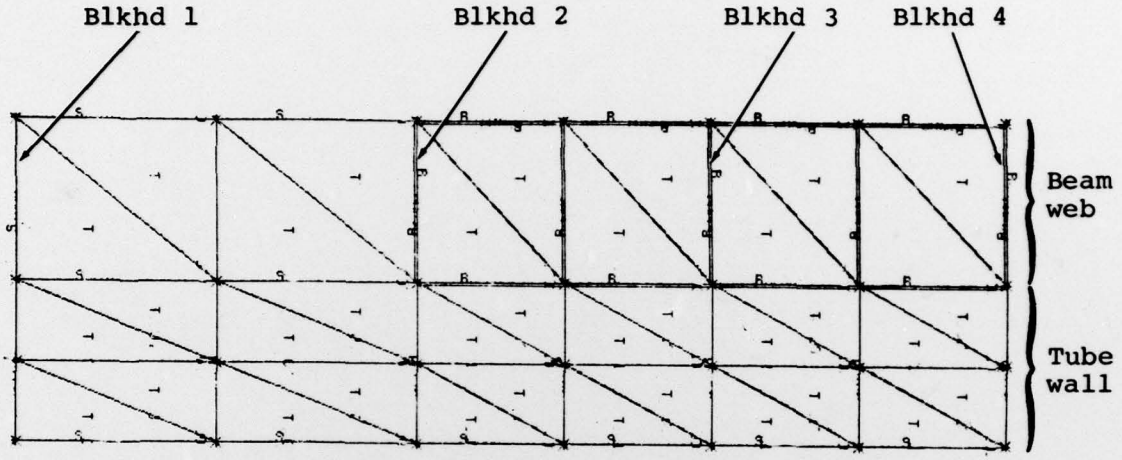

a. Inboard main beam and tube wall.

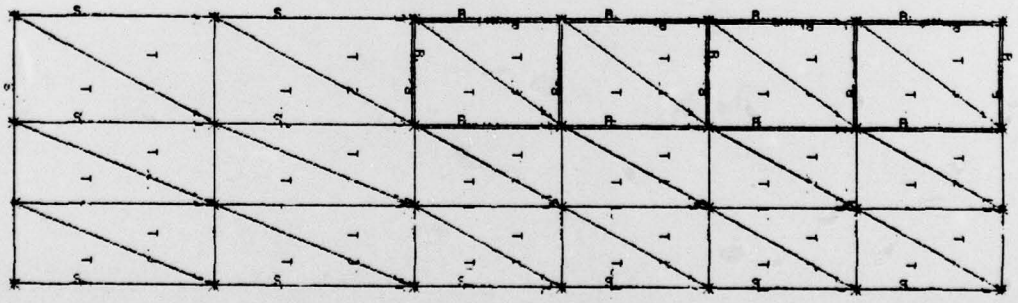

b. Outboard main beam and tube wall.

Figure B-10. Composite section main beam and tube wall elements.

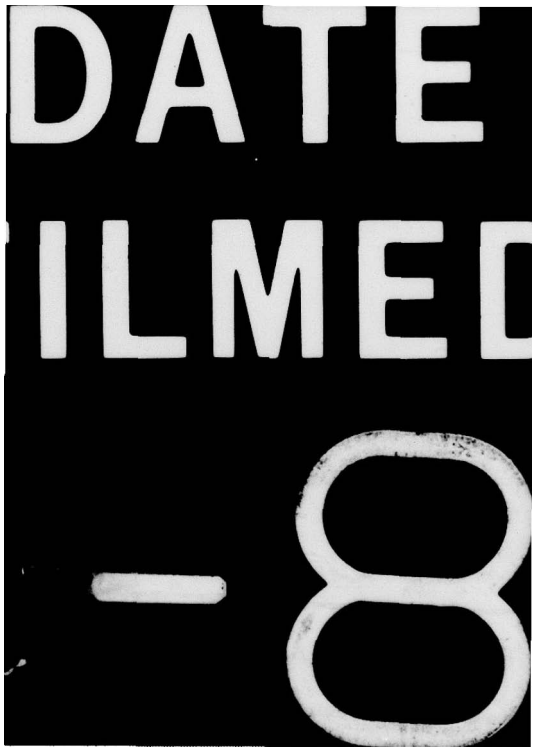
DATE
ILMED
-8